UNIVERSIDAD COMPLUTENSE DE MADRID

FACULTAD DE CIENCIAS QUÍMICAS

DEPARTAMENTO DE QUÍMICA ORGÁNICA

TESIS DOCTORAL

Modificación covalente y supramolecular de derivados de truxeno

Covalent and supramolecular modification of truxene-derivates

MEMORIA PARA OPTAR AL GRADO DE DOCTORA
PRESENTADA POR

María Gallego Capdevila

Directores

Nazario Martín León
Emilo M. Pérez Álvarez

Madrid, 2015

UNIVERSIDAD COMPLUTENSE DE MADRID

FACULTAD DE CIENCIAS QUÍMICAS

Departamento de Química Orgánica I

MODIFICACIÓN COVALENTE Y SUPRAMOLECULAR DE DERIVADOS DE TRUXENO

COVALENT AND SUPRAMOLECULAR MODIFICATION OF TRUXENE-DERIVATIVES

TESIS DOCTORAL

María Gallego Capdevila

Madrid, 2015

MODIFICACIÓN COVALENTE Y SUPRAMOLECULAR DE DERIVADOS DE TRUXENO

COVALENT AND SUPRAMOLECULAR MODIFICATION OF TRUXENE-DERIVATIVES

Directores:

Prof. Dr. Nazario Martín León

Dr. Emilio M. Pérez Álvarez

Memoria que para optar al grado de
DOCTOR EN CIENCIAS QUÍMICAS
presenta

María Gallego Capdevila

Madrid, 2015

References, abbreviations and acronyms

Bibliographic citations have been placed as footnotes in the pages where they were first cited in the section and at the end of this manuscript.

In addition to the standard abbreviations and acronyms in organic chemistry (as defined by the J. Org. Chem. Author Guidelines on January **2015**; http://pubs.acs.org/paragonplus/submission/joceah/joceah_authguide.pdf). The following terms have been used in this manuscript:

1D	one-dimensional
2D	two-dimensional
3D	three-dimensional
A	acceptor
AFM	atomic force microscopy
BHSC	bulk heterojunction solar cell
CNT	carbon nanotube
CT	charge transfer
CTV	cyclotriveratrylene
D	donor
DPP	diketopyrrolopyrrole
DSSC	dye sensitized solar cell
EQE	external quantum efficiency
exTTF	π-extended tetrathiafulvalene
FF	fill factor
FFI	fluoranthene-fused imide
FVP	flash vacuum pyrolysis
IPCE	incident photon to current conversion efficiency
J_{sc}	short-circuit current density
K_a	binding constant
MPP	maximum power point
*o*DCB	*o*-dichlorobenzene
OFET	organic field-effect transistor
OPV	organic photovoltaic
OSC	organic solar cell
PAH	polycyclic aromatic hydrocarbon

PCBM	1-(3-methoxycarbonylpropil)-1-phenyl[6,6] methanofullerene
PCE	power conversion efficiency
PCM	polarizable continuum model
PDI	perylenediimide
PET	photoinduced electron transfer
PhCl	chlorobenzene
PV	photovoltaic
TCO	transparent conducting oxide
TFSC	thin film solar cell
TruxTTF	truxenetetrathiafulvalene
V_{oc}	open-circuit voltage

Table of contents

1. Introduction

1. INTRODUCTION

This year 2015, we commemorate the 150th anniversary of Kekulé's most famous work "*Sur la constitution des substances aromatiques*". The term "aromatic" had been used to classify odoriferous compounds since the beginning of the 19th century. However, the history of aromaticity, as the fundamental chemical concept known nowadays, and as a major branch in chemistry, began with the isolation of benzene by Michael Faraday in 1825 (Figure 1.1).[1]

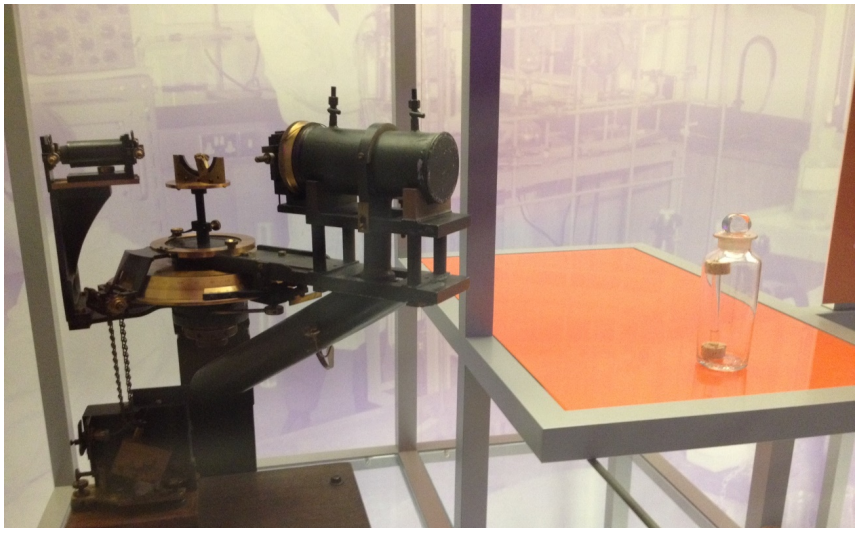

Figure 1.1. It is shown the flask containing the original benzene isolated by Faraday in 1825 and the X-ray diffractometer where the structure of benzene was unambiguously determined to be flat by Kathleen Lonsdate over one century later. Picture by N. Martín in his visit to The Faraday Museum at The Royal Institution in London.

Faraday isolated what he called "bicarburet of hydrogen", a substance obtained by repeated fraction of the fluid obtained during compression of oil gas, a non-aromatic source. He proposed "$(C_2H)_3$" as the empirical formula for this new substance, based on the erroneous carbon equivalent weight of the day, that was thought to be 6 and not 12. He characterized the "dicarburet of hydrogen",

[1] (a) W. H. Brock, "The Norton History of Chemistry", p. 257 "The Triumph of Structural Theory", **1992**; (b) K. Hafner, *Angew. Chem. Int. Ed.,* **1979**, *18,* 641; (c) D. H. Wilcox Jr, F. R. Greenbaum, *J. Chem. Ed.,* **1965**, *42*, 266; (d) A. Kekulé, *Bull. Soc. Chim. Paris,* **1865**, 98.

known nowadays as benzene, determining its boiling and melting points as well as its density quite accurately. Interestingly, just nine years after, Eilhard Mitscherlich heating benzoic acid with lime, an aromatic source, obtained the same hydrocarbon as Faraday. He determined its molecular formula C_6H_6 and named it benzin and later benzene, the name currently accepted by the IUPAC.[2]

It was twenty-five years later after the discovery of Faraday, when A. W. Hofmann recognized benzene and its derivatives as members of the great family of the so-called *aromatic* compounds.

These new aromatic compounds created such expectation that Kekulé and others decided to apply the most recent *structural theory* to unveil the puzzle of its chemical structure. Since the empirical formula of benzene, C_6H_6, as well as the carbon bonding rules were already known, a variety of proposals to describe the benzene molecule were published before Kekulé's solution in 1865. In this regard it is fair to mention the proposals made by Archibald Scott Couper and Josef Loschmidt with the diallene structure of benzene as a circle to note the unknown and elusive structure in his *Chemischen Studien* in 1861 (Figure 1.2), that was considered by Kekulé as misunderstanding.[2]

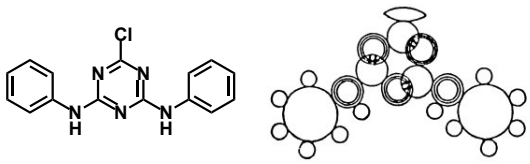

Figure 1.2. (left) modern formula of 2,4-disubstituted 1,3,5-triazine, (right) Loschmidt's drawing.

It was in this atmosphere that Kekulé considered a hexagon as the solution matching all the experimental evidence and the structural theory. If this was the result of a daydream revelation of the Ouroborus in 1862 sitting by his fire in Ghent as he told at the "Benzolfest" in 1890, or not, is a matter of debate.

[2] A. T. Balaban, P.v. R. Schleyer, H. S. Rzepa, *Chem. Rev*. **2005**, *105*, 3436.

"*I was sitting there, working on my textbook, but it was not going well; my mind was on other things. I turned my chair toward the fireplace and sank into half-sleep. Again the atoms fluttered before my eyes. This time smaller groups remained modestly in the background. My mind's eye, sharpened by repeated visions of a similar kind, now distinguished larger forms in a variety of shapes. Long lines, often combined more densely; everything in motion, twisting and turning like snakes. But look, what was that? One of the snakes had seized its own tail, and the figure whirled mockingly before my eyes. I awoke in a flash, and this time, too, I spent the rest of the night working out the consequences of the hypothesis*".[3]

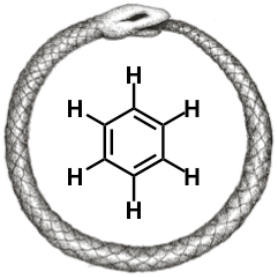

Figure 1.3. The snake seizing its own tail is an ancient symbol known as the Ouroborus.

However, there is no doubt that the formula stemmed from a deductive method resulting in the new ring concept. As stated by Kekulé at the ceremony in Berlin in 1890 to celebrate the twenty-fifth anniversary of his proposal of benzene's structure, "Let us learn to dream, gentlemen, then perhaps we shall find the truth. But let us beware of publishing our dreams until they have been put to the proof by the walking understanding". In January 1865, the recently founded Société Chimiques de Paris, published its "bulletin mensual" containing Kekulé's first paper entitled: "*Sur la constitution des substances aromatiques*". In this paper, he represented benzene as a closed chain of alternating single and double bonds in a linear sausage-shape formula applicable to all the aromatic compounds (Figure 1.4).

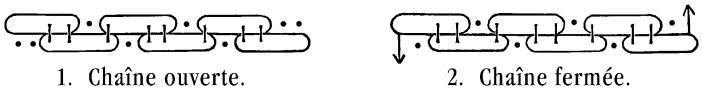

Figure 1.4. Kekulé's "sausages-formulas", they show open and closed chains in benzene.

Soon afterwards, he also published his key postulate, the cyclohexatriene hypothesis (Figure 1.5).[2]

[3] A. J. Rocke, *Angew. Chem. Int. Ed*. **2015**, *54*, 1.

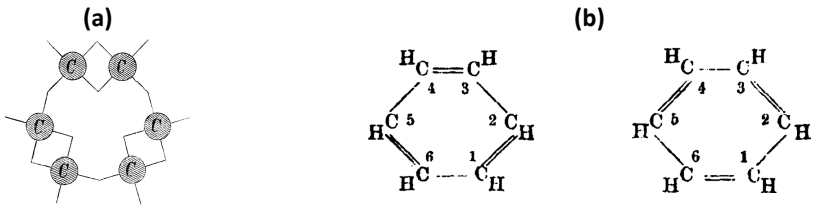

Figure 1.5. (a) Kekulé's 1866 ball-and-stick benzene formula. (b) Kekulé's 1872 oscillating single and double bonds in benzene.

Eventually, Bragg's colleague Kathleen Lonsdale, working at the Royal Institution unambiguously established in 1929 the chemical structure of benzene as well as its planarity by X-ray crystallography.

Since the very beginning, the unraveling and establishment of the concept of aromaticity have been among the most important issues concerning chemistry in general and organic chemistry in particular. In his Kekulé Memorial Lecture to the London Chemical Society in 1898, Francis Japp stated about Kekulé's benzene theory: "The most brilliant piece of scientific production to be found in the world of organic chemistry…three fourths of modern organic chemistry is directly or indirectly, the product of this theory".

With the perspective of time, over one century after Japp's statement, it resulted to be quite modest. Nowadays, aromaticity has a wider meaning referring to those compounds having planar and cyclic conjugated structure obeying Hückel's rule of (4n+2) π electrons. Aromatic compounds are thus not related with the former pleasant odor but to those compounds showing a higher level of stability than that expected from their formulation as conjugated cyclohexatrienes. Although free benzene does not occur naturally, its industrial production is important, at a social level. There is a wide variety of compounds that having benzene as a constituent have been used for applications in areas such as biochemistry, pharmacy, medicine, materials science, including plastics, engineering, etc. with a remarkable social impact.

Inspired in the simple benzene molecule, during the past three decades, new carbon nanoforms, namely fullerenes, carbon nanotubes and graphene, have emerged as most appealing carbon materials exhibiting amazing and outstanding properties. Fullerenes were first discovered as 3D carbon spheres

forming closed cages. Despite fullerenes are formed by twelve pentagons and a variable number of hexagons (n ≥ 20) (cyclohexatrienes), they do not follow Hückel's rule and, therefore, they are not aromatic compounds. Fullerenes have been exhaustively studied as electron acceptors in molecular electronics as well as in other different fields, such as hydrogen storage or medicinal chemistry, just to name a few. Carbon nanotubes are 1D carbon-based analogs to fullerenes forming single and multi-wall nanotubes with a variable diameter and constituted exclusively by carbon hexagonal rings. The mechanical and optoelectronic properties of carbon nanotubes have been extensively exploited to construct a wide variety of devices. Finally, 2D graphene is constituted by a single layer of hexagonal carbon rings, thus forming a planar sheet of carbon atoms. Currently, graphene is considered to be the "panacea" of carbon-based technologies. Diverse applications such as transparent electrodes, super-capacitors, extremely sensitive sensors or lightweight high-performance materials have been postulated for it.

Considering the singularity of this "aromaticity celebration", 150 years after Kekulé's benzene, we wish to contribute with this historical introduction, as benzene is also the cornerstone of the aromatic systems that will be discussed throughout this memory: classic aromatic systems derived from a curved truxene core and bowl shaped polycyclic aromatic compounds. Both type of systems are at the forefront of aromatic compounds, exhibiting less-known features and a high chemical versatility, which make them aromatic compounds of choice in the search for new applications. A non-comprehensive review on the most significant achievements involving truxenes and bowl shaped polycyclic aromatic compounds will be discussed in their respective chapters.

Chapter I.

Covalent modifications on truxTTF core

2. Background

2. BACKGROUND

2.1. TRUXENE

The 10,15-dihydro-*5H*-diindeno[1,2-a:1′,2′-c]fluorene commonly named truxene (**1**), is a planar polycyclic aromatic hydrocarbon with C_3-symetry. Its first synthesis was reported in the literature in 1889.[4] **1** was synthesized by reaction of 3-phenylpropionic acid and phosphorous pentoxide, and directly from 1-indanone by means of aldol-condensation cyclotrimerizations. Alternative synthetic pathways were reported but with an important deficiency: lack of regioselectivity. [5] Truxene was accompanied by its regioisomer isotruxene (**2**), also named β-truxene. Recently, truxene has been successfully synthesized from truxenone (**3**), a polycyclic aromatic ketone with a truxene core.[6]

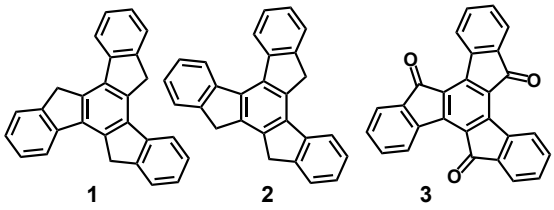

Figure 2.1. Truxene, isotruxene and truxenone.

The high conjugation and the C_3-symmetry of the truxene core make it a useful building block for the construction of new materials with diverse and promising applications. By modifying its periphery at will or using structurally analogous systems we can gain access to:

- Larger polyarenes that might lead to bowl-shaped fullerene fragments or fullerenes.[7]

[4] (a) J. Hausmann, *Ber. Dtsch. Chem. Ges*. **1889**, *22*, 2019; (b) F. S. Kipping, *J. Chem. Soc*. **1894**, 269.

[5] (a) E. Dietzel, U.S. Patent 2,216,001, 1940; (b) Chem. Abstr. **1941**, 35, 4584; (c) K. F. Lang, M. Zander, E. A. Teiling, *Chem. Ber*. **1960**, *93*, 321; (d) G. Merz, *Synthesis* **1972**, 614.

[6] Y. N. Oded, I. Agranat, *Tetrahedron Lett.* **2014**, *55*, 636.

[7] (a) B. Gómez-Lor, O. de Frutos, A. M. Echavarren, *Chem. Commun*. **1999**, 2431; (b) L. T. Scott, M. M. Boorum, B. J. McMahon, S. Hagen, J. Mack, J. Blank, H. Wegner, A. de Meijere, *Science* **2002**, *295*, 1500; (c) K. Y. Amsharov, M. Jansen, *J. Org. Chem*. **2008**, *73*, 2931; (d) K. Amsharov, M. Jansen, *Chem. Commun.* **2009**, 2691; (e) G. Otero, G. Biddau, C. Sánchez-Sánchez, R, Caillard, M. F. López, C. Rogero, F. J. Palomares, N. Cabello, M. A. Basanta, J. Ortega, J.

- Water-soluble anionic fluorophores.[8]
- Candidates for blue light emitting materials.[9]
- Thermally stable cathode buffer materials.[10]
- Active materials for organic field-effect transistors, (OFETs).[11]
- Liquid crystals.[12]
- N-type organic semiconductors for thin-film organic solar cells.[13]

2.1.1. *Synthesis of pristine truxene and its modifications. Truxenes "à la carte"*

Truxene is commonly synthesized by the acid catalyzed trimerization of 1-indanone (Scheme 2.1).[14] It has fifteen positions that can be functionalized. These positions are grouped in three pentagonal rings and three benzene rings.

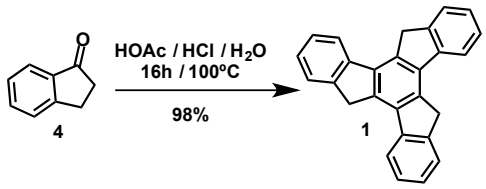

Scheme 2.1. Synthesis of truxene from 1-indanone.[14]

Méndez, A. M. Echavarren, R. Pérez, B. Gómez-Lor, J. A, Martín-Gago, *Nature* **2008**, *445*, 865; (f) K. Amsharov, N. Abdurakhmanova, S. Stepanow, S. Rauschenbach, M. Jansen, K. Kern, *Angew. Chem. Int. Ed*. **2010**, *49*, 9392.

[8] N. Earmrattana, M. Sukwattanasinitt, P. Rashatasakhon, *Dyes and Pigments* **2012**, *93*, 1428.

[9] J. Luo, Y. Zhou, Z.Q. Niu, Q.F. Zhou, Y. Ma, J. Pei, *J. Am. Chem. Soc*. **2007**, *129*, 11314.

[10] H. Tsuji,Y. Ota, S. Furukawa, C. Mitsui, Y. Sato, E. Nakamura, *Asian J. Org. Chem*. **2012**, *1*, 34.

[11] Y. Sun, K. Xiao, Y. Liu, J. Wang, J. Pei, G. Yu, D. Zhu, *Adv. Funct. Mater*. **2005**, *15*, 818.

[12] (a) K.Q. Zhao, C. Chen, H. Monobe, P. Hu, B.Q. Wang, Y. Shimizu, *Chem. Commun.* **2011**, *47*, 6290; (b) K. Isoda, T. Yasuda, T. Kato, *Chem. Asian J*. **2009**, *4*, 1619.

[13] C.B. Nielsen, E. Voroshazi, S. Holliday, K. Cnops, B. P. Rand, I. McCulloch, *J. Mater. Chem*. A, **2013**, *1*, 73.

[14] E. V. Dehmlow, T. Kelle, *Synth. Commun.* **1997**, *27*, 2021.

(a) Modifications at the pentagonal rings

Positions C5, C10 and C15 are generally functionalized with saturated alkyl chains (Scheme 2.2). The objectives of this functionalization are: (1) to reduce the intermolecular π–π stacking, (2) to improve the poor solubility of **1** and thereby facilitate further modifications at other positions.

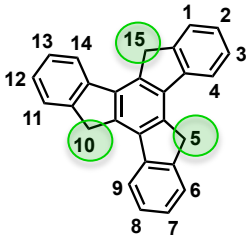

Figure 2.2. Highlighted in green the three pentagonal positions of truxene.

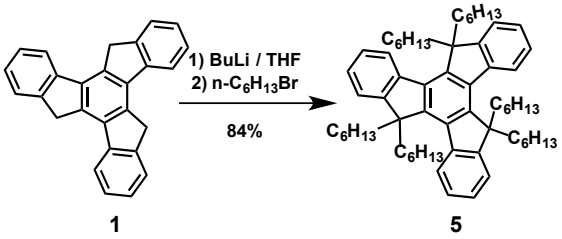

Scheme 2.2. General alkylation conditions.[15]

As aforementioned, truxene has attracted attention for its applicability in molecular electronics. As an example, an artificial antenna system has been reported in which a truxene core is linked at C5 to a C_{60} unit through an aliphatic linker (Scheme 2.3).[16]

There are also some examples of the use of unsaturated alkyl chains and phenyl substituents at these pentagonal positions that open the possibility to the synthesis of new truxene-type building blocks (Scheme 2.4).[17]

[15] S. Diring, R. Ziessel, *Tetrahedron lett.* **2009**, *50*, 1203.
[16] L. Sánchez, N. Martín, E. González-Cantalapiedra, A. M. Echavarren, G. M. A. Rahman, D. M. Guldi, *Org. Let.* **2006**, *8*, 2451.
[17] E. González-Cantalapiedra, M. Ruiz. B. Gómez-Lor, B. Alonso, D. García-Cuadrado, D. J. Cárdenas, A. M. Echavarren. *Eur. J. Org. Chem*. **2005**, 4127.

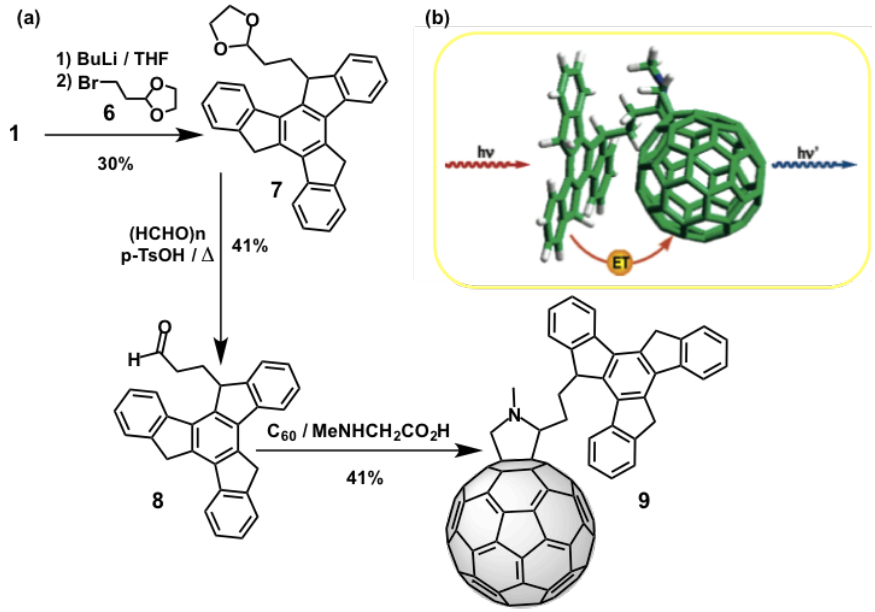

Scheme 2.3. (a) Synthetic route to get photoactive molecule **9**. (b) Figure showing the schematic photoinduced electron transfer of the artificial antenna.

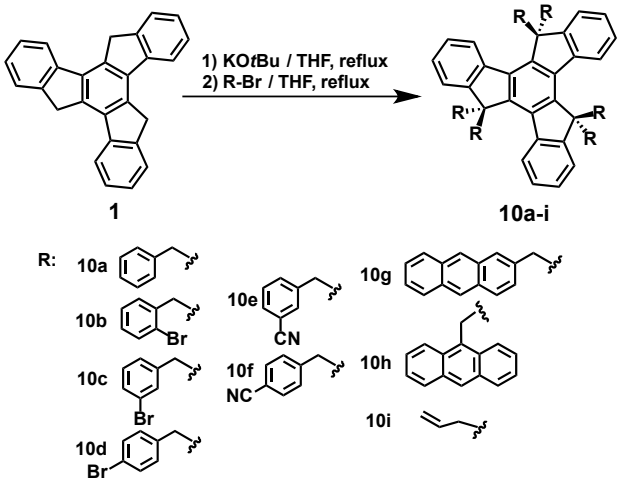

Scheme 2.4. Synthesis of symmetrical hexasubstituted truxenes.[17]

As it is shown in Schemes 2.4 and 2.5, alkylation of **1** in the presence of excess of base and alkyl halides gives the authors a straight pathway to have symmetrically or asymmetrically hexasubstituted truxenes at C5, C10 and C15 positions.

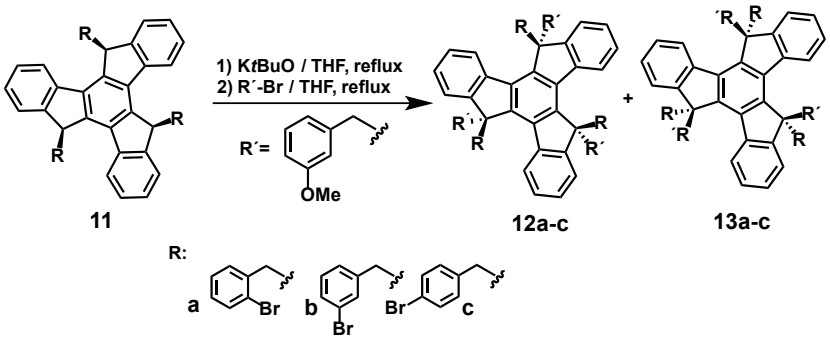

Scheme 2.5. Synthesis of asymmetrical hexabenzyltruxenes.[17]

As mentioned above, the extension of the aromatic core of **1** might lead to fullerenes. A representative example is the synthesis of molecule **16** (Scheme 2.6). **16** is a $C_{84}H_{42}$ hydrocarbon that has more than 83% of the connectivities present in the C_{84}. Through selective cyclodehydrogenation, **16** provides [84]fullerene under flash vacuum pyrolysis (FVP) treatment.[7d]

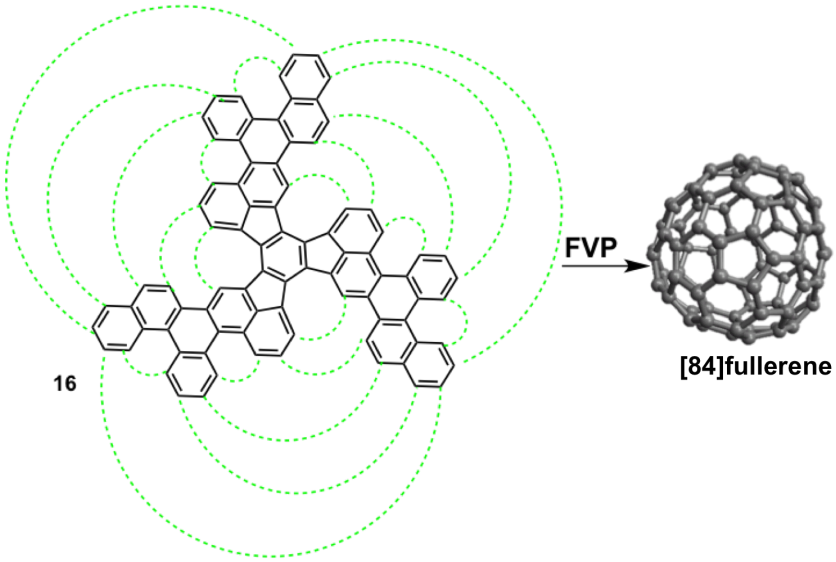

Scheme 2.6. Curved dashed lines show the new C-C bonds that will be created on molecule **16** to construct the close [C_{84}]fullerene cage.

Molecule **16** is achieved in just two synthetic steps (Scheme 2.7): the trianion of truxene is generated in situ by treatment with n-BuLi, dibromide **14** is then added to the trianion to give compound **15** (*anti* isomer) and a subsequent

palladium-catalyzed intramolecular arylation of **15** gives the target molecule **16**.

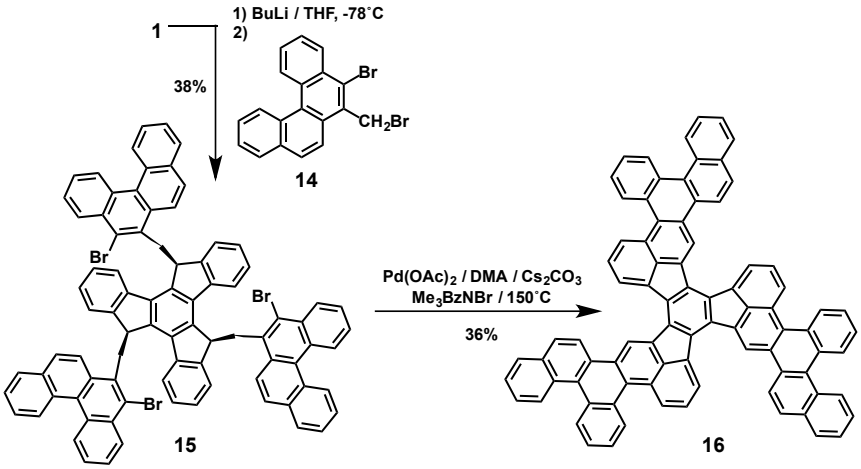

Scheme 2.7. Two-steps synthetic route to obtain molecule **16**.

(b) Modifications at the benzene rings

Within the twelve susceptible positions of reaction at the three benzene rings of truxene, C2, C7 and C12 are the most frequently functionalized (Figure 2.3).

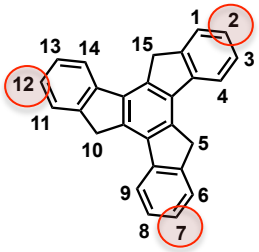

Figure 2.3. Highlighted in red the most frequently functionalizated truxene positions.

In the following example Pei and co-workers, chose the truxene core as building motif, due to its three-dimensional topology, for constructing π-conjugated dendrimers containing up to nine truxene units (Figure 2.4).[18]

To afford dendrimer **19**, pristine truxene is modified with hexahexyl groups at the positions C5, C10 and C15 to enhance the solubility of the starting material and, then, C2 position is modified by Friedel-Crafts acetylation reactions to give molecule **17,** which is followed by cyclotrimerization to give

[18] X. Y. Cao, W. B. Zhang, J. L. Wang, X. H. Zhou, H. Lu, J. Pei, *J. Am. Chem. Soc*. **2003**, *125*, 12430.

molecule **18**. Further repeating the Friedel-Crafts and the cyclotrimerization reactions on **18** leads to dendrimer **19** in an efficient manner (Scheme 2.8).

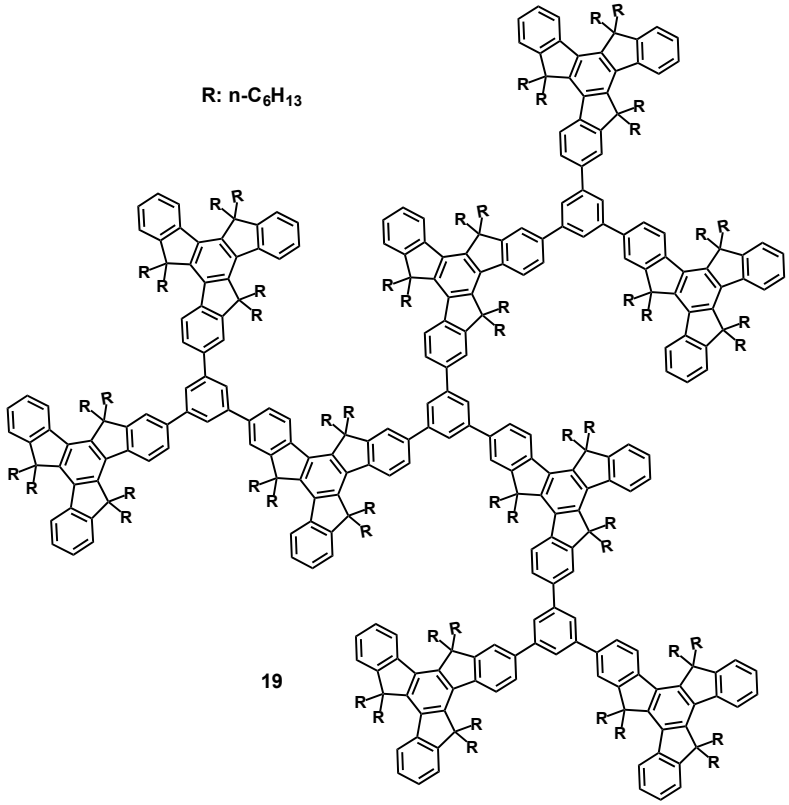

Figure 2.4. π-Conjugated dendrimer **19** endowed with nine units of truxene.

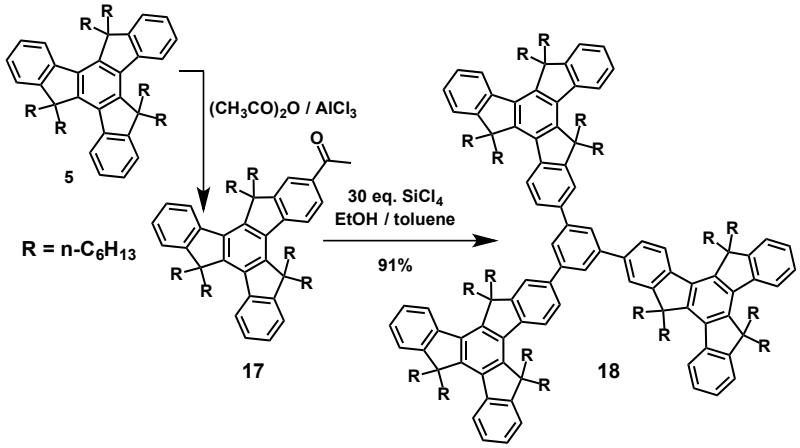

Scheme 2.8. Synthetic route to obtain molecule **18**.

Electrophilic bromination of **1** gives 2,7,12-tribromotruxene (**20**) (Scheme 2.9), which can be used as the starting material for the preparation of C_{3h} trisubstituted truxenes by cross-coupling reactions.

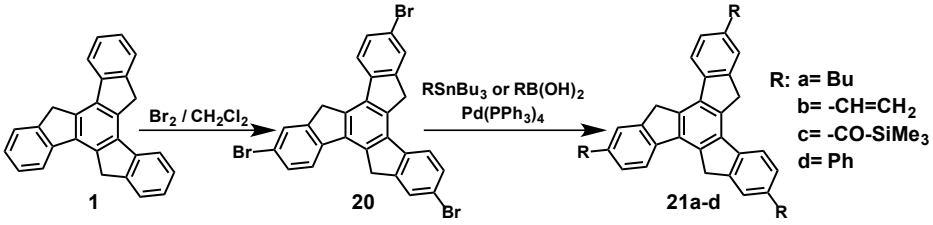

Scheme 2.9. Synthetic route towards C_{3h} trisubstituted truxenes by Stille or Suzuki coupling with organostannanes or boronic acids.[19]

As aforementioned, C5, C10 and C15 positions at the pentagonal rings can be easily modified as well as C2, C7 and C12 positions of the aromatic rings. Modifying the other positions requires alternative routes. C3, C8 and C13 truxene positions can be modified once C2, C7 and C12 are already functionalized.

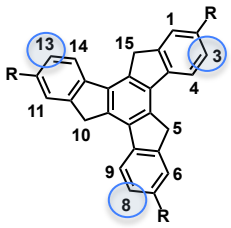

Figure 2.5. Highlighted in blue the C3, C8 and C13 truxene positions.

For example, compound **26** (Trux-PBI) (Figure 2.6) is a star-shaped chromophore, which has recently been reported.[20]

[19] B. Gómez-Lor, O. de Frutos, P. A. Ceballos, T. Granier, A. M. Echavarren, *Eur. J. Org. Chem.* **2001**, 2107.

[20] Y. Xie, X. Zhang, Y. Xiao, Y. Zhang, F. Zhou, J. Qi, J. Qu, *Chem. Commun*. **2012**, *48*, 4338.

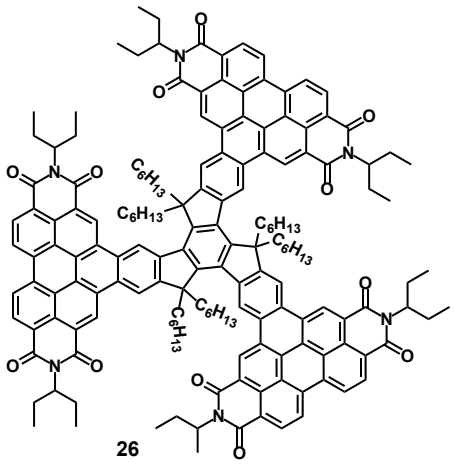

Figure 2.6. Trux-PBI (**26**).

Compound **26** was synthesized by fusing three perylene bisimide branches to a truxene core by Suzuki coupling and later photocyclization to accomplish the fusion (Scheme 2.10). This large rigid and nearly planar conjugated system presents outstanding photostability and remarkable two-photon properties.[20]

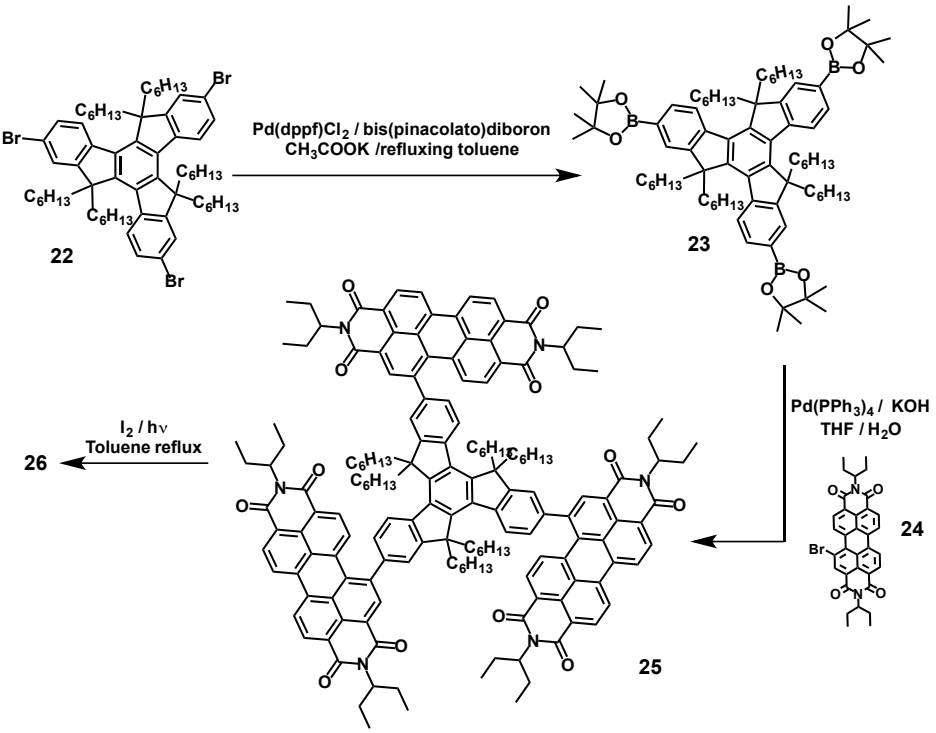

Scheme 2.10. Synthesis of Tr-PBI (**26**).

(c) Condensation of previously modified 1-indanones

A smart solution to get truxenes functionalized at the desired positions with the appropriate functionality is to synthesize truxenes from previously modified 1-indanones (Schemes 2.11, 2.12 and 2.13).[19,12a]

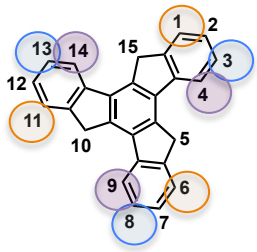

Figure 2.7. Positions of the truxene susceptible to be functionalized from suitably functionalized 1-indanones.

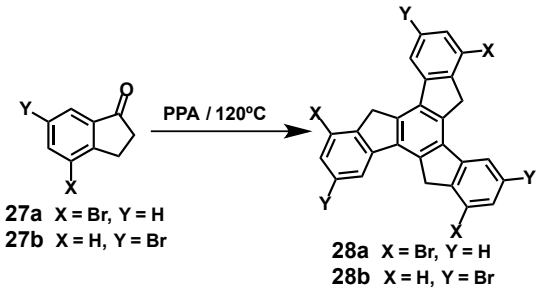

Scheme 2.11. Synthetic pathway to obtain tribrominated truxenes at C1, C6, C11 or C3, C8, C13.

This strategy allows achieving truxenes functionalized at the most hindered positions C4, C9 and C14 (Scheme 2.12).[19]

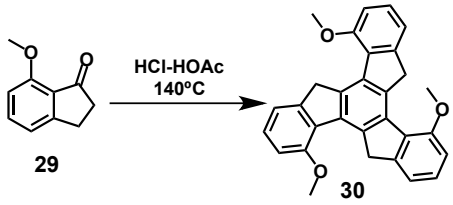

Scheme 2.12. Synthesis of a 4,9,14-substituted truxene.

Molecule **32**, a trioctyloxytruxene, has been synthesized from indanone **31**. Interestingly, compound **32** behaves as a discotic liquid crystal.[12a]

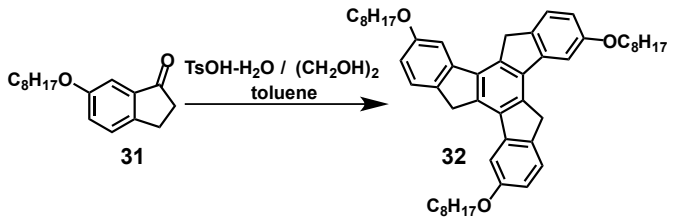

Scheme 2.13. Synthesis of a truxene discotic liquid crystal.

(d) Heteroatom-containing truxene

The truxene core can also present heteroatoms such as oxygen, sulfur or nitrogen in its structure, giving rise to the respective trioxatruxene (**33**), trithiatruxene (**34**) and triazatruxene (**35**). The most common synthetic approach to obtain these kind of derivatives is the cyclocondensation of isobenzofuran-1(3*H*)-one (**36**), benzo[*c*]thiophen-1(3*H*)-one (**37**) and indolin-2-one (**38**), (Figure 2.8).[21]

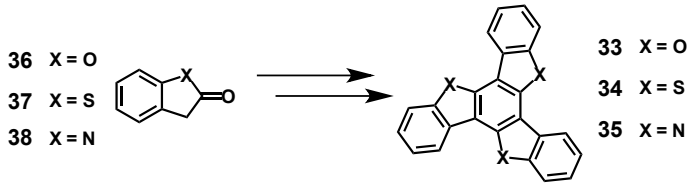

Figure 2.8. Schematic synthesis of trioxatruxene, trithiatruxene and triazatruxene.[21]

Some hexaalkanoates and benzoates of trithiatruxene, trioxatruxene and truxene are known to form discotic liquid crystals (Figure 2.9).[22]

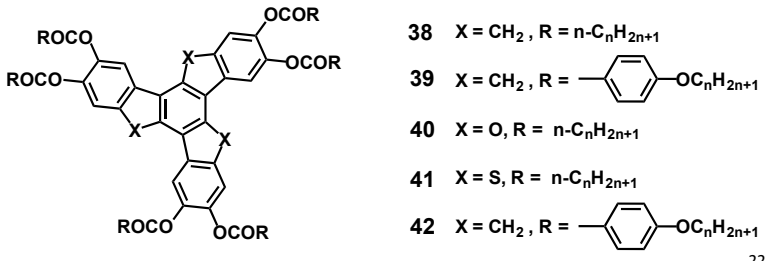

Figure 2.9. Representative examples of truxene-based liquid crystals.[22]

[21] (a) J. Bergman, B. Egestad, *Tetrahedron lett.* **1978**, 3143; (b) J. Bergman, B. Egestad, *Tetrahedron* **1986**, *42*, 763; (c) M. Franceschin, L. Ginnari-satriani, A. Alvino, G. Ortaggi, A. Bianco, *Eur. J. Org. Chem*. **2010**, 134.

[22] H. K. Bisoyi, S. Kumar, *Chem. Soc. Rev.* **2010**, *39*, 264.

Interestingly, some triazatruxene derivatives were synthesized as precursors for less known triazafullerenes (Figure 2.10),[23,7e] as well as precursors for potential blue organic light-emitting diodes,[24] or dyes for organic dye-sensitized solar cells (Figure 2.11).[25]

Triazafullerene $C_{57}N_3$ (**44**) has been synthesized by surface-catalysed cyclodehydrogenation process from triazatruxene $C_{57}H_{33}N_3$ (**43**) as an open precursor. Heating at 750 K **43** deposited onto a platinum (111) surface leads to the triazafullerene **44** in quantitative yield.[23,7e]

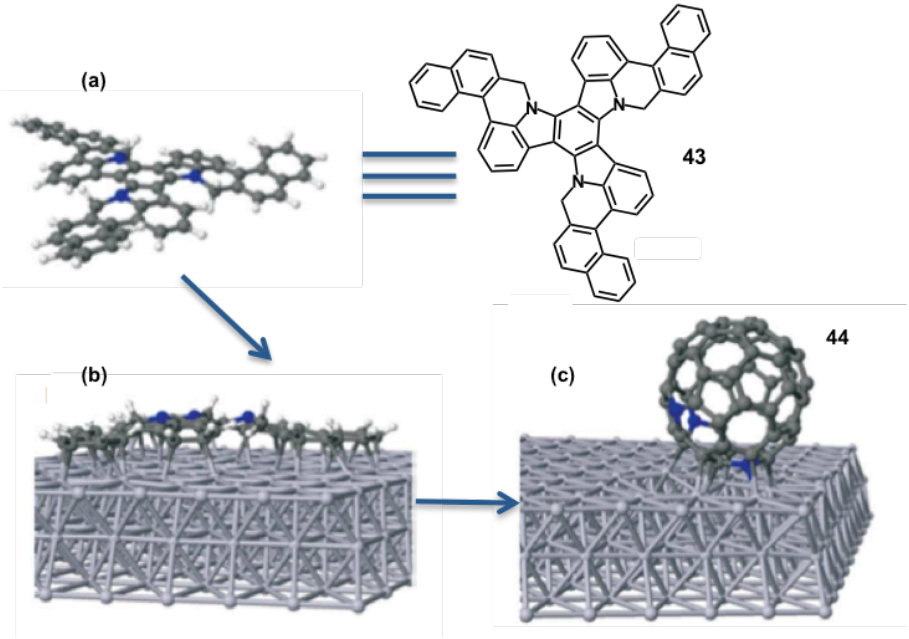

Figure 2.10. (a) Triazatruxene $C_{57}H_{33}N_3$ (**43**), precursor of fullerene $C_{57}N_3$ (**44**). (b) Optimized geometrical structure of **43** adsorbed at 300 K on the platinum surface (111). (c) Optimized geometrical structure for triazafullerene **44** formed after dehydrogenation process at 750 K.[7e]

The triazatruxene core has also been successfully used for designing some organic dyes for dye-sensitized solar cells (Figure 2.11). In these dyes the triazatruxene core provides a delocalized π-donor system.[25]

[23] B. Gómez-Lor, A. Echavarren, *Org. Lett.* **2004**, *6*, 2993.
[24] W. Y Lai, Q. Y He, R. Zhu, Q. Q Chen, W. Huang, *Adv. Funct. Mater.* **2008**, *18*, 265.
[25] X. Quian, Y. Z. Zhu, J. Song, X. P. Gao, J. Y. Zheng, *Org. Lett*. **2013**, *15*, 6034.

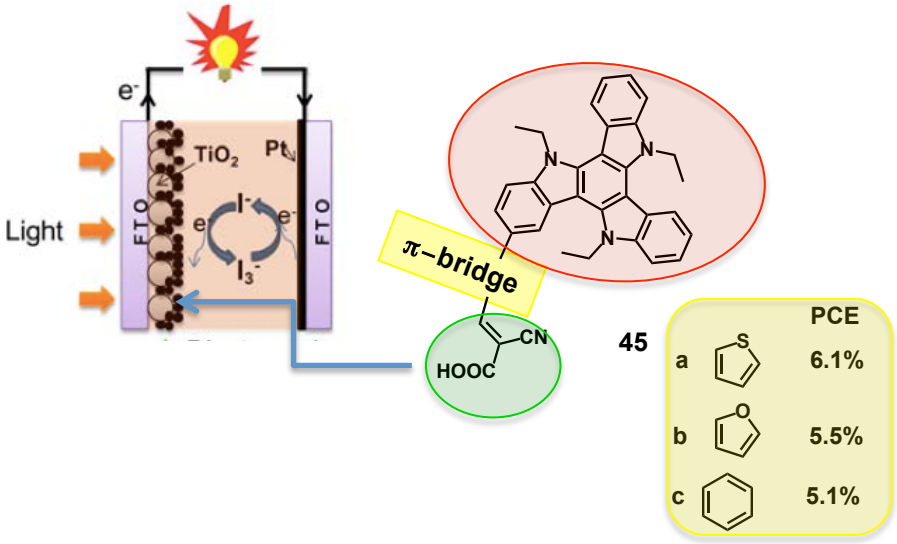

Figure 2.11. Triazatruxene derivatives for dye-sensitized solar cells.

(e) Truxene derivatives from truxenone as starting material

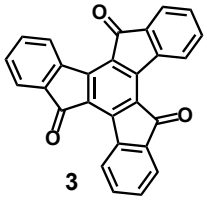

Figure 2.12. Truxenone structure.

Truxenone **3**, 5*H*-diindeno[1,2-*a*:1',2'-*c*]fluorene-5,10,15-trione has a C_{3h} symmetry (Figure 2.12). It can be seen as three fluorenones sharing a common central benzene ring. Furthermore, **3** can also be seen as the "oxidized state" of truxene, **1**.

The presence of the three carbonyl groups on the five membered rings makes **3** an attractive scaffold or component for functional materials. These carbonyl groups make truxene core a relatively strong electron acceptor.

There are several methods to prepare truxenone, but most of them follow one of the two paths shown in Figure 2.13.[26] Compound **3** can be synthesized from cyclotrimerization of **46**, 1*H*-indene-1,3(2*H*)-dione (path A) or, alternatively, by condensation of **48**, 2,2-dibromo-2,3-dihydro-1*H*-inden-1-one (path B).

[26] L. Sanguinet, J. C. Williams, Z. Yang, R. J. Twieg, G. Mao, K. D. Singer, G. Wiggers, R. G. Petscheck, *Chem. Mater.* **2006**, *18*, 4259.

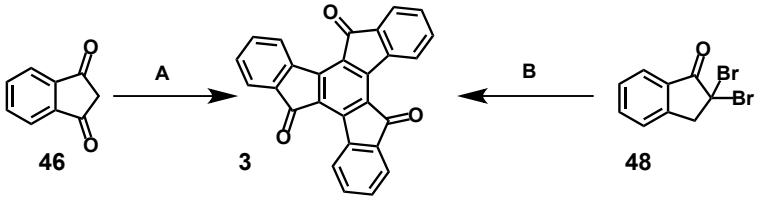

Figure 2.13. Two possible pathways to synthesize truxenone.

Indenones functionalized at C5 with a halogen atom provide truxenone skeletons suitably modified at positions C4, C9 and C14. These halogen atoms are susceptible to suffer further nucleophilic substitution reactions. By following this synthetic strategy, a variety of truxenenone cores with different donor groups at the periphery have been prepared (Scheme 2.14).[26]

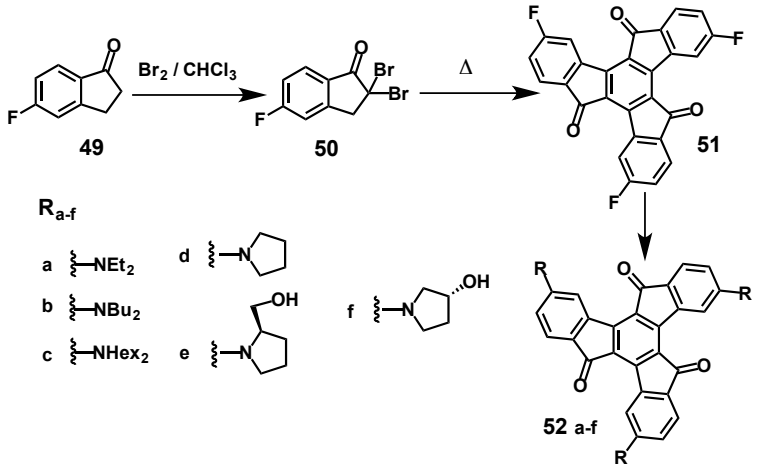

Scheme 2.14. 4,9,14-Tris(dialkylamino)truxenones prepared by nucleophilic substitution from 4,9,14-trifluorotruxenone.

In the following example, the preparation of a truxenone from its homologous truxene derivative is shown (Scheme 2.15)[27]. Compounds **54** and **55** form a supramolecular 1D co-assembly (Figure 2.14). Their donor-acceptor interactions together with the $\pi-\pi$ interactions are the main driving forces for this assembling process.

[27] J. Y. Wang, J. Yan, l. Ding, Y. Ma, J. Pei, *Adv. Funct. Mater.* **2009**, *19*, 1746.

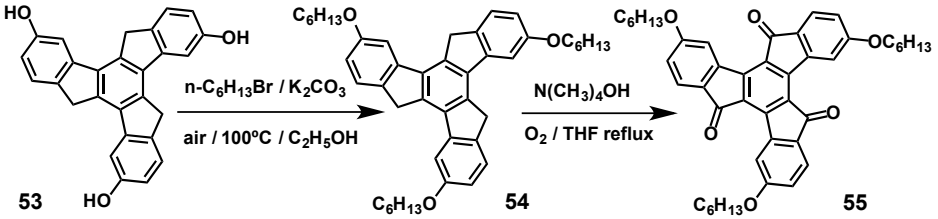

Scheme 2.15. Synthetic route to obtain truxene **54** and truxenone **55**.

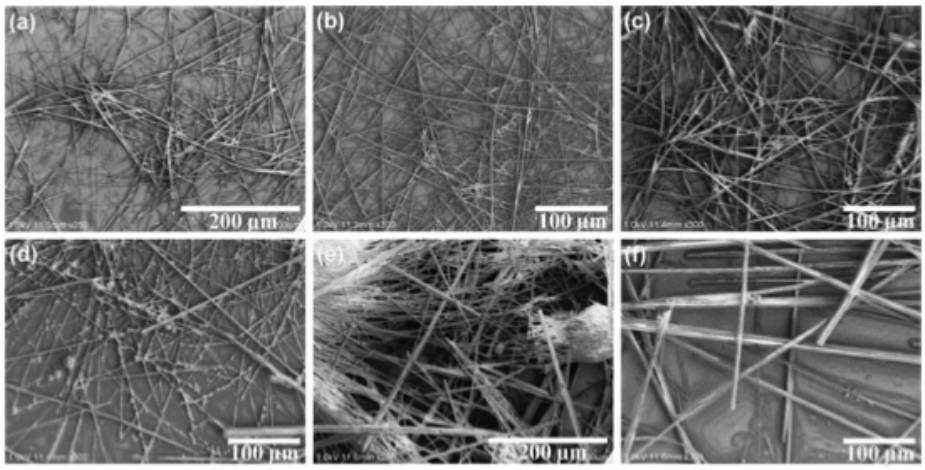

Figure 2.14. SEM images of microwires precipitated from *n*-hexane (1 mg mL^{-1}) solutions of **54** and **55** mixtures: (a) 1:1.5; (b) 1:2; (c) 1:4; (d) 1.5:1; (e) 2:1; (f) 4:1.

In the following example, the authors modified compound **3** at C5, C10 and C15 positions to get a small series of blue emitters with spiro-annulated structural features and a truxene core (Scheme 2.16).[9]

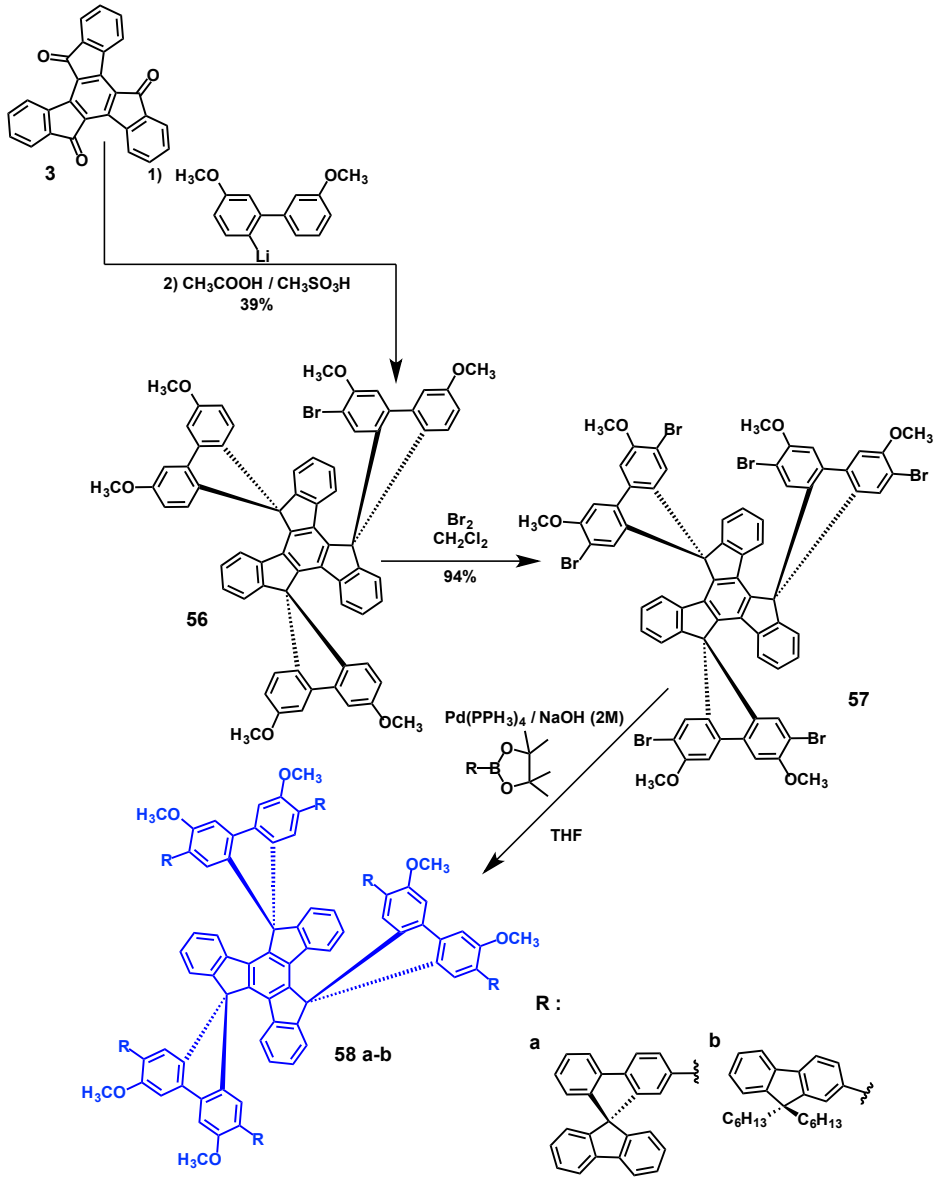

Scheme 2.16. Synthetic route to blue emitters **58**.

In the above paragraphs, we have seen the main covalent modifications carried out on the truxene core to form a wide variety of chemically modified alternatives. In the following, we will focus on one of the potential applications for these materials, namely truxene-based materials for solar cells.

2.2. TRUXENE DERIVATIVES FOR THIN FILM ORGANIC SOLAR CELLS

Thin film solar cell (TFSC) represent an alternative technology to the well-developed crystalline silicon solar cells. A TFSC is a solar cell made by one or more thin layers of a photovoltaic material on a substrate by diverse deposition methods on a wide variety of substrates. According to their composition, the main types of solar cells are classified as follows:

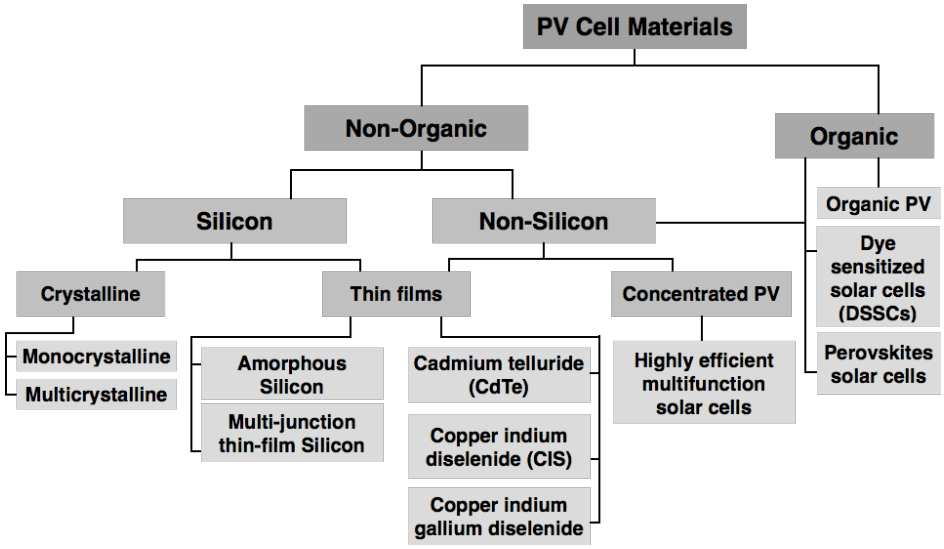

2.2.1. Characterization of solar cell devices

The characterization of a solar cell device comprises mainly the recording of the current-voltage (*J-V*) curves and the measurement of the spectral response, this is, the incident photon to current conversion efficiency (IPCE) for each wavelength, also called external quantum efficiency (EQE) (Figure 2.16).[28]

In order to reproducibly characterize and compare different photovoltaic devices, standardized procedures and conditions have been established. The standard conditions for the photovoltaic measurements are generally AM 1.5

[28](a) A. Mishra, M. K. R. Fischer, P. Bäulerle, *Angew. Chem. Int. Ed.* **2009**, *48*, 2472; (b) S. Zhang, X. Yang, Y. Numata, L. Han, *Energy Environ. Sci.* **2013**, *6*, 1443.

spectrum at an irradiance of 100 mWcm^{-2} and a temperature of 25°C. The air mass 1.5 (AM 1.5) spectrum simulates the terrestrial solar spectrum at the ground when the sun is at 48.2° zenith angle.

The essential parameters that determine the cell performance and that are used for comparing photovoltaic devices are the open-circuit voltage (V_{OC}), the short-circuit current density (J_{SC}), the fill factor (FF) and the external quantum efficiency (EQE).

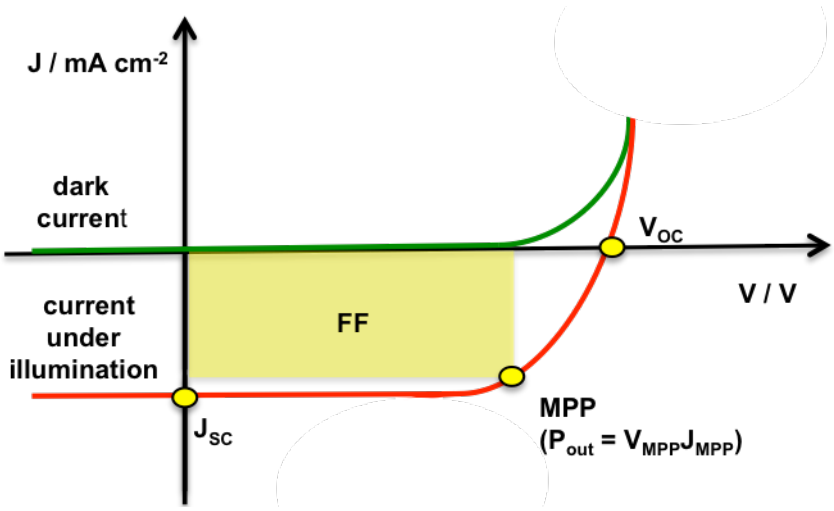

Figure 2.15. Current-voltage (*J-V*) curve characteristic of a typical solar cell device. Essential parameters are shown: V_{OC}, open-circuit voltage; J_{SC}, short-circuit current density; FF, fill factor; MPP, maximum power point, V_{MPP}, J_{MPP}.

The V_{OC} represents the maximum (photo)voltage measured in a solar cell. It is the voltage at the point of zero current flow. The J_{SC} is determined at the point of no counter voltage, it represents the maximum (photo)current that could be obtained in a solar cell. J_{SC} depends on the number of photons absorbed susceptible to be exploited by the device. It also depends on some morphologic characteristics of the device, such as surface area of the active layer and device thickness.

The photogenerated charge carriers and the fraction of them that reach the electrodes determine the fill factor (FF). This FF describes the quality of the device and it is defined as the maximum area within the *J-V* curve (Figure 2.15).

$$FF = \frac{J_{MPP}\, V_{MPP}}{J_{SC}\, V_{OC}}$$

FF is described as the ratio of the output at the maximum power point (MPP) to the ideal power output ($J_{SC}\, V_{OC}$).

The efficiency of a solar cell η, is determined as the ratio of the maximum power produced by the device (P_{out}) to the power of the incident light (P_{in}).

$$\eta = \frac{J_{MPP} V_{MPP}}{P_{in}} = \frac{FF\, J_{SC}\, V_{OC}}{P_{in}}$$

The number of photogenerated charge carriers over the number of incident monochromatic photons defines the external quantum efficiency (EQE). The plot of EQE *vs*. wavelength gives the photovoltaic response of the device. This plot ideally matches with the absorption spectrum of the device.

The efficiencies reached so far by different technologies are depicted in Figure 2.16.

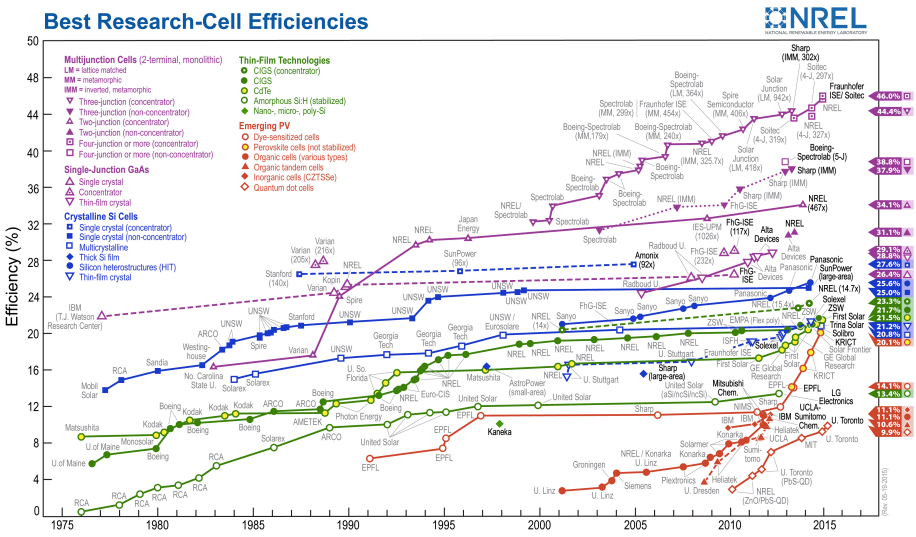

Figure 2.16. Solar cell efficiencies reached so far by different technologies.[29]

[29] http://www.nrel.gov

2.2.2. Organic dyes for metal free dye sensitized solar cells

Standard DSSCs involve a transparent conducting oxide (TCO) electrode, a sensitizer, so called dye, anchored to a mesoporous semiconductor metal oxide (TiO_2 nanocrystals), an electrolyte/hole-transporter material (usually I^-/I_3^- redox couple) and a counter electrode.[28]

The working mode of a DSSCs follows three main steps: (1) the anchored sensitizer molecules absorb incidental light, (2) then charge separation occurs at the interface dye-TiO_2 through photoinduced electron injection from the excited dye to the conduction band of the TiO_2, creating holes in the ground state of the dye, (3) the electrons reach the TCO electrode and the hole-transporter material regenerates the ground state of the dye (Figure 2.17).[28]

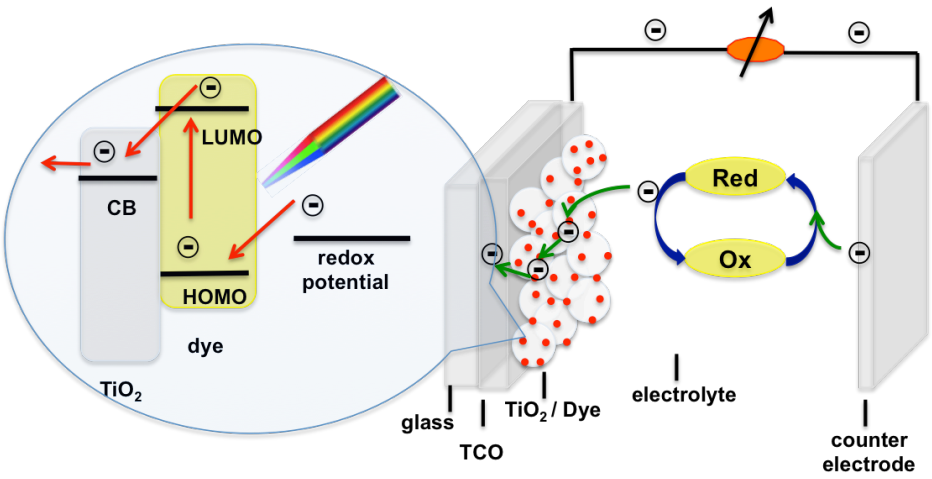

Figure 2.17. Schematic DSSC device.

Regarding the dye, many types of compounds have been synthesized like metal-organic complexes, metal-free organic compounds, Zn-porphyrins and Zn-phthalocyanines. The most successful DSSC made so far featured Ru(II)-polypyridyl complexes dyes as sensitizers.[28] These dyes show broad light absorption ability up to the near infrared region. For example, the so-called

black dye[30a] reported by Grätzel and co-workers reported an efficiency of 11.1% under standard illumination (AM 1.5 G, 1000 W m^{-2}). Recently, the same group has also reported a panchromatic porphyrin sensitizer, **SM315**, that achieved a record 13% PCE under AM 1.5 G illumination (1000 W m^{-2}) (Figure 2.18).[30b]

Metal-free organic dyes are rare metal free, tunable at will, low cost materials, which also present high molecular extinction coefficients. In summary, they are good candidates for DSSCs devices.[28a]

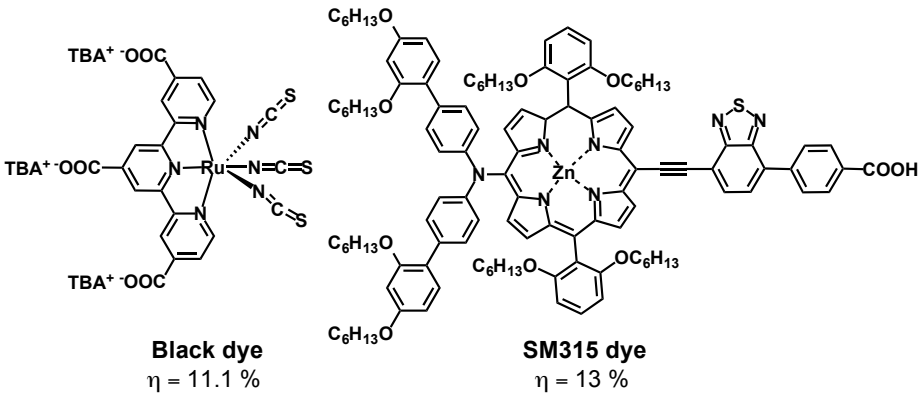

Figure 2.18. Most successful dyes for DSSCs reported by Gräetzel and co-workers.

The schematic structure of a dye for DSSCs is depicted in Figure 2.19. The usual components of a dye are a donor group, a π–bridge and an acceptor group, which usually acts as the anchoring group towards the TiO_2.[28a]

[30] (a) M. K. Nazeeruddin, P. Péchy, T. Renouard, S. M. Zakeeruddin, R. Humphry-Baker, P. Compte, P. Liska, L. Cevey, E. Costa, V. Shklover, L. Spiccia, G. B. Deacon, C. A, Bignozzi, M. Grätzel, *J. Am. Chem. Soc.* **2011**, *123*, 1613; (b) S. Mathew, A. Yella, R. Humphry-Baker, B. Curchod, N. Ashari-Astani, I. Tavernelli, U. Rothlisberger, M. K. Nazeeruddin, M. Grätzel, *Nature Chem.* **2014**, *6*, 262.

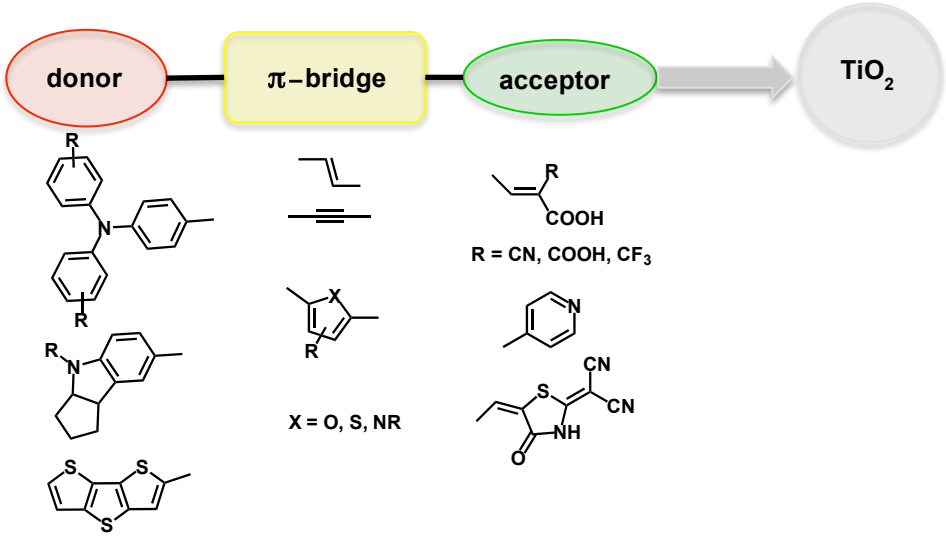

Figure 2.19. Schematic design for a variety of metal-free organic dyes.

There are some examples in the literature in which a truxene core has been used in the design of dyes for DSSCs.[31-32] Recently, a truxene derivative has been synthesized as a donor-π-2acceptor dye for its application in DSSCs (Figure 2.20). A hexahexyltruxene unit acts as the π-bridge, giving an overall power conversion efficiency of 3.62% under simulated solar light (AM 1.5G, 100mW cm^{-2}) irradiation.[31]

[31] L. Yu, J. Xi, H. T. Chan, T. Su, L. J. Antrobus, B. Tong, Y. Dong, W. K. Chan, D. L. Philips, *J. Phys. Chem. C,* **2013**, *177*, 2041.

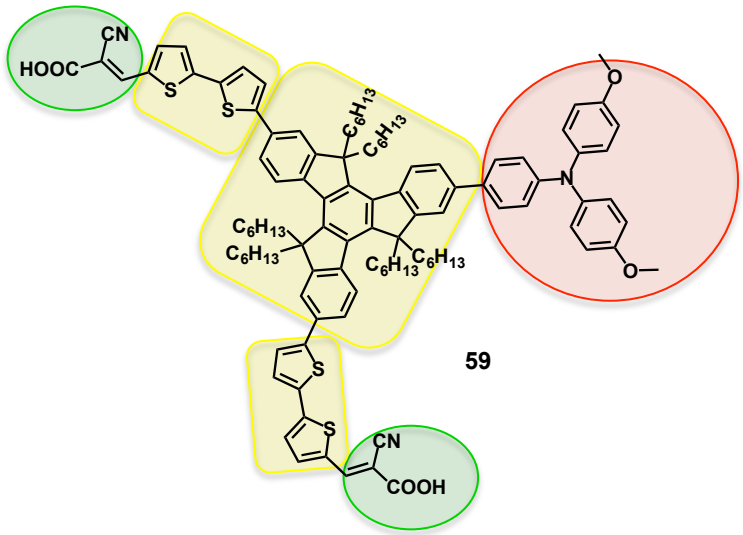

59

Figure 2.20. Chemical structure of truxene-containing dye **59**.

Recently, two push-pull dyes **60** and **61** as photosensitizers for iodine-free DSSCs (Figure 2.21) have also been reported.[32] These dyes feature a hexahexyltruxene unit (HT) substituted at C2 with a 4-(hexyloxy)-*N*-phenylaniline (HPA). This HT-HAP moiety is employed as the donor part in the designed dyes. 4-Hexyl-4H-dithieno[3,2-b:2´,3´-d]pyrrole (H-DTP) and 4-(4-(hexyloxy)phenyl)-4H-dithieno[3,2-b:2´,3´-d]pyrrole (HOP-DTP) are the π-conjugated bridge used by **60** and **61,** respectively. These dyes were compared with the reference DHO-TPA **62** dye that does not have a truxene core in the chemical structure.

The conjugated truxene core of the HT-DTP induces a red-shifted absorption as well as it improves the maximum molar absorption coefficient. The HT-DTP avoids the dye aggregation on the TiO_2 surface and it also inhibits the charge recombination at the interface between the redox shuttle and the titania. Under AM1.5 full conditions **61** achieves a solar to electricity conversion of 8.5% yield (Figure 2.21).[31]

[32] Z. Wanng. M. Liang, H. Wang, P. Wang, F. Cheng, Z. Sun, X. Song, *ChemSusChem* **2014**, *7*, 795.

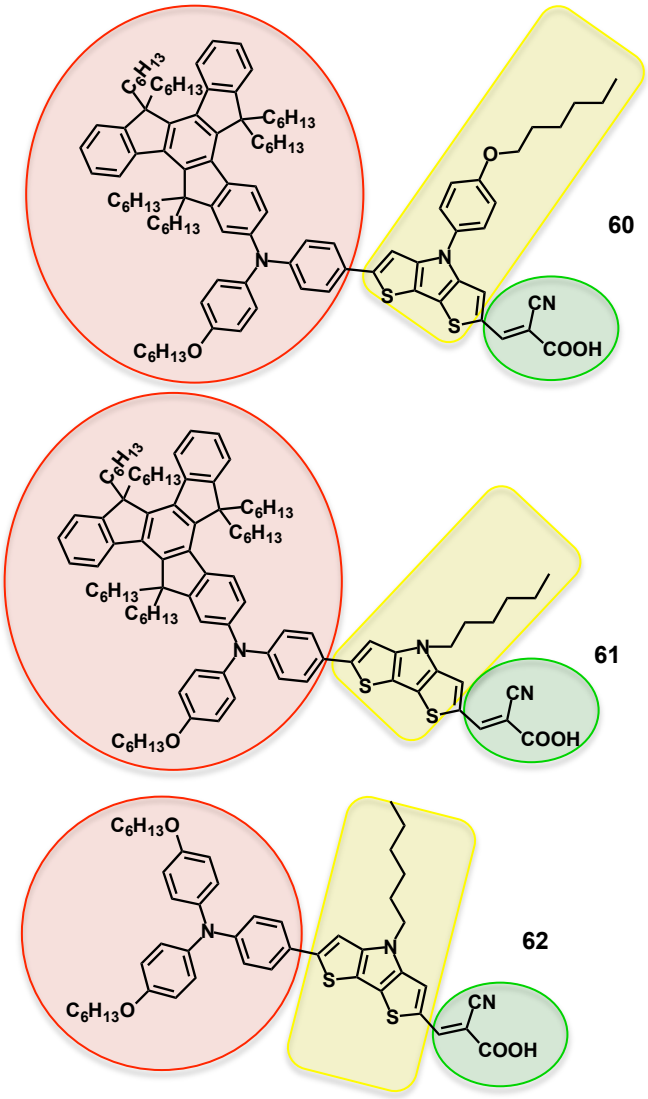

Figure 2.21. Chemical structure of truxene derivatives **60** and **61**. Highlighted in red the donor fragment, in yellow the π-conjugated bridge and in green the acceptor fragment. The PCE obtained by Song and co-workers at the simulated AM1.5 conditions reported in the article for these dyes was 7.9 % and 8.5 % for **60** and **61**, respectively. These values are higher than the value of 7.3% obtained for the reference dye **62**.[32]

2.2.3. Organic semiconductor materials for organic solar cells

Typical organic solar cells (OSCs) are based on a donor (p-type semiconductor) and an acceptor (n-type semiconductor) as active layers, forming donor-acceptor (D-A) heterojunction architectures.

When the donor component is photoexcited, an exciton is created. An exciton is basically an electron-hole pair bound by electrostatic forces. The exciton created in the donor material has to diffuse to the donor-acceptor interface. The excitons that do not manage to reach the interface recombine and, thus, do not contribute to the photocurrent. In contrast, when an exciton reaches the D-A interface it is broken up into free electron-hole pairs. This charge separation requires an optimal energy offset between the LUMO of the donor and the LUMO of the acceptor materials (approximately a 0.3-0.4 eV gap between them). Finally, the last step is the free charge carrier transport and collection at the electrodes. The whole photoinduced process needs high charge-carrier mobility.[33]

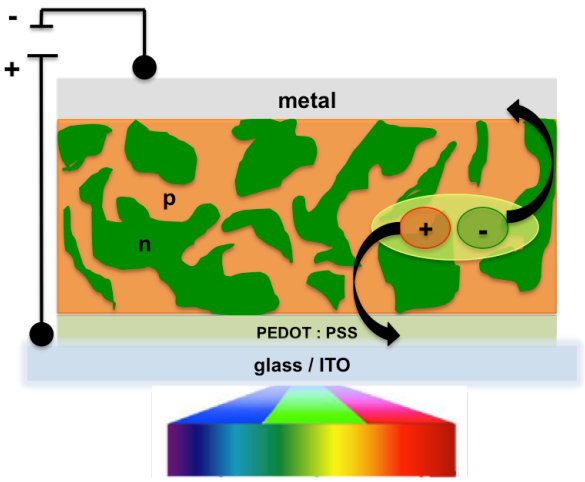

Figure 2.22. Schematic BHJ OSC device and representation of the fundamental photoinduced process.

The D-A heterojunction architectures can have a planar or a bulk configuration. The bulk-heterojunction (BHJ) solar cells (Figure 2.22) overcome the main drawback of the planar-heterojunction (PHJ) solar cells,

[33](a) A. Mishra, P. Bäuerle, *Angew. Chem. Int. Ed.* **2012**, *51*, 2020; (b) J. L. Delgado, P.A. Bouit, S. Filippone, M. A. Herranz, N. Martín, *Chem. Commun.* **2010**, *46*, 4853.

the restricted interfacial area between the donor and acceptor components. Note that only the excitons that reach the interfaces can be efficiently separated into free charge carriers.[33]

The elements that usually form a BHJ solar cell are a mixed film of a conjugated polymer or a small molecule as donor and an acceptor material, usually a fullerene derivative. This film is sandwiched in between an ITO (indium tin oxide) anode and a low work function metal cathode.[33]

Interestingly, very recently McCulloch and co-workers proposed some electron-deficient truxenone derivatives as a non-fullerene type of acceptors or n-type semiconductors for organic solar cells. [13,34]

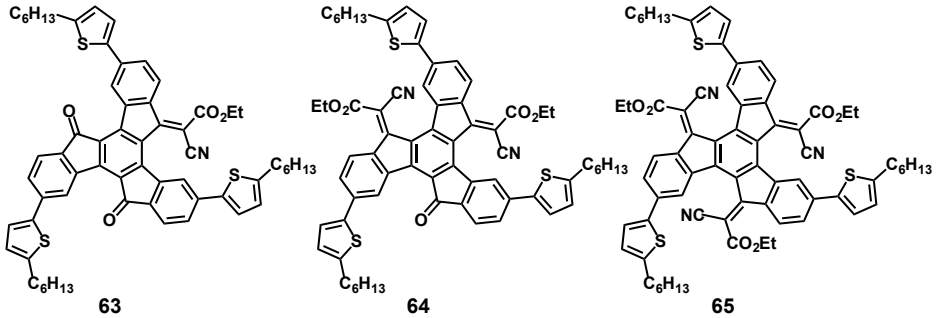

Figure 2.23. Chemical structures of dyes **63**, **64** and **65**.[34]

The potential ability of these new materials to behave as electron acceptors in organic photovoltaic devices was tested towards zinc-phthalocyanine (ZnPc) and subphthalocyanine (SubPc) based materials as electron donor components, respectively, in bilayer devices configuration. The best result was found for the SubPc / **65** device with a poor efficiency of 0.28%.[34]

More remarkably is the example by Ziessel and co-workers; they reported a triazatruxene-diketopyrrolopyrrole dumbel-shaped molecule (**66**) as a photoactive electron donor for OSCs.[35]

Interestingly, triad D-A-D (**66**) blended with $PC_{71}BM$ reached a moderate value, 5.3% of efficiency.[35]

[34] C. B. Nielsen, E. Voroshazi, S. Holliday, K. Cnops, D. Chenys, I. McCulloch, *J. Mater. Chem. A* **2014**, *2*, 12348.

[35] T. Bura, N. Leclerc, R. Bechara, P. Lévêque, T. Heiser and R. Ziessel. *Adv. Energy Mater.* **2013**, *3*, 1118.

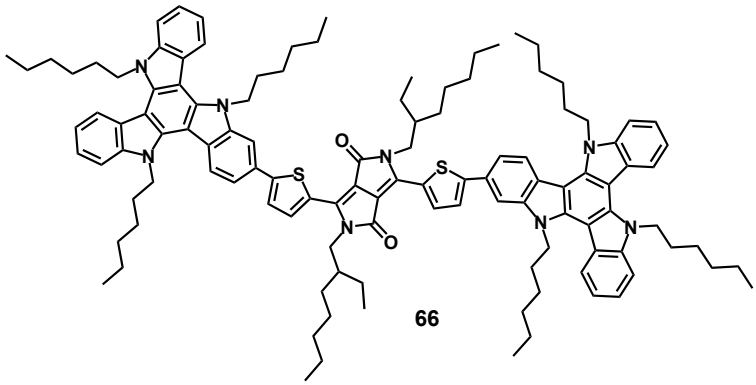

Figure 2.24. Chemical structure of the triazatruxene-diketopyrrolopyrrole dye.[35]

In order to get a better understanding of the progress of this field, in Figure 2.25 it is shown the development of the OPV efficiencies in the last thirty years.[36] Although in general there is a progress in the different types of cells, OPV and, particularly, perovskites are undergoing a significant progress in the recent years, reaching values, which approach to commercial silicon cells.

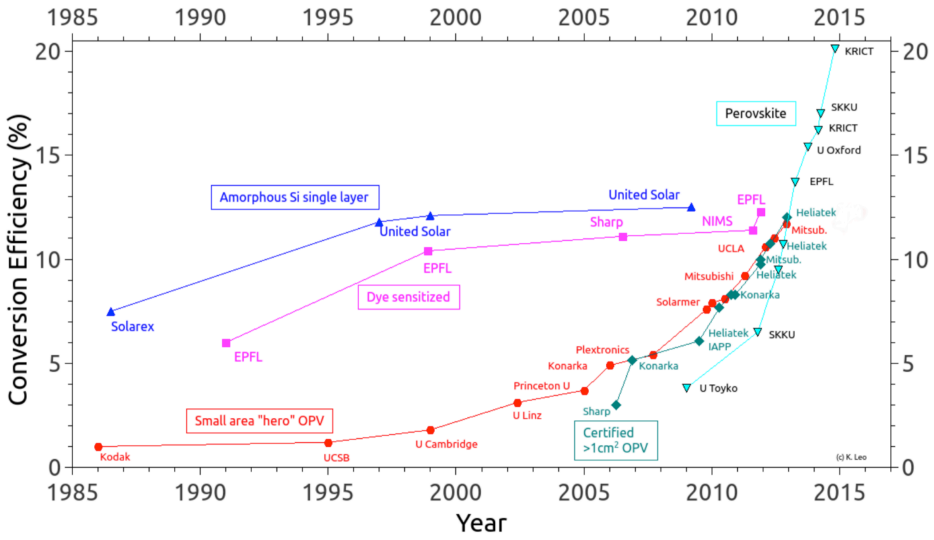

Figure 2.25. Development of the OPV efficiencies in the last 30 years.

A key factor affecting the efficiency of such devices is their morphology. In our research group with the aim of constructing nanostructured optoelectronic

[36] http://www.orgworld.de/

devices, we look for suitable electron-donor partners for fullerenes in order to form supramolecular donor-acceptor pairs. A suitable electron donor partner for fullerenes must show three main features, (i) to have a good electron-donor character, (ii) to present efficient light absorption, preferably in the visible region and, (iii) to have the ability to self-assemble with fullerenes.

The π–extended TTF, exTTF (**67**), a derivate molecule of the well-known donor tetrathiafulvalene, TTF (**68**), in which the dithiole units are connected through a π–conjugated core of anthracene forcing the latter to adopt a butterfly shape, seemed to have those prior requirements (Figure 2.26).[37a-b]

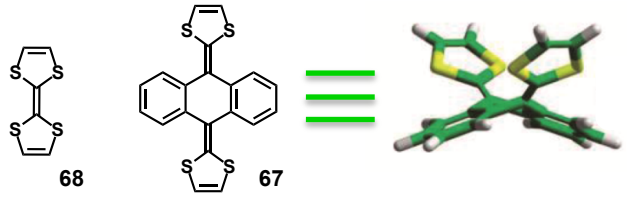

Figure 2.26. TTF (**68**) and exTTF (**67**) structures.

Although the exTTF unit gathers the two first requirements to form a donor-acceptor pair with C_{60}, a single unit of exTTF is not able to bind fullerenes in solution. However, this drawback can be easily solved joining two units of exTTF through an aromatic spacer. In this way, we can construct a simple tweezers-like receptor for fullerenes that comprises two units of exTTF (**69**). Despite the lack of preorganization of **69**, this receptor is able to bind C_{60} in solution in an effective manner. [37d]

The complexation between this receptor **69** and C_{60} was studied in solution by UV/vis titrations revealing a log K_a=3.5 in chlorobenzene at room temperature (Figure 2.27).

[37] (a) F. G. Brunetti, J. L. López, C. Atienza, N. Martín, *J. Mater. Chem.* **2012**, *22*, 4188. (b) N. Martín, L. Sánchez, M. A. Herranz, B. Illescas, D. M. Guldi, *Acc. Chem. Res.* **2007**, *40*(*10)*, 1015; (c) Y. Yamashita, Y. Kobayashi, T. Miyasi, *Angew. Chem. Int. Ed.* **1989**, *28*, 1052; (d) E. M. Pérez, L.Sánchez, G. Fernández, N. Martín, *J. Am. Chem. Soc.* **2006**, *128*, 7172.

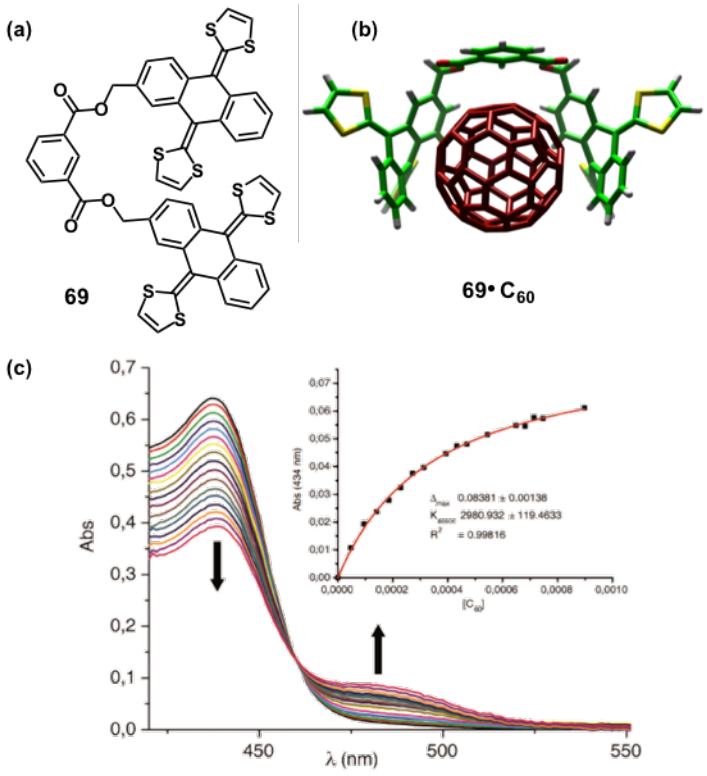

Figure 2.27. (a) Structure of tweezers-like receptor. (b) Complex´s model upon addition of C_{60} to a solution of **69**. (c) Absorption spectral changes of the receptor **69** (chlorobenzene, 298 K, 2.31 x 10^{-5} M) upon addition of the guest, (C_{60} in chlorobenzene, 298 K, 4.05 x 10^{-3} M). Inset shows the fit of ΔAbs to a 1:1 binding isotherm.

To avoid having to connect two units of the π-extended TTF derivative, we searched for an alternative unitary recognition motif for fullerenes. We wanted this new receptor to satisfy: (1) having a larger conjugated surface and (2) being able to host more than two dithiole units, thus increasing its ability to establish dispersion and charge-transfer interactions with fullerenes. The truxenone core seemed to accomplish the expectative as feasible scaffold to build a new receptor for fullerenes; its extended π–delocalized core provides a large aromatic surface suitable for establishing non-covalent interactions towards fullerenes.

A family of truxene-TTFs **70** was thus synthesized by performing a triple Wittig-Horner olefination reaction on truxenone **3** (Scheme 2.17).[38]

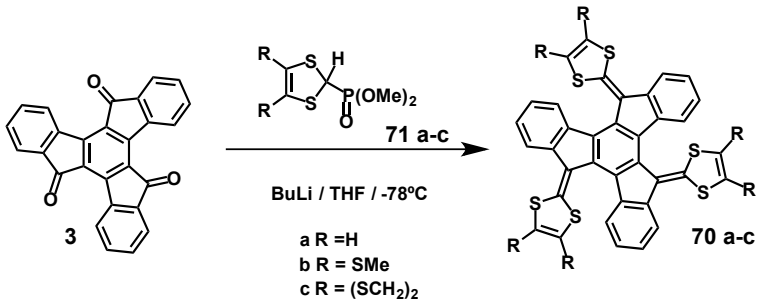

Scheme 2.17. Synthesis of the truxene-TTF derivatives **70 a-c**.

In order to accommodate the three dithiole rings, the planar geometry of the original truxenone is bended adopting an all-*cis* sphere-like geometry (Figure 2.28). This bowl shape adopted by the truxene core is complementary in shape and size with the fullerenes, which should maximize the van der Waals and $\pi-\pi$ interactions between the receptor and C_{60}.

Despite the loss of planarity of the truxene core in truxTTF molecule, the absorption spectra of **70a** shows a bathochromic shifting regarding its reference compounds (Figure 2.29), suggesting a higher degree of conjugation. Theoretical studies assign the band centered around 430 nm to a intramolecular charge transfer process from the dithiole donor units to the truxene core that acts as an acceptor fragment.[38]

[38] E.M. Pérez, M. Sierra, L. Sánchez, M. R. Torres, R. Viruela, P. M. Viruela, E. Ortí, N. Martín, *Angew. Chem. Int. Ed.* **2007**, *46*, 1847.

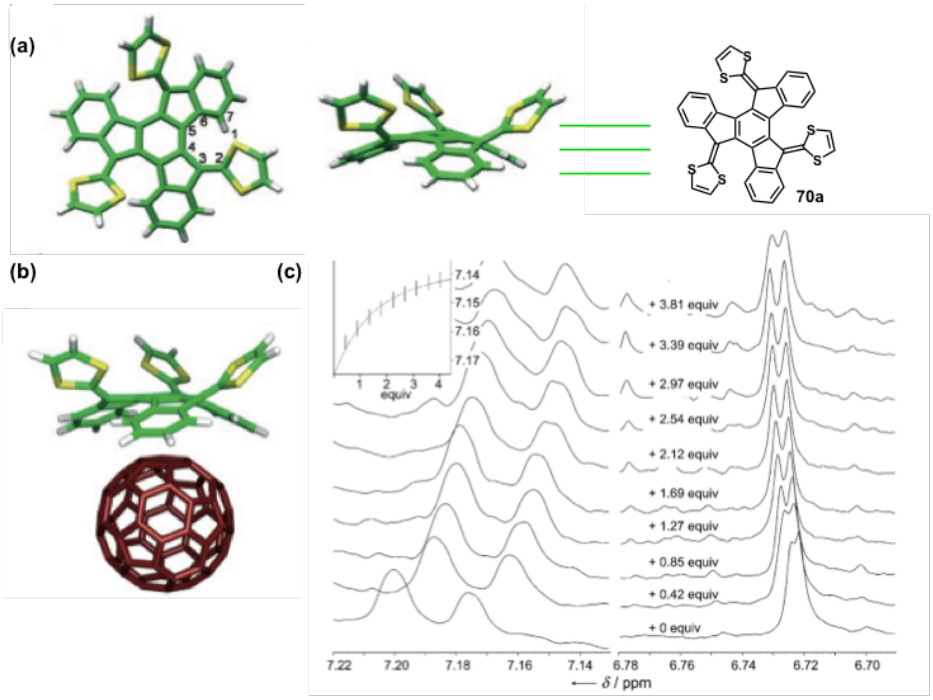

Figure 2.28. (a) X-Ray structure of truxTTF, **70a**, (*P,P,P)* isomer. (b) Structure of the preferred configuration of the trux•TTFC_{60} complex calculated at the MPWB1K/6-31G** level, (c) Partial NMR spectra (300 MHz, 298 K, $CDCl_3/CS_2$) showing the shift suffered by the aromatic protons of the truxTTF upon adition of C_{60}. Inset, fitting of the chemical shifts to a 1:1 binding isotherm giving a $K_a = (1.2 \pm 0.3) \times 10^3\ M^{-1}$.

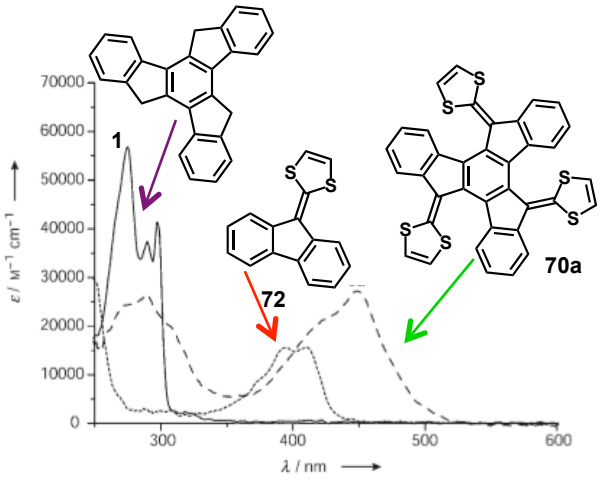

Figure 2.29. UV/vis absorption spectra of truxene, **1**, 9-(1,3-dithiol-2-ylidene)fluorene, **72**, as control molecules and truxTTF (**70a**).

The donor capacity of the truxTTF molecule was evaluated by cyclic voltammetry. Interestingly, the voltammograms showed up to five oxidation waves in solution. The truxTTF molecule is able to give up to five electrons; the three first ones are extracted from the dithiole units, while the truxene core donates the last two. Transient absorption measurements revealed that the fully charge-separated state **70a**$^{\bullet+}$•$C_{60}^{\bullet-}$ is generated with lifetimes of hundreds of picoseconds.[38]

The truxTTF core has recently been used to construct liquid crystals with electro-active properties.[39]

With the aim of improving the light absorption ability of **70a** that absorbs in the visible region range of 350-520 nm, we also synthesized two new truxene-TTF derivatives,[40] **73** and **74** in which one of the three dithiole rings present in truxTTF, is replaced by an electron withdrawing group, a carbonyl or a dicyanomethylene group, respectively (Scheme 2.18). With this chemical modification in the structure we create a push–pull intramolecular effect that turns into a significant bathochromic shift of the electronic spectra of the new derivatives **73** (absorbs all the way to 695 nm) and **74** (reaches 800 nm). The presence of two dithiole rings in the structure assures the bowl-shape fashion of the molecules geometry as well as the ability of these two new compounds to bind C_{60}. The complexation studies of the truxene derivatives and C_{60} were carried out by UV/vis and fluorescence titrations. The molecular structure and electronic properties of **73** and **74** were theoretically studied.

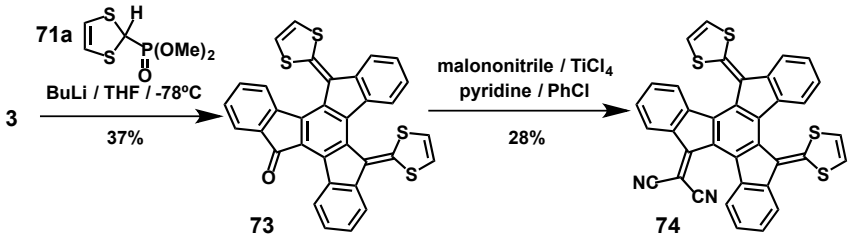

Scheme 2.18. Syntheses of the truxene-TTF derivatives **73** and **74** from truxenone.[40]

[39] K. Isoda, T. Yasuda, T. Kato, *Chem. Asian. J.* **2009**, *4*, 1619.

[40] H. Isla, B. Grimm, E. M. Pérez, M. R. Torres, M. A. Herranz, R. Viruela, J. Aragó, E. Ortí, D. M. Guldi, N. Martín, *Chem. Sci.* **2012**, *3*, 498.

Molecular and supramolecular properties of **70a**, **73** and **74** make these truxene-TTF derivatives a valuable option to test as complementary partners for the C_{60} in organic photovoltaic devices.[40]

3. Objectives

3. OBJECTIVES

Through the aforementioned background of this chapter, we have seen that truxene-based molecules are potential materials for diverse and promising technological applications. Furthermore, molecular and supramolecular properties of truxTTF and other truxene-TTF derivatives make them a valuable option to test as partners for the C_{60} in, for instance, organic photovoltaic devices. Therefore, our aim in this study is to exploit the potential applicability of the truxene-TTF derivatives already reported in our group, as well as constructing new truxene-TTF based molecules that could have potential applications in organic electronics.

We will divide the *Results and Discussion* section of this Chapter I named "Covalent modifications on truxTTF core", according to the following objectives:

- **Synthesis of building blocks**

We will present the synthesis of two suitable functionalized building blocks that will give access to more sophisticated chemical structures of interest for further objectives.

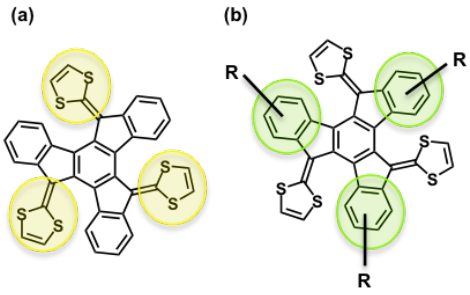

Figure 3.1. Proposed building blocks.

- **Covalent linkage of three fullerenes to a truxTTF core**

The aim is to cover the synthesis and characterization of unprecedented truxTTF-fullerene molecular tetrads, where the central truxene core is connected to three C_{60} units forming DA_3 photo and electroactive systems.

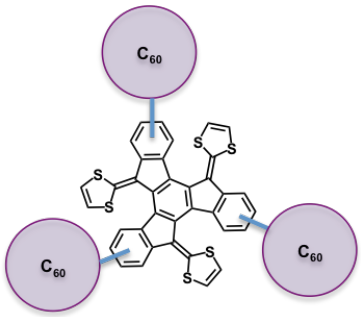

Figure 3.1. tetrad truxTTF-C_{60}

• TruxTTF derivatives for DSSCs

We will report on the synthesis of five truxTTF-based dyes that, according to their chemical structure, could have potential applications as sensitizers in Dye Sensitized Solar Cells devices.

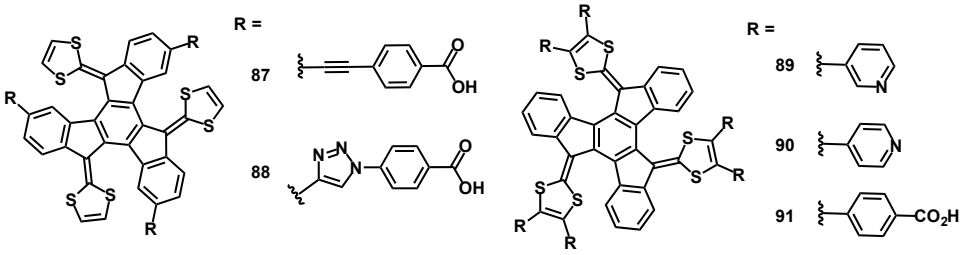

Figure 3.3. truxTTF-based dyes for DSSCs.

• TruxTTF derivatives for BHSCs

The aforementioned interest of the truxene core for DSSCs can be extended to the use of suitably functionalized truxene derivatives, namely truxTTF (**70a**) and truxTTF-CO (**73**) molecules in Bulk Heterojunction Solar Cells devices. Remarkably, to the best of our knowledge, the use of curved molecules for photovoltaic (PV) applications has not been properly addressed in the literature. Therefore, this study could give a valuable hint on the interest of these molecules for PV purposes.

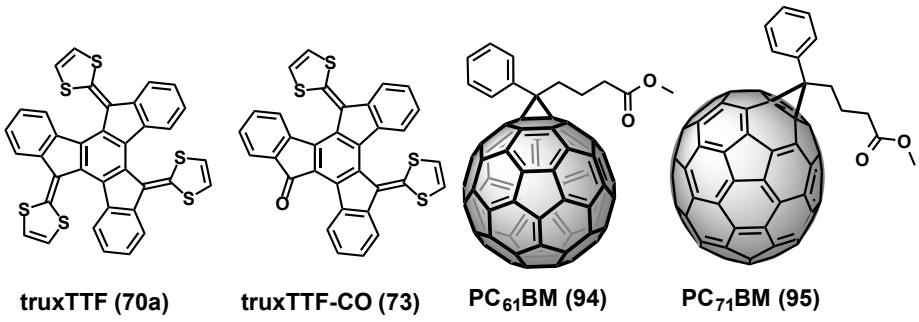

Figure 3.4. Chemical structures of bowl-shape electron-donors truxTTF and truxTTF-CO and electron acceptors phenyl-C_{60}-butyric acid methyl ester ($PC_{61}BM$) and phenyl-C_{70}-butyric acid methyl ester ($PC_{71}BM$).

4. Results and Discussion

4. RESULTS AND DISCUSSION

4.1. SYNTHESIS OF BUILDING BLOCKS

As mentioned in the backgrounds for the truxene molecule, a wide variety of chemical modifications have been carried out on pristine truxene or its precursors, thus affording a great number of derivatives.

In this section we present the synthesis of two building blocks that will give access to the aforementioned proposed objectives.

The truxTTF molecule,[38] offers the possibility of modifying its structure in a covalent manner, either at its 1,3-dithiole rings (highlighted in yellow in Figure 4.1) or at its aromatic core (highlighted in green in Figure 4.1).
If we choose to modify the truxTTF core at the 1,3-dithiole rings, the truxTTF molecule itself will be a suitable building block for this purpose, as the 1,3-dithiole rings of the truxTTF can be easily modified by direct C-H arylation.

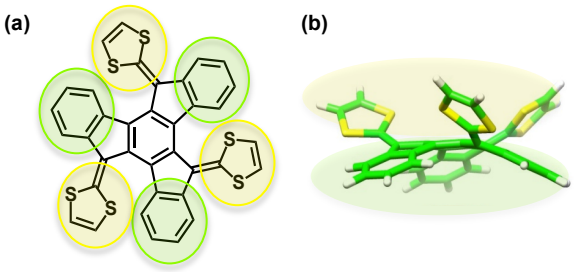

Figure 4.1. (a) Chemical structure of truxTTF (**70a**). Susceptible regions for covalent modification are highlighted in yellow and green. (b) View of the biconcave disposition adopted by the truxene core and the 1,3-dithiole rings in **70a**.

On the other hand, if we want to gain access to the aromatic periphery of the truxene core of the truxTTF, we should design a building block with a suitable functionalization that will allow further and diverse chemical modifications.

4.1.1. *Synthesis of truxTTF: a new building block for modifications at the 1,3-dithiole rings*

Our group firstly reported the truxTTF molecule in 2007.[38] It is synthesized by attaching three 1,3-dithiole rings by a three-fold Horner-Wadsworth-Emmons olefination reaction on truxenone (**3**) (Scheme 4.1).

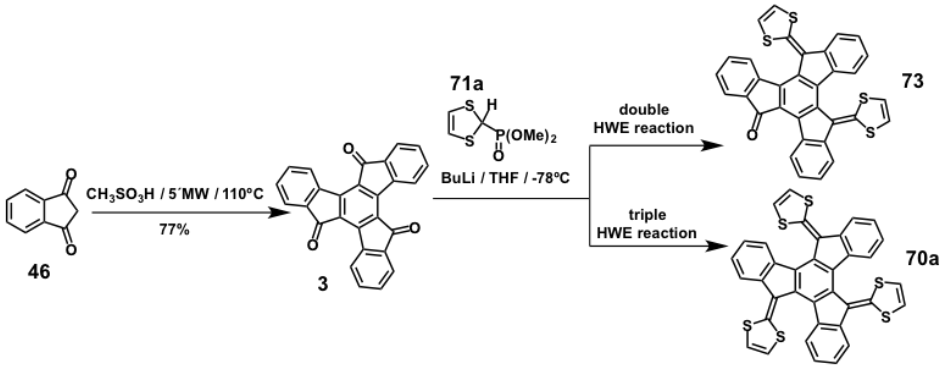

Scheme 4.1. Synthesis of **73** and truxTTF (**70a**).

It is also possible to perform a two-fold Horner-Wadsworth-Emmons olefination reaction on truxenone (**3**), to get a truxTTF derivative, the truxTTF-CO (**73**).[40] This compound, as well as truxTTF, has been tested for BHSC (see last issue of this chapter).

In just one step from truxenone (**3**) we have a useful building block that allows further covalent modifications at the 1,3-dithiole rings of the truxTTF.

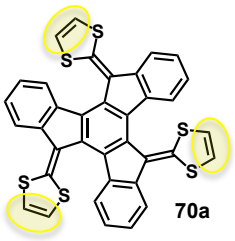

Figure 4.2. Chemical structure of the building block for modifications at the 1,3-dithiole rings of the truxTTF.

4.1.2. *Synthesis of trialkynyl-truxTTF (81): Chemical modifications at the aromatic rings in truxTTF*

In order to design a useful and versatile building block that will provide truxTTF derivatives decorated on its aromatic periphery; we have to resort to the synthesis of a suitably functionalized truxenone and, therefore, to choose a

suitable indanone. In this way, we can construct our building block of choice for further chemical modifications. This strategy is depicted in Figure 4.3.

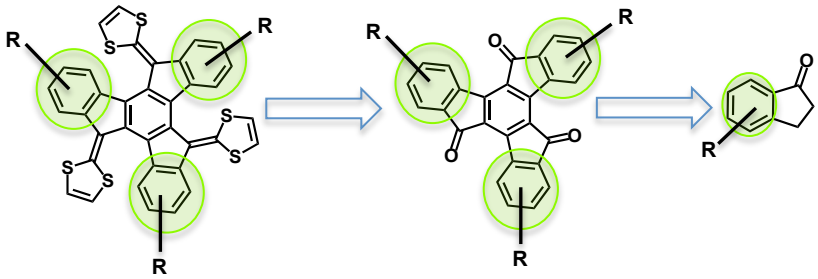

Figure 4.3. Schematic representation of the retrosynthetic strategy followed to build a suitable building block that allows the functionalization at the aromatic core of the truxTTF.

Our truxenone of choice is the tribromotruxenone **75**. Molecule **75** provides the suitable truxene core functionalized with three carbonyl groups and three bromine atoms at its periphery.

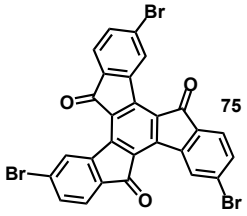

Figure 4.4. Chemical structure of **75**.

The carbonyl groups allow their substitution with 1,3-dithiole rings, as done before with the truxenone molecule and with other related structures. The bromine atoms provide an easy way to functionalize the molecule at its aromatic periphery by cross-coupling reactions.

The synthetic route towards **75** (Scheme 4.2) starts with a double bromination of the 5-bromoindan-1-one (**76**) followed by the condensation of the product, the 2,2,5-tribromoindan-1-one (**77**) at 220 °C to yield compound **75** (7%).[26]

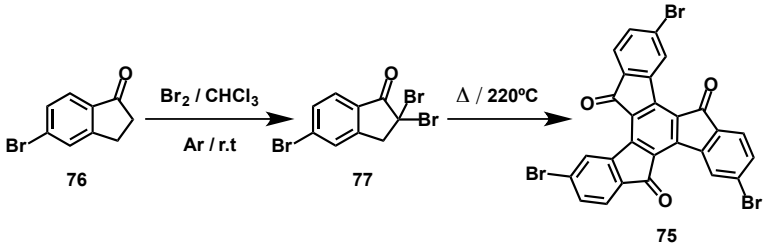

Scheme 4.2. Synthesis of 4,9,14-tribromotruxenone, **75**.

Molecule **75** is conjugated and planar. These characteristics confer the

molecule an extreme insolubility. Any modification done to this structure that disturbs its planarity avoiding its self-aggregation would contribute to the improvement of its solubility.

With **75** in our hands there were two possibilities: (A) to proceed with the functionalization of the carbonyl groups by a three fold Horner-Wadsworth-Emmons reaction to obtain a truxTTF derivative suitably functionalized with three bromine atoms (**78**) or (B) to carry out the functionalization at the aromatic rings (**79**) (Figure 4.5).

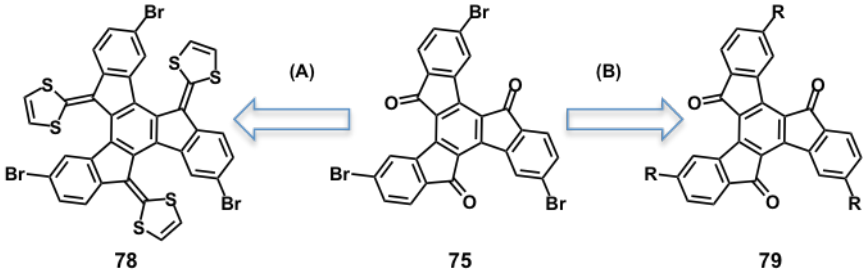

Figure 4.5. Possible paths (A) and (B) to functionalize **75**.

We firstly followed path (A). However, the reaction of **75** with the ylide of the 1,3-dithiol-2-ylphosphonate (**71a**), under similar triple Horner-Wadsworth-Emmons reaction conditions used before in truxenone systems,[38,40] did not work for this substrate. After some attempts we decided to follow path (B).

When following path (B), we decided to include protected alkyne functionalization at the truxenone periphery, because this is a versatile functionality once it is cleavage, and also maintains and extends the conjugation of the molecule.

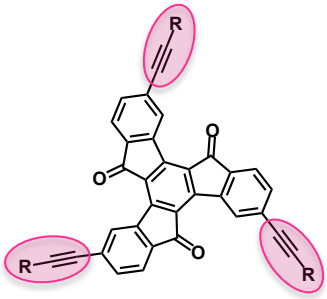

Figure 4.6. Truxenone with general alkyne functionality.

In Scheme 4.3, we show the optimized one-step synthesis from 4,9,14-tribromotruxenone (**75**) to get **80**, a truxenone derivative with alkynes at its aromatic periphery. A three-fold Sonogashira coupling reaction of **75**, with (triisopropylsilyl)acetylene in refluxing THF gives the truxenone derivative **80** (40%).

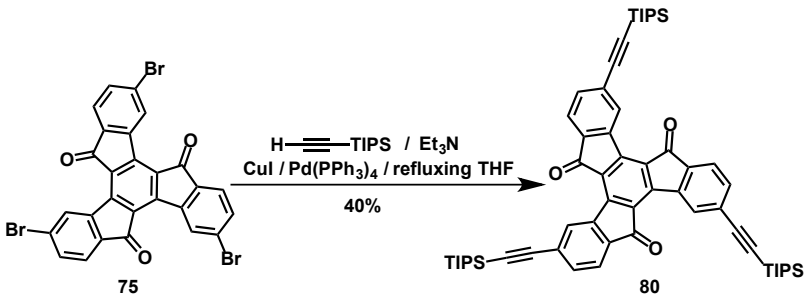

Scheme 4.3. Synthesis of alkynyl-containing truxenone (**80**).

In Table 4.1 some of the experimental conditions tested for this functionalization reaction are shown. The choice of the protecting groups TIPS is not trivial. **75** as well as truxene, is extremely insoluble. Therefore, functional groups are needed in order to prevent the self-aggregation of the core. We were not able to isolate any product when using (trimethylsilyl)acetylene (TMS); however, we succeeded using (triisopropylsilyl)acetylene (TIPS).

Table 4.1. Optimized reaction conditions.

R	Equivalents	Catalyst	Solvent	Conditions	Yield
TMS	6	$PdCl_2(PPh_3)_2$ >30%mmol	DMF	80°C / 7h	-
TMS	6	$Pd(PPh_3)_4$ 20%mmol	THF	))) 15 min / r.t / 24h	-
TMS	12	$Pd(PPh_3)_4$ 20%mmol	THF	))) 15 min / r.t / 24h	-
TIPS	8	$Pd(PPh_3)_4$ 20%mmol	THF	refluxing /3h	40%

The isolated compound **80** is very soluble, unlike its precursor **75**. The trialkynyl-truxenone **80** was easily characterized by the usual spectroscopic techniques. Functionalization of truxenone **75** is rapidly evidenced by the appearance of a band in the IR at 2155 cm^{-1}, characteristic of the carbon-carbon triple bond stretch.

The aromatic ^1H NMR signals of **80** are shown in Figure 4.6. Due to the molecular symmetry, there are just three types of aromatic signals, corresponding to three types of truxene-core protons present in **80**. A typical feature in the ^1H NMR spectrum of this compound is the aromatic singlet signal at 9.07 ppm, a very downfield value for an aromatic ^1H signal (Figure 4.6).

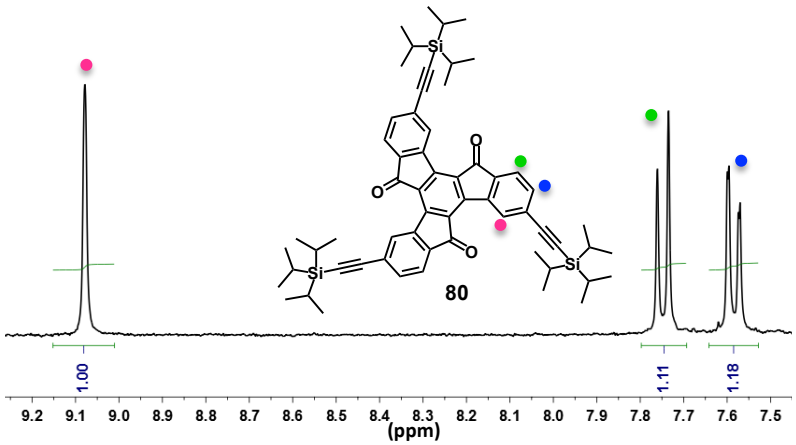

Figure 4.6. ^{1}H NMR (300 MHz, $CDCl_3$, 298 K) of molecule **80**. Aromatic signals are depicted by colored bullets.

Once we have the appropriate functionalization at the truxene core, the next step is the substitution of the carbonyl groups of **80** with 1,3-dithiole rings.

The reaction of **80** with the ylide of the 1,3-dithiol-2-ylphosphonate, **71a**, generated in situ with n-BuLi at -78 °C in THF, gives by a three-fold Horner-Wadsworth-Emmons reaction, product **81** (74%) (Scheme 4.4).

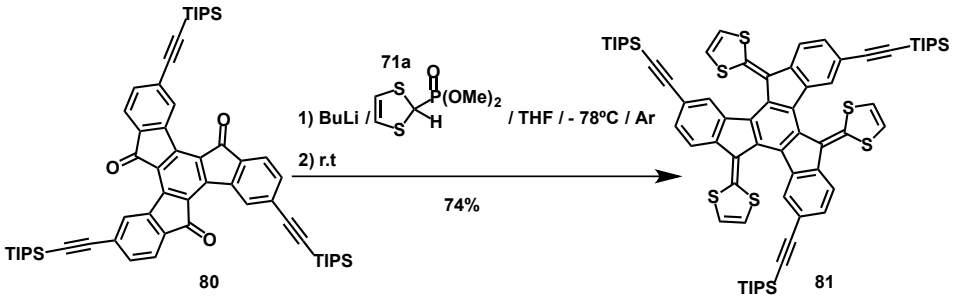

Scheme 4.4. Synthesis of truxTTF derivative **81**.

Besides the characterization in solution, we managed to characterize molecule **81** by solid-state techniques. By slow diffusion of methanol in a semi saturated solution of **81** in chloroform we got single crystals that could be characterized by X-Ray diffraction. As expected, **81** shows a biconcave morphology with triple helical chirality. Attachment of dithioles on either side of the prochiral truxenone produces a racemic mixture of *P,P,P/M,M,M* enantiomers for **81**. The numbering depicted in Figure 4.7 allows an easy visualization of the helices.

In Figure 4.7(a), the C1-C2-C3-C4-C5-C6-S7 series forms an *M*-helix (anticlockwise helix), while in Figure 4.7(b) the equivalent series gives rise to a *P*-helix (clockwise helix). As for truxTTF,[38] we just found the enantiomeric pair *P*,*P*,*P*/*M*,*M*,*M*.

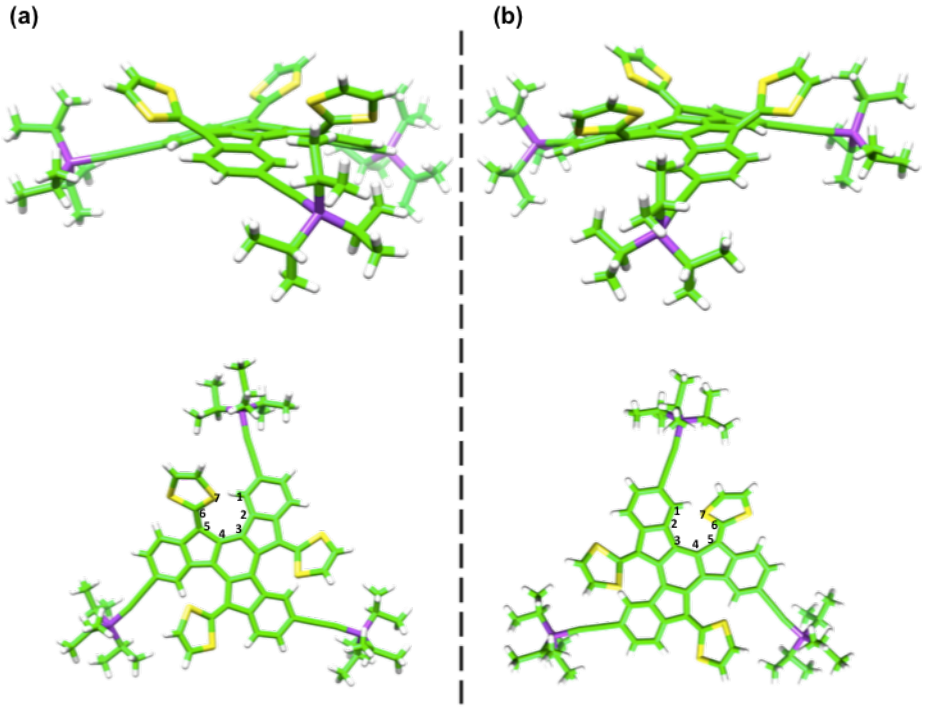

Figure 4.7. X-Ray crystal structure of **81**. (a) Isomer *M*,*M*,*M* left side and (b) isomer *P*,*P*,*P* at the right side of the figure. Carbon atoms are shown in green sulfur in yellow, hydrogens in white and silicon in purple.

Molecule **81** is less concave than the pristine truxTTF molecule. It is demonstrated by the angles defined by the plane of a periphery benzene ring and the plane of the central benzene ring of both molecules. For the truxTTF, this angle is 24.0°, while for the truxTTF derivative **81** this angle is 15.3°. This smaller concavity can be attributed to the increasing in the conjugation of the system in **81** with respect to truxTTF due to the presence of the peripheral alkynes, that should help to the partial recovery of the planarity of the truxene skeleton, achieving a compromise between the steric and conjugative effects.

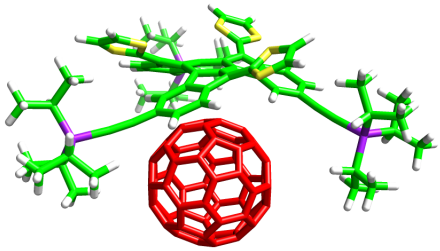

Figure 4.8. Energy minimized Amber force field, simulated complex **81**•C_{60}.

Molecule **81** has a slightly larger aromatic surface than truxTTF. Therefore, **81** results an interesting potential candidate to complex with fullerenes. Thus, we investigated its behavior as molecular receptor for the [60]fullerene.

In Figure 4.9 we can observe the changes in the UV/vis spectra of **81** upon addition of aliquots of C_{60} at room temperature in chlorobenzene. There is a decrease in the absorption band centered at 463 nm while a charge transfer band appears around 545 nm. These spectral changes are accompanied by the formation of an isosbestic point at 507 nm.

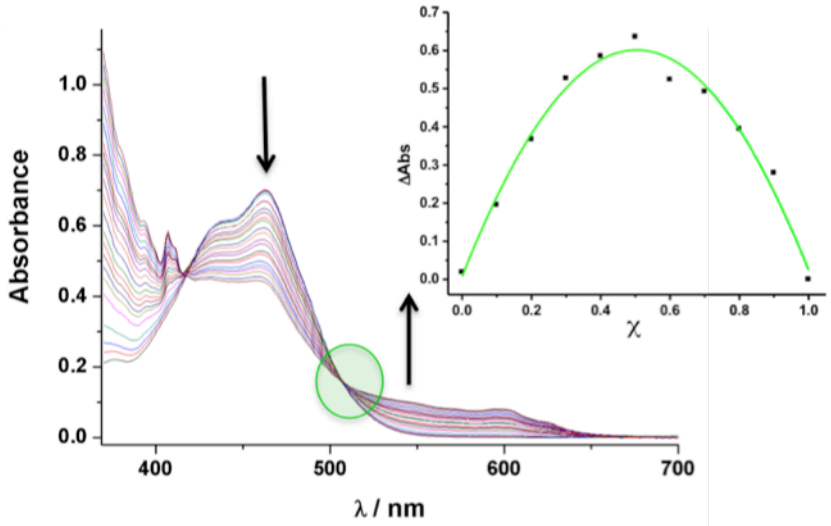

Figure 4.9. Changes in the UV/vis absorption spectra of **81**, upon addition of C_{60} showing log K_a = 4.5 ± 0.5, (PhCl, r.t). Inset Job plot confirming a 1:1 stoichiometry for the complex **81**•C_{60}.

This isosbestic point indicates the formation of just one type of complex, corroborated afterwards by a Job plot (inset in Figure 4.9). The analysis of the Job plot gives a maximum at χ = 0.5, indicative of a 1:1 stoichiometry. Just the 1:1 complex **81**•C_{60} is formed. The analysis of the data of three separate titration experiments to a 1:1 binding mode (utilizing Specfit Software) gave a

log K_a = 4.5 ± 0.5 (PhCl, r.t). This remarkably high value obtained for the binding constant reveals the perfect geometrical and electronic match between the concave surface of the truxTTF derivative and the convex surface of the fullerene unit.

Once obtained the desired building block, a truxTTF derivative functionalized at its periphery with alkynes (**81**), the new compound is ready to undergo further chemical transformations.

The two building blocks satisfactorily synthesized, gave access to more sophisticated truxene-TTF derivatives as described im the following sections.

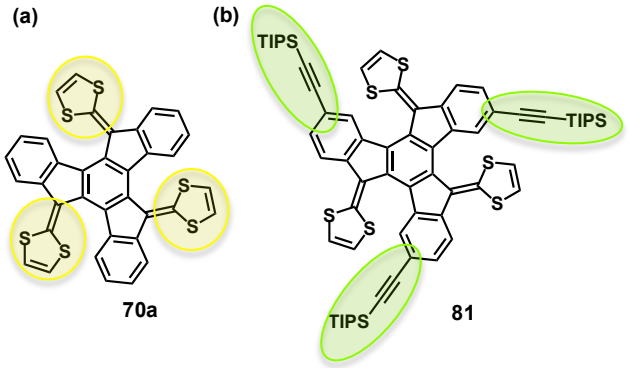

Figure 4.10. Building blocks (a) truxTTF (**70a**) and (b) **81** that will give truxene-TTF derivatives covalently modified at the 1,3-dithiole rings, and at the aromatic periphery, respectively.

4.2. COVALENT LINKAGE OF THREE FULLERENES TO A truxTTF CORE

Several donor-fullerene molecular dyads based on exTTF have previously been reported in our group.[41] Furthermore, the supramolecular behavior between

[41] (a) N. Martín, L. Sánchez, M. A. Herranz and D. M. Guldi, *J. Phys. Chem. A* **2000,** *104*, 4648.;(b) Y. Takano, M. A. Herranz, N. Martín, S. Gayathri-Radhakrishnan, D. M. Guldi, T. Tsuchiya, S. Nagase, T. Akasaka, *J. Am. Chem. Soc.* **2010**, *132,* 8048; (c) F. Giacalone, J. L. Segura, N. Martín, J. Ramey, D. M. Guldi, *Chem. Eur. J.* **2005**, *11*, 4819; (d) D. M. Guldi, F. Giacalone, G. de la Torre, J. L. Segura, N. Martín, *Chem. Eur. J.* **2005**, *11*, 7199; (e) S. Handa, F. Giacalone, S. A. Haque, E. Palomares, N. Martín. J. R. Durran, *Chem. Eur. J.* **2005**, *11*, 7440; (f) L. Sánchez, M. Sierra, N. Martín, D. M. Guldi, M. W. Wienk, R. J. A. Janssen, *Org. Lett.* **2005**, *7*, 1691; (g) C. Atienza, N. Martín, D. M. Guldi, *Chem. Commun.* **2006**, 3202; (h) B. M. Illescas, J. Santos, M. Wielopolski, C. M. Atienza, N. Martín, D. M. Guldi, *Chem. Commun.* **2009**, *74*, 5374; (i) D. M. Guldi, B. M. Illescas, C. M. Atienza, M. Wielopolski, N. Martín, *Chem . Soc. Rev.* **2009**, *38*, 1587.

the C_{60} and the truxTTF (**70a**), has also been extensively studied.[38] However, the covalent linkage of truxTTF to fullerenes has not been addressed in our group so far.

With the main objectives of: (1) covalently linking three [60]fullerene units to the truxTTF, and (2) to study the photophysicall and supramolecular features of the resulting system, we searched for the best synthetic strategy to bring these components together in one molecule.

Our building block of choice is molecule **81**, a truxTTF derivative with alkyne chains at its aromatic periphery that will allow the further covalent linkage of three C_{60} units to the truxene core of the truxTTF (Figure 4.11).

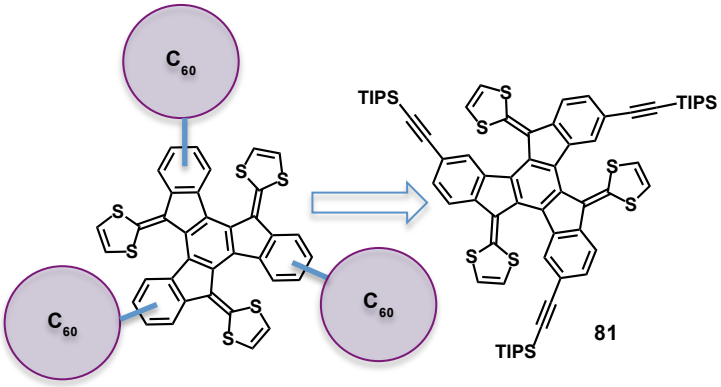

Figure 4.11. Left, proposed general molecule truxTTF-$(C_{60})_3$. Right, building block **81**.

Next we detail the different synthetic strategies followed for the preparation of the truxTTF-$(C_{60})_3$ derivative (Scheme 4.5).

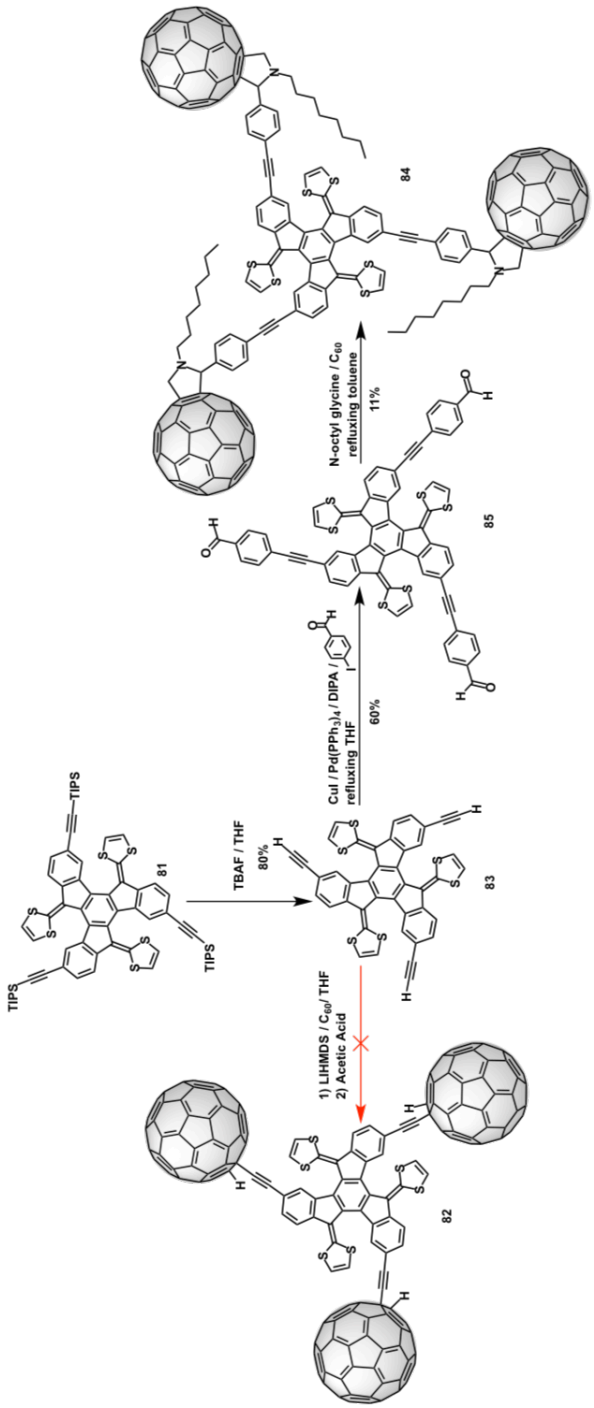

Scheme 4.5. Synthetic strategy towards a truxTTF core linked to three C_{60} units.

Our first strategy to link fullerenes to the truxTTF core, was the direct insertion of an alkyne-truxTTF molecule to [60]fullerene (Figure 4.12). For this purpose, we followed the previously reported methodology by F. Diederich, K. Komatsu, J. Tour and co-workers.[42] (Scheme 4.5).

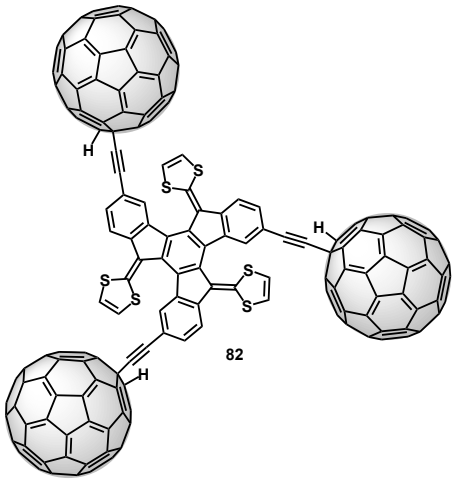

Figure 4.12. Chemical structure of **82**.

The previous step for the linkage of the truxTTF core to the [60]fullerenes is the deprotection of **81**, which is accomplished with tetra-n-butylammonium fluoride (TBAF) in THF at room temperature affording **83** in 80% yield (Scheme 4.5).

83 was characterized by the usual spectroscopic techniques. In the FT-IR we observe the carbon-hydrogen stretch of the terminal alkynes at 3290 cm^{-1}. The ^{1}H NMR of the deprotected trialkyne molecule **83** is shown in Figure 4.13, where all signals are assigned to their respective protons. As expected, the symmetry results in a relatively simple spectrum where the three alkyne-type protons appear as a diagnostic signal as a singlet at around 4.15 ppm and the six dithiole-type protons appear as an AB system at 7.34 ppm, in dimethyl sulfoxide-d_6.

[42] (a) H. L. Anderson, R. Faust, Y. Rubin, F. Diederich, *Angew. Chem. Int. Engl.* **1994**, *33*, 1366; (b) K. Komatsu, Y. Murata, N. Takimoto, S. Mori, N. Sugita, T. S. Wan, *J. Org. Chem.* **1994**, *59*, 6101; (c) G. V. Vives, J. M. Tour, *Acc. Chem. Res.* **2008**, *42*, 473.

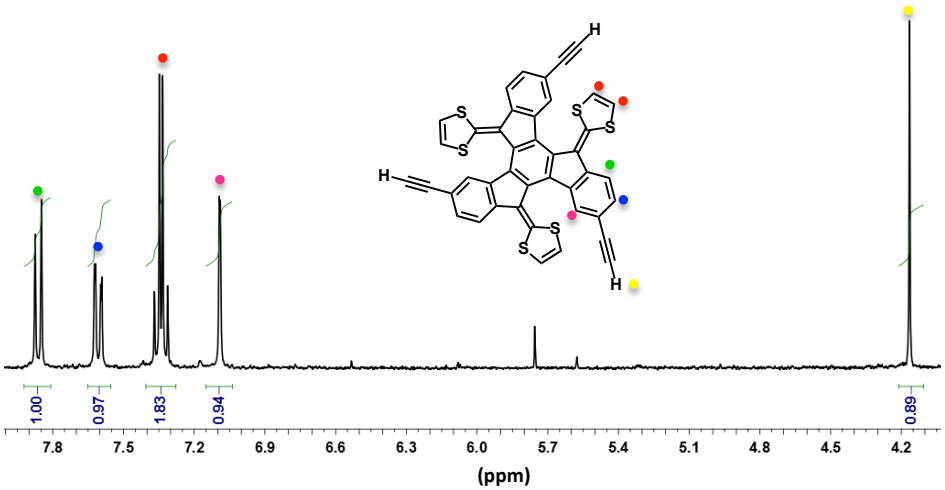

Figure 4.13. ^{1}H NMR (300 MHz, DMSO, 298 K) of compound **83**. Characteristic signals are depicted in colored bullets.

Once we have **83**, it was dissolved in dry THF and deprotonated with lithium bis(trimethylsilyl)amide, LiHMDS. The lithiated-truxTTF is added dropwise to a dispersion of great excess of [60]fullerene in THF. Just three minutes after the addition of the lithium truxTTF derivative, the reaction mixture in THF changes from violet to green; this indicates the generation of the anion of the C_{60}-monoadduct.[42] The last step is the neutralization with acetic acid; the suspension changes its green color and it turns to red-wine, the usual color for the C_{60}-monoadducts.

Unfortunately, HPLC experiments of the crude revealed only the presence of minority peaks of [60]fullerene-monoadducts, which were not possible to isolate from the reaction mixture.

With the idea of bringing together in the same molecule fullerenes and the truxTTF core, we proposed a second synthetic approach in which the three C_{60} units are attached to the truxTTF core by three pyrrolidine rings formed from Prato reactions (Figure 4.14). A similar strategy was followed by Pei and coworkers to link fullerenes to a pristine truxene core.[43]

[43] J.-L. Wang, X.-F. Duan, B. Jiang, L.-B. Gan, J. Pei, *J. Org. Chem.* **2006**, *71*, 4400.

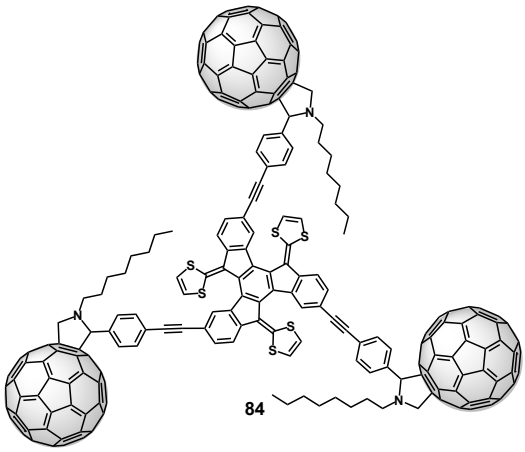

Figure 4.14. Chemical structure of **84**.

The first step in this new synthetic route depicted in Scheme 4.5 is a three-fold Sonogashira coupling in refluxing THF of **83** with 4-iodobenzaldehyde that gives **85** in 60% yield.

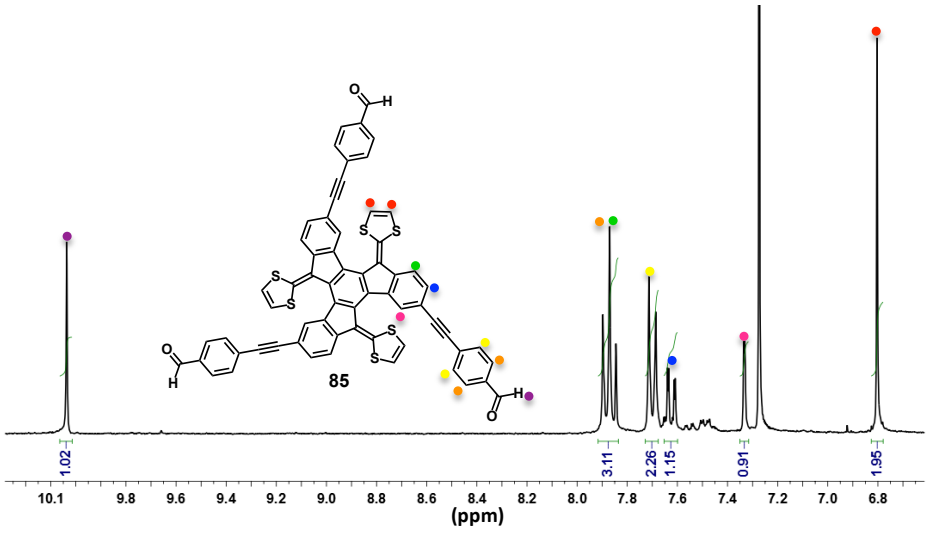

Figure 4.15. ^{1}H NMR (300 MHz, $CDCl_3$, 298 K) of molecule **85**. Characteristic signals are depicted in colored bullets.

This product was satisfactorily characterized by the usual spectroscopic techniques. In Figure 4.15 the characteristic ^{1}H NMR signals of **85** in $CDCl_3$, are shown. Again, the symmetry of the molecule results in a simple spectrum with

just six signals. Among the signals observed, the singlet at 9.95 ppm is the most diagnostic one for this molecule, corresponding to the formyl groups.

Finally, performing a three-fold 1,3-dipolar cycloaddition reaction on trialdehyde **85** with n-octyl glycine, and C_{60} in refluxing toluene we obtained the desired compound **84** in 11% yield after purification by size exclusion chromatography, in the absence of direct light.

Unfortunately, **84** turned to be an unstable compound and difficult to work with. Any experiment done on **84**, had to be carried out in absence of direct light and under inert atmosphere.

When **84** is left in solution, open at the atmosphere and exposed to sunlight, it decomposes loosing the dithiole rings. The UV/vis spectrum of the sample before and after exposure to sunlight is shown in Figure 4.17. The product of decomposition resulted to be molecule **86** (Figure 4.16), which was characterized by NMR experiments.

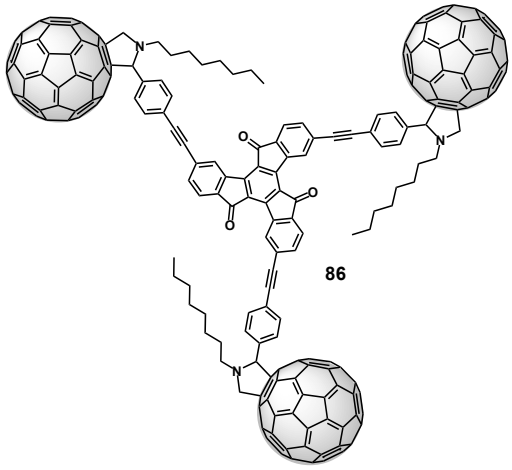

Figure 4.16. Chemical structure of **86**.

The ^{1}H NMR of compound **86** is shown in Figure 4.18. The most diagnostic ^{1}H NMR signals for this compound are: (i) in the aliphatic region: the two doublets, of the AB system formed by the methylene bridge of the pyrrolidine ring (pink bullets), at 5.17 and 4.20 ppm and the singlet at 5.14 ppm of the –CH of the pyrrolidine ring (dark green bullet) and (ii) in the aromatic region: the downfield singlet at 9.22 ppm (light green bullet), which belongs to the aromatic truxenone core. This downfield singlet has been found as well in molecule **80**, but when truxenone core is turned into truxTTF core, the same proton appears more shielded, as it has been seen for molecules **81**, **83** and **85**.

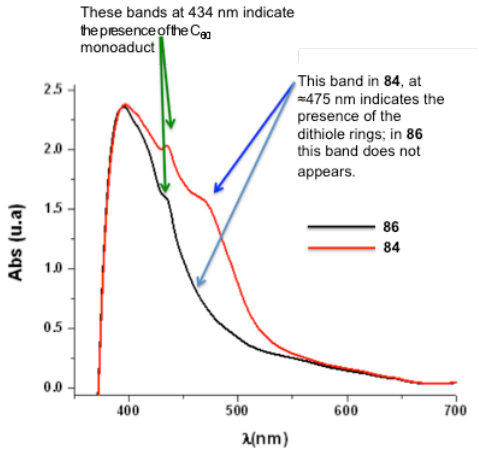

Figure 4.17. UV/vis spectra of the sample before and after exposure to sunlight.

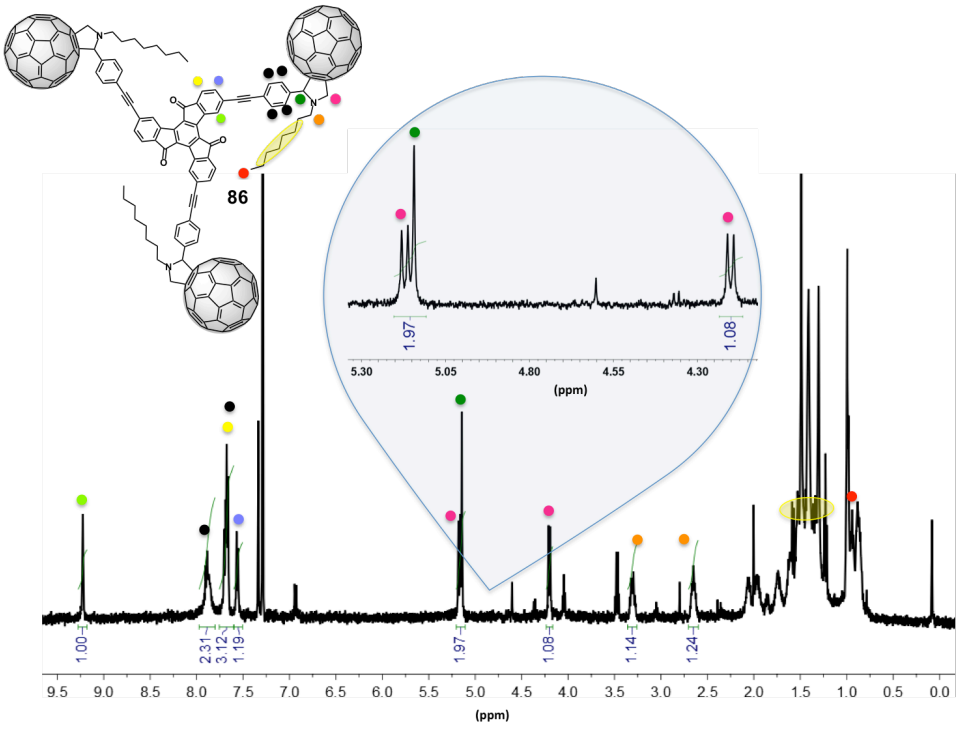

Figure 4.18. ^{1}H NMR (500 MHz, CS_2 with inner $CDCl_3$ reference, 298 K) of **86**. Characteristic signals are depicted in colored bullets.

The chemical structure of molecule **86** is further elucidated by ^{13}C NMR and 2D experiments (HSQC, COSY). In Figure 4.19, the –CH, -CH_2 and –CH_3 carbon signals are depicted in colored bullets on the DEPT-135, some of them are depicted again on the ^{13}C NMR together with some of the quaternary carbons present in **86**. The highlighted signals on the ^{13}C NMR in Figure 4.19 are: the carbonyl group at 190.1 ppm (highlighted in red), the sp^2 carbons of the C_{60} (highlighted in pink), the –CH of the pyrrolidine at 82.9 ppm (highlighted in blue), the –CH_2 at 67.4 ppm (purple bullet), the set of –CH_2 of the octyl chain from 32.9 to 27.9 ppm (highlighted in yellow) and the –CH_3 group of the same chain at 23.8 ppm (red bullet).

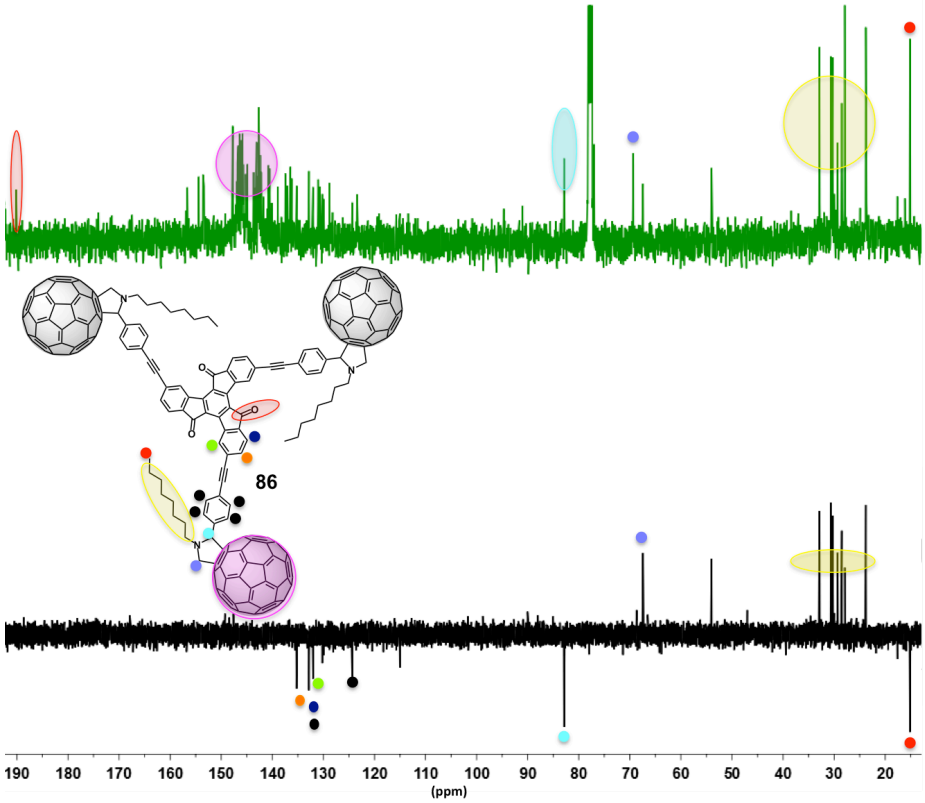

Figure 4.19. ^{13}C NMR and DEPT-135 (125 MHz, CS_2 with inner $CDCl_3$ reference, 298 K) of molecule **86**. Characteristic signals are highlighted in colored bullets.

The characterization of molecule **86** is very helpful for the understanding of the characterization of molecule **84**.

The ^{1}H NMR of molecule **84** shows broad, and not well defined signals, but in contrast to molecule **86**, **84** does not have the downfield aromatic singlet, characteristic of the truxenone core, and it has a broad singlet around 7 ppm that correlates in 2D NMR experiments with carbon signals at around 120 ppm characteristic of the –CH groups of the 1,3-dithiole rings. In the aliphatic region of the ^{1}H NMR we can observe the same characteristic signals (for the pyrrolidine ring and for the octyl chain) that were observed in **86** but shielded. A comparison of the ^{1}H NMR of these two molecules is shown in Figure 4.20. When comparing the ^{13}C NMR of **84** and **86** (Figure 4.21), we observe the same major characteristic signals for both compounds and a very important difference, the quaternary carbon at 189.60 ppm, related to a carbonyl group is just present in **86**.

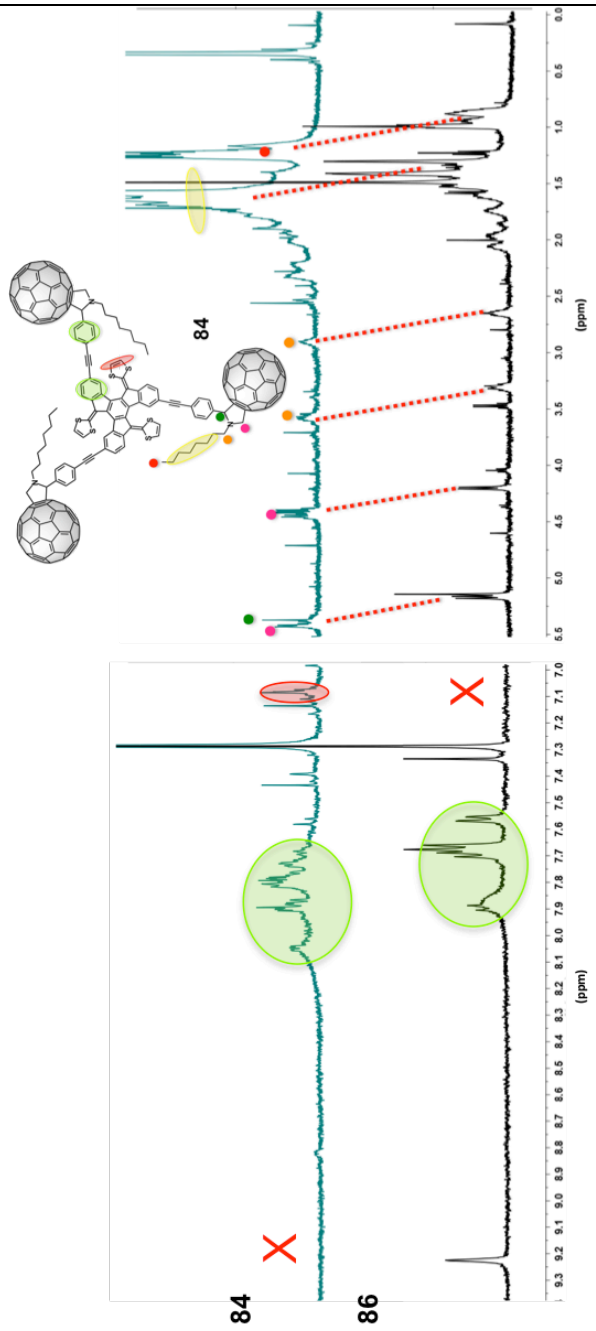

Figure 4.20. Superimposition of ^{1}H NMR: molecules **86** (green, 700 MHz, CS_2 with inner $CDCl_3$ reference, 298 K) and **84** (black, 700 MHz, CS_2 with inner $CDCl_3$ reference, 298 K). Characteristic signals of molecule **86** are depicted in colored bullets.

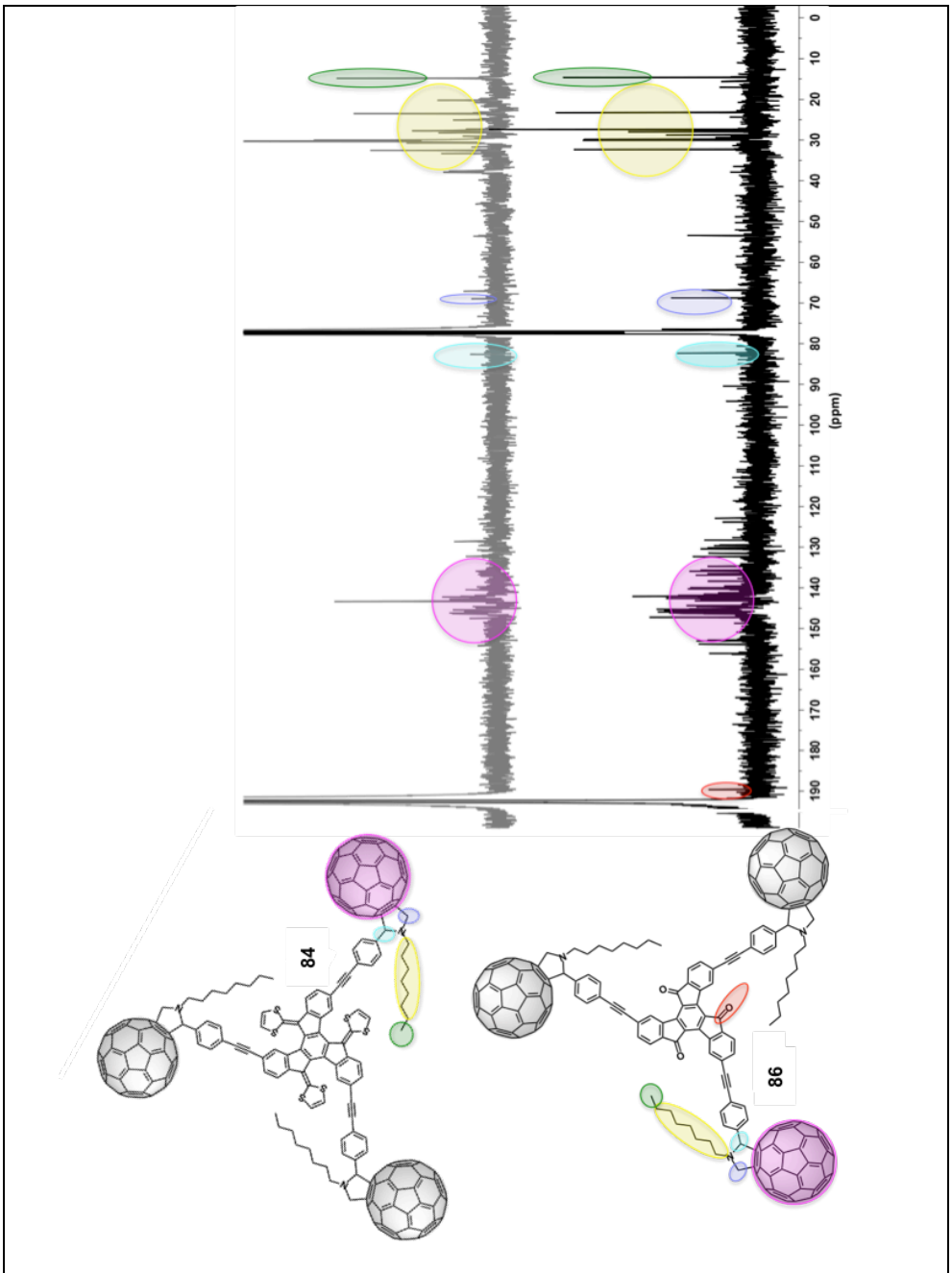

Figure 4.21. Superimposition of ^{13}C NMR: **84** (grey, 125 MHz, CS_2 with inner $CDCl_3$ reference, 298 K) and **86** (black, (175 MHz, CS_2 with inner $CDCl_3$ reference, 298 K). Characteristic signals of molecule **86** are highlighted in colors.

It is important to note that the unstable compound **84** could not be properly characterized, however, based on spectroscopic data of its decomposition product **86**, both structures could be confirmed despite the lack of mass spectra.

Once we accomplished the synthesis and the characterization of **84**, we studied its supramolecular behavior. Apparently, **84** resulted a good receptor for fullerenes. It exploits fullerene-fullerene interactions to bind [70]fullerene. In Figure 4.22 we can see a UV/vis titration experiment of a solution of C_{70} ($1x10^{-5}$ M) with **84** ($1x10^{-4}$ M) at room temperature in 1,2-dichlorobenzene. The results of three separate titration experiments were analyzed with Specfit software affording a binding constant of log K_a = 6.8 ± 0.5.

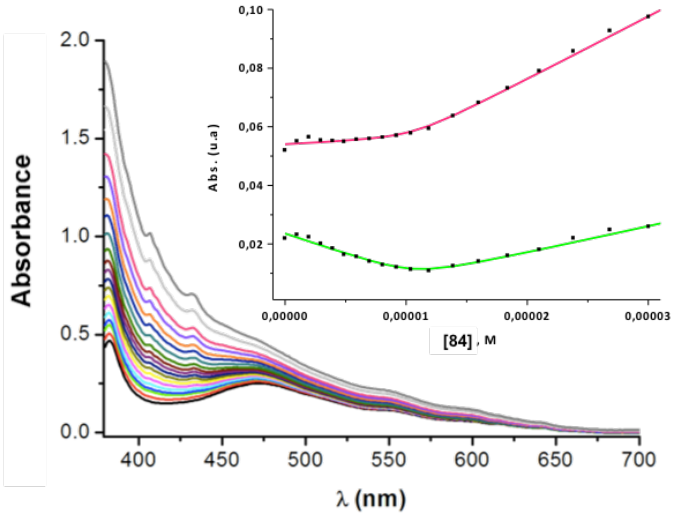

Figure 4.22. Changes in the UV/vis absorption spectra of C_{70} upon addition of **84** showing log K_a = 6.8 ± 0.5 (*o*DCB, r.t). Inset: binding isotherms at 605 nm (in pink) and 653 nm (in green).

Unfortunately upon femtosecond flash photolysis experiments, the sample decomposed. The UV/vis spectra before and after the measurements, after the exposition to the laser beam, did not remain equivalents, so it was impossible to determine whether there were or not intermolecular o intramolecular charge transfer processes.

4.3. TruxTTF DERIVATIVES AS METAL FREE ORGANIC SENSITIZERS FOR DYE SENSITIZED SOLAR CELLS (DSSCs)

Among the components of a typical Dye Sensitized Solar Cells device, the sensitizer is one of the key components for achieving a high efficiency. In this regard, despite the fact that the ruthenium (II) polypyridyl complexes are beyond the most successful dyes for DSSCs, they are expensive due to the used metal. Metal free and porphyrin-like dyes are an alternative kind of sensitizers for DSSCs devices. However, the molecular aggregation of these kind of dyes typically decreases the efficiency of the device since aggregation may lead to efficient intermolecular quenching and, also, to the coating of the TiO_2 surface with molecules unattached to it. These facts will greatly reduce the electron injection, thus lowering the efficiency of the device. One strategy to avoid the aggregation of these dyes is to design sensitizers with non-planar groups such as diphenylamines.[44] In this regard, truxTTF could be a versatile building block for constructing metal-free organic sensitizers that may have a potential use in DSSCs. As already mentioned before, the biconcave shape of the truxTTF molecule provides steric hindrance, preventing the self-aggregation of the truxene core and, in addition, truxTTF is a good electron donor system.

The truxTTF molecule provides a truxene aromatic core, this is, a π-conjugated bridge (Figure 4.23, highlighted in green) and three 1,3-dithiole units, which behave as three donor units (Figure 4.23, highlighted in yellow). The presence of appropriate anchoring groups would allow synthesizing a suitable functionalized sensitizer. As mentioned in the background of this chapter, there are several examples exploiting the planar truxene core as π-bridge for DSSCs.[31,32]

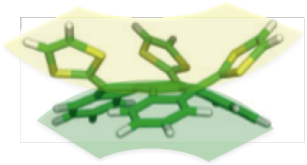

Figure 4.23. truxTTF molecule **70a**.

The biconcave disposition of the truxTTF molecule offers not only a hindrance to prevent the aggregation of the dye but also the possibility of organizing donor groups, π-bridge and anchoring groups.

[44] Z. Ning, Y. Fu, H. Tian, *Energy Environ. Sci.* **2010**, *3*, 1170.

Recently, the study on annulated TTF-acceptor system for DSSCs has been reported.[45] There are also some studies carried out in our group on exTTF-based organic dyes for DSSCs.[46] Unfortunately, up to now, they show a moderate power conversion efficiency (1.6-3.8%) due to thermodynamically unfavorable dye-regeneration after electron injection.

Here, we propose the synthesis of metal-free organic sensitizers based on the truxTTF core. To do so, we will link anchoring groups to a truxTTF. The linkage of these anchoring groups to the truxTTF molecule will be done through the aromatic truxene core or, alternatively, through the dithiole donor units (Figure 4.24). The sensitizers will feature multiple anchoring groups, namely pyridines or carboxylic acids.

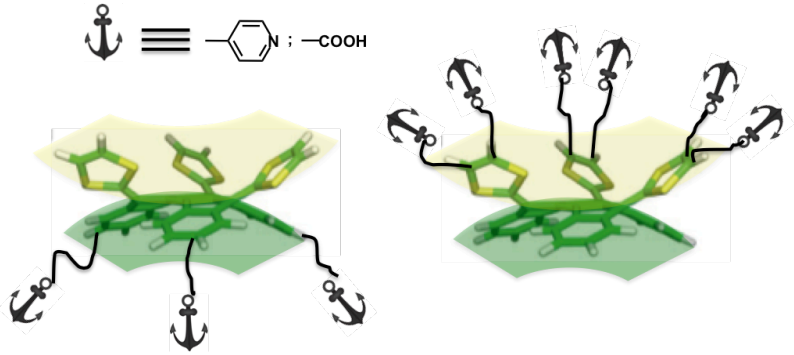

Figure 4.24. Schematic representation of the truxTTF dyes.

There are several studies on systems with multiple anchoring groups.[47] This "multi-anchoring" exhibits some advantages, namely: dye-bonding enhancement on the surface of the photo-electrode, superior electron injection efficiency and reduced recombination rate. Most of the donor-acceptor π-conjugated (D-π-A) organic dyes have carboxyl groups (carboxylic acid,

[45] A. Amacher, C. Yi, J. Yang, M. P. Bircher, Y. Fu, M. Cascella, M. Grätzel, S. Decurtis, S.-X. Liu, *Chem. Commun.* **2014**, *50*, 6540.

[46] (a) S. Wenger, P.-A. Bouit, Q. Chen, J. Teuscher, D. Di Censo, R. Humphry-Baker, J.-E Moser, J. L. Delgado, N. Martín, S. M. Zakeeruddin, M. Gräetzel, *J. Am. Chem. Soc.* **2010**, *132*, 5164; (b) C. A. Echeverry, M. A. Herranz, A. Ortiz, B. Insuasty, N. Martín, *New J. Chem.* **2014**, *38,* 5801.

[47] (a) S. P. Singh, M. S. Roy, K. R. J. Thomas, S. Balaiah, K. Bhanuprakash, G. D. Sharma, *J. Phys. Chem. C* **2012**, *116*, 5941; (b) D. Cao, J. *Peng*, Y. Hong, X. Fang, L. Wang, H. Meier, *Org. Lett.* **2011**, *13*, 1610; (c) Y.-S. Yen, W.-T Chen, C.-Y. Hsu, H.-H Chou, J. T. Lin, M.-C. P. Yeh, *Org. Lett.* **2011**, *13*, 4930.

cyanoacrylic acid or rhodanine-3-acetic acid) in order to link the dye to the TiO_2 surface. The carboxyl group forms strong ester linkage with Brönsted acid sites of the TiO_2 surface, enabling good electron communication between the dye and the TiO_2. Just a few years ago, Harima and co-workers reported the use of a pyridine ring as electron-withdrawing and anchoring group in dyes.[48] The pyridine ring forms a strong coordinated bond between the lone pair of electrons of the nitrogen atom and the Lewis acid sites of the TiO_2. This new type of D-π-A dye gave electron injection efficiencies comparable to, or even higher, than the equivalent dye featuring carboxyphenyl group as anchoring group.

Herein we report the design of five new molecules that could have potential application in dye sensitized solar cells devices. (Figure 4.25 and 4.26). All of them feature a truxTTF core. Two of them, **87** and **88** are constructed from the building block **81**, while **89**, **90**, and **91**, are constructed from pristine truxTTF, **70a**.

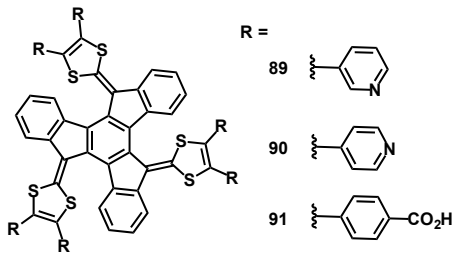

Figure 4.25. Chemical structure of dyes **89**, **90** and **91.**

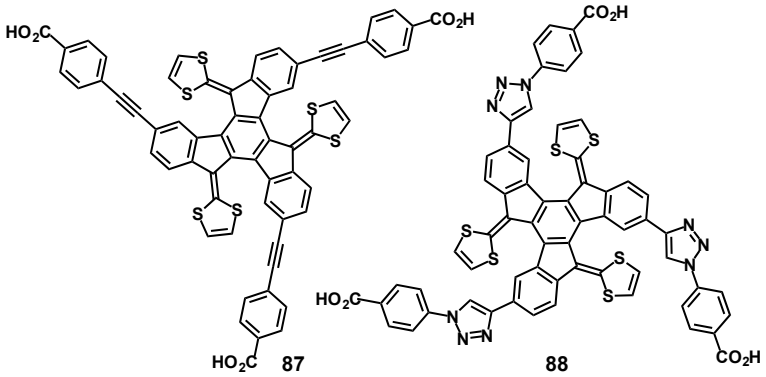

Figure 4.26. Chemical structure of dyes **87** and **88.**

[48] (a) Y. Ooyama, S. Inove, T. Nagano, K. Kushimoto, J. Ohshita, I. Imae, K. Komaguchi, Y. Harima, *Angew*. *Chem*. **2011**, *123*, 7567. (b) Y. Ooyama, T. Nagano, S. Inoue, I. Imae, K. Komaguchi, J. Ohshita, Y. Harima, *Chem. Eur. J*. **2011**, *17*, 14837.

4.3.1. *Synthesis of truxTTF derivatives for DSSCs with three anchoring groups*

As mentioned before, molecule **81** is an usefull building block to expand the truxTTF core (Figure 4.27). It offers the posibility to modify the aromatic periphery in order to attach linkers to construct dyes for DSSCs.

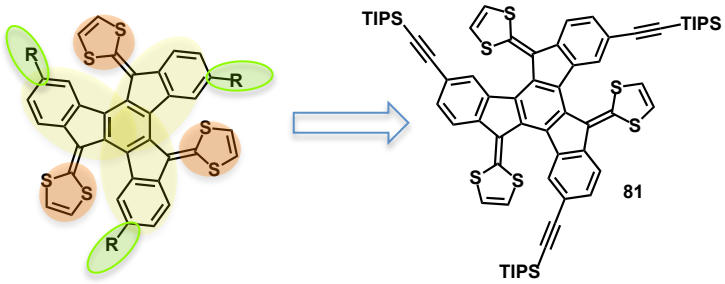

Figure 4.27. Retrosynthetic scheme of truxTTF-based dyes with three anchoring groups. Highlighted in yellow the π-bridge, in orange the donor units and in green the anchoring groups.

Building block **81** provides three alkyne groups that can be chemically modified. Therefore, we followed two strategies: (1) modification via three-fold Sonogashira coupling reaction and (2) modification via "click chemistry".

Both strategies start with the cleavage of the protecting groups TIPS with tetra-n-butylammonium fluoride (TBAF) in THF at room temperature to afford molecule **83** (Scheme 4.5).

(a) Modification via triple Sonogashira coupling reaction

Molecule **87** is prepared from **83** in a two steps synthesis (Scheme 4.6); firstly a three-fold Sonogashira coupling reaction is carried out on **83** with 4-iodomethylbenzoate. After purification of the corresponding methylester truxTTF-derivative **92** (50% yield), it is hydrolized to yield **87** in 30%.

Compounds **92** and **87** were satisfactorily characterized by different spectroscopic techniques.

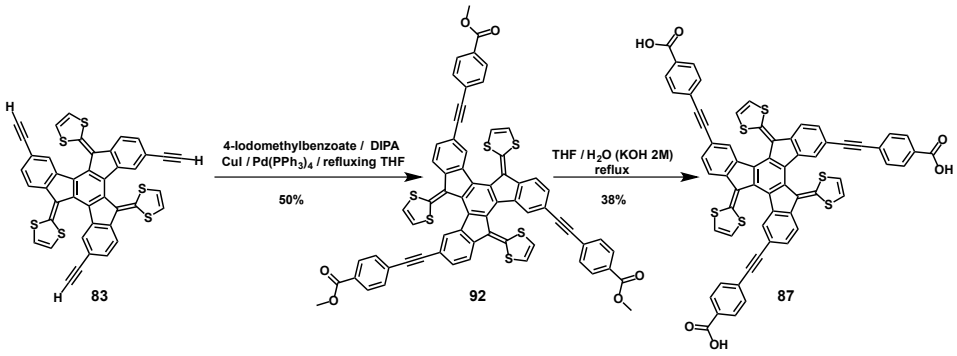

Scheme 4.5. Synthesis of **87**.

The transformation of **83** in **92** is easily evidenced by ^{1}H NMR. The disappearance of the singlet signal for the terminal alkynes at 4.17 ppm is accompained by the appearance of three new diagnostic signals for the new molecule, two duplets in the aromatic region and a singlet at 3.95 ppm, characteristic of the methoxy groups (Figure 4.28).

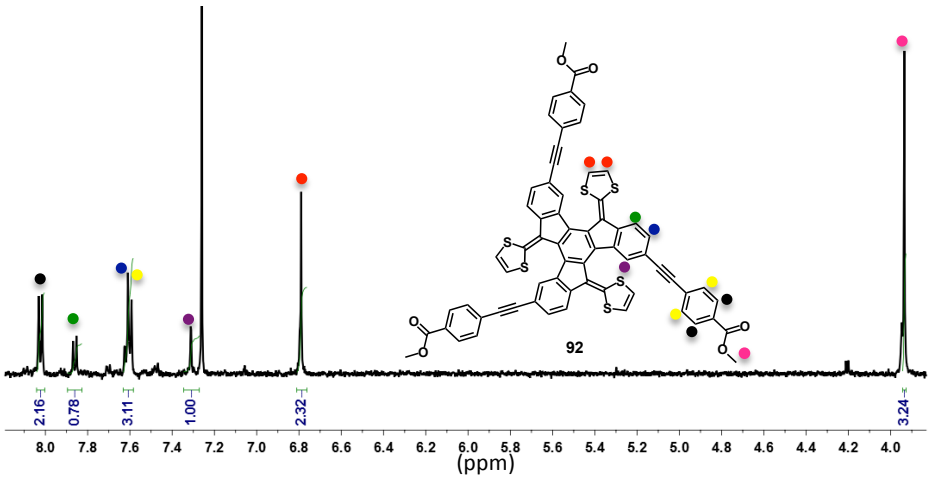

Figure 4.28. ^{1}H NMR (500 MHz, $CDCl_3$, 298 K) of molecule **92**. Characteristic signals are depicted in colored bullets.

The hydrolysis of the methyl esters of compound **92** in basic medium is evidenced in the ^{1}H NMR of the new compound **87** by the absence of the signal for the methoxy groups of the precursor molecule. Further NMR experiments and MS allowed us to unambiguously characterize the product. The aromatic region of ^{1}H NMR of **87** is shown in Figure 4.29.

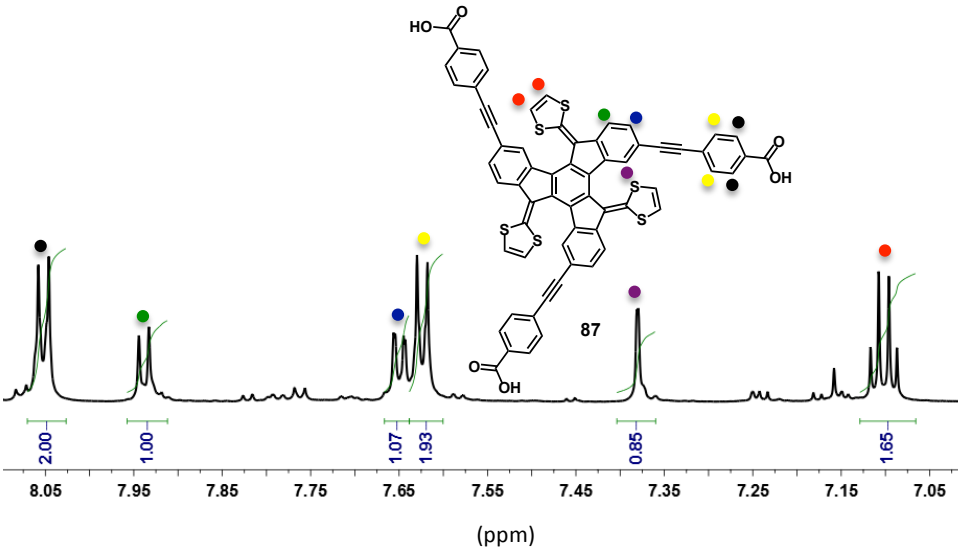

Figure 4.29. ^{1}H NMR (700 MHz, THF, 298 K) of molecule **87**. Characteristic signals are depicted in colored bullets.

(b) Modification via "click Chemistry"

Compound **88** is obtained from **83** in 65% yield in just one step via "click chemistry" [49] by a three-fold 1,3-dipolar cycloaddition reaction of 4-azidobenzoic acid with the alkyne units of truxTTF derivative **81**, catalyzed by Cu(I) at room temperature in DMSO. The source of Cu (I) is $CuBr{\bullet}CH_3SCH_3$, the sodium L-ascorbate acts as reductor and metallic Cu wire assures the presence of Cu(I) under reducing conditions and oxygen free reaction medium. Under these conditions we obtain a truxTTF core linked to a benzoic acid through a 1,4-disubstituted triazol ring (Scheme 4.7).

[49] H. C. Kolb, M. G. Finn, K. B. Sharpless, *Angew. Chem. Int. Ed.* **2001**, *40*, 2004.

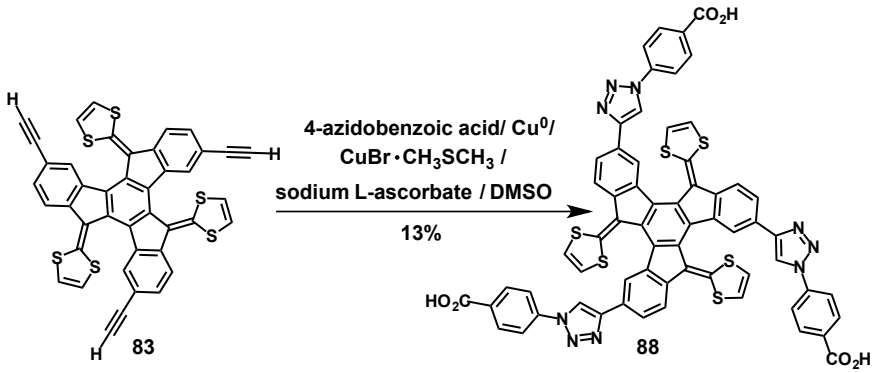

Scheme 4.7. Synthesis of **88**.

Molecule **88** was successfully characterized by the usual spectroscopic techniques. The ^{1}H NMR signals for molecule **88**, as well as some of the most diagnostic ^{13}C NMR ones are depicted in colored bullets in Figure 4.30. For example, the singlet at 9.37 ppm that correlates with a –CH in ^{13}C NMR at 119.57 ppm, belongs to the ^{1}H of the triazole ring (light blue bullet), the protons of the dithiole rings appear as an AX system, two duplets at 7.25 ppm and 7.35 ppm (red bullets).

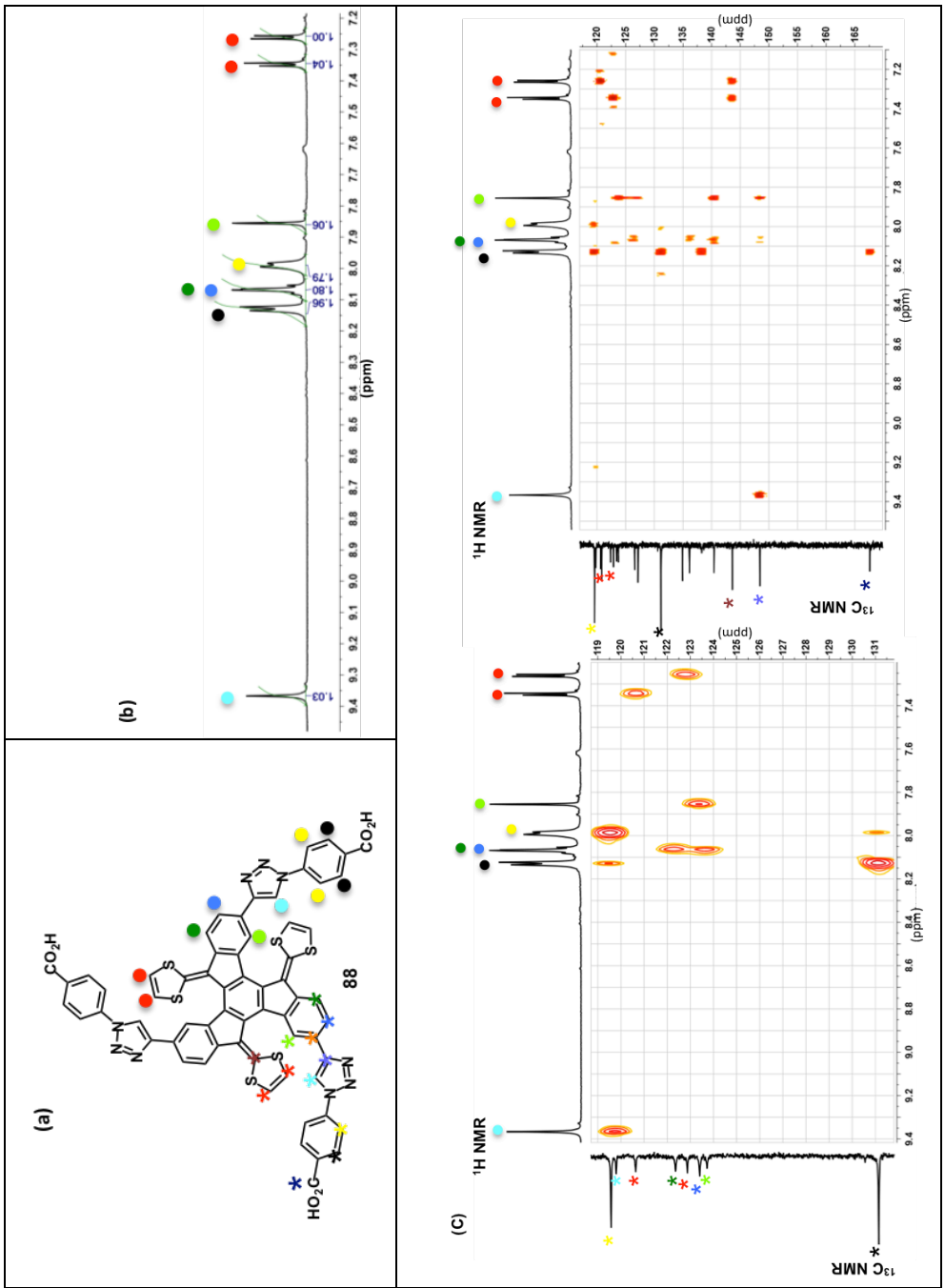

Figure 4.30. (a) Chemical structure, (b) ^{1}H NMR (700 MHz, DMSO, 298 K), (c) HSQC, (d) HMBC of molecule **88**. Characteristic signals are depicted in colored bullets.

4.3.2. Syntheses of truxTTF derivatives for DSSCs with six anchoring groups

Our building block for these syntheses is the truxTTF molecule (Figure 4.31).

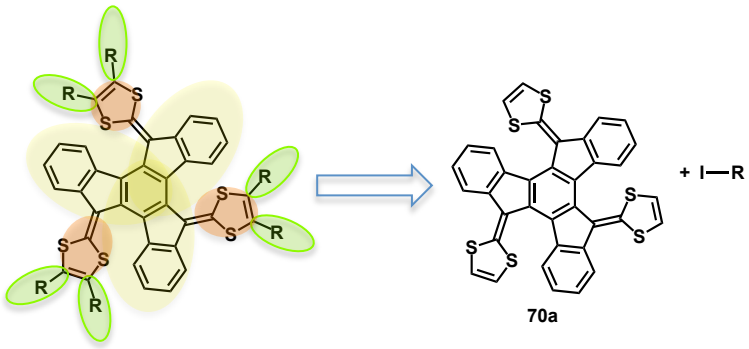

Figure 4.31. Retrosynthetic scheme of the truxTTF-based dyes. Highlighted in yellow the π-bridge, in orange the donor units and in green the anchoring groups.

The three dithiole rings of the truxTTF can be easily modified by direct C-H arylation with palladium catalysis in one-pot reaction. By this methodology, we synthesized the hexasubstituted truxTTF molecules **89**, **90** and **91**. An analogous substitution-type has also been reported on TTF and exTTF molecules.[50]

Treatment of aryl iodides (3-iodopyridine and 4-iodopyridine for **89** and **90**, respectively, and methyl 4-iodobenzoate for **93**) with truxTTF (**70a**) in the presence of cesium carbonate, a catalytic amount of palladium acetate and tri-*tert*-butylphosphonium tetrafluoroborate in refluxing dioxane provided the corresponding hexa-arylated compounds **89**, **90** and **93** in moderate yields (around 50%). Ester saponification of **93** under basic conditions and subsequent acid treatment gives **91** in 80% yield, (Scheme 4.8).

[50] (a) Y. Mitamura, H. Shima, A. Osuka, *Chem. Sci*. **2011**, *2*, 2017; (b) S. Bivaud, S. Goeb, V. Croeué, P. I. Dron. M. Allain, M. Sallé. *J. Am. Chem. Soc.* **2013**, *135*, 10018.

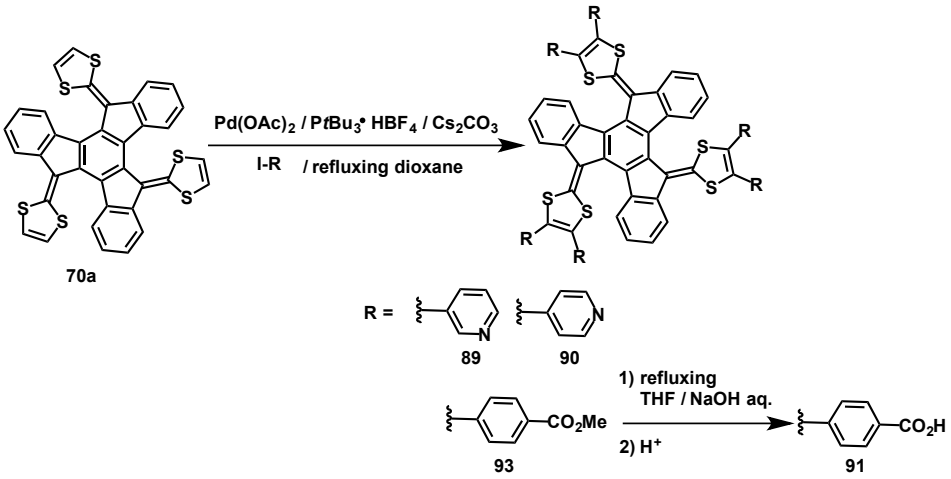

Scheme 4.8. Synthesis of **89**, **90**, **93** and **91**.

All new products were satisfactorily characterized by the ususal spectroscopic techniques.

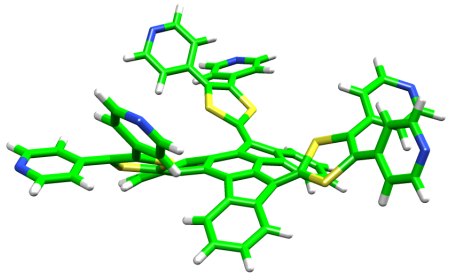

Figure 4.33. Energy minimized Amber force field modelization of **89**.

As a general feature in molecules **88**, **89**, **93** and **91**, the two aromatic rings at the 1,3-dithioles show different chemical shifts. In Figure 4.33 the energy minimized Amber force field modelization of **89** is presented revealing the different environment for the pyridine units.

As an example, the ^{1}H NMR of molecule **89** is shown in Figure 4.32. Note that each pyridine ring shows two distinct duplets for their proton signals.

In Figure 4.34 we show how the functionalization on the 1,3-dithiole rings of truxTTF affects their UV/vis spectra. The comparison of truxTTF UV/vis spectra vs the new synthesized dyes UV/vis spectra at constant concentration (1.8 x 10^{-4} M in THF, room temperature) reveals a slightly bathocromic shift of the maximun absorbance centered at 448 nm in truxTTF to 456 nm in the new dyes, as well as a broadening of the band. Interestingly, the carboxyl groups induce a weak absortion at 600 nm most probably due to an intramolecular charge-

transfer process.

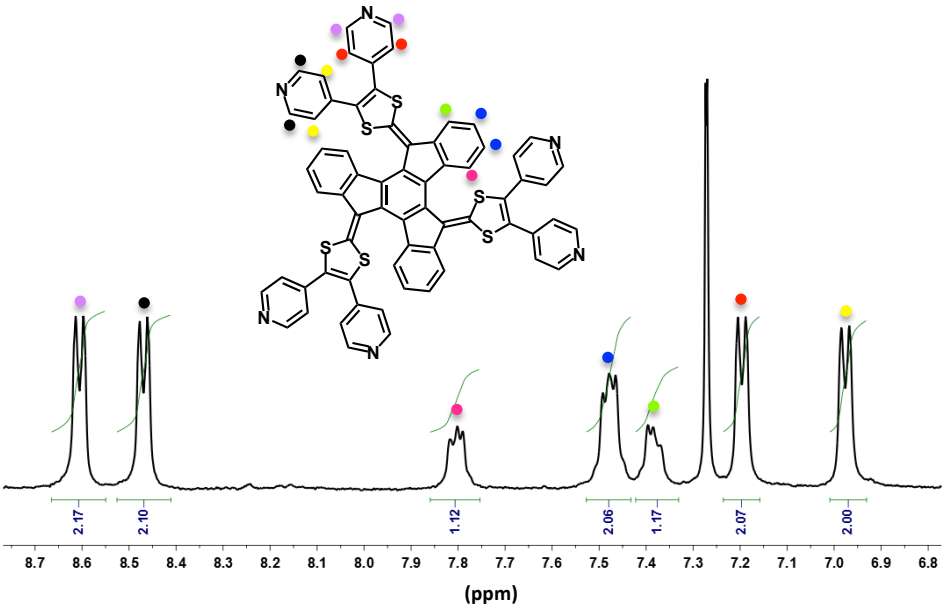

Figure 4.32. ^{1}H NMR (300 MHz, $CDCl_3$, 298 K) of molecule **89**. Characteristic signals are depicted in colored bullets.

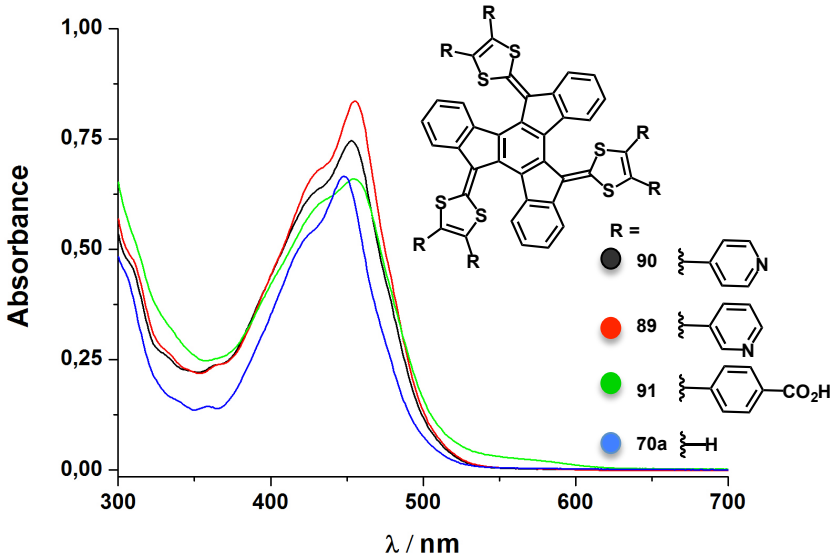

Figure 4.34. UV/vis spectra of molecules **89**, **90**, **91** and truxTTF (**70a**). (1.8 x 10^{-4} M in THF, room temperatures.

4.4. TruxTTF derivatives for Bulk Heterojunction Solar Cells (BHSCs)

The following results have been extracted from the article " Organic solar cells based on bowl-shape small molecules". The results described in the original publication have been complemented with the synthesis and characterization of another truxTTF-derivative, the truxTTF-3F, which was not reported in the above-mentioned publication.

Agustín Molina-Ontoria, María Gallego, Luis Echegoyen, Emilio M. Pérez and Nazario Martín, *RSC* Adv., **2015**, *5*, 31541.

Light absorption ability and morphology of the active components are two of the key factors that determine the energy conversion efficiency in organic solar cells (OSCs). Determining the relative importance of each of these aspects is decisive for the construction of more efficient OSCs. Here we introduce two π-extended derivatives of tetrathiafulvalene as electron donors for solution-processed small-molecule bulk-heterojunction solar cells. Both of them exhibit similar bowl-shape geometry, excellent electron-donor behaviour and moderately high association constants with fullerenes in solution (around 10^4 M^{-1} for truxTTF (**70a**) and 10^3 M^{-1} for truxTTF-CO (**73**) in several solvents at room temperature)[40]. The substitution of one dithiole ring in truxTTF-CO for a carbonyl group results in an intramolecular push-pull effect, which enhances its light-harvesting properties, with the onset of absorbance reaching 650 nm. The introduction of a third dithiole ring, results in a more pronounced concave shape in truxTTF, allowing better self-assembly with fullerenes which, in turn, leads to a more favorable morphology of the active layer. However, the light-absorption ability of the truxTTF is limited to ca. 500 nm. We have prepared bulk-heterojunction solar cells using phenyl-C_{60}-butyric acid methyl ester ($PC_{61}BM$) and $PC_{71}BM$ as electron-acceptors and bowl shape truxTTF and truxTTF-CO as electron-donors. The devices prepared utilizing truxTTF performed significantly better (PCE up to 1.77% with $PC_{71}BM$ and 0.92% with $PC_{61}BM$) than the truxTTF-CO counterpart (PCE up to 1.19% with $PC_{71}BM$ and 0.56% with $PC_{61}BM$). These results suggest that a more favorably morphology of the active layer is, in this case, more relevant for efficiency of OSCs than the light absorption properties of the active layer.

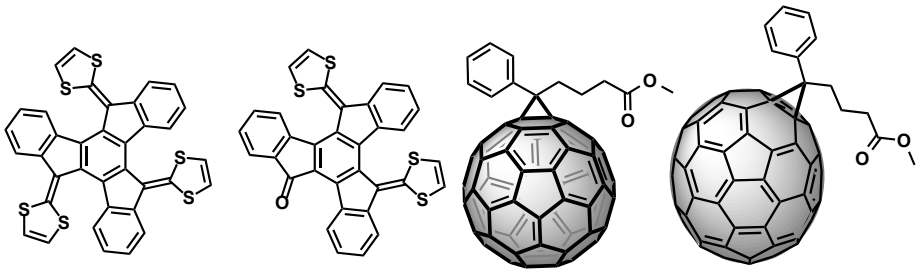

truxTTF (70a) **truxTTF-CO (73)** **$PC_{61}BM$ (94)** **$PC_{71}BM$ (95)**

Figure 4.35. Chemical structures of bowl-shape electron-donors truxTTF and truxTTF-CO and electron acceptors phenyl-C_{60}-butyric acid methyl ester ($PC_{61}BM$) and phenyl-C_{70}-butyric acid methyl ester ($PC_{71}BM$).

The photoactive layer of a bulk-heterojunction solar cell (BHJ) is composed of a blend of either a π-conjugated semiconductor polymer or other small-molecule as electron donor and a fullerene derivative or a small acceptor molecule, such as diketopyrrolopyrrole (DPP), perylenediimide (PDI) or fluoranthene-fused imide (FFI), as electron acceptor. An interpenetrating network at the nanometer scale (shorter than the exciton diffusion length ≈ 3-10 nm) of these two components is crucial for efficient exciton diffusion to the interfaces, followed by exciton dissociation into charges. Formation of percolating pathways for electrons and holes to be efficiently collected at the external electrodes is also needed to avoid undesired charge recombination processes. Therefore, a more favorable morphology of the active layer is a key issue in the preparation of BHJ solar cells, given its critical influence on the device performance.[51] There are several macroscopic methods to assist the control of the morphology, including the use of solvent additives[52] or solvent thermal annealing.[53] Moreover, a molecular approach has been used to control the

[51] (a) B. C. Thompson, J. M. Frechet, *Angew. Chem. Int. Ed.* **2008**, *47*, 58; (b) A. J. Moulé,K. Meerholz, *Adv. Funct. Mater.* **2009**, *19*, 3028; (c) G. Dennler, M. C. Scharber, C. J. Brabec. *Adv. Mater.* **2009**, *21*, 1353; (d) F. Yang, M. Shttein, S. R. Forrest, *Nat. Mater.* **2004**, *4*, 37; (e) J. Peet, M. L. Senatore, A. J. Heeger, G. C. Bazan, *Adv. Mater.* **2009**, *21*, 1521; (f) X. Yang, J. Loos, *Macromolecules*, **2007**, *40*, 1353; (g) Y. Huang, E. J. Kramer, A. J. Heeger, G. C. Bazan, *Chem. Rev.* **2014**, *114*, 7006.

[52] (a) J. Peet, J. Y. Kim, N. E. Coates, W. L. Ma, D. Moses, A. J. Heeger, G. C. Bazan, *Nat. Mater.* **2007**, *6*, 497; (b) S. J. Lou, J. M. Szarko, T. Xu, T. J. Marks, L. X. Chen, *J. Am. Soc.* **2011**, *133*, 20661; (c) J. K. Lee, W. L. Ma, C. J. Brabec, J. Yuen, J. S. Moon, J. Y. Kim, K. Kee, G. C. Bazan, A. J. Heeger, *J. Am. Chem. Soc*. **2008**, *130*, 3619.

[53] (a) G. Li, V. Shrotriya, J. Huang, Y. Yao, T. Moriarty, K. Emery, Y. Yang, *Nat. Mater.* **2005**, *4*, 864; (b) G. Li, Y. Yao, H. Yang, V. Shrotriya, G. Yang, Y. Yang, *Adv. Funct. Mater.* **2007**, *17*, 1636; (c) W.

phase segregation, for instance, by self-assembling fullerene derivatives,[54] by using the side chains of the polymers to accommodate the acceptor moieties[55] or by means of hydrogen-bonding.[56] However, in these macroscopic and molecular approaches, the donor and acceptor moieties act individually, since there are no specific interactions between them. On the other hand, a supramolecular approach in which both components interact through their complementary shapes has been only recently reported.[57] Coronene derivatives (donor) were found to form supramolecular complexes with $PC_{71}BM$ (acceptor) through dispersion-type concave-convex interactions.[58] Both materials were used in order to control the morphology of thin-film solar cells by self-assembly, yielding devices with power conversion efficiency (PCE) values of up to 2.6%.

In 2007, truxene-tetrathiafulvalene (truxTTF, **70a**) emerged as an excellent supramolecular partner for recognition of C_{60} as well as C_{70}.[38] TruxTTF features a truxene core, which is decorated with three covalently linked dithiole units. The

Ma, C. Yang, X. Gong, K. Lee, A. J. Heeger, *Adv. Funct. Mater.* **2005**, *15*, 1617; (d) M. Campoy-Quiles, T. Ferenczi, T. Agostinelli, P. G. Etchegoin, Y. Kim, T. D. Anthopoulos, P. N. Stavrinou, D. D. C. Bradley, J. Nelson, *Nat. Mater.* **2008**, *7*, 158; (e) S. Miller, G. Franchini, Y. Y. Lin, C. Li, C. W. Chen, W. F. Su, M. Chowalla, J. Mater. Chem. **2008**, *18*, 306; (f) G. Wei, S. Wang, K. Sun, M. E. Thompson, S. R. Forrest, *Adv. Energy Mater.* **2011**, *1*, 184; (g) G. Wei, R. R. Lunt, K. Sun, S. Wang, M. E. Thompson, S. R. Forrest, *Nano Lett.* **2009**, *3*, 627; (h) T. A. Bull, L. S. C. Pingree, S. A. Jenekhe, D. S. Ginger, C. K. Luscombe, *ACS Nano*, **2009**, *3*, 627.

[54] (a) R. D. Kennedy, A. L. Ayzner, D. D. Wanger, C. T. Day, M. Halim, S. I. Khan, S. H. Tolbert, B. J. Schwartz, Y. Rubin, *J. Am. Chem. Soc.* **2008**, *130*, 17290; (b) C. J. Tassone, A. L. Ayzner, R. D. Kennedy, M. Halim, M. So, Y. Rubin, S. H. Tolbert, B. J. Schwartz, *J. Phys. Chem. C.* **2011**, *115*, 22563.

[55] (a) N. C. Cates, R. Gysel, Z. Beiley, C. E. Miller, M. F. Tonet, M. Heeney, I. McCulloch, M. D. McGehee, *Nano Lett.* **2009**, *9*, 4153; (b) C. Bruner, N. C. Miller, M. D. McGehee, R. H. Dauskardt, *Adv. Funct. Mater.* **2013**, *23*, 2863; (c) N. C. Miller, S. Sweetnam, E. T. Hoke, R. Gysel, C. E. Miller, J. A. Barlet, X. Xie, M. F. Toney, M. D. McGehee, *Nano Lett.* **2012**, *12*, 1566.

[56] (a) K. H. Lam, T. R. B. Foong, Z. E. Ooi, J. Zhang, A. C. Grimsdale, Y. M. Lam, *ACS Appl. Mater. Interfaces,* **2013**, *5*, 13265; (b) B. M. Schulze, N. T. Shewmon, J. Zhang, D. L. Watkins, J. P. Mudrick, W. Cao, R. B. Zerdan, A. J. Quartararo, I. Ghiviringa, J. Xue, R. K. Castellano, *J. Mater. Chem. A*. **2014**, *2*, 1541; (c) A. Ruiz-Carretero, T. Aytun, C. J. Bruns, C. J. Newcomb, W. W. Tsai, S. I. Stupp, *J. Mater. Chem. A.* **2013**, *1*, 11674; (d) C. H. Huang, N. D. McClenaghan, A. Kuhn, J. W. Hofstraat, D. M. Bassani, *Org. Lett*. **2005**, *7*, 3409.

[57] (a) S. J Kang, J. B. Kim, C. Y. Chiu, S. Ahn, T. Schiros, S. S. Lee, K. G. Yager, M. F. Toney, Y. L. Loo, C. Nuckolls, *Angew. Chem. Int. Ed.* **2012**, *51*, 8594; (b) S. J. Kang, S. Ahn, J. B. Kim, C. Schenck, A. M. Hiszpanski, S. Oh, T. Schiros, Y. L. Loo, C. Nuckolls, *J. Am. Chem. Soc.* **2013**, *135*, 2207.

[58] (a) E. M. Pérez, N. Martín, *Chem. Soc. Rev.* **2008**, *37*, 1512; (b) M. Gallego, J. Calbo, J. Aragó, R. M. K. Calderón, F. H. Líquido, A. Iwamoto, A. K. Greene, E. A. Jackson, E. M. Pérez, E. Ortí, D. M. Guldi, L. T. Scott, N. Martín, *Angew. Chem. Int. Ed.* **2014**, *53*, 2170.

introduction of these dithiole rings in an all-*cis* configuration leads to a deviation from planarity of the truxene core, which adopts bowl-shape geometry. Its relatively large concave aromatic surface allows for the self-assembly with fullerenes with binding constants (K_a) in the range of 10^4 M^{-1}.[40] Recently, a new truxTTF-like derivative truxTTF-CO was synthesized; truxTTF-CO shows enhaced absorption properties, compared to truxTTF, while retaining the ability to bind with C_{60}, albeit with a significantly lower binding constant (K_a = 10^3 M^{-1}). The truxTTF-CO exhibits a push-pull structure where one dithiole ring is substituted for a weak electron-withdrawing carbonyl group. As a consequence, a new bathocromically shifted intramolecular charge-transfer band is observed in its electronic absorption spectrum, which expands to ca. 650 nm.

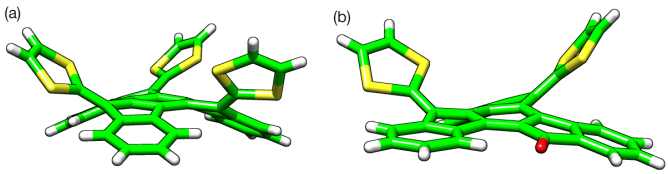

Figure 4.36. (a) X-ray crystal structure of truxTTF and (b) X-ray crystal structure of truxTTF-CO. Carbon atoms are shown in green sulfur in yellow and oxygen in red.

This represents a significant enhancement of the spectral light absorption of truxTTF-CO with respect to truxTTF.

We have also synthesized a new truxTTF derivative in which three hydrogen atoms of the truxene core are substituted by three fluorine atoms, the truxTTF-3F (**96**). To do so, we synthesized the 4,9,14-trifluorotruxenone (Scheme 4.9) by the methodology described by Petschek and co-workers,[26] and then we attached three dithiole units to the core by the methodology reported by N. Martín and co-workers for truxenones.[40]

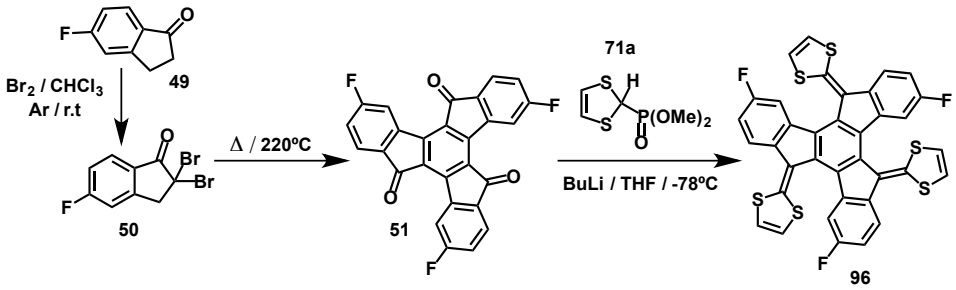

Scheme 4.9. Synthesis of truxTTF-3F (**96**).

The truxTTF-3F ability to bind C_{60} in solution was confirmed by three independent titrations of C_{60} with truxTTF-3F in toluene at 298 K. Thus, to a solution of **96** in toluene (0.32 mM) aliquots of a C_{60} solution (1.47 mM) were added working at constant concentration of the host. The truxTTF-3F showed a binding constant of log K_a = 3.7 ± 0.5 towards C_{60}, similar to the one obtained for the truxTTF-C_{60} system.[40]

The spectral features show that increasing the concentration of C_{60} decreases the absorption of **96** at 454 nm, which occurs together with the appearance of a new band centered at 560 nm and an isosbestic point at 497 nm due to the formation of the complex truxTTF-3F•C_{60} (Figure 4.37).

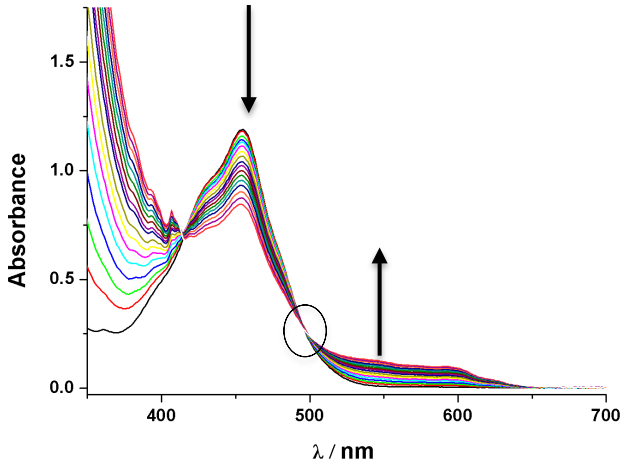

Figure 4.37. Spectral changes in a UV/vis titration experiment for truxTTF-3F *vs* C_{60} in toluene at 298 K.

Spectroscopic light absorption features and the ability to bind fullerenes in

solution make truxTTF, truxTTF-3F and truxTTF-CO ideal candidates to investigate the relative importance of morphology *vs* light absorption on the efficiency of OSCs.

When using an electron acceptor with limited absorption properties, such as $PC_{61}BM$, morphology is a very important parameter to control. The stronger interactions (π-π, charge transfer and van der Waals interactions) between the concave face of the truxTTF and the convex face of the $PC_{61}BM$ could eventually lead to a better self-organization of the photoactive layer. These interactions between the donor and the acceptor are even stronger when using larger fullerene cages, such as $PC_{71}BM$, which could promote a more successful formation of the supramolecular complex.

Herein, we demonstrate that, at least for our particular systems, morphology of the photoactive layer plays a more important role in determining the PCE than the corresponding light absorbance.

Unfortunately, the truxTTF-3F is invalid for constructing these devices. The truxTTF-3F was not able to form a thin film of few nm either with [61]PCBM or [71]PCBM.

Figure 4.38 shows optical absorption spectra of truxTTF and truxTTF-CO in dilute $CHCl_3$ solution and for spin-coated thin films. In solution, truxTTF-CO absorbs over a wider spectral range (300-655 nm) than truxTTF. TruxTTF-CO exhibits maximum absorption band (λ_{max}) at 400 nm and an intramolecular charge transfer (CT) band with a low absorption at 550 nm, which is originated from transitions from the dithiole rings to the carbonyl group.[40] On the other hand, truxTTF displays a sharper absorption peak centered at 449 nm, reflecting the lack of an intramolecular push-pull effect and loss of planarity. In the solid state, truxTTF and truxTTF-CO show broader absorptions, compared with those in solid solution, extending the absorption to 618 and 677 nm, for truxTTF and truxTTF-CO, respectively. Although not as pronounced as in solution, truxTTF-CO still absorbs over a wider spectral range in thin films.

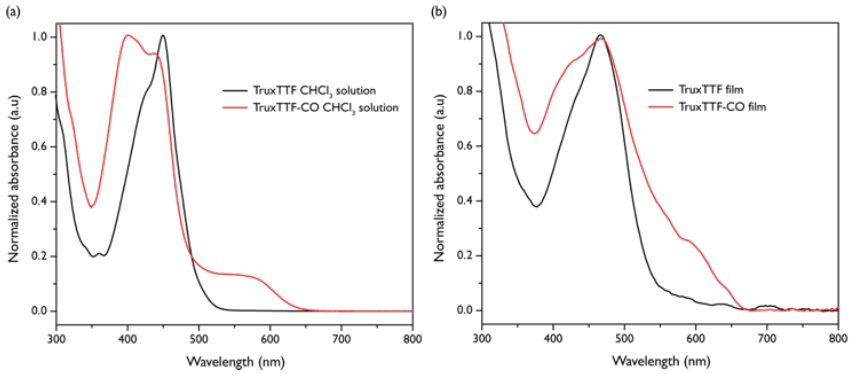

Figure 4.38. UV/vis absortion spectra of truxTTF and truxTTF-CO in (a) diluted chloroform solution and in (b) thin films.

Based on previous DFT calculations, HOMO and LUMO levels for truxTTF are located at -4.72 and -1.48 eV, respectively. TruxTTF-CO exhibits a lower band gap than truxTTF, due to the lack of one 1,3-dithiole ring. This fact leads to a deeper HOMO level (-4.46 eV), which should lead to an enhancement in the V_{oc} (Figure 4.39).[40]

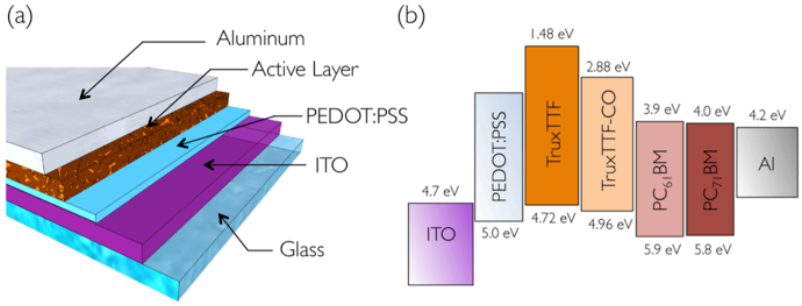

Figure 4.39. (a) Device structure of the conventional sandwich solar cells (ITO/PEDOT:PSS/Active layer/Al) and (b) energy-level diagram of the device.

To explore the properties of truxTTF and truxTTF-CO in photovoltaic devices, solar cells were fabricated using the conventional sandwich structure of ITO/PEDOT:PSS/Donor:Acceptor/Al or Ca/Al by using a varying weight ratio of the donor:$PC_{61}BM$ from 1:2 to 1:6 in a chlorobenzene:*ortho*-dichlorobenzene (3:1) mixture. These experiments were performed under an ambient atmosphere employing AM 1.5G simulated illumination in an intensity of 100

mW cm^{-2}. The current density-voltage (*J-V*) characteristics and the external quantum efficiency (EQE) for the conventional device architecture ITO/PEDOT/active layer/Al are shown in Figure 4.40 (a-d) and the performance parameters are summarized in table 4.2 as a function of the weight ratios of donor:$PC_{61}BM$.

Table 4.2. Device performance parameters of the devices fabricated with truxTTF and truxTTF-CO blended with $PC_{61}BM$.

Active layer	V_{OC} (V)	J_{SC} (mA cm^{-2})	FF (%)	PCE [Highest](%)
truxTTF:$PC_{61}BM$ (1:6)	0.53±0.03	4.34±0.21	30.1±0.21	0.69±0.1 [0.72]
truxTTF:$PC_{61}BM$ (1:4)	0.57±0.01	4.42±0.17	30.2±0.19	0.76±0.1 [0.80]
truxTTF:$PC_{61}BM$ (1:2)	0.63±0.02	4.28±0.10	31.2±0.11	0.81±0.1 [0.92]
truxTTF-CO:$PC_{61}BM$ (1:6)	0.40±0.01	3.13±0.11	28.1±0.18	0.34±0.04 [0.36]
truxTTF-CO:$PC_{61}BM$ (1:4)	0.50±0.02	3.24±0.21	28.7±0.26	0.47±0.1 [0.56]
truxTTF-CO:$PC_{61}BM$ (1:2)	0.50±0.02	3.31±0.23	27.7±0.18	0.44±0.04 [0.47]

It is important to note that the D/A ratio strongly affects the V_{OC}, which can be attributed to a more effective supramolecular complexation (lower association constants were obtained using $PC_{61}BM$), but only slightly affects the fill factor (FF) and the short-circuit current density (J_{SC}). A photovoltaic device using truxTTF as a donor yielded an average power conversion efficiency of 0.81%, with a V_{OC} of 0.63 V, a short-circuit current density (J_{SC}) of 4.28 mA cm^{-2} and a FF of 31.2%. Average values were taken from 10 devices. In addition, the overall efficiency and the V_{OC} decreased upon further increasing of the $PC_{61}BM$ ratio, but the FF and the J_{SC} remained almost constant. On the other hand, the devices with a blend of the truxTTF-CO:$PC_{61}BM$ exhibited a PCE of 0.56%, with J_{SC} of 3.5 mA/cm^2 and with significantly lower FF values than those observed for truxTTF (28.7%), which is indicative of an unfavorable morphology of the active layer.

The external quantum efficiency (EQE) curves for devices based on different donor/acceptor (D/A) ratios, displayed in Figure 4.40(b), were investigated under monochromatic light. Both donor systems when blended with $PC_{61}BM$ exhibited a narrow spectral response, ranging from 300 to 700 nm. The devices

containing truxTTF and $PC_{61}BM$ exhibited EQEs of 43% and 36% at 343 and 459 nm, respectively. The former corresponds to the photocurrent arising from the truxTTF. On the other hand, devices incorporating a blend of truxTTF-CO:$PC_{61}BM$ exhibited a broader but lower intensity photoresponse with a shoulder at 594 nm, due to the broader light-harvesting abilities of the truxTTF-CO. The higher EQE values obtained for truxTTF indicate a better capacity to dissociate excitons and extract charge carriers than truxTTF-CO, which suggest a better morphological arrangement in the former. The J_{sc} obtained from the *J-V* measurements and the integrated current densities from the EQEs are in good agreement, within ± 5%.

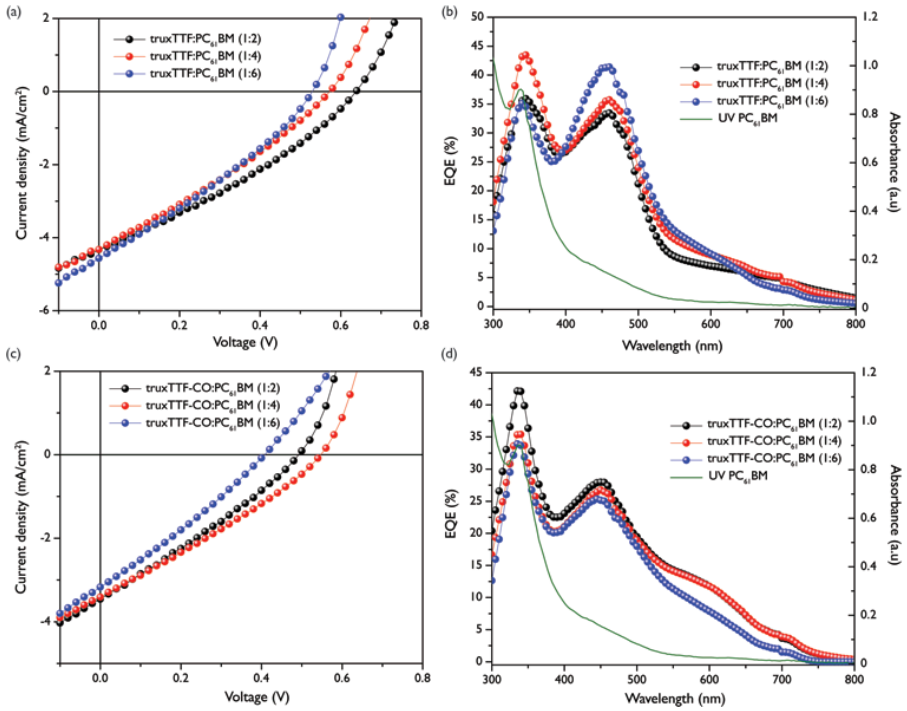

Figure 4.40. (a) Current density-voltage (*J-V*) curves of the blend truxTTF:$OC_{61}BM$, (b) EQE plots for the devices derived from truxTTF:$PC_{61}BM$ at different w/w ratio, (c) current density-voltage (*J-V*) curves of the blend truxTTF-CO-$PC_{61}BM$ and (d) EQE plots for the devices derived from truxTTF-CO:$PC_{61}BM$ at different w/w ratio.

To further explore the photovoltaic performances of truxTTF and truxTTF-CO donor compounds, solar cells were investigated with a different electron acceptor, namely $PC_{71}BM$ (Figure 4.41, table 4.3). It is known that the $PC_{61}BM$

absorbs over a narrower range and has a lower extinction coefficient than $PC_{71}BM$ in the visible region. In thin film, $PC_{71}BM$ displays a broad absorption from 300 to 750 nm, whereas $PC_{61}BM$ has limited photo-response in the same region.

Table 4.3. Device performance parameters of the devices fabricated with truxTTF and truxTTF-CO blended with $PC_{71}BM$.

Active layer	V_{OC} (V)	J_{SC}(mA cm^{-2})	FF (%)	PCE [Highest](%)
truxTTF:$PC_{71}BM$ (1:8)	0.55±0.01	4.81±0.37	29.8±0.17	0.80±0.1 [0.89]
truxTTF:$PC_{71}BM$ (1:6)	0.60±0.03	8.11±0.22	33.1±0.28	1.61±0.1 [1.77]
truxTTF:$PC_{71}BM$ (1:4)	0.53±0.01	6.38±0.12	31.9±0.24	1.07±0.1 [1.15]
truxTTF:$PC_{71}BM$ (1:2)	0.58±0.02	4.87±0.10	30.8±0.11	0.83±0.1 [0.88]
truxTTF-CO:$PC_{71}BM$ (1:6)	0.51±0.01	1.49±0.14	26.3±0.15	0.2±0.02 [0.22]
truxTTF-CO:$PC_{71}BM$ (1:4)	0.61±0.02	5.78±0.31	30.2±0.22	1.06±0.1 [1.19]
truxTTF-CO:$PC_{71}BM$ (1:2)	0.56±0.02	3.82±0.25	29.0±0.21	0.62±0.04 [0.68]

Photovoltaic devices incorporating truxTTF exhibited a higher power conversion efficiency for a blend ratio 1:6 w/w, with an V_{OC} of 0.6 V, a short-circuit current (J_{SC}) of 8.11 mA cm^{-2} and a maximum PCE of 1.77% which corresponds to an improvement of almost 100% with respect to those devices containing $PC_{61}BM$ as the electron acceptor.

When the D/A ratio was adjusted from 1:2 to 1:6, the J_{SC} increased from 4.87 to 8.11 mA cm^{-2} and the FF increases from 30.8 to 33.1. This experimental finding could be explained in terms of aggregation of truxTTF molecules when the amount of the donor increases, which results in the formation of larger domains of truxTTF, and therefore unsuccessful creation of the supramolecular complex. In contrast, the best photovoltaic performance for truxTTF-CO was provided by the blend with a 1:4 w/w ratio (average PCE 1.06%, maximum of 1.19%), with a V_{OC} of 0.61 V, J_{SC} of 5.78 mA cm^{-2} and a FF of 30.2%. The V_{OC} values obtained are consistent with the difference between the donor HOMO and the LUMO of the $PC_{71}BM$ in both cases. Furthermore, the photovoltaic properties were investigated employing the best ratios for each donor molecule,

with the device architecture of ITO/PEDOT:PSS/active layer (ETL) provides a higher built-in potential and a more efficient electron transport and collection process (increasing the FF). As expected, a remarkable improvement of 66 mV in the V_{OC} and more than 3% in the FF was achieved in a blend of truxTTF:$PC_{71}BM$, for a maximum efficiency of 1.77%. Surprisingly, no improvement was observed for the blend containing truxTTF-CO and $PC_{71}BM$ (1:4 w/w).

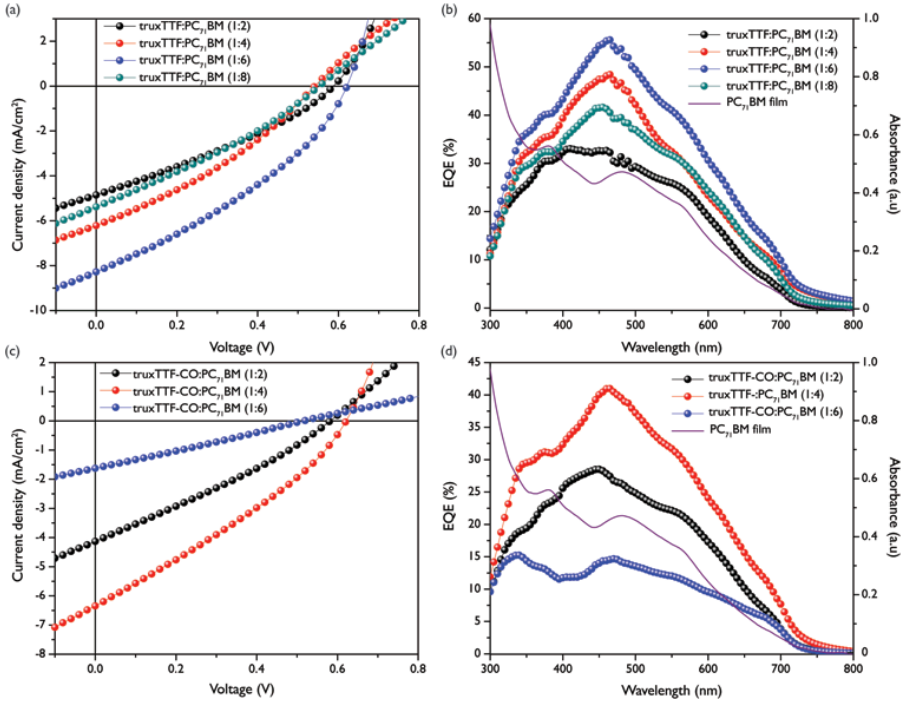

Figure 4.41. (a) Current density-voltage (*J-V*) curves of the blend truxTTF:$PC_{71}BM$, (b) EQE plots for the devices derived from truxTTF:$PC_{71}BM$ at different w/w ratio, (c) current density-voltage (*J-V*) curves of the blend truxTTF-CO: $PC_{71}BM$ and (d) EQE plots for the devices derived from truxTTF-CO: $PC_{71}BM$ at different w/w ratio.

The study in solution of the formation of the complexes truxTTF•$PC_{61}BM$ and truxTTF•$PC_{71}BM$ by UV/vis titrations, revealed binding values of log K_a = 3.10 ± 0.08 ($CHCl_3$, r.t) and log K_a = 3.44 ± 0.03 (PhCl, r.t) for truxTTF•$PC_{61}BM$ and log K_a = 4.8 ± 0.4 ($CHCl_3$, r.t) and log K_a= 4.1 ± 0.8 (PhCl, r.t) for truxTTF•$PC_{71}BM$. These values are in agreement with the better result obtained for the devices fabricated with $PC_{71}BM$.

In Figure 4.42 we can observe the spectroscopic changes in the UV/vis spectra of truxTTF (1.15 x 10^{-4} M) upon addition of $PC_{61}BM$ (4.9 x 10^{-4} M), (Figure 4.42a) or $PC_{71}BM$ (4.37 x 10^{-4} M), (Figure 4.42b) in chlorobenzene at room temperature. We observed a decrease in the intensity of the truxTTF absorption band at λ = 450 nm, accompanied by the increase of a broad band in the 500-600 nm region and the formation of a well defined isosbestic point at 490 nm for the truxTTF•$PC_{61}BM$ and 475 nm for the truxTTF•$PC_{71}BM$. These spectral changes are analogous to those found in the titration of truxTTF vs. C_{60} and C_{70}.[40]

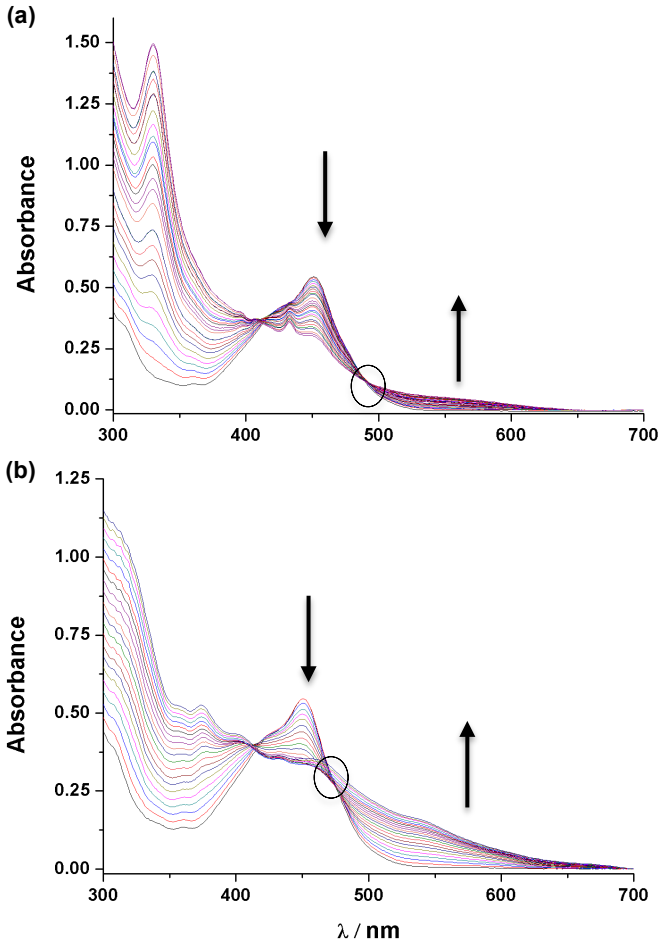

Figure 4.42. UV/vis spectra as obtained during the titration of (a) truxTTF (1.15 x 10^{-4} M) with $PC_{61}BM$ (4.9 x 10^{-4} M) and (b) truxTTF (1.15 x 10^{-4} M) with $PC_{71}BM$ (4.37 x 10^{-4} M), in chlorobenzene at room temperature. Each addition corresponds to 0.1 equiv.

It is important to emphasize that the FF was higher when truxTTF was used as electron donor. The FF is known to depend heavily on morphology/charge-recombination, [59] so this fact can safely be attributed to the stronger interactions between truxTTF and $PC_{71}BM$, which seems to allow a more favorable morphology of the active layer, when compared to truxTTF-CO.

Figure 4.41b shows the external quantum efficiency (EQE) curves for those devices based on varying D/A ratios. Both spectra of donor units blended with $PC_{71}BM$ exhibited a broader spectral response that those with $PC_{61}BM$, ranging from 300 to 750 nm, whereas the mixture of truxTTF:$PC_{71}BM$ at 1:6 w/w ratio reached the highest value of EQE (55%) at 463 nm. When the donor ratio decreases to 1:4 or 1:6, the contribution to the EQE is mainly from $PC_{71}BM$, but when the ratio is increased to 1:2 the contribution of the donor is similar to the contribution of the $PC_{71}BM$. For the blend based on truxeneTTF/ $PC_{71}BM$ (1:6 w/w), the higher experimental J_{SC} values were 8.31 mA cm^{-2}. The corresponding devices containing truxTTF-CO:$PC_{71}BM$ gave a lower EQE (41% at 460 nm for 1:4 ratio), which confirms a less favorable morphology of the active layer.

The active layer morphologies incorporating truxTTF and truxTTF-CO were characterized by atomic force microscopy (AFM) in tapping mode, as shown in Figure 4.43, to confirm that the former leads to a more favorable morphology of the active layer.

The surface topographies of truxTTF:$PC_{61}BM$ (1:6) and truxTTF:$PC_{71}BM$ blend films exhibit evenly distributed nanometer-sized features with a root-mean-square roughness (rms) value of 0.33 nm and 0.31 nm, respectively, indicating good miscibility of the donor unit with $PC_{61}BM$ or $PC_{71}BM$. In addition, the truxTTF: $PC_{71}BM$ reveals the formation of more grains with thinner morphological features (10-30 nm), measured from cross-sectional profiles, which is beneficial for exciton dissociation and charge transport.[60]

[59] (a) V. D. Mihailetchi, H. X. Xie, B. de Boer, L. J. A. Koster, P. W. M. Blom, *Adv. Funct. Mater.* **2006**, *16*, 699; (b) B. Qui, J. Wang, *Phys. Chem. Chem. Phys.* **2013**, *15*, 8972; (c) D. Gupta, S. Mukhopadhyay, K. S. Narayan, *Sol. Energy. Mater. Sol. Cells,* **2010***, 94*, 1309; (d) G. Li, R. Zhu, Y. Yang, *Nature Photonics*, **2012**, *6*, 153.

[60] (a) C. R. McNeill, S. Westenhoff, C. Groves, R. h. Friend, N. C. Greenham, *J. Phys. Chem. C.* **2007**, *111*, 19153; (b) Y. Yao, J. Hou, Z. Xu, G. Li, Y. Yang, *Adv. Funct. Mater.* **2008**, *18*, 1783.

The blends containing truxTTF-CO blended with $PC_{61}BM$ and $PC_{71}BM$ display featureless and slightly coarser topographies, with higher root mean square (rms) values of 0.47 nm and 0.43 nm, respectively. These results suggest that truxTTF may form a better interpenetrating network with the fullerene acceptors than truxTTF-CO (Figure 4.23(e-h)). These experimental findings can be accounted for its larger concave aromatic surface and higher binding constants with the fullerene derivatives, which lead to a better self-assembly, a more favorable morphology of the active layer and to enhance device performance.

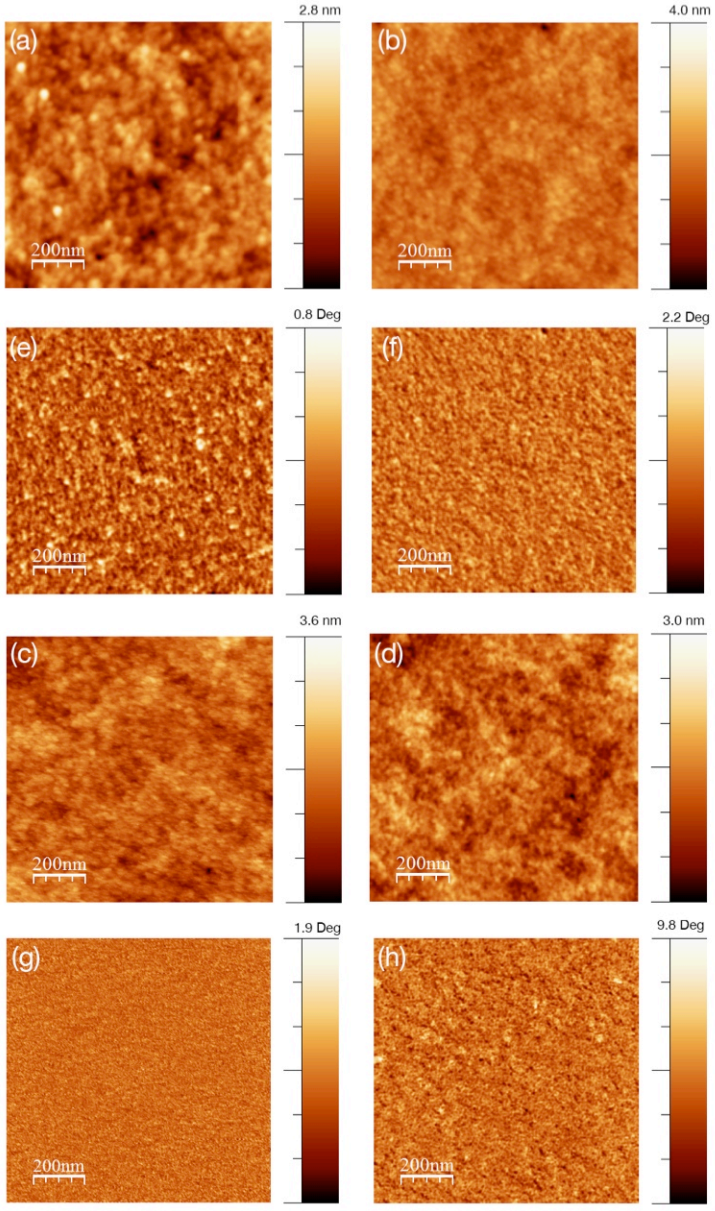

Figure 4.43. Tapping mode AFM height and phase images (1μm x 1 μm) of blends films spin-coated from chlorobenxene:*ortho*dichlorobenzene of (a and e) truxTTF:$PC_{61}BM$ (1:6), (b and f) truxTTF:$PC_{71}BM$ (1:6), (c and g) truxTTF-CO:$PC_{61}BM$ (1:4) and (d and h) truxTTF-CO:$PC_{71}BM$ (1:4).

In conclusion, a less-explored supramolecular approach has been used for the preparation of efficient small-molecule solar cells. The highest PCE based on a truxTTF was 1.77% while incorporating truxTTF-CO yielded 1.19%. Although, both of them posess similar bowl-shape geometries that allow the formation of supramolecular complexes when blended with $PC_{61}BM$ or $PC_{71}BM$, they show different binding constants with fullerenes and also different optical properties. Despite the broader absorption and the deeper HOMO of truxTTF-CO, the stronger non-covalent interactions between the concave shape of the electron donating truxTTF and the surface of the fullerene derivatives lead to higher J_{sc} and FF, attributed to a more favorable morphology of the active layer.

5. Experimental Section

5. EXPERIMENTAL SECTION

5.1. GENERALITIES

All solvents were dried according to standard procedures.[61] Reagents were used as purchased. All air-sensitive reactions were carried out under argon atmosphere. Flash chromatography was performed using silica gel (Merck, Kieselgel 60, 230-240 mesh, or Scharlau 60, 230-240 mesh). Analytical thin layer chromatography (TLC) was performed using aluminium-coated Merck Kieselgel 60 F_{254} plates. Visualization was made by UV light (λ=254 or 365 nm). Microwave reactions were performed in sealed vessels in an Anton Paar Monowave 300 and the reaction mixture temperature was controlled with an external surface sensor. NMR spectra were recorded on a Bruker Avance 300 (^{1}H: 300 MHz; ^{13}C: 75 MHz) a Bruker Avance 500 (^{1}H: 500 MHz; ^{13}C: 125 MHz) or a Bruker AvanceIII 700 (^{1}H: 700 MHz; ^{13}C 175 MHz) spectrometers at 298 K, using partially deuterated solvents as internal standards. Coupling constants (J) are denoted in Hz and chemical shifts (d) in ppm. Multiplicities are denoted as follows: s = singlet, d = doublet, t = triplet, m = multiplet, b = broad. Matrix assisted Laser desorption ionization (coupled to a Time-of-Flight analyzer) experiments (MALDI-TOF) were recorded on a HP1100MSD spectrometer and a Bruker REFLEX spectrometer. UV/vis spectra were recorded with a Simadzu Spectrophotometer UV-3600 at 298K or with a Varian Cary 50 at 298K.

5.2. SYNTHESYS OF COMPOUNDS

Synthesis of 4, 9, 14-tribromotruxenone (75)[26]

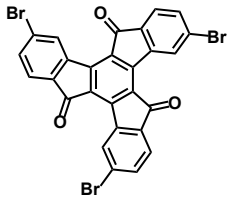

To a solution of commercial 5-bromoindanone (5 g, 23.7 mmol) in 50 mL of $CHCl_3$, 3mL of bromine (9 g, 56 mmol) diluted in 5 mL of $CHCl_3$ are added drop-

[61] D. D. Perrin, I. F. Amariego, D. R. Perrin, Purification of laboratory Chemicals, Pergamon Press, Oxford, **1980**.

wise. After stirring for 2 h, excess Br_2 was removed bubbling argon through the solution. The solvent was removed in vacuum. The crude was placed in a round-bottom flask on a heating system at 220 °C and it was stirred until gas evolution cessed. After cooling, the dark brown residue was treated with methylene chloride, filtered and washed with methylene chloride to yield a brown solid (1.04 g, 7%).

FT-IR (KBR) 1712 cm^{-1}.

Synthesis of compound 80

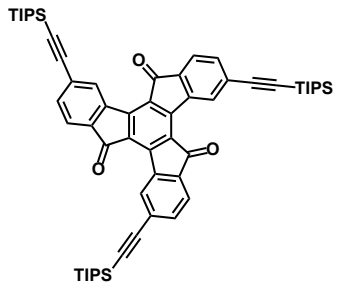

A dispersion of **75** (100 mg, 0.16 mmol), (triisopropylsilyl)acetylene (227.44 g, 1.28 mmol), tetrakis(triphenylphosphine)palladium(0) (36 mg, 20% mmol), CuI (4.57 mg, 15% mmol), and dry triethylamine (0.29 mL, 1.28 mmol) is stirred under argon refluxing for 3 hours in 5 mL of dry THF. Then the solvent was removed under reduced pressure and the brownish reaction crude is dispersed in aqueous NH_4Cl and extracted with dichloromethane. The organic phase was washed with brine and water, and finally dried over $MgSO_4$ and filtered. After evaporation of the solvents under reduced pressure, the crude is purified by column chromatography (SiO_2, hexane/dichloromethane 2:1), to afford 60 mg of **80**, yellow solid (40%).

FT-IR (KBR) 2929, 2862, 2155, 1713 cm^{-1}.

^{1}H NMR (300 MHz, $CDCl_3$, 298 K) δ 9.07 (3H, s), 7.74 (3H, d, J=7.6 Hz), 7.58 (3H, dd, J=7.6 Hz, J=1.1 Hz), 1.24 (63H, m) ppm.

^{13}C NMR (125 MHz, $CDCl_3$, 298 K) δ 190.4, 146.8, 141.1, 136.1, 134.9, 131.7, 130.9, 130.1, 124.1, 106.9, 96.4, 19.2, 11.9 ppm.

MS (MALDI TOF) m/z calcd for $C_{60}H_{72}O_3Si_3$ 924.48, m/z found 924.39.

Synthesis of compound 81

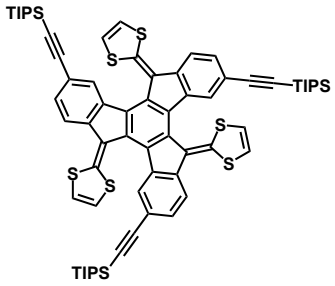

To a solution of dimethyl 1,3-dithiol-2-ylphosphonate 190 mg (0.9 mmol) in dry THF (3 mL) at –78°C BuLi (1.44 mL, 1.6 M in hexane, 0.9 mmol) was added drop-wise. The solution is stirred at –78°C for 25 minutes under argon, and a yellow slurry appears. In the meantime, a suspension of 100 mg (0.1 mmol) of the truxenone precursor **80** in 5 mL of dry THF is dispersed with sonication for *ca.* 30 min. The resulting suspension was added to the phosphorous ylide suspension, and the cooling bath is immediately removed. The mixture is allowed to warm to room temperature and left to stir until no reactant **80** is left. Then methanol is added to the crude of the reaction and solvents are removed under reduced pressure. The crude is purified by column chromatography (SiO_2, hexane/dichloromethane, 1:1) to yield 85 mg of an orange solid, **81** (72%).

FT-IR (KBR) 2924, 2852, 2148 cm^{-1}.

^{1}H NMR (300 MHz, $CDCl_3$, 298 K) δ 7.81 (3H, d, 8.0 Hz), 7.56 (3H, dd, J=8.0 Hz, J=1.23 Hz), 7.31 (3H, d, J=1.23 Hz), 6.75 (6H, m), 1.14 (63H, m) ppm.

^{13}C NMR (125 MHz, $CDCl_3$, 298 K) δ 141.8, 140.1, 136.1, 135.3, 131.3, 129.1, 127.9, 122.4, 121.6, 121.3, 119.2, 118.9, 109.2, 90.3, 19.2, 11.8 ppm.

MS (MALDI TOF) m/z calcd for $C_{69}H_{78}S_6Si_3$ 1182.37, m/z found 1182.34.

X-RAY

Bond precision:	C-C = 0.0103 A	Wavelength=0.71073

Cell:	a=22.781(3)	b=22.781(3)	c=21.448(4)
	alpha=90	beta=90	gamma=120
Temperature:	100 K		

	Calculated	Reported
Volume	9640(4)	9640(3)
Space group	R -3	¿
Hall group	-R 3	¿
Moiety formula	C69 H78 S6 Si3	¿
Sum formula	C69 H78 S6 Si3	C69 H78 S6 Si3
Mr	1183.95	1183.94
Dx,g cm-3	1.224	1.224
Z	6	6
Mu (mm-1)	0.309	0.309
F000	3780.0	3780.0
F000’	3786.92	
h,k,lmax	30,30,28	30,25,27
Nref	5274	4938
Tmin,Tmax	0.932,0.955	
Tmin’	0.931	

Data completeness= 0.936	Theta(max)= 28.210
R(reflections)= 0.1344(3348)	wR2(reflections)= 0.4383(4938)
S = 1.813	Npar= 242

Synthesis of compound 83

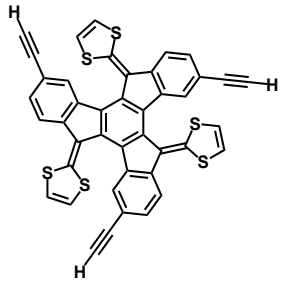

To a solution of **81** (70 mg, 0.06 mmol) in 10 mL of dry THF, 0.9 mL (0.9 mmol) of tetrabutylammonium fluoride solution 1 M in THF were added. The reaction mixture was stirred for 2 hours. After evaporation of the solvents under reduced pressure, the crude was purified by column chromatography (SiO_2, hexane/dichloromethane, 1:1). After purification, 34.2 mg (80%) of **83** were obtained as an orange solid.

FT-IR (KBR) 3291, 2927, 2859, 2358 cm^{-1}.

^{1}H NMR (300 MHz, DMSO) δ 7.86 (d, *J* = 8.0 Hz, 3H), 7.61 (dd, *J* = 8.0 Hz, *J*= 1.4 Hz, 3H), 7.34 (AB, *J* = 6.12 Hz, 6H), 7.09 (d, *J* = 1.4 Hz 3H), 4.17 (s, 3H) ppm.

^{13}C NMR (175 MHz, DMSO-D6, 298K) δ 144.9, 140.7, 135.2, 134.8, 129.9, 129.3, 126.2, 123.0, 122.0, 121.1, 120.2, 117.6, 84.9, 80.9 ppm.

MS (MALDI TOF) m/z calcd for $C_{42}H_{18}S_6$ 713.97, m/z found 713.86.

Synthesis of compound 85

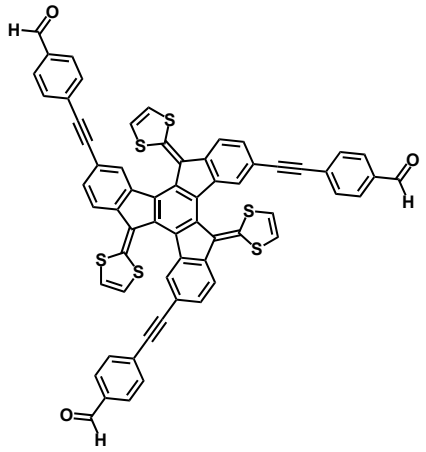

A solution of **83** (34 mg, 0.045 mmol), 4-iodobenzaldehyde (99.7 mg, 0.43 mmol), 0.06 mL of diisopropylamine, CuI (2.4 mg, 25% mmol), and tetrakis(triphenylphosphine)palladium(0) (13 mg, 25% mmol) were stirred under reflux in 20 mL of dry THF. The reaction was followed by thin film chromatography, until **83** was exhausted; the solvents were removed under reduced pressure. Then, the crude was purified by column chromatography (SiO_2, CH_2Cl_2). After purification 31 mg (60%) of **85** were obtained as an orange solid.

^{1}H NMR (300 MHz, $CDCl_3$) δ 10.02 (s, 3H), 7.86 (m, 9H), 7.69 (d, *J* = 8.1 Hz, 6H), 7.62 (dd, *J* = 8.1 Hz, *J*= 1.2 Hz, 3H), 7.32 (d, *J*= 1.2 Hz, 3H), 6.79 (s, 6H) ppm.

^{13}C NMR (125 MHz, $CDCl_3$) δ 191.8, 142.5, 141.5, 136.5, 135.8, 135.6, 132.5, 132.5, 130.5, 130.5, 130.0, 129.8, 128.9, 128.9, 128.1, 127.73 122.5, 122.1, 121.7, 119.1, 118.3, 95.8, 88.9 ppm.

MS (MALDI TOF) m/z calcd for $C_{63}H_{30}O_3S_6$ 1026.05, m/z found 1026.85.

Synthesis of compound 84

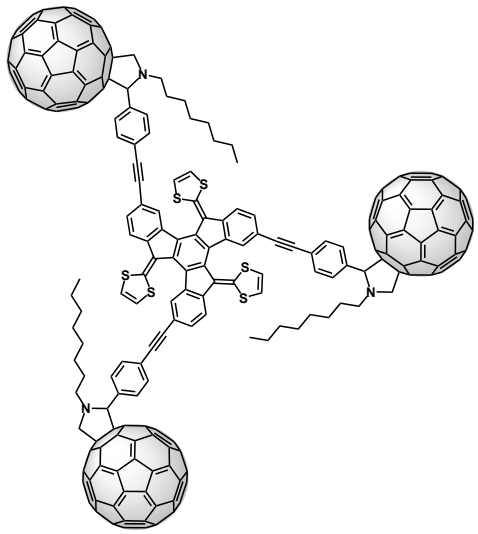

C_{60} (648 mg, 0.15 mmol) and n-octylglycine (320 mg, 1.8 mmol) were sonicated for 30 minutes in 300 mL of toluene at room temperature. Afterwards trialdehyde **85** (150 mg, 0.15 mmol) was added to the flask and the reaction mixture was refluxed until the color of the crude changes from purple to red-wine. The reaction mixture is then cooled down to room temperature and after evaporation of the toluene under reduced pressure, the crude is purified by size exclusion chromatography, BioBeads^{TM} SX-12 as stationary phase and o-DCB as eluent to yield 60 mg of **84** (11% yield) as a black solid.

The elucidation of this compound was done from the NMR characterization of its decomposition product **86**, see Figures 4.20 and 4.21 on pages 71 and 72 respectively. As NMR signals of **84** are broad and not well defined they are not listed here. The most characteristic signals for **86** are listed coming up next.

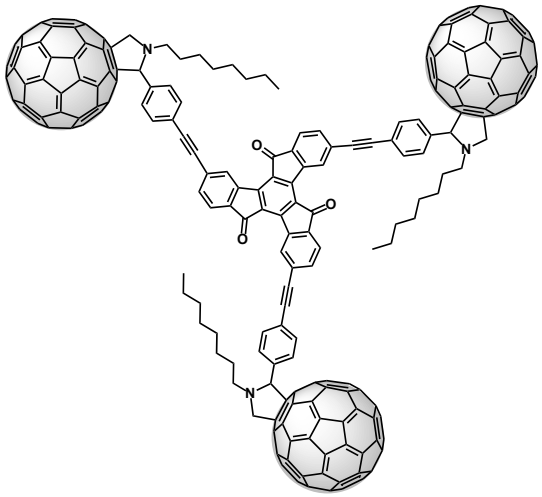

^{1}H NMR (500 MHz, $CDCl_3$) δ 9.23 (s, 3H), 8.06 – 7.79 (m, 6H), 7.68 (m,9H), 7.56 (d, *J* = 7.7 Hz, 3H), 5.17 (d, *J* = 9.3 Hz, 3H), 5.14 (s, 3H), 4.20 (d, *J* = 9.2 Hz, 3H), 3.31 (m, 3H), 2.65 (m, 3H) ppm.

^{13}C NMR (126 MHz, $CDCl_3$) δ 190.1, 156.6, 154.4, 153.6, 153.4, 147.8, 146.9, 146.4, 146.2, 146.1, 145.8, 145.7, 145.2, 144.9, 143.7, 143.5, 143.1, 142.6, 142.6, 142.4, 142.2, 140.8, 140.5, 138.9, 137.4, 137.0, 136.4, 136.2, 135.2, 132.8, 132.0, 131.0, 130.7, 130.2, 129.9, 128.8, 124.3, 123.4, 82.9, 69.3, 32.9, 30.6, 30.3, 29.3, 28.5, 27.9, 23.8, 15.1 ppm.

Synthesis of compound 92

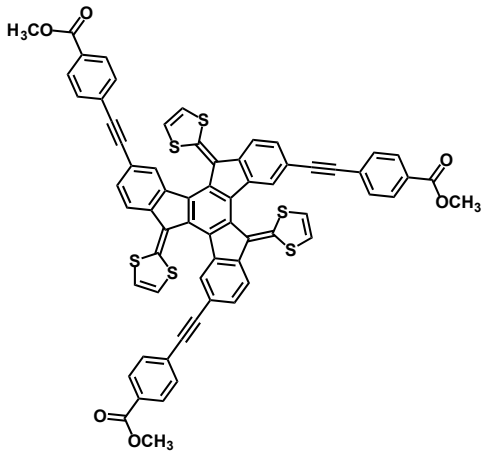

32 mg (0.0448 mmol) of trialkyne-truxTTF derivative **83**, 15.5 mg (30% mmol) of tetrakis(triphenylphosphine)palladium(0), 2.1 mg of CuI (25% mmol), diisopropylamine (6 equivalents), and 106 mg (0.403 mmol) of 4-iodobenzoate are refluxed in 13 mL of dry THF. The reaction is followed by TLC, until **83** is exhausted, the reaction is cooled down at room temperature. After evaporation of the solvents under reduced pressure, the crude is purified by column chromatography (SiO_2, Hx/CH_2Cl_2) to yield 26 mg of a red-orange solid **92** (50% yield).

^{1}H NMR (500 MHz, $CDCl_3$) δ 8.05 (d, *J* = 8.4 Hz, 6H), 7.89 (d, *J* = 7.9 Hz, 3H), 7.66-7.61 (m, 9H), 7.34 (d, *J*=1.1 Hz, 3H), 6.82 (s, 6H), 3.95 (s, 9H) ppm.

^{13}C NMR (126 MHz, $CDCl_3$) δ 167.06, 142.18, 141.37, 136.57, 135.75, 131.89, 129.90, 129.55, 129.74, 128.91, 122.64, 122.10, 121.67, 119.19, 119.04, 118.51, 94.56, 89.82, 88.86, 52.62 ppm.

MS (MALDI TOF) m/z calcd for $C_{63}H_{36}O_6S_6$ 1116.08, m/z found 1116.09.

Synthesis of compound 87

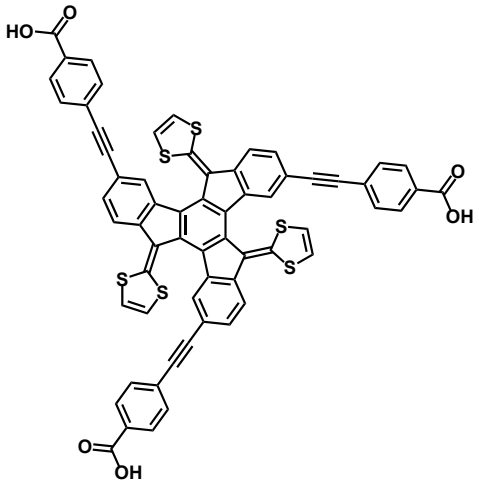

26 mg of **92** (0.02 mmol) are stirred and refluxed in a mixture of THF/$NaOH_{aq}$(1M) 9:1 for 3 h, meanwhile, the reaction is followed by TLC. When **92** is exhausted, the THF is evaporated under reduced pressure and then the crude is dissolved in more water. The aqueous phase is extracted with ethyl acetate and then is acidified dropwise with HCl aq. 1M. The aqueous phase is

extracted with ethyl acetate and the organic phase is washed with brine and then dried over Mg_2SO_4, the solvents are removed under reduced pressure to yield a dark red solid **87** (8.2 mg, 38%).

^{1}H NMR (700 MHz, THF-d_5) δ 8.05 (d, *J* = 8.3 Hz, 6H), 7.94 (d, *J* = 7.9 Hz, 3H), 7.65 (dd, *J* = 7.9, 1.0 Hz, 3H), 7.62 (d, *J* = 8.3 Hz, 6H), 7.38 (d, *J* = 1.0 Hz, 3H), 7.10 (AB, *J* = 6.12 Hz, 6H) ppm.

^{13}C NMR (176 MHz, THF-d_5) δ 166.12, 143.31, 140.92, 136.13, 135.26, 131.11, 130.12, 129.51, 129.28, 128.92, 126.93, 121.63, 121.48, 121.29, 119.13, 118.04, 113.57, 93.53, 88.20 ppm.

MS (MALDI TOF) m/z calc. for $C_{63}H_{30}O_6S_6$ 1074.04, m/z found 1074.03.

Synthesis of compound 88

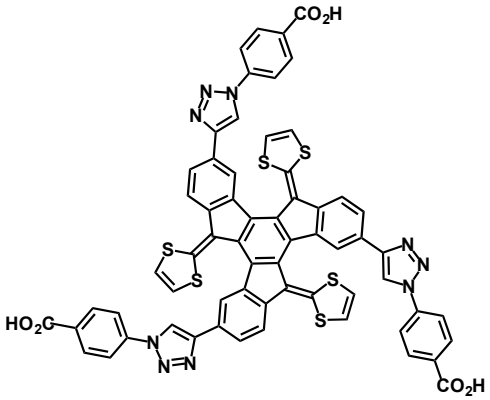

24 mg (0.033 mmol) of **83**, 4-azidobenzoic acid (24.8 mg, 0.152 mmol), CuBr•$S(CH_3)_2$ (5.21 mg, 0.152 MMOL), sodium L-ascorbate (10.54 mg, 0.08 mmol) and Cu metallic, were dispersed in 2 ml of dimethyl sulfoxide and purged with Ar. The reaction was sealed under argon and stirred for 2 days. Then, the crude is dispersed in a mixture of DMSO/ethyl acetate and centrifuged three times for 15 minutes at 6000 rpm. The obtained precipitate was washed with water and dichloromethane to yield a dark red solid (26 mg, 65%) (**88**), that needs no further purification.

^{1}H NMR (700 MHz, DMSO-d_6) δ 9.37 (s, 3H), 8.13 (d, *J* = 7.7 Hz, 6H), 8.10 – 8.04 (m, 6H), 7.99 (d, *J* = 7.7 Hz, 6H), 7.86 (s, 3H), 7.35 (d, *J* = 6.4 Hz, 3H), 7.26 (d, *J* = 6.4 Hz, 3H) ppm.

^{13}C NMR (175 MHz, DMSO-d_6) δ 167.56, 148.45, 143.63, 140.43, 136.12, 134.91, 131.16, 127.15, 126.56, 123.72, 123.41, 122.87, 122.36, 120.81, 120.64, 119.80, 119.57 ppm.

MS (MALDI TOF) m/z calcd for $C_{63}H_{33}N_9O_6S_6$ 1203.09, m/z found 1203.97.

Synthesis of truxenone (3)[26]

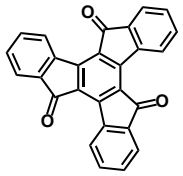

1,3–Indandione (1g, 6.8 mmol) was dissolved in 16 mL of methanesulfonic acid, and the solution was placed in an standard microwave 30 mL vial equipped with a magnetic stirrer bar. This solution was heated to 110 °C in an Anton Paar Monowave 300 microwave synthesis reactor utilizing the “as fast as possible” heating mode with stirring, and a hold temperature time of 5 seconds. The resulting suspension was poured into 10 mL of water and filtered. The solid was successively washed with copious amounts of water and methanol, then recrystallized from propylene carbonate and from picoline, and finally washed with diethyl ether and dried, to obtain 0.5 g (1.3 mmol, 60%) of truxenone.

FT-IR (KBR) 1713 cm^{-1}.

Synthesis of truxTTF (70a)[38,40]

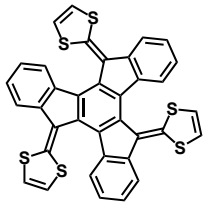

To a solution of dimethyl 1,3-dithiol-2-ylphosphonate 2.48 g (11.7 mmol) in dry THF (10 mL) at –78 °C, BuLi (4.68 mL, 2.5 M in hexane, 11.7 mmol) is added

drop-wise. The solution is stirred at –78 °C for 25 minutes under argon, and a yellow slurry appears. In the meantime, a suspension of 500 mg (1.3 mmol) of the truxenone precursor **3** in 15 mL of dry THF is dispersed with sonication for *ca.* 30 min. The resulting suspension was added to the phosphorous ylide suspension, and the cooling bath is immediately removed. The mixture is allowed to warm to room temperature and left stirring for 3 hours. Then methanol is added to the crude of the reaction and solvents are removed under reduced pressure. The crude is purified by column chromatography (SiO_2, hexane/dichloromethane, 1:1) to yield 425 mg of a red solid, **70a** (74%).

^{1}H NMR (300 MHz, $CDCl_3$) δ 7.77 (d, *J* = 7.3 Hz, 3H), 7.36 (t, *J* = 6.8 Hz, 3H), 7.29 (t, *J* = 6.8 Hz, 3H), 7.16 (d, *J* = 7.3 Hz, 3H), 6.63 (s, 6H) ppm.

General procedure for the synthesis of compounds 89 and 90

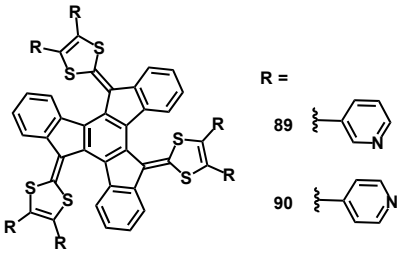

A suspension of palladium (II) acetate (12.57 mg, 0.06 mmol), tri-*tert*-butylphosphonium tetrafluoroborate (68.98 mg, 0.22 mmol) and cesium carbonate (546 mg, 1.4 mmol) in dry degased dioxane (5mL) is heated at 80°C for ten minutes. To this suspension a degased solution of truxTTF (**70a**) (120 mg, 0.19 mmol) and the corresponding iodo-pyridine (287 mg, 1.4 mmol) in 10 mL of dioxane, is added dropwise. The reaction was stirred under reflux for 48 hours. After cooling and evaporation of the solvents under reduced pressure, the crude is dispersed in a pyridine/dichloromethane mixture (1:10). The organic phase is washed with water and brine and then dried over Mg_2SO_4. The solvents are removed under reduced pressure and the purification is done by column chromatography on silica gel with an increasing polarity from methylene chloride and hexane (3:1), methylene chloride and methylene chloride and pyridine (10:1) as eluents. After purification, the desired products are obtained as orange solids in 49% yield for **89** and 52% for **90**.

Characterization of **89**:

^{1}H NMR (300 MHz, CD_2Cl_2) δ 8.56 (bs, 3H), 8.46 (d, *J* = 4.7 Hz, 3H), 8.36 (bs, 3H), 7.88 – 7.81 (m, 3H), 7.67 (d, *J* = 8.0 Hz, 3H), 7.53 – 7.41 (m, 12H), 7.30 (dd, *J* = 7.9, 4.9 Hz, 3H), 7.16 (dd, *J* = 7.8, 4.8 Hz, 3H) ppm.

^{13}C NMR (175 MHz, $CDCl_3$) δ 149.94, 149.89, 140.80, 136.67, 136.61, 136.48, 134.60, 133.45, 129.76, 129.56, 127.76, 127.53, 126.66, 126.53, 126.16, 125.12, 124.19, 123.63, 123.55, 122.45 ppm.

MS (MALDI TOF) m/z calcd for $C_{66}H_{36}N_6S_6$ 1104.13, m/z found 1104.04.

Characterization of **90**:

^{1}H NMR (300 MHz, $CDCl_3$) δ 8.61 (d, *J* = 4.9 Hz, 6 H), 8.47 (d, *J* = 5.0 Hz, 6 H), 7.80 (d, *J* = 3.4 Hz, 3 H), 7.52 – 7.45 (m, 6 H), 7.39 (d, *J* = 3.2 Hz, 3 H), 7.20 (d, *J* = 4.9 Hz, 6 H), 6.98 (d, *J* = 5.0 Hz, 6 H) ppm.

^{13}C NMR (175 MHz, $CDCl_3$) δ 150.70, 150.56, 140.76, 138.97, 138.74, 136.41, 134.52, 132.71, 132.45, 131.17, 130.91, 129.93, 128.82, 128.26, 126.70, 126.34, 125.29, 124.36, 123.37, 123.32, 122.52 ppm.

MS (MALDI TOF) m/z calc for $C_{66}H_{36}N_6S_6$ 1104.13, m/z found 1104.04.

Synthesis of compound 93

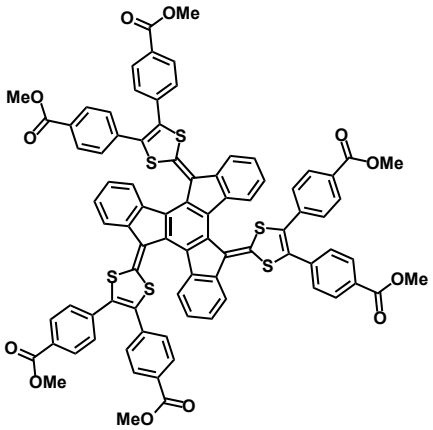

A suspension of palladium (II) acetate (8.38 mg, 0.04 mmol), tri-*tert*-butylphosphonium tetrafluoroborate (43.2 mg, 0.14 mmol) and cesium

carbonate (293.23 mg, 0.9 mmol) in dry degased dioxane (5mL) is heated at 80°C for ten minutes. To this suspension, a degased solution of truxTTF (**70a**) (80 mg, 0.12 mmol) and methyl 4-iodobenzoate (244 mg, 0.93 mmol) in 10 mL of dioxane, is added dropwise. The reaction was stirred under reflux for 48 hours. After cooling and evaporation of the solvents under reduced pressure, the crude is dissolved in ethyl acetate/water mixture. The organic phase is washed with water and brine and then dried over Mg_2SO_4. The solvents are removed by evaporation under reduced pressure and the purification is done by column chromatography on silica gel with methylene chloride and methylene chloride/ethyl acetate (1:1) as eluents to give compound **93** (85 mg, 47%) as an orange solid.

FT-IR (KBr) 2924, 2853, 1725, 1604, 1509, 1436, 1278, 1108, 760 cm^{-1}.

^{1}H NMR (700 MHz, $CDCl_3$) δ 7.96 (d, *J* = 8.9 Hz, 6H), 7.85 – 7.79 (m, 9H), 7.49 – 7.41 (m, *J* =, 9H), 7.37 (d, *J* = 7.9 Hz, 6H), 7.15 (d, *J* = 7.9 Hz, 6H), 3.94 (s, 9H), 3.87 (s, 9H) ppm.

^{13}C NMR (175 MHz, $CDCl_3$) δ 166.31, 166.20, 140.87, 136.49, 136.11, 135.83, 134.61, 133.95, 131.74, 130.25, 130.21, 130.08, 129.97, 129.52, 129.35, 128.65, 126.67, 125.96, 124.89, 123.63, 122.35, 52.34, 52.26 ppm.

MS (MALDI TOF) m/z calcd for $C_{84}H_{54}0_{12}S_6$ 1446.19, m/z found 1446.74.

Synthesis of compound 91

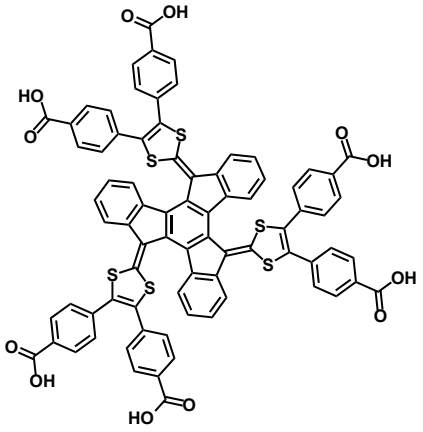

60 mg of **93** (0.04 mmol) are stirred and refluxed in a mixture of THF/$NaOH_{aq}$ (1M) 9:1 overnight. Solvents are evaporated under reduced pressure and then, the crude is dissolved in water. The aqueous phase is extracted with ethyl acetate and then is neutralized dropwise with TFA. The aqueous phase is extracted with ethyl acetate and the organic phase is washed with brine and then dried over Mg_2SO_4. The solvents are removed under reduced pressure under reduced pressure to yield a dark red solid **91** (45 mg, 80%).

FT-IR (KBr) 2925, 2854, 1695, 1606, 1512, 1272, 764 cm^{-1}.

^1H NMR (700 MHz, THF-d_5) δ 8.02 – 7.97 (m, 6H), 7.90 – 7.83 (m, 9H), 7.46 (d, *J* = 7.3 Hz, 15H), 7.24 (d, *J* = 7.4 Hz, 6H) ppm.

^{13}C NMR (175 MHz, THF-d_5) δ 166.01, 165.84, 140.85, 138.81, 136.42, 135.68, 135.42, 134.38, 131.58, 131.17, 130.02, 129.98, 129.44, 129.26, 129.13, 128.75, 126.45, 125.80, 124.56, 123.31, 122.40, 121.15 ppm.

MS (MALDI TOF) m/z calcd for $C_{78}H_{42}O_{12}S_6$ 1362.10, m/z found 1362.15.

Synthesis of compound truxTTF-CO (73)[40]

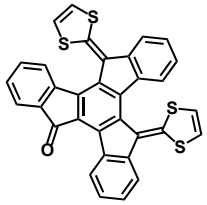

A solution of dimethyl 1,3-dithiol-2-ylphosphonate (200 mg, 0.9 mmol) in 2.5 mL of dry THF was cooled to –78 °C under argon. Then BuLi (0.6 mL, 1.6 M in hexane, 0.96 mmol) was added dropwise. The solution was left to stir at –78°C for 20 min, with appearance of a yellow precipitate. In the meantime, a suspension of truxenone (**3**) (100 mg, 0.26 mmol) in 15 mL of dry THF was dispersed with sonication for *ca.* 30 min. The resulting suspension was added to the phosphorous ylide suspension, and the cooling was kept. The mixture was allowed to warm slowly to room temperature and left to stir for 3 h. The solvent was removed under reduced pressure and the residue was purified by column chromatography (SiO_2, hexane: dichloromethane 3:1). After purification the product **73** was obtained as a black solid (50 mg, 42%).

^{1}H NMR (300 MHz, $CDCl_3$) δ 9.54 (d, *J* = 7.5 Hz, 1H), 7.83 (d, *J* = 5.4 Hz, 1H), 7.77 (d, *J* = 7.0 Hz, 1H), 7.63 – 7.42 (m, 5H), 7.39 (t, *J* = 7.0 Hz, 1H), 7.31 (d, *J* = 6.8 Hz, 1H), 7.23 (d, *J* = 7.5 Hz, 1H), 7.11 (d, *J* = 7.5 Hz, 1H), 6.93 – 6.56 (m, 4H) ppm.

Synthesis of 4, 9, 14-trifluorotruxenone (97)[26]

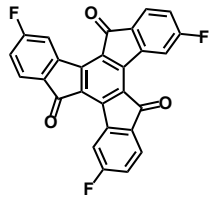

Commercially available 5-fluoroindanone (5 g, 0.033 mmol) was dissolved in 125 ml of $CHCl_3$ and 3.4 mL (0.066 mol) of Br_2 were added dropwise. The reaction mixture was stirred for two hours and then, the mixture was purged with Ar during 1h. Afterwards, the solvent was eliminated under vacuum. The resulting product reaction crude, without further purification, was heated at 220 °C in a 100 mL round flask until no bromine gas was further eliminated. Then, the crude of the reaction was sonicated with CH_2Cl_2 and eventually, the mixture was filtered off with a Büchner and washed with CH_2Cl_2 to obtain a yellow solid. The global yield was 5% (700 mg).

FT-IR (KBR) 1707 cm^{-1}

Synthesis of 4, 9, 14-trifluorotruxTTF (96)

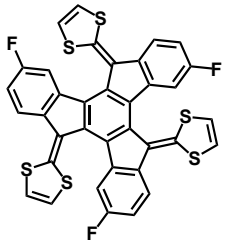

A solution of 1,3-dithiol-2-ylphosphonate (435 mg, 2.05 mmol) in 3 mL of dry THF, was cooled to -78 °C under Ar. Then, 1.3 mL of BuLi (1.6 M in hexane, 2.08 mmol) were added dropwise. The solution was left to stir for 20 minutes at -78 °C under Ar with appearance of a yellow precipitate. In the meantime, 100 mg of truxenone **97** (0.23 mmol) were dispersed with sonication for *ca.* 20 minutes in 3 mL of dry THF. The resulting suspension was added to the

phosphorous ylide suspension, and the cooling bath is immediately removed. The mixture is allowed to warm up to room temperature and left stirring for 3 hours. Then methanol is added to the crude of the reaction and solvents are removed under reduced pressure. The crude is purified by column chromatography (SiO_2, hexane/dichloromethane, 3:1) to yield 110 mg of a dark orange solid, **96** (69%).

^{1}H NMR (300 MHz, $CDCl_3$) δ 7.70 (dd, *J* = 8.4, 5.0 Hz, 3H), 7.05 (td, *J* = 8.8, 2.4 Hz, 3H), 6.83 (dd, *J* = 9.7, 2.4 Hz, 3H), 6.67 (s, 6H) ppm.

^{13}C NMR (175 MHz, $CDCl_3$) δ 161.20, 159.83, 139.85, 137.90, 137.02, 136.23, 129.05, 128.24, 127.53, 125.31, 122.44, 121.67, 120.97, 118.17, 113.73, 113.59, 111.93 (d, *J* = 25 Hz), 111.80(d, *J* = 25 Hz) ppm.

MS (MALDI TOF) *m/z* calcd for $C_{36}H_{15}F_3S_6$ 695.954, *m/z* found 695.767.

General procedure for the synthesis of phenyl-C_{60} butyric acid methyl ester (94) and phenyl-C_{70} butyric acid methyl ester (95).[62]

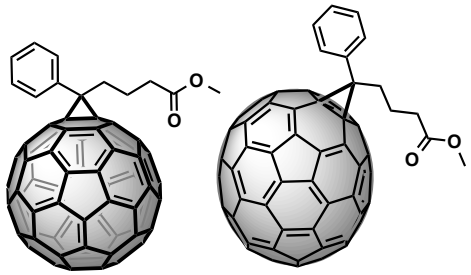

p-Tosilhydrazone (26.37 mg, 0.09 mmol) and MeONa (0.83 mmol, 46 mg) were stirred in 12 mL of dry pyridine at room temperature under argon for 25 minutes. To this solution, a solution of 0.09 mmol of C_{60} or C_{70} in *o*-DCB (45 mL) was then added. The reaction mixture was refluxed for 16 hours. After cooling to room temperature, the solvents were removed under reduced pressure under reduced pressure and the crude of the reaction is purified by column chromatography (SiO_2, Cs_2 and hexane/toluene). To yield black solids (25 mg, 30% **[61]PCBM**), (34 mg, 37% **[71]PCBM**).

[62] J. C. Hummelen, B. W. Knight, F. LePeq, F. Wudl, *J. Org. Chem.* **1995**, *60*, 532.

[61]PCBM (94)

^{1}H NMR (300 MHz, $CDCl_3$) δ 7.91-7.75 (m, 2H), 7.53-7.32 (m, 3H), 3.61 (s, 3H), 2.95-2.72 (m, 2H), 2.45 (t, *J*= 7.5 Hz, 2H), 2.18-2.08 (m, 2H) ppm.

[71]PCBM (95)

^{1}H NMR (300 MHz, $CDCl_3$) δ 7.76 (d, *J*= 8.75 Hz, 2H), 7.68 (m, 2H), 4.46 (m, 1H), 3.87 (s, 3H), 2.68(t, 2H, *J* = 8.75), 2.1-2.3 (m, 2H), 1.65-1.90 (m, 2H) ppm.

Chapter II. *Supramolecular complexation of truxene derivatives with bowl-shaped PAHs*

6. Background

6. BACKGROUND

6.1. BOWL-SHAPED POLYCYCLIC AROMATIC HYDROCARBONS

Polycyclic aromatic hydrocarbons (PAHs) represent an important and large family of compounds composed of multiple fused aromatic rings. When PAHs are formed entirely by fused benzene rings their structure remains planar except in some isolated examples such as helicenes.[63] When PAHs show five-membered rings inserted in their structure, they adopt non-planar equilibrium geometries. Actually, fullerenes are the result of embedding twelve five-membered rings in the PAHs structure. Any number fewer than twelve produces bowl-shape molecules, also named "fullerene fragments" or "buckybowls". Despite this last name, there is no requirement that these buckybowls should map the C_{60}-fullerene structure.[64]

Bowl-shape polycyclic aromatic hydrocarbons can be seen as the unclosed geodesic polyarenes family set, while fullerenes will constitute the set of the closed ones.[64]

Corannulene (**98**) $C_{20}H_{10}$, named so after its concentric zwitterion resonance structure, "annulene-within-an-annulene", is the smallest elemental bowl-shape subunit of C_{60}.[65] It was the first known geodesic polyarene, first synthesized by Lawton and Barth in a multi-step synthesis in 1966, eighteen years before the discovery of the first closed geodesic polyarenes by H. Kroto, J. Heath, S. O´Brien, R. Curl and R. Smalley.[66]

$C_{20}H_{10}$ (**98**)

C_{60}

Figure 6.1. Chemical structure of corannulene (**98**), and [60]fullerene.

[63] (a) M. Gingras, *Chem. Soc. Rev.* **2013**, *42*, 968; (b) M. Gingras, G. Félix, R. Peresutti, *Chem. Soc. Rev.* **2013**, *42*, 1007; (c) M. Gingras, *Chem. Soc. Rev.* **2013**, *42*, 1051.

[64] L. T. Scott, H. E. Bronstein, D. V. Preda, R. B. M. Ansems, M. S. Bratcher, S. Hagen, *Pure & Appl. Chem*. **1999**, *71*, 209.

[65] (a) W. E. Barth, R. G. Lawton, *J. Am. Chem. Soc.* **1966**, *88*, 380; (b) R. G. Lawton, W. E. Barth, *J. Am. Chem. Soc.* **1971**, *93*, 1730.

[66] H. W.Kroto, J. R. Heath, S. C. O´Brien, R. F. Curl, R. E. Smalley, *Nature,* **1985**, *318*, 162.

C_{60} was named Buckminsterfullerene in honor of the futuristic American architect Buckminster Fuller, author of the geodesic dome. Both fullerene and the geodesic dome have surfaces comprised by assemblies of interconnected polygonal faces that share edges and vertices one with another. The full assembly defines a surface that looks like the earth surface. [60]fullerene has the geometry of a truncated icosahedron, a convex isogonal non-prismatic Archimedean solid. It has twelve regular pentagonal faces, twenty regular hexagonal faces, sixty vertices and ninety edges. Fullerenes, as geodesic spheres, obey Euler´s formula for polyhedra, ($V - E + F = 2$). The number of vertices (carbon atoms, 60), minus the number of edges (covalent bonds among carbon atoms, 90), plus the number of faces (hexagons, 20, and pentagons, 12, defined by the carbon atoms and covalent bonds among them), is equal to 2. Partial geodesic dome and fullerene fragments obey the rule $V - E + F = 1$, as in corannulene, the number of carbon atoms, 20, minus the number of covalent bonds, 25, plus the number of faces, 6, is equal to 1.

During the first years after the discovery of C_{60} and other related fullerenes, many scientists, fascinated by their unusual properties, focused their efforts in the achievement of macroscopic amounts of these substances. Once Wolfgang Krätschmer fulfilled this goal in 1990,[67] the field was open to the nowadays known chemistry of fullerenes.[68]

The total chemical synthesis of C_{60} was an appealing challenge for many organic chemists soon after its discovery. Undoubtedly, the key step in the synthesis would be the achievement of the characteristic curvature of this system. Although many groups figured out that this could be overcome synthesizing

[67] W. Krätschmer, L. D. Lamb, K. Fostiropoulos, D. R. Huffman, *Nature*, **1990**, *347*, 354.

[68] (a) D. M. Guldi, N. Martín, "Fullerenes: From synthesis to Optoelectronic Properties", Kluwer Academic Publishers, **2002**; (b) A. Hirsh, M. Brettreich, "Fullerenes", Wiley-VCH: New York, NY, **2005***;* (c) F. Langa, J. F. Nierengarten, "Fullerenes: Principles and Applications", RSC Nanoscience and Nanotechnology, **2007**; (d) N. Martin, J. F. Nierengarten, "Supramolecular Chemistry of Fullerenes and Carbon Nanotubes", Wiley-VCH Verlag GmbH and Co. KGaA, **2010**; For references on the aromaticity in fullerenes see (e) A. Hirsch, Z. Chen, H. Jiao, *Angew. Chem. Int. Ed.* **2000**, *39*, 3915; (f) A. rodriguez-Fortea, N. Alegret, A. L. Balch, J. M. Poblet, *Nature Chem*. **2010**, *2*, 955; (g) M. García-Borrás, S. Osuna, M. Swart, J. M. Luis, M. Solá, *Angew. Chem. Int. Ed.* **2013**, *52*, 9275.

bowl-shaped intermediates, and stitching them together afterwards, the idea of watching the fullerene as a set of bowl-shaped fragments put all together was not new. In 1970 even before the discovery of fullerenes, soon afterwards the discovery of corannulene, Eiji Osawa predicted the existence of C_{60} as the combination of corannulene subunits forming a soccer ball.[69] Going back to the early nineties, the $C_{30}H_{12}$ PAH was proposed as a suitable bowl-shape fullerene fragment for the synthesis of C_{60}, as it contains exactly half of the C_{60} carbon framework. Many groups embarked themselves in the synthesis of this buckybowl ($C_{30}H_{12}$) with the final aim of fusing two of those molecules together, unfortunately, even nowadays, there are no methods for stitching molecules in such a way.[70]

L. T. Scott and co-workers eventually accomplished the synthesis of C_{60} in 2001, from a non-bowl-shaped molecule, $C_{60}H_{27}Cl_3$ (99), under flash vacuum pyrolysis (FVP) treatment.[7b] (Scheme 6.1)

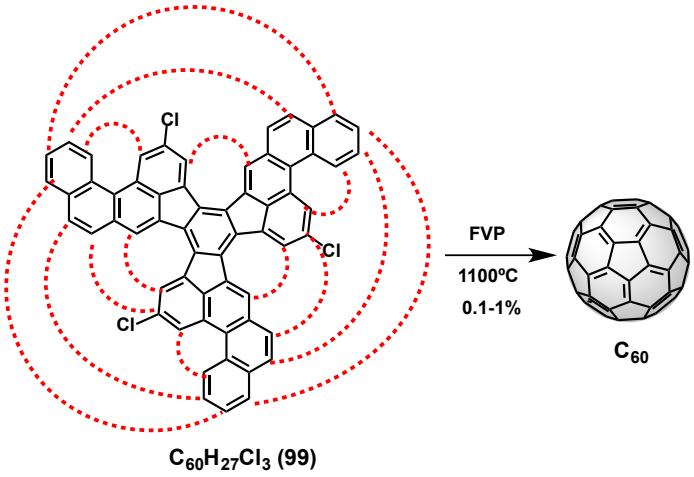

Scheme 6.1. Chemical synthesis of C_{60} from $C_{60}H_{27}Cl_3$ (**99**) under FVP treatment. Dashed red lines represent the C(aryl)-C(aryl) bonds that are still needed to be formed to get the target molecule.

Buckybowls are not only interesting precursors for the synthesis of fullerenes. Contrary to planar PAHs, bowl-shaped PAHs show two different surfaces for the

[69] Z. Yoshuda, E. Osawa, Aromaticity, Kagakudojin: Kyoto, 1971, p. 174.

[70] (a) A. H. Abdouzarak, Z. Marcinow, A. Sygula, R. Sygula, P. W. Rabideau, *J. Am. Chem. Soc.* **1995**, *117*, 6410; (b) S. Hagen, M. S. Bratcher, M. S. Erickson, G. Zimmermann, L. T. Scott. *Angew. Chem. Int. Ed.* **1997**, *36*, 406.

same molecule, the convex and the concave sides. Those, provide different chemical and physical environments. Despite having a convex accessible face as fullerenes, they have edges susceptible of being chemically modified, and a concave exposed surface as well. These features have attracted the interest of the chemical community and many open questions still remain in this research topic.

6.1.1. *Synthesis of buckybowls*

The most significant feature of geodesic polyarenes is the curved π-system composed by piramidalized carbon atoms (Figure 6.2). Those piramidalized carbon atoms force the curvature and induce electronic perturbations such as π-orbital misalignement between adjacent pairs of carbon atoms, that will lead to weaker π-bonds, increased s-character in the π-system and lowered LUMO energy.

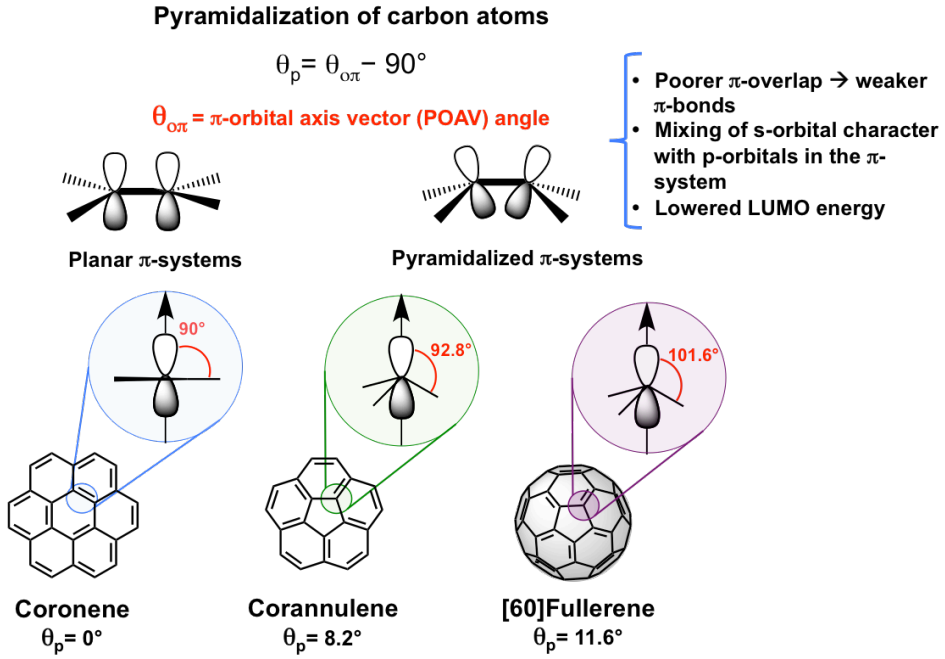

Figure 6.2. π-orbital axis vector angle and θ_p of coronene, corannulene and [60]fullerene.

The development of different strategies for the synthesis of bowl-shape PAHs by means of FVP or solution synthetic techniques lead to the synthesis of an

increasing library of fullerene fragments (Figure 6.3).[71] As these fragments present not only the curvature but also some of the chemical features of fullerenes, these molecules and their inherent reactivity resemble in some way the fullerene properties. Actually, they can be considered as the bridge in between planar PAHs and fullerenes.

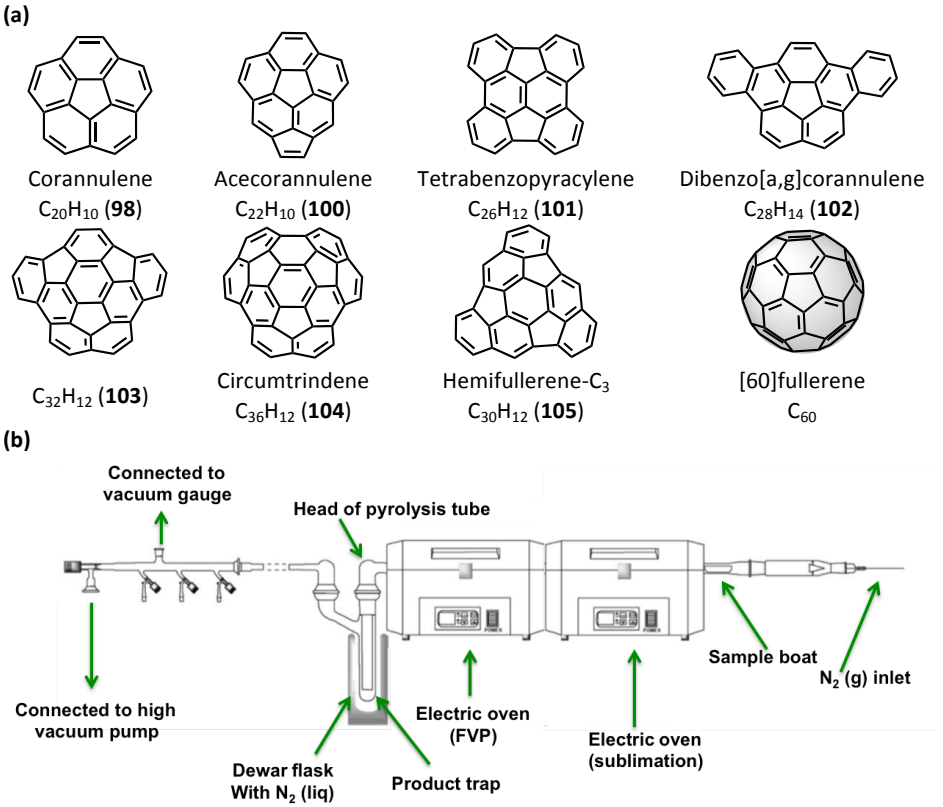

Figure 6.3. (a) Representative examples of geodesic polyarenes prepared by FVP. (b) Schematic view of a FVP display.[72b]

FVP is a technique that allows the heating of molecules in their gas phase to very high temperatures, reaching up to 1100 °C, for a very short period of time. The sample is sublimed under vacuum at the first oven. The vapors pass through a hot zone, the "FVP oven", helped by a nitrogen flow that gets into the system through capillary tubing. Under thermal activation, the organic flat

[71] M. A. Petrukhina, L. T. Scott, *Fragments of Fullerenes and Carbon Nanotubes: Designed Synthesis, Unusual Reactions, and Coordination Chemistry,* Wiley, Hoboken **2012**.

molecules can be turned into, temporarily, highly distorted conformations that can then be trapped to make bowl-shaped polyarenes by joining together distant parts of the molecule.[72]

6.1.2. *Reactivity on the convex surface*

Some buckybowls share reactivity patterns with fullerenes. For example, when **101** ($C_{26}H_{12}$), the smallest fullerene fragment featuring a "[6,6] double bond type", is treated under 1,3-dipolar cycloaddition conditions, carbine additions or nucleophilic addition of MeLi, it behaves as [60]fullerene, suffering the addition reactions at the central [6,6] ring junction.[64] This double bond exhibits the greater curvature, and reacts forming new covalent bonds that destroy the cyclic conjugation in the adjacent benzene rings (Scheme 6.2).

If the same molecule is exposed to Friedel-Crafts alkylation conditions, this bowl-shaped molecule behaves as an ordinary PAH, reacting at the double bonds located at the edges (Scheme 6.3).

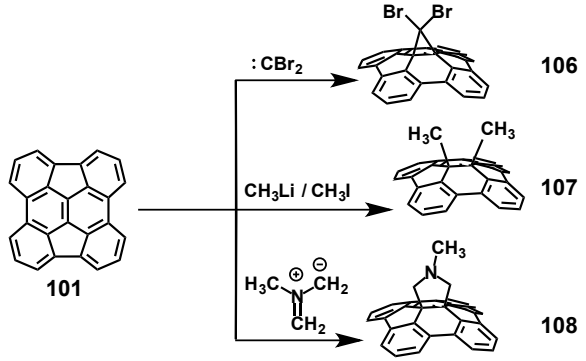

Scheme 6.2. Chemical behavior of buckybowls as fullerenes.

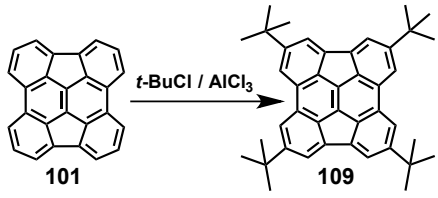

Scheme 6.3. Chemical behavior of buckybowls as PAHs do.

[72] (a) L. T. Scott, *Angew. Chem. Int. Ed.* **2004**, *43*, 4994; (b) V. M. Tsefrikas, L. T. Scott, *Chem. Rev.* **2006**, *106*, 4868.

A more complex situation occurs when more than one type of [6,6] double bond is present in the molecule. Thus, when **104** undergoes the Prato reaction, the process is site-selective for the [6,6] bond located at the point of greatest curvature (Scheme 6.4). This chemical behavior resembles that observed for C_{70}. In the case of C_{70} having five types of [6,6] bonding sites, only α and β isomers ($\alpha >> \beta$) are typically detected and in some cases, traces of the γ isomer are also observed.[73]

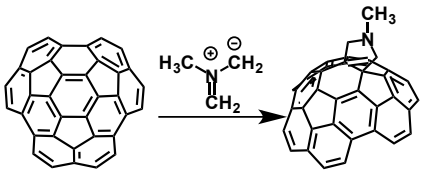

104 **110**

Scheme 6.4. Chemical behavior of buckybowls as C_{70}.

[73] E. Maroto, A. de Cózar, S. Filippone, A. Martín-Domenech, M. Suárez, F. P. Cossío, N. Martín, *Angew. Chem. Int. Ed.* **2011**, *50,* 6060.

6.1.3. *Stacking and molecular packing*

When two bowl-shaped conjugated systems interact, stacking structures in a concave-convex face could be expected as a potential way of supramolecular arrangement. However, this does not occur with the corannulene.

Corannulene shows almost the same degree of curvature as C_{60}. However, in contrast to fullerenes, its curvature is not permanent since the molecule undergoes a rapid bowl-to-bowl inversion in solution (10-11 Kcal mol^{-1}).[74] Furthermore, corannulene shows a complete lack of bowl stacking in its crystal packing.

Corannulene
$C_{20}H_{10}$ (**98**)

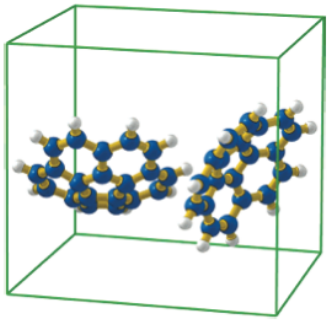

Figure 6.4. Orientation of two independent corannulene molecules in the unit cell of the crystal. [75]

When a second pentagonal ring is added to the corannulene, the molecular rigidity and curvature are slightly increased. This way, the bowl conformation is apparently locked. P. W. Rabideau and co-workers found that, in this case, the rapid bowl inversion is not observed; at least at the NMR time scale.

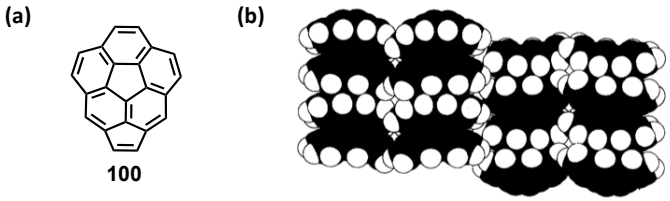

Figure 6.5. (a) Cyclopentacorannulene (**100**). (b) Crystal packing of **100**.

Additionally, cyclopentacorannulene (**100**), with deeper depth of the bowl and larger surface area than corannulene, shows short-range concave-convex

[74] L. T. Scott, M. M. Hashemi, M. S. Bratcher, *J. Am. Soc.* **1992**, *114*, 1920.
[75] M. A. Petrukhina, K. W. Andrenini, J. Mack, L. T. Scott, *J. Org. Chem.* **2005**, *70*, 5713.

crystal packing along the α-axis.[76]

When the concave-convex packing turns into a long-range characteristic, it affects the dipoles and the electronic properties. Two major kinds of stacking motifs can be distinguished (Figure 6.6).[77]

- Type 1: bowl-in-bowl stacks where all columns are oriented towards the same direction. This kind of stacking leads to polar crystals. The molecules showing this kind of crystallization are potential candidates for organic semiconductor materials or for non-linear optoelectronic materials. The molecules forming each column can slip from side to side within each stack; this non-perfect bowl-in-bowl stack results as a compromise between intrastack and interstack interactions given by the π–π and CH-π interactions.
- Type 2: bowl-in-bowl stacks where adjacent columns are oriented toward opposite directions. This kind of stacking gives apolar crystals.

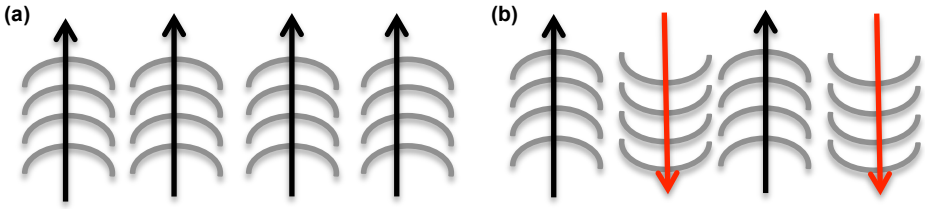

Figure 6.6. Schematic representation of (a) Type 1 and (b) Type 2 of bowl-in-bowl stacking.

Y. T. Wu and co-workers reported the synthesis of some buckybowls showing crystallization type 1 (Figure 6.7).[78] As a few examples, the packing patterns of buckybowls **111**, **112** and **113** are shown in Figure 6.7. Notice that **113** is a bowl shaped fragment of C_{70}. These packing patterns revealed that the curvature of **112** is greater than the curvature of **113**. On the other hand, the less curved shape of **113** together with a larger π–π surface, results in a larger π–π overlap and a smaller slipping angle. The methylene protons of **111** take part in strong

[76] A. Sygula, H. E. Folsom, R. Sygula, A. H. Abdourazak, Z. Marcinow, R. Fronczek, P. W. Rabideau, *Chem. Soc., Chem. Commun.* **1994**, 2571.
[77] Y. T. Wu, J. S. Siegel, *Chem. Rev.***2006**, *106*, 4843.
[78] (a) T. C. Wu, M. K. Chen, Y. W. Lee, M. Y. Kuo, Y. T. Wu, *Angew. Chem. Int. Ed.* **2013**, *52*, 1289; (b) Y. T. Wu, T. C. Wu, M. K. Chen, H. J. Hsin, *Pure Appl. Chem.* **2014**, *86*, 539.

intermolecular CH–π interactions within a columnar stack.

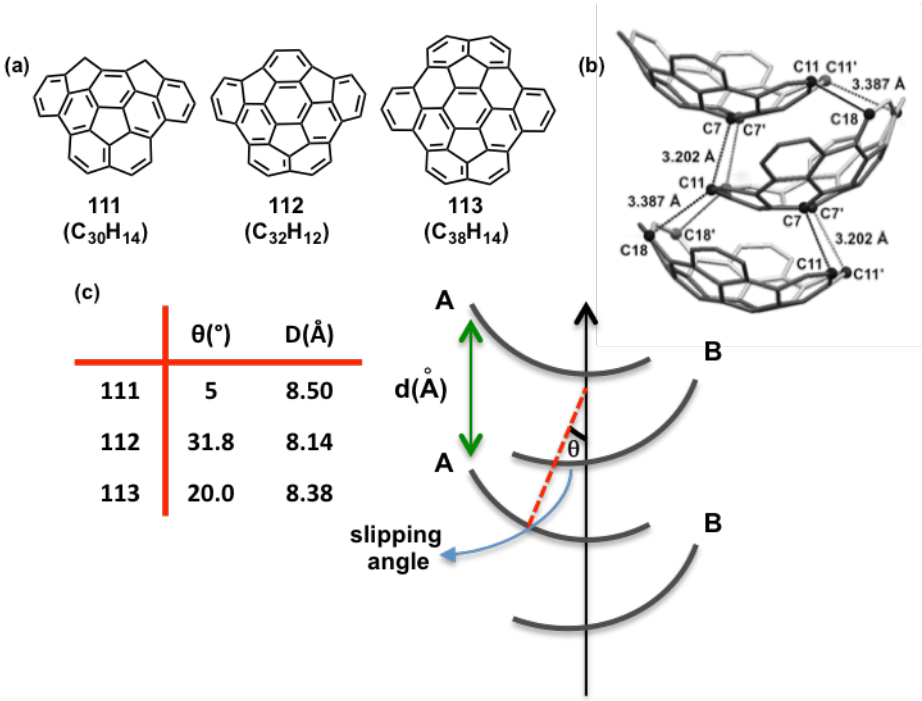

Figure 6.7. (a) **111**, **112** and **113** bowl-shaped molecules reported by Wu and co-workers. (b) Bowl-in-bowl stack and intermolecular interaction of **113**. (c) Packing patterns of **111**, **112** and **113**.

Scott and co-workers synthesized circumtrindene,[79] ($C_{36}H_{12}$) **104**, and the hemifullerene $C_{30}H_{12}$ (**105**), their solid-state packing motives are depicted on Figure 6.8, to further illustrate the possible stacking motifs. **104** shows a deep concave cavity and forms polar crystals with linear bowl-in-bowl stacks, maximizing π–π interactions. On the other hand, X-ray diffraction studies on **105** revealed two polymorphs,[80] namely trigonal (**105-t**) and orthorhombic (**105-o**). **105-t** shows the same stacking behavior as circutrimdene, while the orthorhombic one shows the type 2 stacking, interlocking *exo-exo* and *endo-endo* columnar stacks.

[79] (a) L. T. Scott, M. S. Bratcher, S. Hagen, *J. Am. Chem. Soc.* **1996**, *118*, 8743; (b) R. B. M. Ansems, L. T. Scott, *J. Am. Chem. Soc.* **2000**, *122*, 2719.
[80] M. A. Petrukhina, K. W. Andrenini, L. Peng, L. T. Scott, *Angew. Chem. Int. Ed.* **2004**, *43*, 5477.

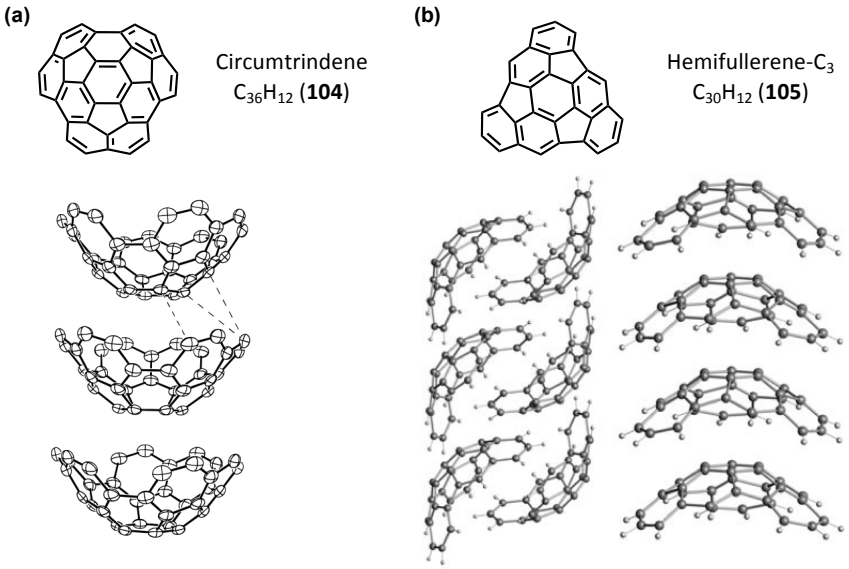

Figure 6.8. Solid-state packing of (a) **104** and (b) **105**.

6.1.4. *Coordination chemistry of buckybowls*

Buckybowls as ligands present multi-site coordination possibilities.[81] They have edge or rim carbon atoms capped with hydrogen atoms, a concave and a convex three-dimensional surface of unsaturated carbon atoms and, therefore, they will exhibit preferences for metal binding.

The formation of both *endo* or *exo*-complexes of these buckybowls (this is, complexes at the concave or convex surface of hemifullerenes respectively) have caught researchers attraction as they are somehow structurally related to fullerenes. With the long-term goal of being able to synthesize fullerenes from these bowl-shaped molecules. The control over the arrangement of metal centers at the concave surface, will ideally open the possibility to synthesize endohedral fullerenes, which are of great interest for their peculiar properties and that nowadays are not available in great amount.[82]

[81] M. A. Petrukhina, L. T. Scott, *Fragments of Fullerenes and Carbon Nanotubes: Designed Synthesis, Unusual Reactions, and Coordination Chemistry,* Wiley, Hoboken **2012**, p. 413.
[82] A. A. Popov, S. Yang, L. Dunsch, *Chem. Rev.* **2013**, *113*, 5989.

Some buckybowls show different coordination modes that will be summarized in the following examples.

The first corannulene complex structurally charactericed was the $[(Cp^*Ru)_2\mu_2\text{-}\eta^6, \eta^6\text{-}C_{20}H_{10})]^{2+}$ reported by Rabideau and co-workers.[83] In this complex, two $\{Cp^*Ru\}^+$ units are bound to non-adjacent arene rings on opposite sides of the corannulene (Figure 6.9). The η^6-coordination causes reduction of the curvature of the corannulene flattening it.

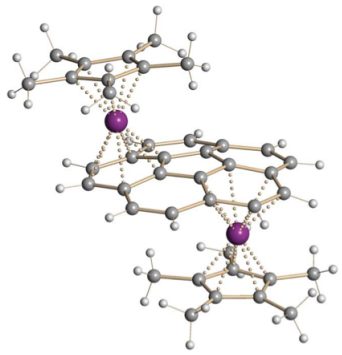

Figure 6.9. Coordination complex $[(Cp^*Ru)_2\mu_2\text{-}\eta^6, \eta^6\text{-}C_{20}H_{10})]^{2+}$; Ru purple, C gray, H light grey.

The $[CpFe(sumanene)]^+$ was the first concave-selective coordination complex of a buckybowl reported (Figure 6.10).[84] The sumanene ($C_{21}H_{12}$) is another symmetric subunit of C_{60}.

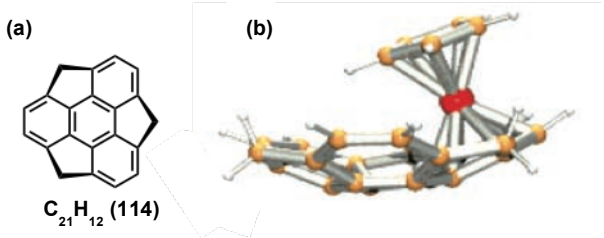

Figure 6.10. (a) Chemical structure of sumanene (**114**), (b) coordination motif of $[CpFe(sumanene)]^+$. C orange, H, white, Fe red.

For a given metal system complex, there are various bonding motifs towards different buckybowls. As an example Scott and co-workers tested three buckybowls (Figure 6.11), each of them exhibiting different geometry and curvature towards the dimetal complex $Rh_2(OCCF_3)_4$.[85]

[83] P. A. Vecci, C. M. Alvarez, A. Ellern, J. Angelici, A. Sygula, P. W. Rabideau, *Angew. Int. Ed.* **2004**, *43*, 4497.
[84] T. Amaya, H. Sakane, T. Hirao, *Angew. Chem. Int. Ed.* **2007**, *46*, 8376.
[85] M. A. Petrukhina, L. T. Scott, *Dalton Trans.* **2005**, 2969.

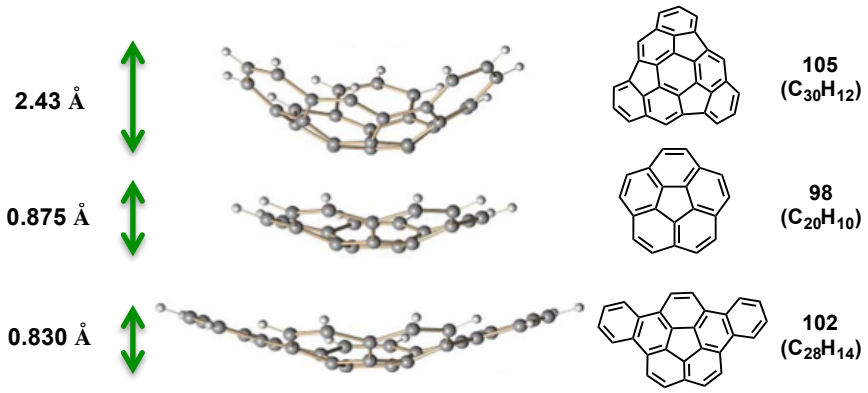

Figure 6.11. Chemical structure and bowl depth of the three buckybowls ligands tested.

X-ray diffraction studies revealed unique structural motifs for the new metal complexes generated (Figure 6.12). In all of them, rhodium (II) centers approach the bowls in different fashion but interacting just with the rim C=C bonds of the hemifullerenes.

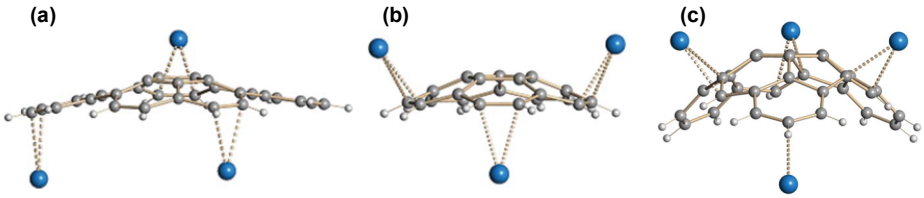

Figure 6.12. (a) Tridentate η^2: η^2: η^2-bridging coordination of $C_{20}H_{10}$ (**98**) . (b) Tridentate η^2: η^2: η^2-bridging coordination of $C_{28}H_{14}$ (**102**) . (c) Tetradentate η^2: η^2: η^2: η^1-bridging coordination of $C_{30}H_{12}$ (**105**) . Ru blue, C gray, H light grey.

We can conclude that the overall binding mode will be determined by the buckybowl-metal system complex chosen. Same metal complexes will lead to different binding modes towards different hemifullerenes, and a given buckybowl will show different bonding motifs towards different metal complexes (Figures 6.9, 6.12 and 6.13).

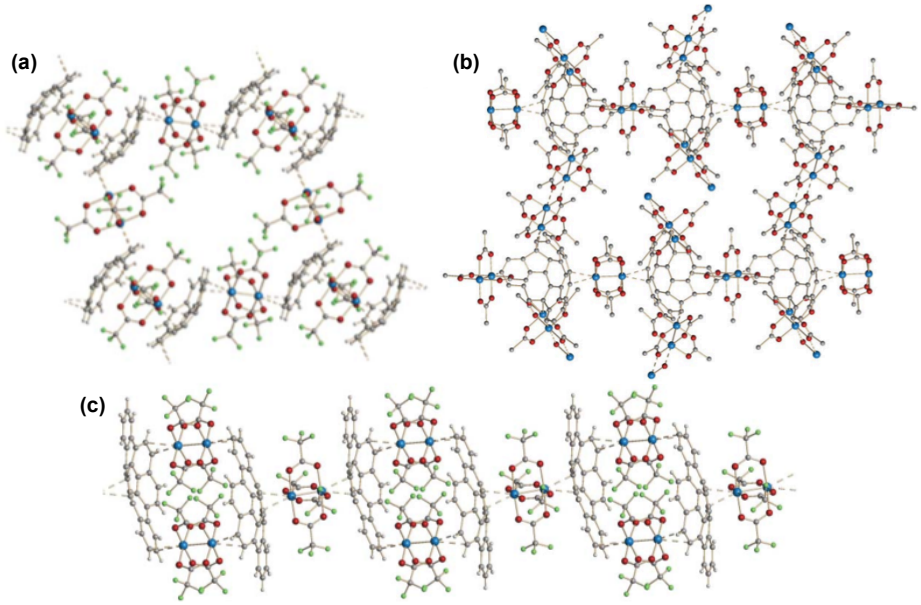

Figure 6.13. A view of the structure: (a) $\{[Rh_2(O_2CCF_3)_4]_3 \bullet (C_{20}H_{10})_2\}_\infty$, (b) $\{[Rh_2(O_2CCF_3)_4]_3 \bullet (C_{30}H_{12})_2\}_\infty$, (c) $\{[Rh_2(O_2CCF_3)_4]_3 \bullet (C_{28}H_{14})_2\}_\infty$.

6.1.5. *Supramolecular chemistry and host properties of buckybowls*

Since the discovery of fullerenes and their further potential applications, the search for appropriate concave receptors complementing their convex surfaces is still a challenging issue. The interest for designing such receptors obey two main needs: the purification of fullerenes from fullerite and the construction of organized electroactive nanostructures by self-assembly. Both of them share the same preliminary condition: the formation of stable associates.[86]

One of many strategies followed to find adequate receptors to associate fullerenes is to exploit the complementarity host-guest shape that will maximize π–π interactions; this is, to design concave receptors that will match the convex surface of fullerenes. In this sense, several authors noticing the shape complementarity among the π-faces of the C_{60} and corannulene designed several corannulene-based receptors for fullerenes, featuring one or more corannulene units.

[86] (a) E. M. Pérez, N. Martín, *Chem. Soc. Rev.* **2008**, *37*, 1512; (b) D. Canevet, E. M. Pérez, N. Martín, *Angew. Int. Ed.* **2011**, *50*, 9248.

When the first corannulene-based receptors for fullerenes were reported, the only experimental evidence to bet on the corannulene as an adequate recognition motif towards C_{60} was the fact that corannulene forms a stable complex with $(C_{60})^+$ in the gas phase.[87] It took until 2012 to achieve the co-crystallization of C_{60} and corannulene (Figure 6.14).[88]

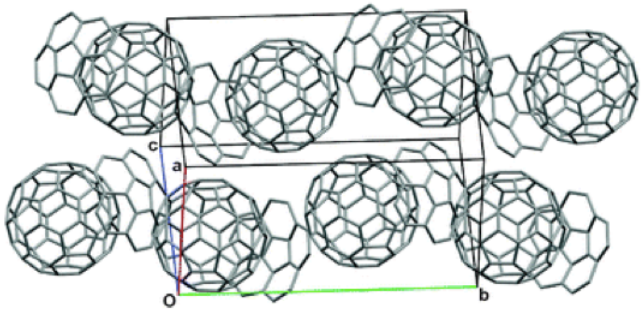

Figure 6.14. Representation of the extended packed unit cell for **98**•C_{60}.

Scott and co-workers reported a series of fullerenes receptors synthesized from the modification of a single corannulene unit (Figure 6.15).[89]

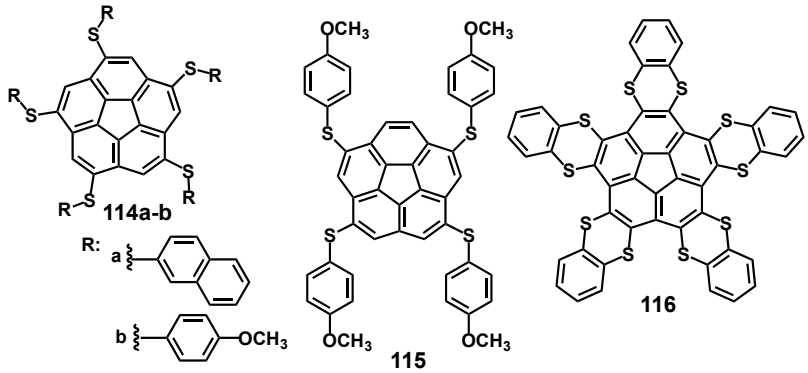

Figure 6.15. Chemical structure of the receptors reported by Scott and co-workers. **114a-b** and **115** showed binding constant values of 280-475 M^{-1} measured by ^{1}H-NMR in toluene-d_8. The corannulene "Venus fly-trap", **116**, has a better affinity towards C_{60}, having a binding constant of 1420 M^{-1} also measured by ^{1}H-NMR in toluene-d_8.

Sygula *et al*. reported a tweezer like corannulene receptor, named

[87] S. Mizyed, P. E. Georghiou, M. Bancu, B. Cuadra, A. K. Rai, P. Cheng, L. T. Scott, *J. Am. Chem. Soc.* **2001**, *123*, 12770.
[88] L. N. Dawe, T. A. AlHujran, H. A. Tran, J. I. Mercer, E. A. Jackson, L. T. Scott, P. E. Georghiou, *Chem. Commun.* **2012**, *48*, 5563.
[89] P. E. Georghiou, A. H. Tran, S. Mizyed, M. Bancu, L. T. Scott, *J. Org. Chem.* **2005**, *70*, 6158.

buckycatcher (**117**), for C_{60} and C_{70},[90] showing a binding constant value of K_a = 8600 ± 500 M^{-1}, towards C_{60}, obtained by ^{1}H-NMR studies in toluene-d_8. The crystal structure of the complex system **117**•C_{60} was also studied resulting the first evidence of a corannulene concave face binding to C_{60} (Figure 6.16).

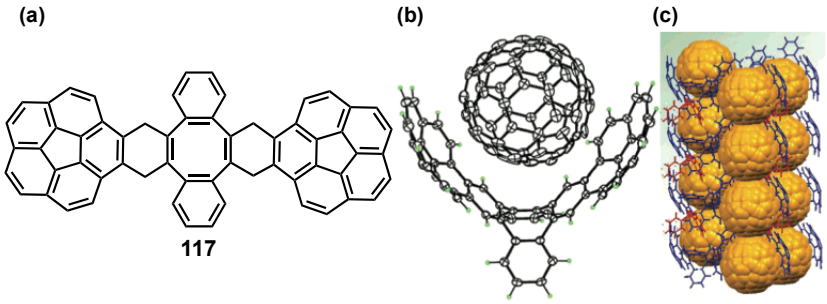

Figure 6.16. (a) Chemical structure of **117**, (b) crystal arrangement of **117**•C_{60} and (c) crystal packing pattern of **117**•C_{60}.

Sygula also reported the synthesis of a cyclotriveratrylene (CTV) receptor for C_{60} and C_{70} featuring three recognition units of corannulene (Figure 6.17). However, despite having a third unit of corannulene the values obtained for the association binding constants are notably lower than the ones found for the buckycatcher.[91]

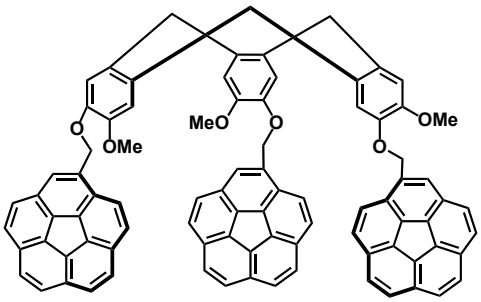

Figure 6.17. Tripodal corannulene based CTV receptor for fullerenes (**118**).

Stuparu reported a series of corannulene-encoded polymers able to interact towards C_{60}.[92] This example represents the multivalent recognition towards C_{60} using the corannulene as the recognition motif.

[90] A. Sygula, F. R. Fronczek, R. Sygula, P. W. Rabideau, M. M Olmstead, *J. Am. Chem. Soc.* **2007**, *129*, 3842.
[91] M. Yanney, A. Sygula, *Tetrahedron Letters* **2013**, *54*, 2604.
[92] M. C. Stuparu, *Angew. Chem. Int. Ed.* **2013**, *52*, 7786.

Fukuzumi and co-workers, have recently reported a charge-transfer complex formed between corannulene and lithium ion-encapsulated [60]fullerene ($Li^{+}@C_{60}$) showing a binding constant of K_a = 1.9 x 10 M^{-1} in benzonitrile at 298 K.[93]

Interestingly, corannulene has been the only bowl-shaped PAH used as a fullerene-binding motif. However, no receptors for buckybowls have been reported so far.

6.1.6. *Potential applications of buckybowls*

Bowl-shaped fullerenes fragments have recently shown diverse potential applications. For example this kind of compounds could have potential application as optoelectronic organic materials. Recently, Aida designed a liquid crystal made by modifying the corannulene framework with amidated paraffinic side chains[94].

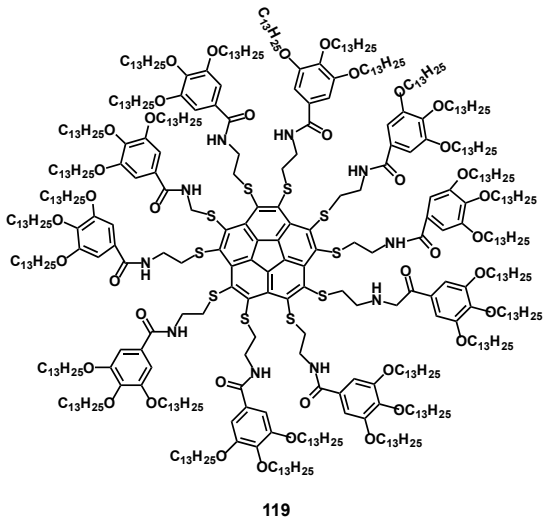

119

Figure 6.18. Chemical structure of a corannulene-based liquid crystal reported by T. Aida.

Due to a multivalent H-bonding interaction between the peripheral amide groups along with the van der Waals interactions, this molecule forms a hexagonal columnar mesophase even at room temperature. The π-stacked columns of **119** are aligned in response to an applied electric field.

[93] M. Yamada, K. Ohkubo, M. Shionoya, S. Fukuzumi, *J. Am. Chem. Soc*. **2014**, *136*, 13240.

[94] D. Miyajima, K. Tashiro, F. Araoka, H. Takezoe, J. Kim, K. Kato, M. Takata, T. Aida, *J. Am. Chem. Soc.* **2009**, *131*, 44.

Buckybowls could also act as organic semiconductors. Recently, single crystals of sumanene revealed to show high electronic mobility with large anisotropy measured by the charge-carrier time-resolved microwave conductivity method (7.5×10^{-1} cm^2 V^{-1} s^{-1}).[95] This would in principle, allows the development of electrical materials based on buckybowls.[95]

Buckybowls have also found application in the synthesis of larger allotropes of carbon.[96] Scott and co-workers reported a short [5,5] carbon nanotube chemically synthesized from corannulene. The strategy of the bottom up synthesis and elongation of short [5,5] CNT would lead to the growth of [5,5] CNTs with controlled size, diameter and chirality CNT. This new approach represents a current challenge in the science of CNTs because of the still lack of synthetic control in the preparation of these allotropes of carbon.

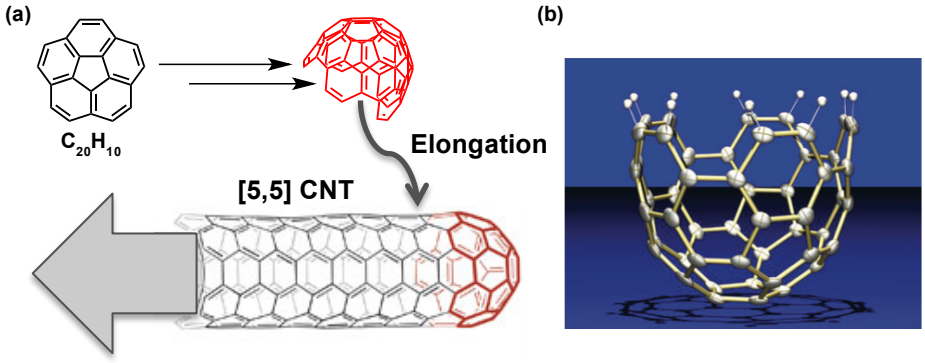

Figure 6.19. (a) Chemical structure of a short [5,5] carbon nanotube. (b) Molecular structure of a short [5,5] carbon nanotube determined by X- ray crystallography.

[95] T. Amaya, S. Seki, T. Moriuchi, K. Nakamoto, T. Nakata, H. Sakane, A. Saeki, S. Tagawa, T. Hirao, *J. Am. Chem. Soc.* **2009**, *131*, 408.
[96] L. T. Scott, E. A. Jackson, Q. Zhang, B. D. Steinberg, M. Bancu, B. Li, *J. Am. Chem. Soc.* **2012**, *134*, 107.

7. Objectives

7. OBJECTIVES

The synthesis of curve PAHs (open geodesic cages) is currently a mayor topic in chemistry and different preparation procedures as well as covalent chemical modifications have been reported during the last recent years. However, to the best of our knowledge the supramolecular chemistry of these systems with complementary concave-convex partners has not been properly addressed so far. In this chapter we will present our studies directed to the supramolecular understanding between curved PAHs and electron-donor (truxTTF, **70a**) and electron acceptor (trux6CN, **128**) as efficient recognition partners of choice in order to determine the main supramolecular interactions governing the complexation process. Thus the following topics are discussed in this Chapter II:

• Supramolecular chemistry of truxTTF and $C_{30}H_{12}$, a singular case of study

We will study the association of a fullerene fragment, the hemifullerene $C_{30}H_{12}$ (**105**), with an electron-donating bowl-shaped tetrathiafulvalene derivative (truxTTF, **70a**).

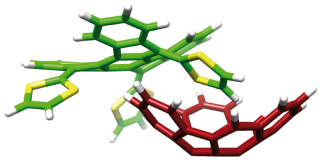

Figure 7.1. truxTTF•$C_{30}H_{12}$ complex.

• Extension to other curved PAHs systems, a comparative study

Encouraged by the good results obtained for the previous study, we decided to widen the scope and explore the complexation processes between bowl-shaped PAHs **112** and **113** molecules with truxTTF, as well as to explore if the n/p electronic behavior of the buckybowls **105** and **112** could be tuned depending on the counterpart in the formed complexes, to do so we resort to an electron acceptor truxene derivative, the trux6CN (**128**).

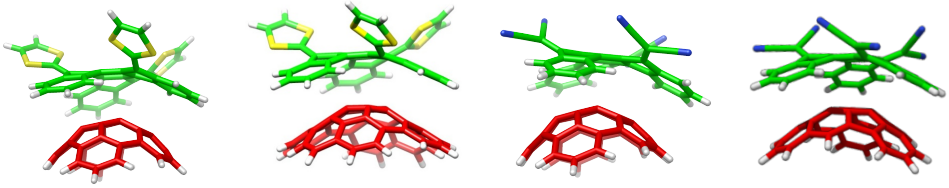

truxTTF•$C_{32}H_{12}$ truxTTF•$C_{38}H_{14}$ Trux6CN•$C_{32}H_{12}$ Trux6CN•$C_{30}H_{12}$

8. Results and Discussion

8. RESULTS AND DISCUSSION

8.1. SUPRAMOLECULAR CHEMISTRY OF truxTTF AND $C_{30}H_{12}$. A SINGULAR CASE OF STUDY

The following results have been extracted from the published article "Electron Transfer in a Supramolecular Associate of a Fullerene Fragment". The results described in the original publication have been complemented with the synthesis and characterization of the fullerene fragment $C_{30}H_{12}$ that was carried out during my short stay at the Boston College under the supervision of Prof. L. T. Scott.

María Gallego, Joaquín Calbo, Juan Aragó, Rafael M. Krick Calderón, Fernando H. Líquido, Takahiro Iwamoto, Allison K. Greene, Edward. A. Jackson, Emilio M. Pérez, Enrique Ortí, Dirk M. Guldi, Lawrence T. Scott, Nazario Martín, *Angew. Chem. Int. Ed.* **2014**, *53*, 2170.

Herein, we investigate the association of a fullerene fragment, hemifullerene $C_{30}H_{12}$, with an electron-donating bowl-shaped tetrathiafulvalene derivative (truxTTF). UV/vis titrations and DFT calculations support the formation of the complex, for which an association constant of log K_a = 3.6 ± 0.3 in $CHCl_3$ at room temperature was determined. Remarkably, electron transfer from truxTTF to $C_{30}H_{12}$ to form the fully charge-separated species takes place upon irradiation of the associate with light, constituting the first example in which a fullerene fragment mimics the electron accepting behavior of fullerenes within a supramolecular complex.

The different nanoforms of carbon,[97] namely fullerenes,[98] carbon nanotubes,[99] and graphene,[100] each present distinct extraordinary properties that have

[97] J. L. Delgado, M. A. Herranz, N. Martín, *J. Mater. Chem.* **2008**, *18*, 1417.

[98] (a) N. Martín, *Chem. Commun.* **2006**, *42*, 2093; (b) J. Delgado, S. Filippone, F. Giacalone, M. Herranz, B. Illescas, E. Pérez, N. Martín, *Top. Curr. Chem.* **2014**, *350*, 1.

[99] *Carbon Nanotubes And Related Structures: Synthesis, Characterization, Functionalization, and Aplications* (Eds. D. M. Guldi, N. Martín), Wiley-VCH, Weinheim, **2010**.

[100] (a) M. J. Allen, V. C. Tung, R. B. Kaner, *Chem. Rev.* **2010**, *110*, 132; (b) C. N. R. Rao, A. K. Sood, K. S. Subrahmanyam, A. Govindaraj, *Angew. Chem., Int. Ed.* **2009**, *48*, 7752; (c) A. K. Geim, *Science* **2009**, *324*, 1530; (d) A. K. Geim, K. S. Novoselov, *Nat. Mater.* **2007**, *6*, 183; (e) L. Rodríguez-Pérez, M. A. Herranz, N. Martín, *Chem. Commun.* **2013**, *49,* 3721; (f) K. Dirian, M.

attracted a great deal of attention in different areas of research. Fullerenes, in particular C_{60} and its derivatives, have been thoroughly studied as electron acceptors in fundamental investigations of photoinduced electron transfer (PET) processes, combined with a variety of electron donors in covalent and non-covalent dyads.[101,37b] From an application point of view, C_{60} and C_{70} derivatives are by far the most commonly utilized n-type semiconducting materials in organic solar cells.[102,33b] In the case of carbon nanotubes, both their mechanical and optoelectronic properties have been exploited to construct a variety of devices, including field-effect transistors and sensors.[103] Finally, graphene is currently considered to have the potential to be the "balm of Fierabras" of carbon-based technologies. Transparent electrodes,[104] extremely sensitive sensors,[105] super-capacitors,[106] and lightweight high-performance materials[107] have all been postulated as potential applications of graphene.[108]

A. Herranz, G. Katsukis, J. Malig, L. Rodríguez-Pérez, C. Romero-Nieto, V. Strauss, N. Martín, D. M. Guldi *Chem. Sci.,* **2013**, *4,* 4335.

[101] (a) D. Wróbel, A. Graja, *Coord. Chem. Rev.* **2011**, *255*, 2555; (b) S. Fukuzumi, T. Kojima, *J. Mater. Chem.* **2008**, *18*, 1427; (c) H. Imahori, *Org. Biomol. Chem.* **2004**, *2*, 1425.

[102] (a) G. Dennler, M. C. Scharber, C. J. Brabec, *Adv. Mater.* **2009**, *21*, 1323; (b) M. Helgesen, R. Søndergaard, F. C. Krebs, *J. Mater. Chem.* **2010**, *20*, 36; (c) C. J. Brabec, S. Gowrisanker, J. J. M. Halls, D. Laird, S. Jia, S. P. Williams, *Adv. Mater.* **2010**, *22*, 3839; (d) H. Hoppe, N. S. Sariciftci, *J. Mater. Chem.* **2006**, *16*, 45.

[103] (a) J. M. Schnorr, T. M. Swager, *Chem. Mater.* **2011**, *23*, 646; (b) C. Wang, K. Takei, T. Takahashi, A. Javey, *Chem. Soc. Rev.* **2013**, *42*, 2592; (c) S. Park, M. Vosguerichian, Z. Bao, *Nanoscale* **2013**, *5*, 1727. (d) S. N. Kim, J. F. Rusling, F. Papadimitrakopoulos, *Adv. Mater.* **2007**, *19*, 3214.

[104] (a) S. Bae, H. Kim, Y. Lee, X. Xu, J.-S. Park, Y. Zheng, J. Balakrishnan, T. Lei, H. R. Kim, Y. I. Song, Y.-J. Kim, K. S. Kim, B. Oezyilmaz, J.-H. Ahn, B. H. Hong, S. Iijima, *Nat. Nanotechnol.* **2010**, *5*, 574; (b) X. Li, Y. Zhu, W. Cai, M. Borysiak, B. Han, D. Chen, R. D. Piner, L. Colombo, R. S. Ruoff, *Nano Lett.* **2009**, *9*, 4359; (c) K. S. Kim, Y. Zhao, H. Jang, S. Y. Lee, J. M. Kim, K. S. Kim, J.-H. Ahn, P. Kim, J.-Y. Choi, B. H. Hong, *Nature* **2009**, *457*, 706; d) X. Wang, L. Zhi, K. Müllen, *Nano Lett.* **2008**, *8*, 323.

[105] (a) C.-H. Lu, H.-H. Yang, C.-L. Zhu, X. Chen, G.-N. Chen, *Angew. Chem. Int. Ed.* **2009**, *48*, 4785; (b) J. T. Robinson, F. K. Perkins, E. S. Snow, Z. Wei, P. E. Sheehan, *Nano Lett.* **2008**, *8*, 3137; (c) F. Schedin, A. K. Geim, S. V. Morozov, E. W. Hill, P. Blake, M. I. Katsnelson, K. S. Novoselov, *Nat. Mater.* **2007**, *6*, 652.

[106] (a)Y. Zhu, S. Murali, M. D. Stoller, K. J. Ganesh, W. Cai, P. J. Ferreira, A. Pirkle, R. M. Wallace, K. A. Cychosz, M. Thommes, D. Su, E. A. Stach, R. S. Ruoff, *Science* **2011**, *332*, 1537; (b) K. Zhang, L. L. Zhang, X. S. Zhao, J. Wu, *Chem. Mater.* **2010**, *22*, 1392; (c) Y. Wang, Z. Shi, Y. Huang, Y. Ma, C. Wang, M. Chen, Y. Chen, *J. Phys. Chem. C* **2009**, *113*, 13103.

[107] H. Hu, Z. Zhao, W. Wan, Y. Gogotsi, J. Qiu, *Adv. Mater.* **2013**, *25*, 2219.

[108] X. Huang, Z. Yin, S. Wu, X. Qi, Q. He, Q. Zhang, Q. Yan, F. Boey, H. Zhang, *Small* **2011**, *7*, 1876.

Molecular fragments of these carbon nanoforms[71] can serve as model systems for their investigation, with the added value of their synthetic availability in pure form with a well-defined molecular structure. The coordination of metal cations by fullerene fragments has been thoroughly studied, and they have also been used frequently to construct receptors for fullerenes,[87,89,88] but their binding by other organic hosts has not been investigated thus far. Herein, we present the first insights into the supramolecular association of a fullerene fragment (hemifullerene, $C_{30}H_{12}$) with a bowl-shaped electron donor molecule, based on a truxene core to which three dithiole rings are covalently attached (truxTTF).[38] The chemical structures of $C_{30}H_{12}$ and truxTTF are shown in Figure 8.1(a).

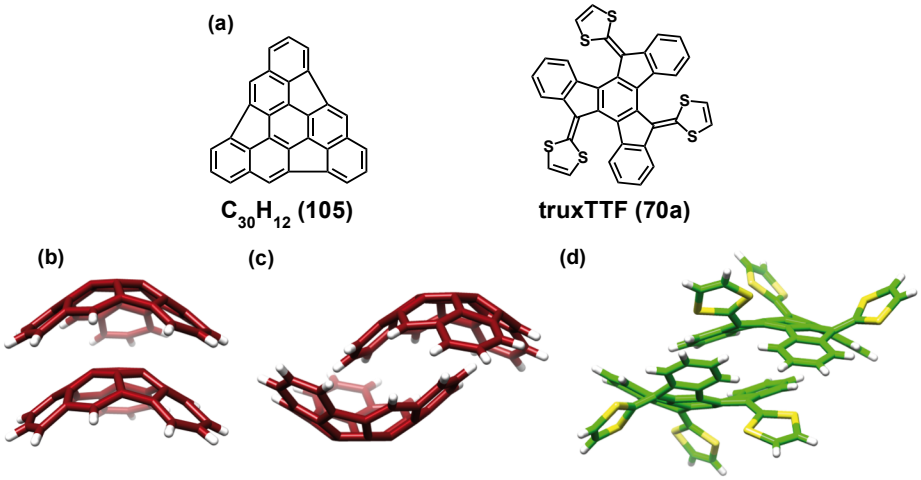

Figure 8.1. (a) Chemical structures of hemifullerene $C_{30}H_{12}$ and truxTTF. (b), (c) Structures of the dimers formed by $C_{30}H_{12}$ in its trigonal and orthorhombic crystal polymorphs, respectively. (d) Structure of the dimers formed by truxTTF in its crystal packing.

Several syntheses[70] and two crystal structures[80] of hemifullerene $C_{30}H_{12}$ were reported a few years ago. In the solid state, two polymorphs were found, each of which showed a different packing motif, originating from the interaction between the $C_{30}H_{12}$ molecules. In the trigonal polymorph, bowl-in-bowl columnar stacks were found, an arrangement in which π–π interactions are maximized (Figure 8.1(b)). In the orthorhombic polymorph, each hemifullerene inserts one of its six-membered rings into the cavity of a neighboring molecule, forming dimers in which both CH–π and π–

π interactions play a primary role (Figure 8.1(c)). On the other hand, in truxTTF, a bowl-in-bowl arrangement is prevented by the protruding dithiole rings and, consequently, only the dimeric form in which one of the aromatic rings of each monomer is placed inside the cavity of the other is found (Figure 8.1(d)). Because of their concave shape both $C_{30}H_{12}$ and truxTTF are inherently chiral, [109] consequently, each is obtained as a racemic mixture of two enantiomers.

The synthesis of the hemifullerene $C_{30}H_{12}$ (**105**) was carried out at the laboratory of professor L. T. Scott at Boston College, following the previously reported synthetic strategy.[70b]

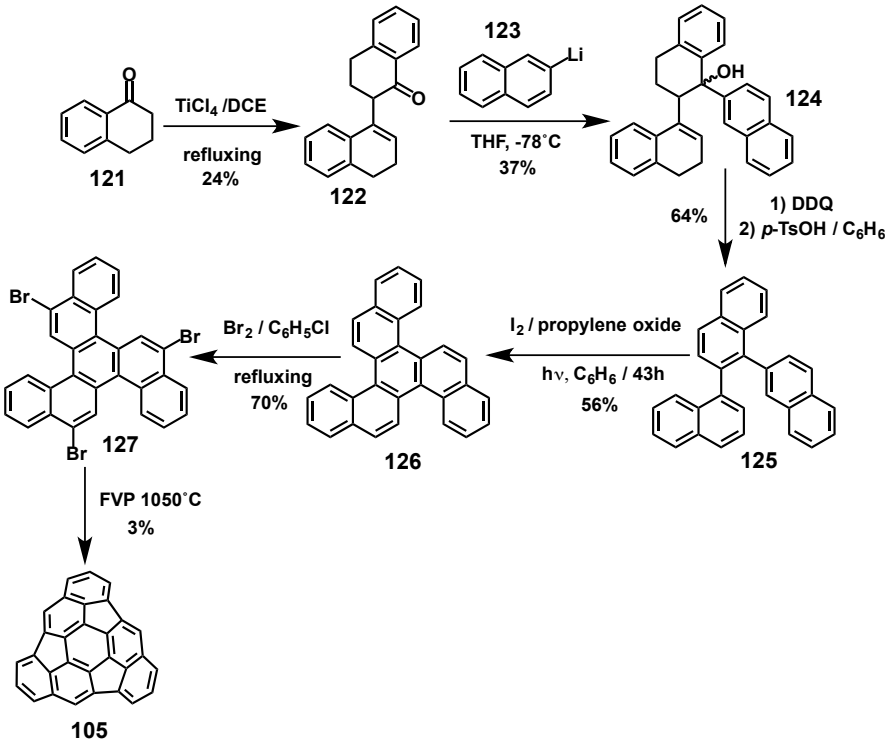

Scheme 8.1. Synthetic route towards hemifullerene $C_{30}H_{12}$ (**105**).

The aldol condensation of commercially available α-tetralone (**121**) with $TiCl_4$ in refluxing 1,2-diclhoroethane gives the ketone **122** in 24% yield. The reaction of **122** with 2-naphthyllithium (**123**), generated in situ from 2-

[109] A. Dalla Cort, L. Mandolini, C. Pasquini, L. Schiaffino, *New J. Chem.* **2004**, *28*, 1198.

bromonaphthalene and BuLi, at -78°C gives the alcohol **124** (37%); this alcohol is then aromatized to **125** by treatment with 2,3-dichloro-5,6-dicyano-1,4-benzoquinone (DDQ) and a catalytic amount of *p*-toluensulfonic acid (*p*-TsOH) in refluxing benzene (64%). Irradiation of **125** in benzene with a 450 W medium-pressure mercury UV-lamp with iodine and propylene oxide provokes the photocyclization of **125** to give **126** (56%). Bromination of **126** with Br_2 in refluxing chlorobenzene results in the selective formation of **127** (70%), which is the precursor of hemifullerene **105**. In a last step, samples up to 1g of tribromide **127** undergo FVP treatment (1050°C, pressure range [0.763-0.758] Torr, N_2 as the carrier gas) to produce hemifullerene $C_{30}H_{12}$ in 3% yield.

The transformation of **127** into **105** is believed to occur by a stepwise loss of the halogen atoms, the homolysis of a C-Br bond leads to an aryl radical; the sterically hindered H atom at the adjacent carbon shifts by a 1,2-H migration giving rise to a new aryl radical reactive at the site where ring closure occurs.

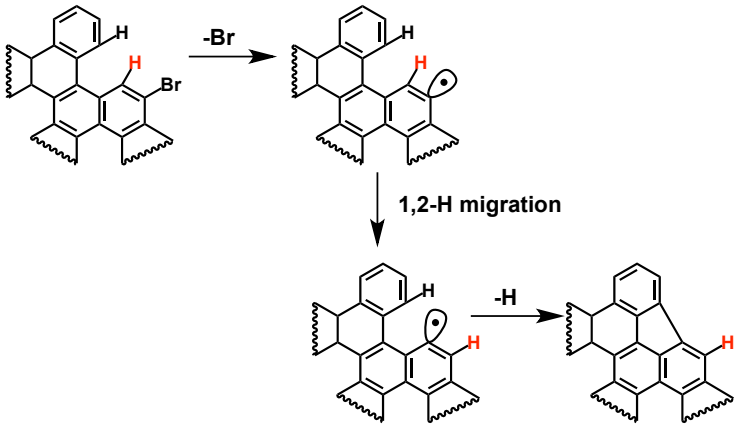

Scheme 8.2. Proposed mechanism for the formation of **105**.

The chemical structure of hemifullerene $C_{30}H_{12}$ has been fully established. Interestingly, the ^1H NMR spectrum is relatively simple due to the molecular symmetry (Figure 8.2).

The synthesis of the truxTTF has already been mentioned in the first chapter of this memory.

Considering the ability of truxTTF to associate fullerenes,[38,40] and its electron-donating character, we reasoned that it should also be able to bind $C_{30}H_{12}$, forming hetero-molecular bowl-bowl complexes. To explore this possibility, we first carried out density functional theory (DFT) calculations on four different supramolecular truxTTF•$C_{30}H_{12}$ models, which were rationally constructed from the crystallographic information on both $C_{30}H_{12}$ and truxTTF. All of the models proposed were fully optimized using the revPBE0-D3 functional,[110] which is capable of capturing the dispersion effects and is one of the best density functional to accurately describe supramolecular complexes governed by π–π interactions.[111] The revPBE0-D3 functional has been successfully applied in the structural and energetic characterization of related supramolecular nanoarchitectures between a tetrathiafulvalene derivative and a graphene sheet model.[112]

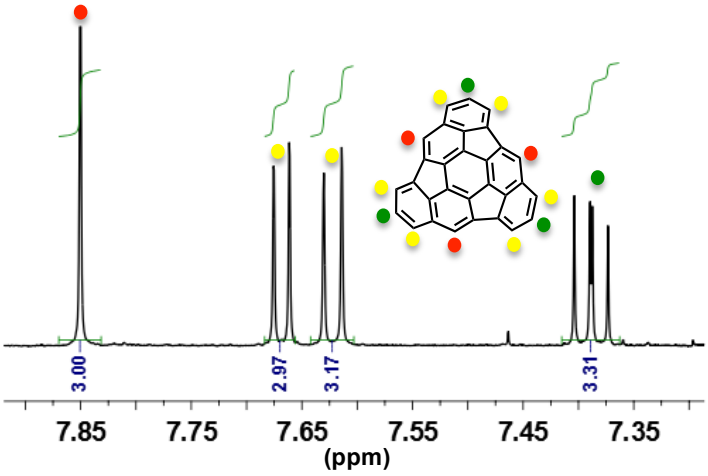

Figure 8.2. ^{1}H-NMR (500 MHz, $CDCl_3$, 298K) spectra of **105**.

Figure **8.3** displays the minimum-energy structures (**1**-**4**) computed for the truxTTF•$C_{30}H_{12}$ heterodimer at the revPBE0-D3/cc-pVTZ level. The most relevant intermolecular distances in **1**-**4** are given in Figure 8.4(a).

[110] (a) Y. Zhang, W. Yang, *Phys. Rev. Lett.* **1998**, *80*, 890; (b)S. Grimme, J. Antony, S. Ehrlich, H. Krieg, *J. Chem. Phys.* **2010**, *132*, 154104.
[111] W. Hujo, S. Grimme, *J. Chem. Theory Comput.* **2011**, *7*, 3866.
[112] F. G. Brunetti, H. Isla, J. Aragó, E. Ortí, E. M. Pérez, N. Martín, *Chem. Eur. J.* **2013**, *19*, 9843.

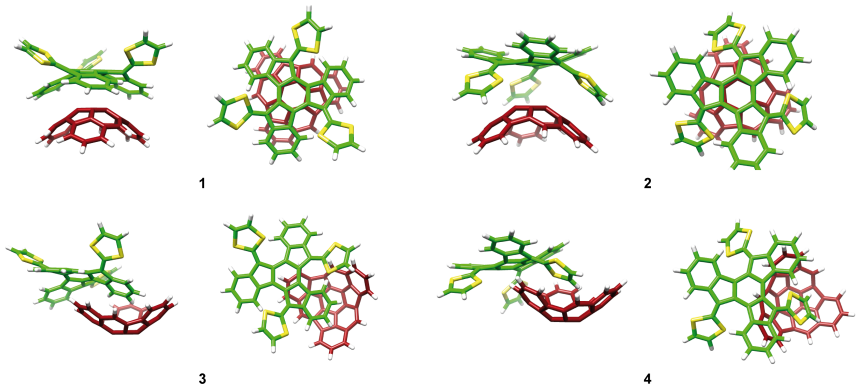

Figure 8.3. Minimum-energy structures (**1**-**4**) computed for the truxTTF•$C_{30}H_{12}$ heterodimer at the revPBE0-D3/cc-pVTZ level.

The truxTTF•C_{60} associate was also calculated at the same level of theory (Figure 8.4(b)). In structures **1** and **2** the convex surface of the $C_{30}H_{12}$ bowl perfectly matches the two concave cavities of the truxTTF host; that is, either through the cavity formed by the carbon backbone (structure **1**) or through the cavity formed by the central benzene ring and the three dithiole rings (structure **2**). Both structures can be thus seen as bowl-in-bowl arrangements where π–π interactions are maximized. The concave cavities of truxTTF and $C_{30}H_{12}$ can also interact, giving rise to heterodimers in which either a benzene ring or a dithiole ring of the truxTTF molecule is placed inside the concave cavity of the hemifullerene bowl (structures **3** and **4,** respectively). The optimized heterodimeric structures **1**-**4** all show close intermolecular contacts in the 2.5-3.7 Å range (Figure 8.4(a)), which is indicative of the positive non-covalent interactions between both molecular bowls.

(a)

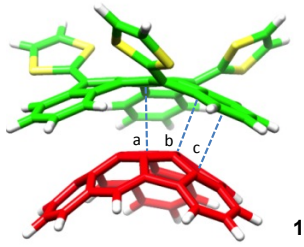

1

Distance	revPBE0-D3/cc-pVTZ (Å)
a	3.26
b	3.08
c	3.28

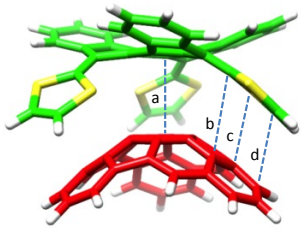

2

Distance	revPBE0-D3/cc-pVTZ (Å)
a	3.71
b	3.66
c	3.37
d	3.49

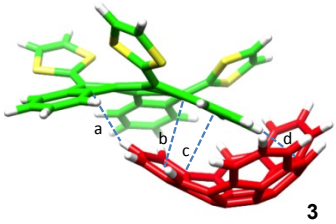

3

Distance	revPBE0-D3/cc-pVTZ (Å)
a	2.73
b	3.65
c	3.54
d	2.56

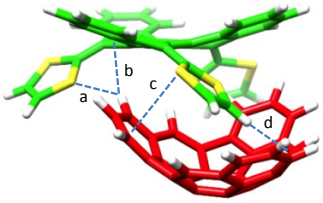

4

Distance	revPBE0-D3/cc-pVTZ (Å)
a	2.76
b	2.69
c	3.62
d	2.52

(b)

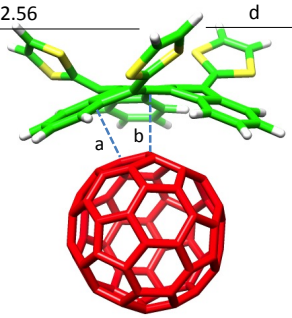

Distance	revPBE0-D3/cc-pVTZ (Å)
a	3.27
b	3.07

Figure 8.4. Selected intermolecular distances computed at the revPBE0-D3/cc-pVTZ level for structures (a) **1**-**4** and (b) truxTTF•C_{60} associate.

To assess the strength of the interactions between the truxTTF and $C_{30}H_{12}$ bowls, association energies for the previously optimized heterodimers were also calculated at the revPBE0-D3/cc-pVTZ. The four supramolecular structures **1**-**4** exhibit significant gas-phase association energies, ranging from -21.0 and -19.4 kcal mol^{-1} for **1** and **2**, respectively, to -25.2 and -28.5 kcal mol^{-1} for **3** and **4**, respectively. The bowl-in-bowl arrangements are therefore significantly less stable than the staggered ones. The truxTTF•C_{60} model system, for which we have experimentally calculated association constants in the range of log K_a = 3-4 in a variety of solvents at room temperature,[38,40] presents an association energy of -22.1 Kcal mol^{-1}, which is very close to that computed for structure **1**, owing to the similarity in the concave-convex interaction.

The electronic properties of the truxTTF•$C_{30}H_{12}$ associate have also been theoretically investigated. Figure **8.5** sketches the highest occupied (HOMO-2 to HOMO) and lowest unoccupied (LUMO to LUMO+4) molecular orbitals computed at the revPBE0-D3/cc-pVTZ level for the most stable structure (**4**) of truxTTF•$C_{30}H_{12}$. Similar molecular orbital distributions are found for the rest of supramolecular structures **1**-**3** (Figure 8.5(b)). The HOMO, HOMO-1, and HOMO-2 spread over the electron-donating truxTTF moiety. In contrast, the LUMO, LUMO+1, and LUMO+2 are localized on the electron-accepting $C_{30}H_{12}$ bowl, with LUMO+1 and LUMO+2 being almost degenerate. Above LUMO+2, LUMO+3 and LUMO+4 are again concentrated on the truxTTF bowl. The nature and energies calculated for the HOMOs and LUMOs of truxTTF•$C_{30}H_{12}$ therefore suggest that photoinduced charge-transfer processes from the truxTTF to $C_{30}H_{12}$ should take place in the UV/vis range.

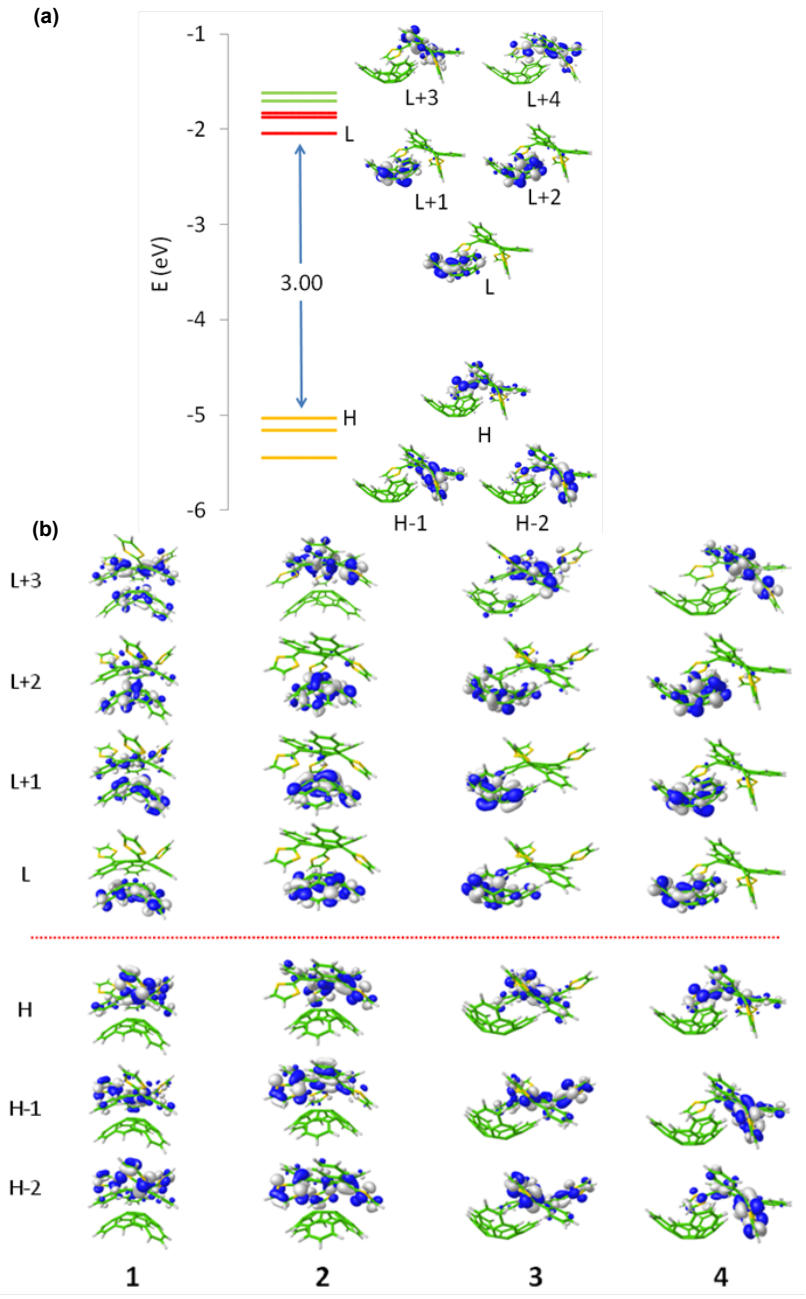

Figure 8.5. (a) Electron density contours (0.03 e bohr^{-3}) and energies calculated for the HOMOs and LUMOs of the structure **4** at the revPBE0-D3/cc-pVTZ level. H and L denote HOMO and LUMO, respectively. (b) Electron density contours (0.03 e bohr^{-3}) computed for structures 1-4 at the revPBE0-D3/cc-pVTZ level.

Encouraged by the results of the theoretical calculations, we titrated truxTTF (1.7×10^{-4} M) with $C_{30}H_{12}$ (0.8×10^{-3} M) in $CHCl_3$ at room temperature. The electronic absorption spectra resulting from this titration experiment are depicted in Figure 8.6(a). We observed a decrease in the intensity of the truxTTF absorption at λ = 450 nm, accompanied by the increase of a broad band and a charge-transfer band in the 500-600 nm region. These spectral changes are analogous to those found in the titration of truxTTF *vs*. C_{60}, albeit with a significantly less intense charge-transfer feature.[40] The results of three separate titration experiments were analyzed with Reactlab Equilibria software, affording a binding constant of log K_a = 3.6 ± 0.3.

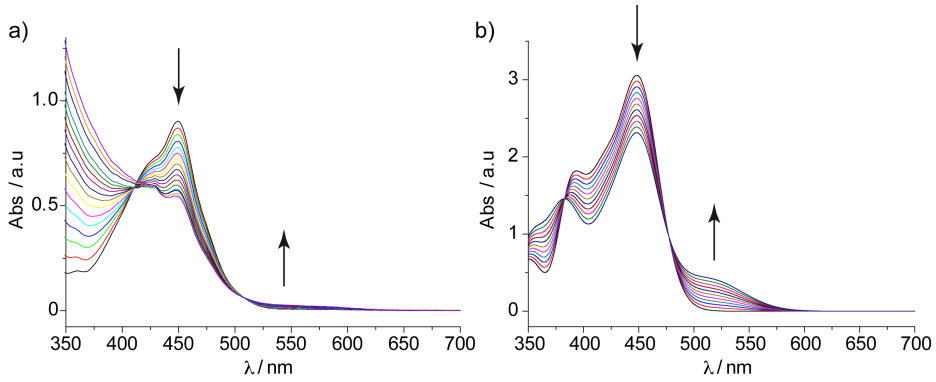

Figure 8.6. (a) Experimental UV/vis spectra as obtained during the titration of truxTTF (1.7×10^{-4} M) with $C_{30}H_{12}$ (0.8×10^{-3} M) in $CHCl_3$ at room temperature. Each addition corresponds to 0.2 eq. (b) TDDFT simulation of the absorption spectra of truxTTF as the ratio of truxTTF•$C_{30}H_{12}$ increases from 0 to 100% (B3LYP/cc-pVDZ calculations including $CHCl_3$ as solvent).

To gain more insight into the electronic nature of the absorption bands observed experimentally, and their evolution during the titration experiment, the lowest-energy singlet excited states (S_n) of the truxTTF•$C_{30}H_{12}$ heterodimer and of isolated truxTTF were computed using time-dependent DFT (TDDFT) approach, taking into account the solvent effects. Only the results obtained for the most stable structure (**4**) of truxTTF•$C_{30}H_{12}$ are discussed. TDDFT calculations predict the first two excited stated S_1 and S_2 at 537 nm (2.31 eV) and 516 nm (2.40 eV) above the ground state S_0 with moderate oscillator strengths (*f*) of 0.036 and 0.046, respectively. The $S_0 \rightarrow S_1$ and $S_1 \rightarrow S_2$ electronic transitions are mainly described by one-electron

promotions from the HOMO to the LUMO and LUMO+1, respectively. These transitions therefore imply a charge transfer from the electron-donor, truxTTF, where the HOMO is located, to the electron-acceptor, $C_{30}H_{12}$, where the LUMO and LUMO+1 are spread (Figure 8.5(a)), and are the major contribution to the charge-transfer band experimentally recorded in the 500-600 nm range. Other charge-transfer transitions are computed around 500 nm, but they are less intense. At higher energies, the S_9 (454 nm, 2.73 eV), S_{10} (452 nm, 2.75 eV), and S_{11} (445 nm, 2.78 eV) states are calculated to be very close in energy and present higher oscillator strengths (0.178, 0.178 and 0.093, respectively). The $S_0 \rightarrow S_9$, $S_0 \rightarrow S_{10}$ and $S_0 \rightarrow S_{11}$ electronic transitions mainly originate from the HOMO, HOMO-1→LUMO+3, LUMO+4 one-electron excitations localized on truxTTF (Figure 8.5(a)), and give rise to the absorption band observed at 450 nm. The oscillator strengths calculated for these transitions are significantly smaller than those computed for isolated truxTTF (0.277, 0.320, and 0.145, respectively).

A TDDFT simulation of the absorption spectra of the truxTTF chromophore as the amount of truxTTF•$C_{30}H_{12}$ increases from 0 (spectrum of truxTTF) to 100% is shown in Figure 8.6(b). The simulation clearly reveals that the truxTTF band decreases in intensity as truxTTF•$C_{30}H_{12}$ forms. This is due to the smaller oscillator strengths computed for the truxTTF-centered transitions in the truxTTF•$C_{30}H_{12}$ complex. The charge-transfer band associated with the formation of truxTTF•$C_{30}H_{12}$ simultaneously increases in intensity. The theoretical simulation is in notable agreement with the experimental evolution of the absorption spectra, and supports the formation of the supramolecular donor-acceptor truxTTF•$C_{30}H_{12}$ heterodimer.

In addition to the ground-state interactions, we turned to pump probe absorption measurements to unravel the processes following photoexcitation of truxTTF•$C_{30}H_{12}$ and their references truxTTF and $C_{30}H_{12}$. Upon 470 nm excitation of truxTTF, a new transient immediately develops (Figure 8.7). Characteristics of the latter are a marked maximum in the visible at 530 nm and a broad, featureless transition that spans all throughout the near infrared. Furthermore, a marked ground-state bleaching is observed around 450 nm. This excited state decays rapidly, as in other sulfur rich electron donors, with a lifetime of only 1.0 ± 0.1 ps. The short lifetime is rationalized by the presence

of the sulfur atoms, with a strong second-order vibronic spin-orbit coupling, as it transforms into a much weaker absorbing state, for which a lifetime of 20 ± 1 ps is detected.

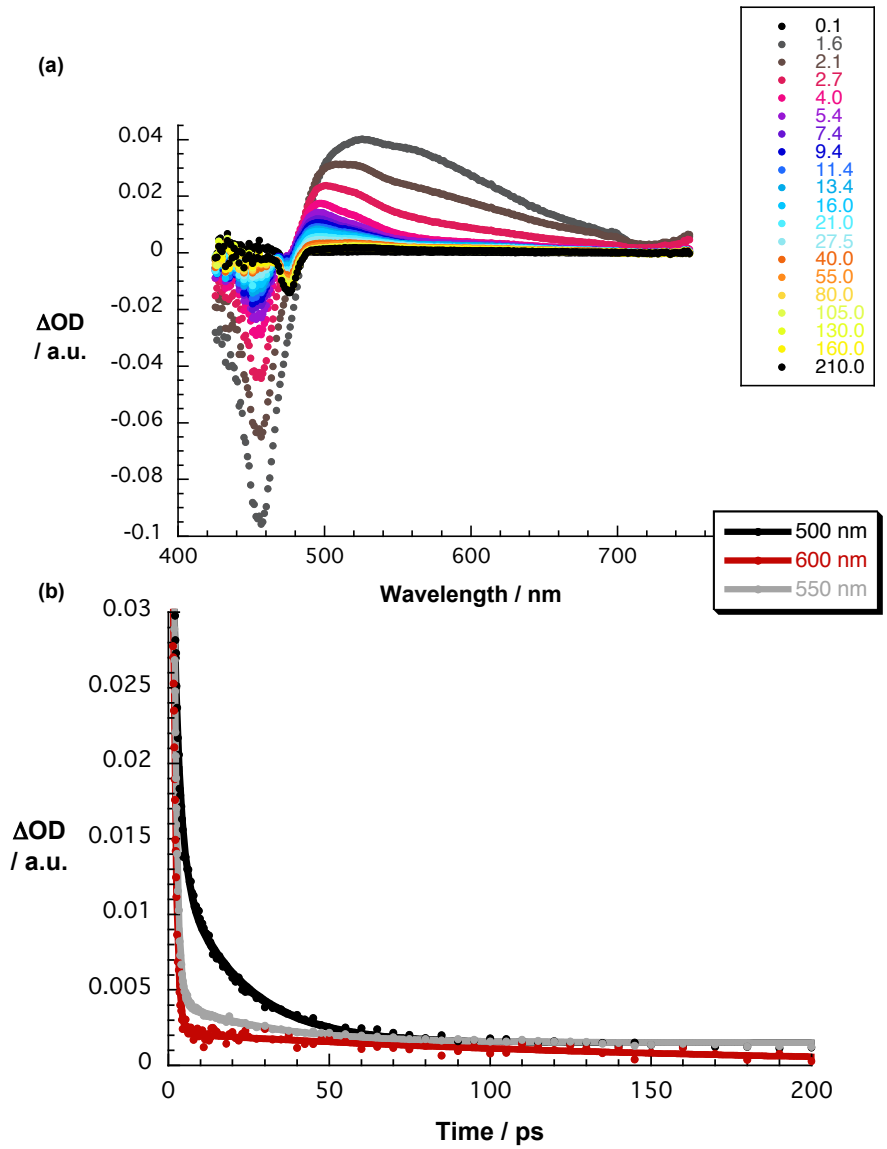

Figure 8.7. (a) Differential absorption spectra (visible) obtained upon femtosecond pump probe experiments (470 nm) of truxTTF in chlorobenzene with time delays between 0.1 and 210.0 ps at room temperature. (b) Time absorption profiles of the spectra shown above at 500, 550 and 600 nm monitoring the excited state deactivation.

For $C_{30}H_{12}$, the singlet and triplet excited states upon 387 nm excitation include transient maxima at 515 and 516 nm, respectively (Figure 8.8). These reflect the singlet excited state that decays within 11 ns through intersystem crossing to the energetically low-lying triplet excited state.

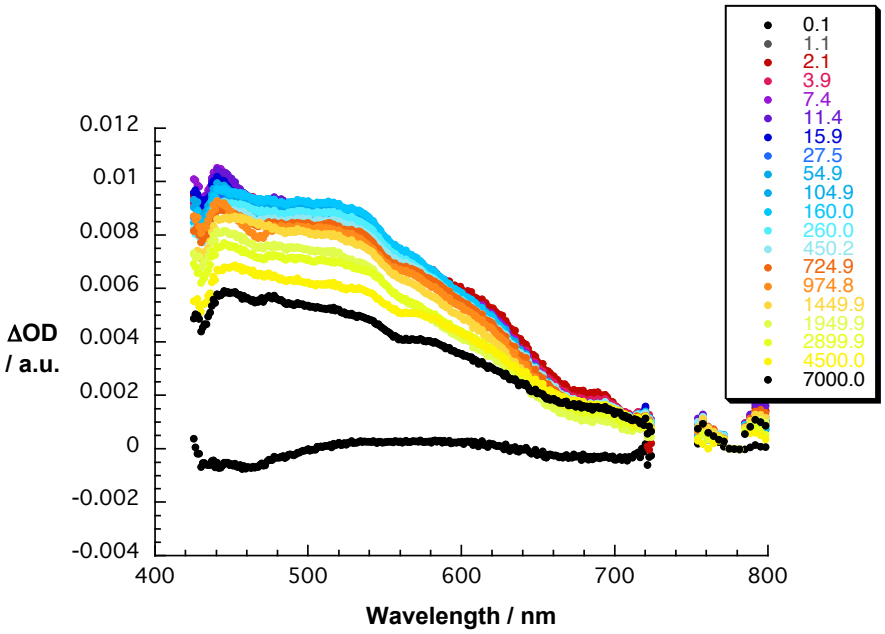

Figure 8.8. Differential absorption spectra (visible) obtained upon femtosecond pump probe experiments (387 nm) of hemifullerene $C_{30}H_{12}$ in toluene with time delays between 0.1 and 7000 ps at room temperature.

Following 470 nm photoexcitation of truxTTF•$C_{30}H_{12}$ (1:5 ratio), the differential absorption changes are dominated by truxTTF-centered features (Figure 8.9). Within approximately 1.5 ± 0.5 ps, the latter gives place, however, to a new transient with characteristics that include maxima at 440, 475, 495, 530 (sh), and 615 nm, as well as a minimum at 450 nm. Neither photoexcited $C_{30}H_{12}$ nor photoexcited truxTTF exhibit differential absorption changes that bear any significant resemblance to these data (Figure 8.7 and 8.8). Thus a tentative assignment of these features implies the formation of a charge-separated state.

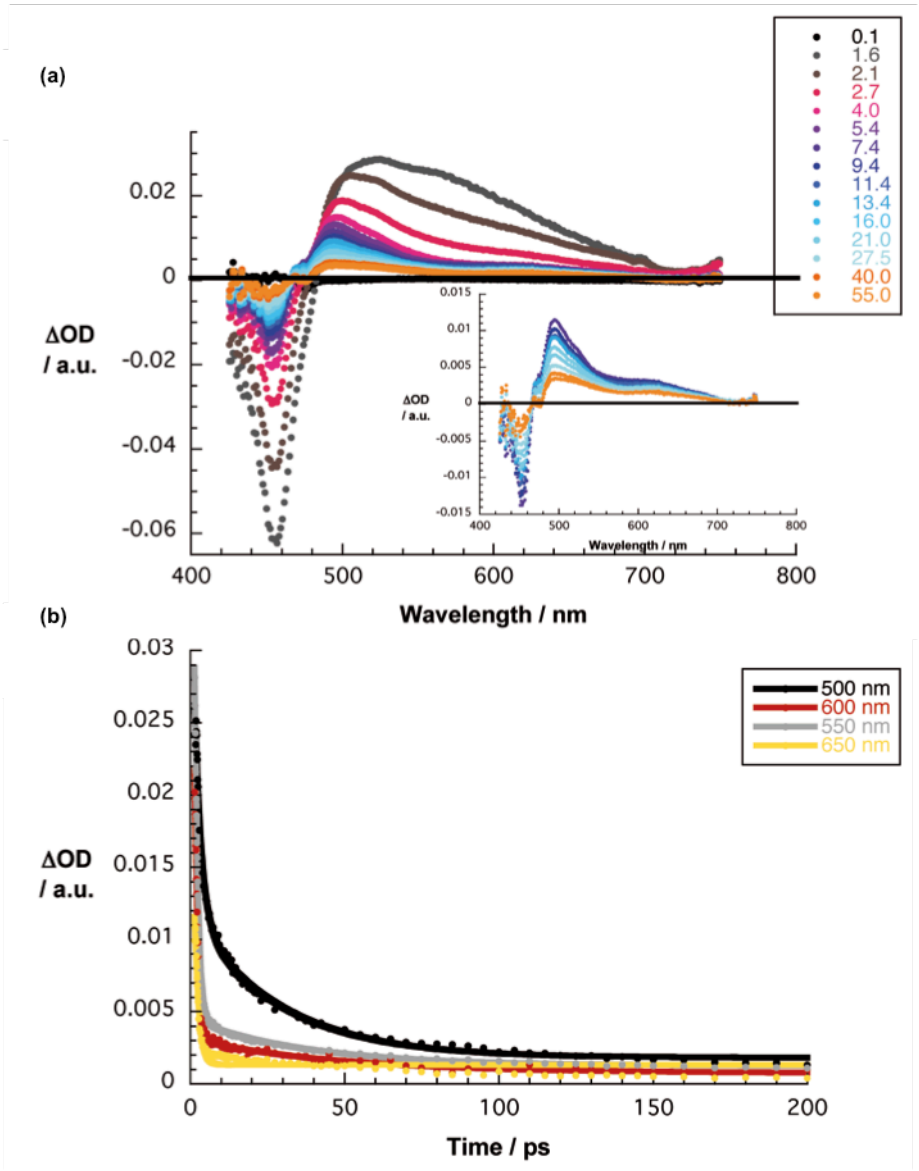

Figure 8.9. (a) Differential absorption spectra (visible) obtained upon femtosecond pump probe experiments (470 nm) of truxTTF•$C_{30}H_{12}$ (1:5 ratio) in chlorobenzene with time delays of 0.1-55.0 ps at room temperature. (b) Time absorption profiles of the spectra shown in (a) at 500, 550, 600 and 650 nm monitoring the charge transfer.

Support for this interpretation comes from spectroelectrochemical oxidation and reduction experiments with truxTTF and $C_{30}H_{12}$ in *ortho*-dichlorobenzene, respectively. For the former, upon applying a potential of +0.8 V versus Ag

wire, maxima at 500 and 615 nm and minimum at 450 nm are noted (Figure 8.10(a)). Again, these changes were reversed upon resetting the applied potential back to 0 V. As such, the differential absorption changes upon photoexciting truxTTF•$C_{30}H_{12}$ (Figure 8.9) are in sound agreement with the superimposition of the spectroelectrochemically initiated oxidation and reduction of the truxTTF and hemifullerene, respectively. From multiwavelength analyses we derive rate constants of 6.6 x 10^{11} and 1.0 x 10^{10} s^{-1} for the charge separation and charge recombination dynamics, respectively.

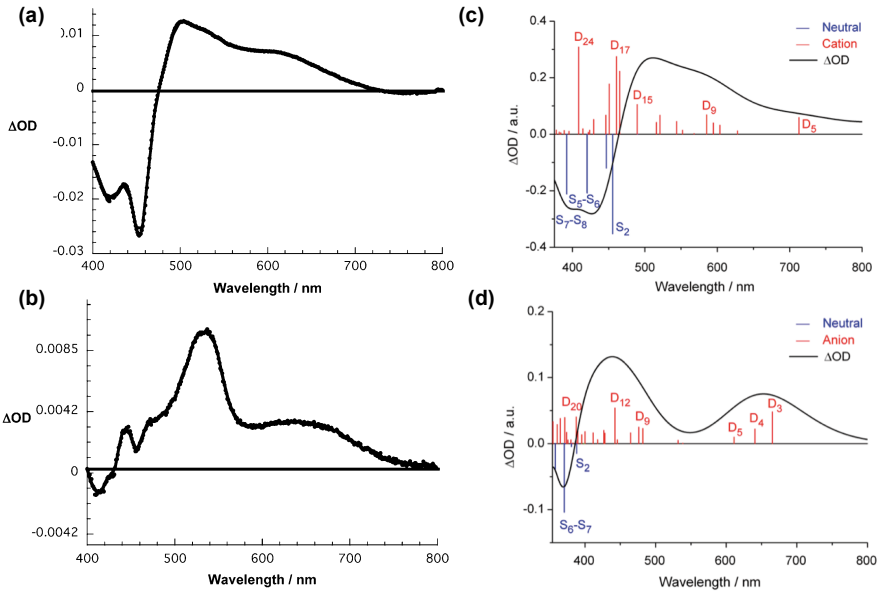

Figure 8.10. Differential absorption spectra (visible) obtained upon spectroelectrochemical oxidation of truxTTF (a) and reduction of $C_{30}H_{12}$ (b) in deoxygenated *ortho*-dichlorobenzene containing 0.1 M $TBAPF_6$ with potentials versus Ag wire of +0.8 and –1.0 V, respectively. TDDFT simulation of the differential absorption spectra calculated for truxTTF$^{\bullet+}$ (c) and $C_{30}H_{12}^{\bullet-}$ (d) at the B3LYP/cc-pVDZ level using ortho-dichlorobenzene as solvent.

To better understand the spectroelectrochemical data recorded for the truxTTF and $C_{30}H_{12}$ fragments, the theoretical absorption spectra of the singly oxidized truxTTF$^{\bullet+}$ and singly reduced $C_{30}H_{12}^{\bullet-}$ species were computed. The spectra calculated for the neutral species were substracted from the spectra

of the oxidized/reduced systems to obtain a theoretical simulation of the differential absorption spectra. For the truxTTF fragment, the predicted spectrum (Figure 8.10(c)) is in excellent agreement with the experimental spectrum (Figure 8.10(a)). The long tail over 550-800 nm originates from electron promotions from high-energy, doubly occupied molecular orbitals to the single-occupied molecular orbital (SOMO) (doublet states D_5 to D_9). The peak observed at 500 nm is due to higher-energy excitations (states D_{12} to D_{15}), where SOMO→LUMO transitions are involved. The steep slope experimentally recorded at around 480 nm is nicely reproduced by the theoretical simulation and originates from the proximity in energy of the intense excitation to the double state D_{17} in the cation and the excitation to the singlet state S_2 in the neutral species. The two peaks bleaching in the 400-450 nm region is due to the intense transitions (S_5→S_6 and S_7→S_8) of neutral truxTTF counterbalanced between them by the intense doublet excitation (D_{24}) in the cation. For the hemifullerene fragment, the theoretical simulation (Figure 8.10(d)) is in worse agreement with the experimental spectrum (Figure 8.10(b)) because the most intense band is calculated too high in energy. The lower-energy band appearing at 600-700 nm corresponds to doublet excitations (D_3-D_5) from the SOMO to higher-unoccupied molecular orbitals. The near-degeneracy of the LUMOs in neutral $C_{30}H_{12}$ is the origin of these low-energy transitions. Otherwise, the main features experimentally observed above 420 nm are assigned to doublet transitions (D_8 to D_{20}) implying electron excitations from doubly occupied molecular orbitals to the SOMO.

In summary, we have corroborated the association of a fullerene fragment, namely hemifullerene $C_{30}H_{12}$, with a bowl-shaped electron-donor, truxTTF. The association was investigated experimentally through UV/vis titrations. To this end, changes in the absorption spectra, most notably a decrease in the truxTTF absorption and the formation of a weak charge transfer band, are clearly indicative for the truxTTF•$C_{30}H_{12}$ heterodimer in solution. Quantitatively, we calculated a binding constant of log K_a = 3.6 ± 0.3 in $CHCl_3$ at room temperature, which is comparable to that found for the association of truxTTF with C_{60}. Calculations at the revPBE0-D3/cc-pVTZ level of theory supported the non-covalent interactions between the truxTTF and the $C_{30}H_{12}$; providing insight into the possible structure of the heterodimer and the

nature of the changes observed during the UV/vis titration.

Remarkably, femtosecond pump-probe experiments reveal the formation of a transient species that corresponds to a charge-separated truxTTF$^{\bullet+}$•$C_{30}H_{12}^{\bullet-}$ state. Overall, the latter assignment was backed by both spectroelectrochemical measurements and theoretical calculations. Analysis of the time evolution of these features afforded rate constants of 6.6 x 10^{11} and 1.0 x 10^{10} s^{-1} for the charge separation and charge recombination dynamics respectively. This is the first example of a fullerene fragment mimicking the charge transfer behavior of C_{60}, which paves the way to the study of other related known fullerene fragments, thus opening a new avenue for these electronically less-known carbon-based materials.

Computational details: Geometry optimizations of the supramolecular truxTTF•$C_{30}H_{12}$ heterodimers **1–4** were performed within the density functional theory (DFT) framework using the revPBE0 correlation-exchange functional in combination with the Grimme dispersion correction –D3 (revPBE0-D3).[110] Note that the original damping function in the –D3 approach has been replaced by the Becke-Johnson damping function to provide a better performance.[113] The choice of the exchange-correlation functional revPBE0 is justified by its excellent performance when studying the very popular S22[114] and S66[115] non-covalent interaction databases[116,111] as well as when applied to other related supramolecular systems.[117] The correlation-consistent cc-pVTZ basis set was applied throughtout.[118] The "resolution of identity" (RI)[119] and "chain of spheres" (COSX)[120] techniques, for the Coulomb and exchange integrals, respectively, were used to alleviate the computational cost of the more demanding steps.

[113] S. Grimme, S. Ehrlich, L. Goerigk, *J. Comput. Chem.* **2011**, *32*, 1456.
[114] P. Jurecka, J. Sponer, J. Cerny, P. Hobza, *PCCP* **2006**, *8*, 1985.
[115] J. Řezáč, K. E. Riley, P. Hobza, *J. Chem. Theory Comput.* **2011**, *7*, 2427.
[116] W. Hujo, S. Grimme, *J. Chem. Theory Comput.* **2011**, *7*, 3866.
[117] (a) S. Grimme, W. Hujo, B. Kirchner, *Phys. Chem. Chem. Phys.* 2012, 14, 4875; (b) M. K. Rana, H. S. Koh, J. Hwang, D. J. Siegel, *J.* Phys. *Chem. C.* **2012**, *116*, 16957; (c) A. Tkatchenko, O. A von Lilienfeld, *Phys. Rev. B* **2008**, *78*, 045116; (d) F. Goltl, J. Hafner, *J. Chem. Phys.* **2011**, *134*, 064102.
[118] J. T. H. Dunning, *J. Chem. Phys.* **1989**, *90*, 1007.
[119] K. Eichkorn, O. Treutler, H. Öhm, M. Häser, R. Ahlrichs, *Chem. Phys. Lett.* **1995**, *240*, 283.
[120] F. Neese, F. Wennmohs, A. Hansen, U. Becker, *Chem. Phys.* **2009**, *356*, 98.

On the previously optimized structures (both for the heterodimer and for the isolated moieties), single- energy calculations at the revPBE0-D3/cc-pVTZ level were performed to compute the association binding energies. Note that the three-body contribution to the dispersion energy has been included because it can be significant for medium and large supramolecular systems.[121] The association energy in each heterodimer was computed as the difference between the energy of the associate and the sum of the energies for the two constituting fragments [Δe_{assoc} = *E*(heterodimer) – *E*(truxTTF) – *E*($C_{30}H_{12}$ or C_{60})]. Geometry optimizations and single-point energy calculations at the revPBE0-D3/cc-pVTZ level were performed using the ORCA program package (version 2.9.0).[122] Molecular orbitals were plotted using the Chemcraft 1.6 software with electron density contours of 0.03 e $bohr^{-3}$.[123]

Vertical electronic transition energies for the ground-state optimized geometries of structures **1–4** were computed in the framework of the time-dependent density functional theory (TDDFT) [124] using the Gaussian 09 (revision D.01)[125] suite of programs. The lowest 40 singlet excited states of the truxTTF•$C_{30}H_{12}$ heterodimer and its individual fragments were computed at the B3LYP/cc-pVDZ level of theory. Solvent effects were taken into account by means of the polarizable continuum model (PCM) using chloroform ($CHCl_3$) as a solvent.[126] The TDDFT simulation displayed on Figure 8.6 (b) corresponds to the absorption spectra of truxTTF as the ratio of truxTTF•$C_{30}H_{12}$ increases

[121] S. Grimme, *Chem. Eur. J.* **2012**, *2*, 9955.
[122] F. Neese. *WIREs Comput. Mol. Sci.* **2012**, *2*, 73.
[123] http://www.chemcraftprog.com
[124] E. M. Casida, C. Jamorski, K. C. Casida, D. R. Salahub, *J. Chem. Phys.* **1998**, *108*, 4439.
[125] Gaussian 09, revisión D.01, M. J. Frisch, G. W Trucks, H. B. Schlegel, G. E. Scuseria, M. A. Robb, J. R. Cheeseman, G. Scalmani, V. Barone, B. Mennucci, G. A. Petersson, H. Nakatsuji, M. Caricato, X. Li, H. P. Hratchian, A. F. Izmaylov, J. Bloino, G. Zheng, J. L. Sonnenberg, M. Hada, M. Ehara, K. Toyota, R. Fukuda, J. Hasegawa, M. Ishida, T. Nakajima, Y. Honda, O. Kitao, H. Nakai, T. Vreven, J. A. Montgomery, J. E. Peralta, F. Ogliaro, M. Bearpark, J. J. Heyd, E. Brothers, K. N. Kudin, V. N. Staroverov, R. Kobayashi, J. Normand, K. Raghavachari, A. Rendell, J. C. Burant, S. S. Iyengar, J. Tomasi, M. Cossi, N. Rega, J. M. Millam, M. Klene, J. E. Knox, J. B. Cross, V. Bakken, C. Adamo, J. Jaramillo, R. Gomperts, R. E Stratmann, O. Yazyev, A. J. Austin, R. Cammi, C. Pomelli, J. W. Ochterski, R. L. Martin, K. Morokuma, V. G. Zakrzewski, G. A. Voth, P. Salvador, J. J. Dannenberg, S. Dapprich, A. D. Daniels, Farkas, J. B. Foresman, J. V. Ortiz, J. Cioslowski, D. J. Fox, Gaussian, Inc., Wallingford CT, **2009**.
[126] (a) J. Tomasi, M. Perisco, *Chem. Rev.* **1994**, 2027; (b) C. S. Cramer, D. G. *Solvent Effects and Chemical reactivity;* Kluwer: Dordrecht, 1996.

from 0 (pure truxTTF) to 100% (all the truxTTF is complexed as truxTTF•$C_{30}H_{12}$) in steps of 10%. The sigma parameter used for the Gaussian functions in the convolution of the spectra was set to 0.15 eV. During the titration experiment, there is an increasing amount of $C_{30}H_{12}$ that is not associated to truxTTF and contributes to the experimental absorption spectrum with the growth of an intense band below 350 nm where the characteristic intense peak of $C_{30}H_{12}$ is found. The theoretical simulation does not consider the electronic transitions of isolated $C_{30}H_{12}$ involved in this band because they are not relevant for the characterization of the supramolecular truxTTF•$C_{30}H_{12}$ complex.

The truxTTF and hemifullerene fragments in its cation and anion state, respectively, were also computed in order to understand the spectroelectrochemical oxidation and reduction experiments carried out in *ortho*-dichlorobenzene. The $truxTTF^{+}$ and $C_{30}H_{12}^{-}$ species were fully optimized at the rev-PBE0- D3/cc-pVTZ level taking into account solvent effects using PCM and *ortho*-dichlorobenzene as solvent. Their neutral counterparts were also optimized at the same level of theory. The TDDFT simulation of the differential absorption spectra for $truxTTF^{+}$ and $C_{30}H_{12}^{-}$ (Figure 8.10 (c and d)) was obtained by subtracting the spectrum of the neutral form of each fragment to the calculated spectrum of the cation and anion, respectively. TDDFT calculations were performed at the B3LYP/cc-pVDZ level using *ortho*-dichlorobenzene as solvent.

8.2. EXTENSION TO OTHER CURVED PAH SYSTEMS. A COMPARATIVE STUDY

Encouraged by the aforementioned results we decided to extend these systematic studies to two more buckybowls **112** and **113**, provided by Prof. Yao-Ting Wu from the National Cheng Kung University (Taiwan). Therefore, we will study the supramolecular complexation among truxTTF molecule and these two new buckybowls. Notice that if **105** could be seen as the hemifullerene of C_{60}, **113** could be seen as the analogous hemifullerene of C_{70}.

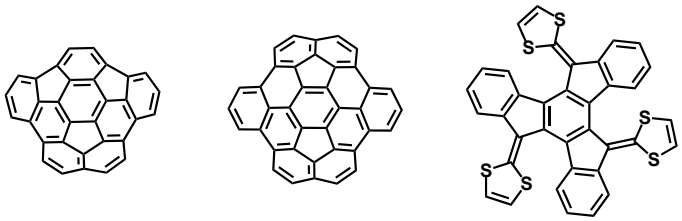

$C_{32}H_{12}$ (**112**) $C_{38}H_{14}$ (**113**) truxTTF (**70a**)

Figure 8.11. Chemical structures of buckybowls **112**, **113**, and truxTTF **70a**.

We also wanted to explore if the n/p electronic behavior of the buckybowls can be tuned depending on the counterpart in the formed complexes. For this purpose, we have firstly investigated the association behavior in solution of buckybowls $C_{32}H_{12}$ **112** and $C_{30}H_{12}$ **105** towards truxene derivative molecule **128** the trux6CN. Please note that **128** is the analogous acceptor system to truxTTF in which the three 1,3-dithiole rings are replaced by three cyanovinylene units.

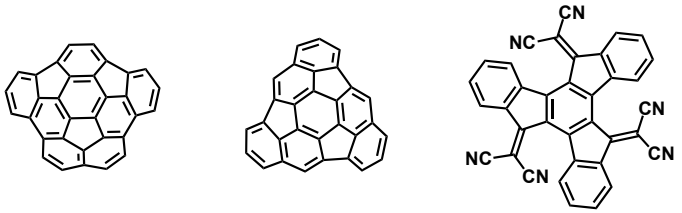

$C_{32}H_{12}$ (**112**) $C_{30}H_{12}$ (**105**) Trux6CN (**128**)

Figure 8.12. Chemical structures of buckybowls **112** and **113**, and truxene acceptor derivative **128**.

Electron acceptor trux6CN (**128**) was synthesized following the method described by V. Khodorkovsky and co-workers,[127] buckybowls **112** and **113** were provided by Y. T. Wu, and $C_{30}H_{12}$ (**105**) was synthesized at the laboratory of L. T. Scott.

128 was synthesized performing a triple Knoevenagel reaction on truxenone **3** with malononitrile, pyridine and titanium tetrachloride in chlorobenzene at 70°C.

[127] K. Jacob, J. Y. Becker, A. Ellern, V. Khodorkovsky, *Tetrahedron Lett.* **1999**, *40*, 8625.

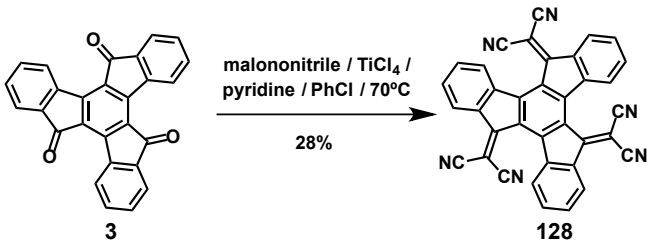

Scheme 8.3. Synthetic route towards **128**.

Although electron acceptor **128** has already been fully reported, the ^{1}H NMR spectrum is relatively simple due to the inherent molecular symmetry (Figure 8.13).

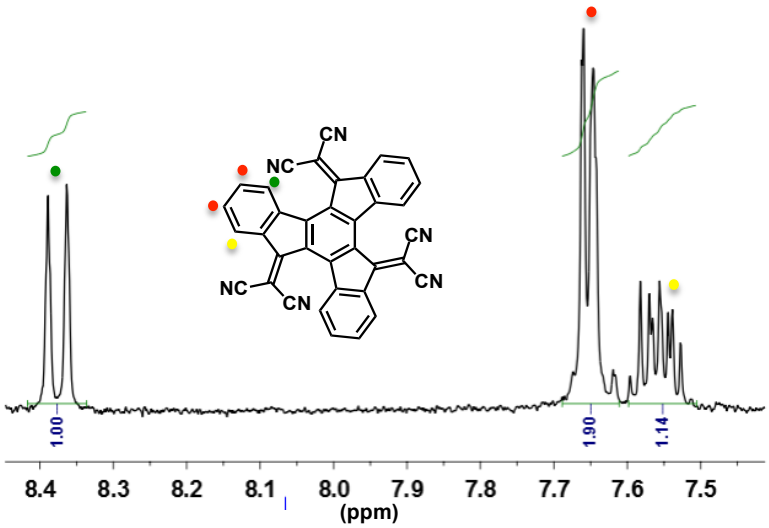

Figure 8.13. ^{1}H NMR (700 MHz, $CDCl_3$, 298 K) spectra of **128**. ^{1}H signals are depicted in colored bullets.

8.2.1. Supramolecular chemistry of electron donor truxTTF and electron acceptor trux6CN with $C_{32}H_{12}$

We firstly investigated the association in solution of the truxTTF and the trux6CN with the buckybowl $C_{32}H_{12}$. To do so, we titrated both truxTTF and trux6CN with $C_{32}H_{12}$ (**112**), in a variety of solvents at room temperature. The results of three separate titration experiments for each scenario (solvent/truxene derivative) were analyzed with Reactlab Equilibria software, affording the binding constants listed in Table 8.1.

The association constants for truxTTF•$C_{32}H_{12}$ and for trux6CN•$C_{32}H_{12}$ complexes are in the same order of magnitude as the one obtained for the truxTTF•$C_{30}H_{12}$ heterodimer.

Table 8.1. Binding constants obtained for truxTTF•$C_{32}H_{12}$ and for trux6CN•$C_{32}H_{12}$ complexes by UV/vis titrations.

Solvent	truxene derivative	buckybowl	log K_a
	[truxTTF] mM	[$C_{32}H_{12}$] mM	
PhCl	0.18	0.88	3.19±0.02
$CHCl_3$	0.17	0.76	2.90±0.40
THF	0.17	0.81	3.30±0.20
solvent	**[trux6CN] mM**	**[$C_{32}H_{12}$] mM**	**log K_a**
PhCl	0.12	0.71	3.20±0.20
$CHCl_3$	0.16	0.52	3.40±0.20
THF	0.11	0.56	3.21±0.05

In Figure 8.14 and Figure 8.15 are depicted two of the experimental UV/vis experiments carried out. Note that no isosbestic point is observed in any of the titrations, however, when analyzing these titrations at a fixed wavelength, both experimental and theoretical binding isotherms fit.

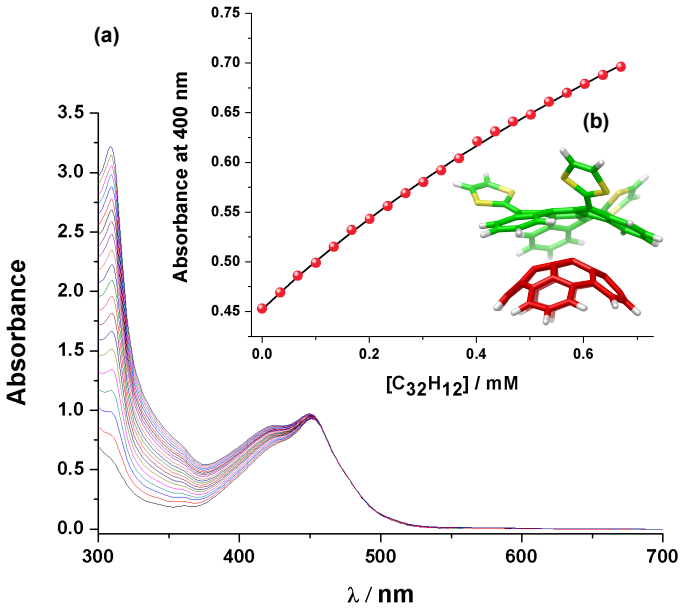

Figure 8.14. (a) Experimental UV/vis spectra as obtained during the titration of truxTTF (1.76×10^{-4} M) with $C_{32}H_{12}$ (8.78×10^{-4} M) in PhCl at room temperature, 3.81 equivalents of $C_{32}H_{12}$ were added; Inset experimental (red dots) and theoretical (black line) binding isotherm at 400 nm. (b) DFT calculated heterodimer for truxTTF•$C_{32}H_{12}$.

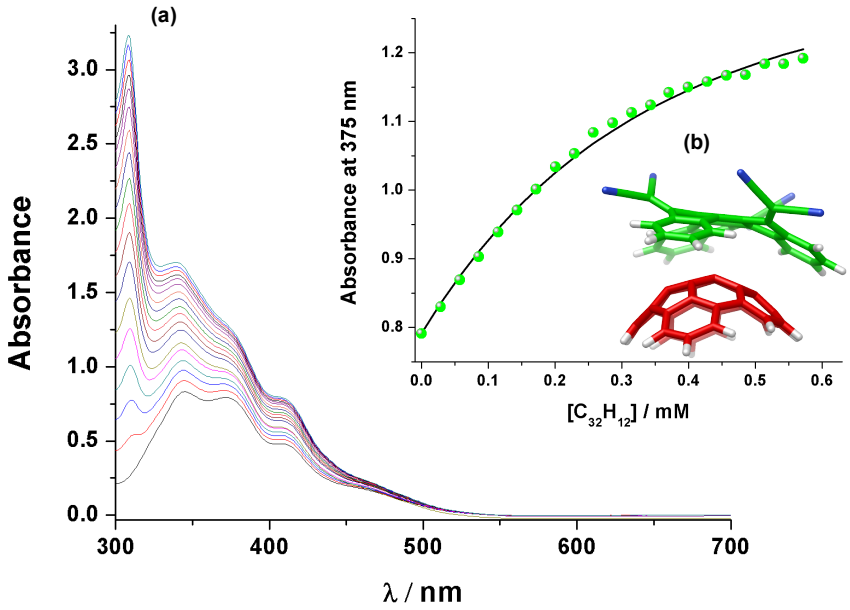

Figure 8.15. (a) Supramolecular heterodimer trux6CN•$C_{32}H_{12}$. Experimental UV/vis spectra as obtained during the titration of trux6CN (1.55 x 10^{-4} M) with $C_{32}H_{12}$ (5.25 x 10^{-4} M) in $CHCl_3$ at room temperature, 3.13 equivalents of $C_{32}H_{12}$ were added; Inset experimental (green dots) and theoretical (black line) binding isotherm at 400 nm. (b) DFT calculated heterodimer for trux6CN•$C_{32}H_{12}$.

Once we have experimentally proven the formation of these heterodimers, we turn to density functional theory (DFT) calculations to further explore these complexes.

There are four different ways in which truxTTF molecule and the $C_{32}H_{12}$ fullerene fragment can interact with each other. These four-modeled configurations are depicted in Figure 8.16.

In structures **1** and **2**, the convex surface of the $C_{32}H_{12}$ bowl perfectly matches the two concave cavities of the truxTTF host; i. e., either through the cavity formed by the truxene core (structure **1**) or through the cavity formed by the three 1,3-dithiole rings and the central benzene ring of the truxene core (structure **2**). Both structures can be thus seen as bowl-in-bowl arrangements where π–π interactions are maximized. The concave cavities of truxTTF and $C_{32}H_{12}$ can also interact giving rise to heterodimers in which either a benzene or a dithiole ring of the truxTTF molecule is placed inside the concave cavity of

the hemifullerene bowl (structures **3** and **4**, respectively). These two dispositions resemble the arrangement found in the crystal packing for the homodimers of truxTTF and the related fullerene fragment $C_{32}H_{12}$, implying a mixture of π–π and CH-π interactions. All the optimized heterodimeric structures **1**-**4** show close molecular contacts in the range of 2.5-3.7 Å range (Figure 8.17), indicative of the positive non-covalent interaction between both bowls.

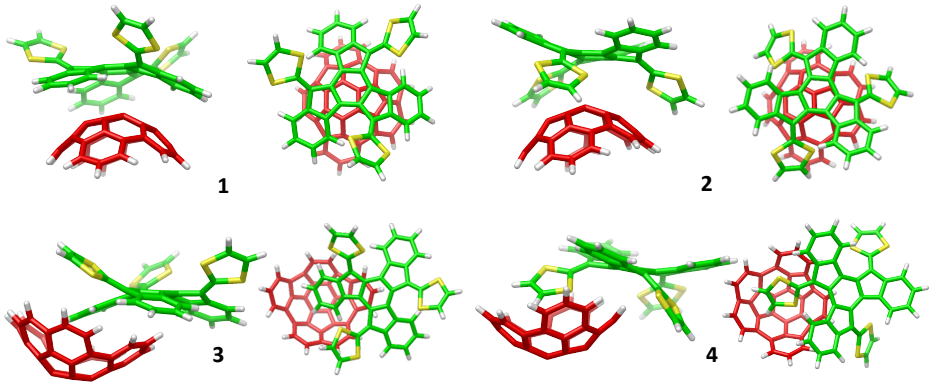

Figure 8.16. Minimum-energy structures (**1**-**4**) computed at the revPBE0-D3/cc-pVTZ level for the most stable conformations of the heterodimer formed by the $C_{32}H_{12}$ fullerene fragment with truxTTF (truxTTF•$C_{32}H_{12}$). Carbon atoms of the truxTTF are depicted in green, sulfur in yellow and hydrogen in white. Carbon atoms of $C_{32}H_{12}$ are depicted in red and hydrogen in white.

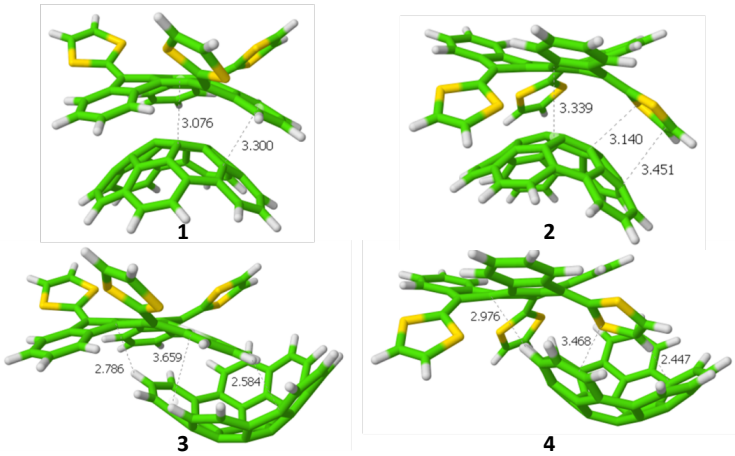

Figure 8.17. Selected intermolecular distances computed for structures **1**-**4** of the truxTTF•$C_{32}H_{12}$ heterodimer at the revPBE0-D3/cc-pVTZ level.

Analogous arrangements to the truxTTF•$C_{32}H_{12}$ complex were obtained for the associate between the trux6CN and the $C_{32}H_{12}$, trux6CN•$C_{32}H_{12}$, with two bowl-in-bowl (structure **1** and **2**) and two staggered (structure **3** and **4**) conformations (Figure 8.18).

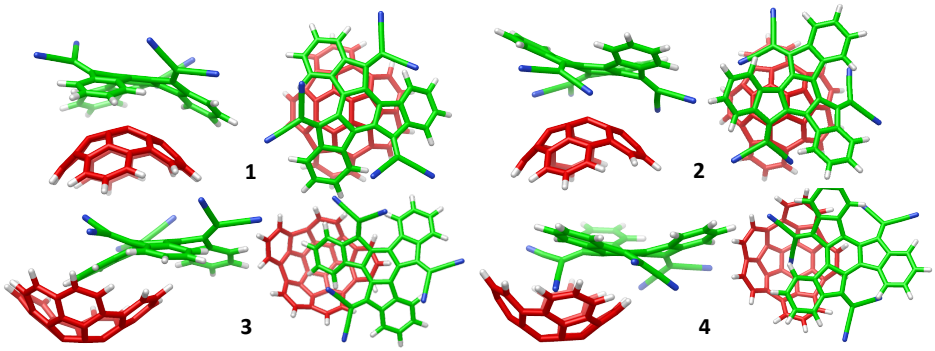

Figure 8.18. Minimum-energy structures (**1**-**4**) computed at the revPBE0-D3/cc-pVTZ level for the most stable conformations of the heterodimer formed by the $C_{32}H_{12}$ fullerene fragment with truxTTF (trux6CN•$C_{32}H_{12}$). Carbon atoms of the truxTTF are depicted in green, sulfur in yellow and hydrogen in white. Carbon atoms of $C_{32}H_{12}$ are depicted in red and hydrogen in white.

Similarly to the structures of truxTTF•$C_{32}H_{12}$ complex, close contacts are computed for the different arrangements governed by π–π interactions in structure **1** and **2** (3.0 – 3.5 Å), and by a mixture of π–π and CH-π forces in structures **3** and **4** (Figure 8.19).

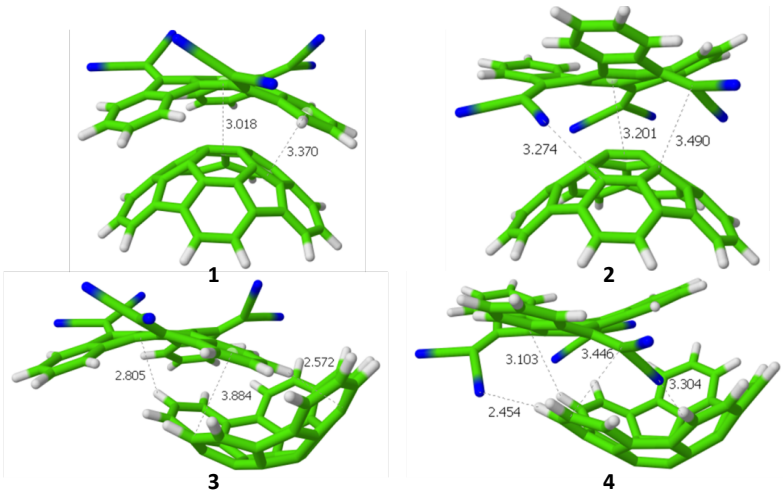

Figure 8.19. Selected intermolecular distances computed for structures **1**-**4** of the trux6CN•$C_{32}H_{12}$ heterodimer at the revPBE0-D3/cc-pVTZ level.

To assess the strength of the interaction between the truxTTF and $C_{32}H_{12}$ bowls association energies for the previously optimized heterodimers were also calculated at the revPBE0-D3/cc-pVTZ, including the three-body correction to the dispersion interaction. The four supramolecular structures **1**-**4** exhibit significant gas-phase association energies, ranging from -20.4 and -20.0 kcal/mol for structures **1** and **2** respectively, to -24.7 and -29.9 kcal/mol for structures **3** and **4**. The bowl-in-bowl arrangements are therefore significantly less stable than the staggered ones.

Moving to the associate formed by the electron-acceptor trux6CN with the $C_{32}H_{12}$ fragment, a different situation in the relative association energies is computed along the conformers studied (Table 8.2). The bowl in bowl conformer **2** remains the least stable conformer (-17.1 kcal/mol) whereas the staggered associate, in which a benzene is placed inside the concave cavity of the $C_{32}H_{12}$ bowl (conformer **3**), is computed to be the most stable one (-24.3 kcal/mol). The increase in stability of the conformer **3** with respect to the conformer **4**, as an opposite situation predicted for the truxTTF•$C_{32}H_{12}$ analogues, stems from the different nature of the truxene derivative moiety: the truxTTF behaves as an electron-donor system through its dithiole rings (HOMO localized in the truxTTF moiety and LUMO in $C_{32}H_{12}$, Figure 8.21), whereas the trux6CN stands as an electron-accepting fragment (HOMO located in the fullerene fragment and LUMO in trux6CN). The accumulated Mullinken net charges computed for the fullerene fragment of -0.03 and +0.02 e in truxTTF•$C_{32}H_{12}$ conformer **4** and in trux6CN•$C_{32}H_{12}$ conformer **3**, respectively, corroborate this hypothesis. Moreover, the dicyanomethylene groups do not provide as many stabilizing non-covalent interactions as the dithiole rings do (Figure 8.20). Thus, in the trux6CN•$C_{32}H_{12}$ associate, the trux6CN prefers to interact with the $C_{32}H_{12}$ moiety through its aromatic core (conformer **3**) although small differences of less than 2 Kcal/mol are predicted between conformers **1**, **3** and **4** (Table 8.2).

Table 8.2. Association energy (in kcal/mol) for the different conformations of truxTTF•$C_{32}H_{12}$ and trux6CN•$C_{32}H_{12}$.

Conformer	truxTTF•$C_{32}H_{12}$	trux6CN•$C_{32}H_{12}$
1	-20.44	-22.89
2	-19.97	-17.09
3	-24.69	-24.33
4	-29.91	-22.82

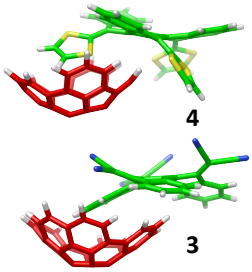

Figure 8.20. Most stable conformer for each heterodimer.

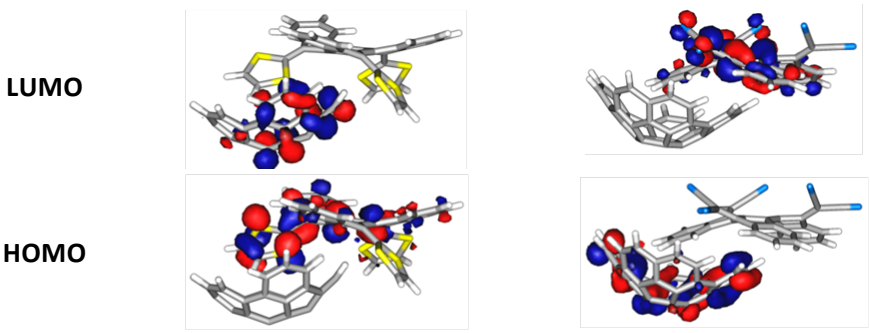

Figure 8.21. Frontier molecular orbitals computed for the most stable conformations of truxTTF•$C_{32}H_{12}$ and trux6CN•$C_{32}H_{12}$.

8.2.2. Supramolecular chemistry of truxTTF with $C_{38}H_{14}$

When studying UV/vis titrations of truxTTF with the largest buckybowl $C_{38}H_{14}$, **113**, the "hemi-C_{70}" in THF and PhCl at room temperature, we also obtained a log $K_a \approx 3$ (Table 8.3). The magnitude of the association constant obtained for truxTTF•$C_{38}H_{14}$ is the same as the one obtained for the truxTTF•$C_{30}H_{12}$ heterodimer and it is also in the same range of the values obtained for the complexation of C_{70} by the truxTTF.[38,40]

Table 8.3. Binding constants obtained for truxTTF•$C_{38}H_{14}$ complex.

Solvent	**truxene derivative**	**buckybowl**	**log K_a**
	[truxTTF] mM	**[$C_{38}H_{14}$] mM**	
PhCl	0.15	0.77	3.4±0.1
THF	0.14	0.72	3.5±0.2

In the UV/vis experimental spectra obtained during the titration of truxTTF

with $C_{38}H_{14}$ we observed a decrease in the intensity of the truxTTF absorption band at $\lambda \approx 450$ nm, accompanied by the increase of a broad band and a charge-transfer band in the 500-600 nm region (Figure 8.22).

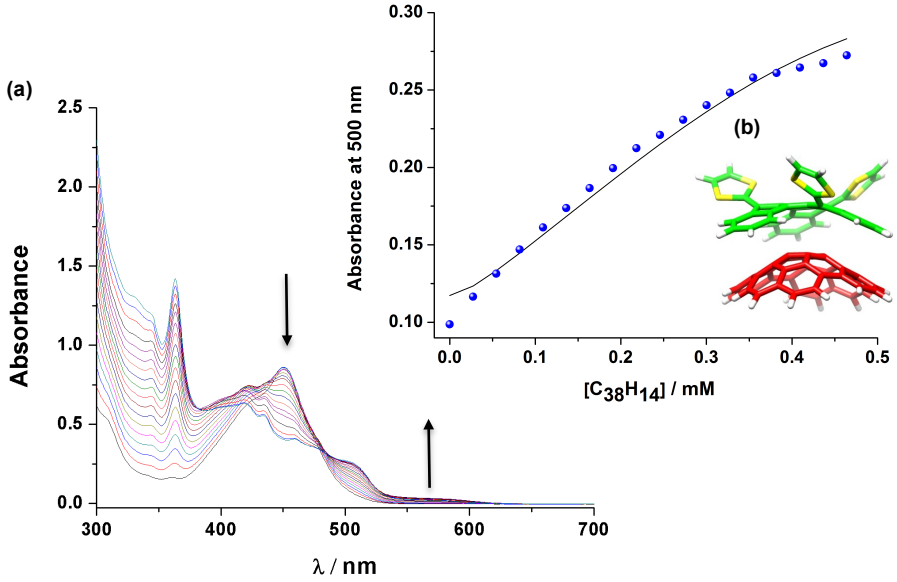

Figure 8.22. (a) Experimental UV/vis spectra as obtained during the titration of truxTTF (1.5×10^{-4} M) with $C_{38}H_{14}$ (7.7×10^{-4} M) in PhCl at room temperature; Inset experimental (blue dots) and theoretical (black line) binding isotherm at 500 nm. (b) DFT calculated heterodimer for truxTTF•$C_{38}H_{14}$.

Again, the supramolecular aggregate formed by the electron donor truxTTF molecule and the $C_{38}H_{14}$ fullerene fragment was modeled in several conformations in resemble to the previously studied truxTTF•$C_{30}H_{12}$, truxTTF•$C_{32}H_{12}$ and trux6CN•$C_{32}H_{12}$ associates (Figure 8.23). Depending on the relative disposition of one moiety with respect to the other, two bowl-in-bowl (**1** and **2**) and four staggered (**3**-**6**) conformations were optimized at the revPBE0-D3/cc-pVTZ+E_{abc} level of theory. Conformers **3** and **4** differ from **5** and **6**, respectively, into a small rotation of the bowl-in-bowl arrangements where π–π interactions are maximized with short intramolecular contacts in the 3.2-3.8 Å range (Figure 8.24). On the other hand, staggered arrangements **3**-**6** are governed by a mixture of π–π and CH–π interactions between the electron donor truxTTF and the electron acceptor $C_{38}H_{14}$ fullerene fragment with short intermolecular contacts ranging 2.7-3.9 Å (Figure 8.24).

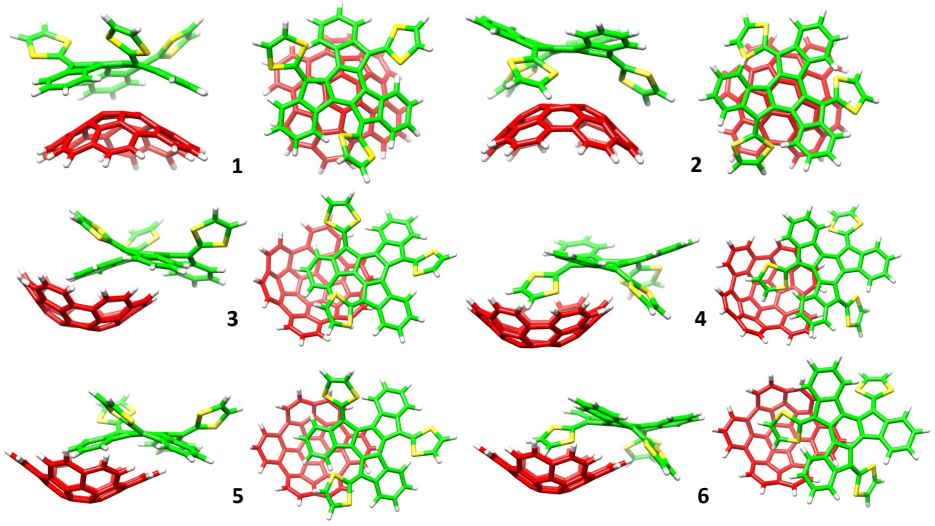

Figure 8.23. Minimum-energy structures (**1**-**6**) computed at the revPBE0-D3/cc-pVTZ level for the most stable conformations of the heterodimer formed by the $C_{32}H_{12}$ fullerene fragment with truxTTF (truxTTF•$C_{38}H_{14}$). Carbon atoms of the truxTTF are depicted in green, sulfur in yellow and hydrogen in white. Carbon atoms of $C_{38}H_{14}$ are depicted in red and hydrogen in white.

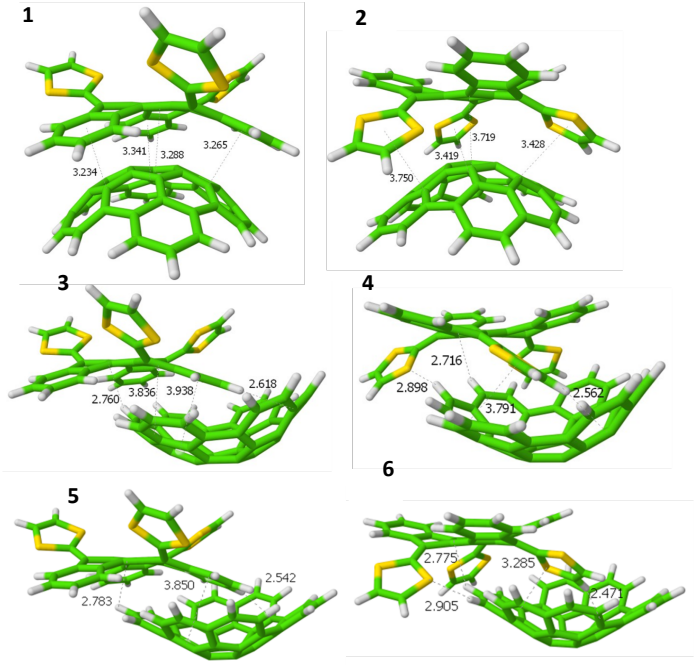

Figure 8.24. Selected intermolecular distances computed for structures **1**-**6** of the truxTTF•$C_{38}H_{14}$ heterodimer at the revPBE0-D3/cc-pVTZ level.

The association energy values computed for the different conformers of truxTTF•$C_{38}H_{14}$ are summarized in Table 8.4. The bowl-in-bowl arrangements in which the convex surface of the $C_{38}H_{14}$ bowl perfectly matches the two concave cavities of the truxTTF host, i. e. either through the cavity formed by the carbon backbone (**1**) or through the cavity formed by the central benzene ring and the three dithiole rings (**2**), are computed the less stable with -23.4 and -21.6 kcal/mol, respectively. On the other hand, the staggered arrangements **3**-**6** are computed to be more stable compared to the bowl-in-bowl analogues. The conformer in which a dithiole ring of the truxTTF molecule is placed inside the concave cavity of the $C_{38}H_{14}$ bowl is computed to be the most stable arrangement with -33.5 kcal/mol in **4** and -34.2 kcal/mol in **6**.

Table 8.4. Association energy (in kcal/mol) for the different conformations of truxTTF•$C_{38}H_{14}$

Conformer	truxTTF•$C_{38}H_{14}$
1	-23.37
2	-21.63
3	-29.09
4	-33.48
5	-31.57
6	-34.25

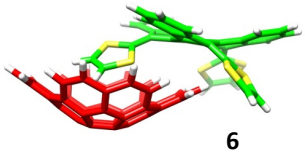

6

Figure 8.25. Most stable conformer of truxTTF•$C_{38}H_{14}$.

As for the others truxTTF•buckybowl heterodimers, the truxTTF behaves as an electron-donor system through its dithiole rings (HOMO localized in the truxTTF moiety and LUMO in $C_{38}H_{14}$, Figure 8.26).

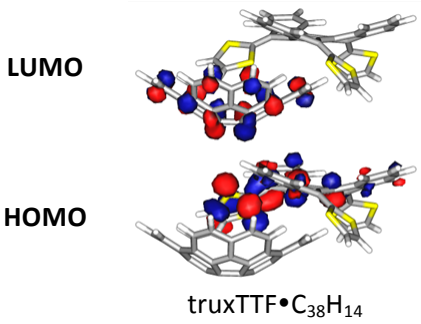

Figure 8.26. Frontier molecular orbitals computed for the most stable conformation of truxTTF•$C_{38}H_{14}$.

To shed light onto excited state properties of truxTTF, $C_{38}H_{14}$ and their supramolecular associate truxTTF•$C_{38}H_{14}$, transient absorption experiments were conducted. As mention before, upon 480 nm excitation of truxTTF in chlorobenzene, a new transient immediately develops (Figure 8.27). Characteristics of the latter are a marked maximum in the visible at 530 nm and a broad, featureless transition that spans all throughout the near infrared. Furthermore, a marked ground-state bleaching is observed around 450 nm. This excited state decays rapidly, as in other sulfur-rich electron donors, with a lifetime of only 1.0 ps. The short lifetime is rationalized by the presence of the sulfur atoms, with a strong second-order vibronic spin-orbit coupling, as it transforms into a much weaker absorbing state, for which a lifetime of 20 ps is detected.

When exciting $C_{38}H_{14}$ at 480 nm in chlorobenzene, several strong transient maxima evolve with completion of the laser pulse. Three sharp maxima at 450, 546 and 800 nm are accompanied by broad transients ranging from 625 to 725 nm and at wavelengths >1000 nm (Figure 8.27). After excitation, a multiexponential deactivation of these features is observed. While the 546 nm maxima persists, the features at 450, 800 and from 625 to 725 nm and >1000 nm deactivate within 46 ps (20%) and 3.5 ns (80%). The earlier is assigned to non-radiative deactivation, e.g. quenching processes in aggregated species. The latter reflects the intersystem crossing to the triplet excited state $^{3*}C_{38}H_{14}$. The triplet excited state shows a transient absorption maximum at 546 nm and two broad transients around 670 and 845 nm that deactivate within 18 µs to the ground state. Experiments in toluene and benzonitrile gave similar results.

In order to gain insight into the processes occurring after photoexcitation, spectroelectrochemical measurements were conducted, i.e. recording differential absorption spectra upon electrochemical oxidation of TruxTTF and reduction of $C_{38}H_{14}$ (Figure 8.28).

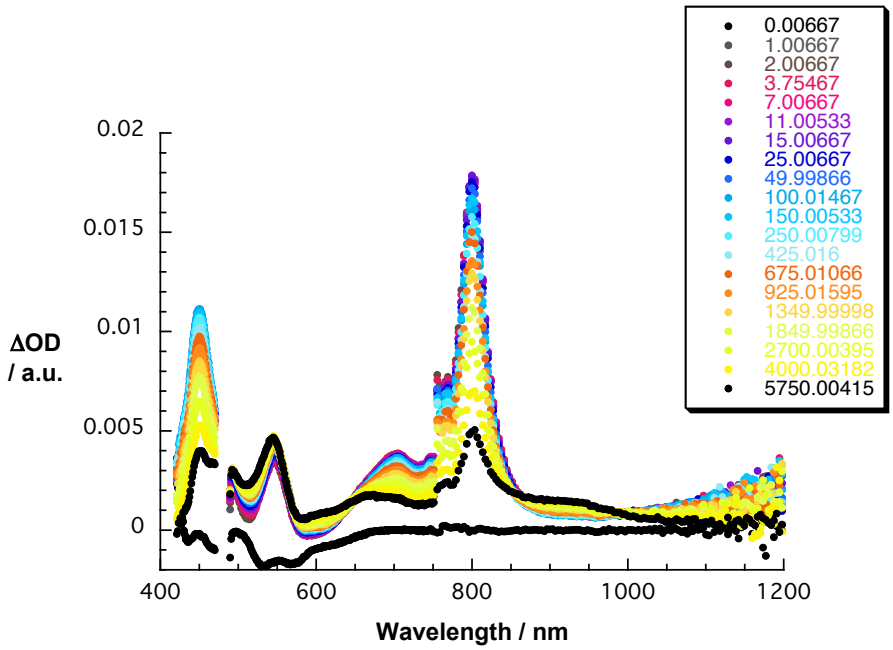

Figure 8.27. Differential absorption spectra obtained upon femtosecond pump probe experiments (480 nm) of $C_{38}H_{14}$ in chlorobenzene with time delays of 0–5750 ps at room temperature.

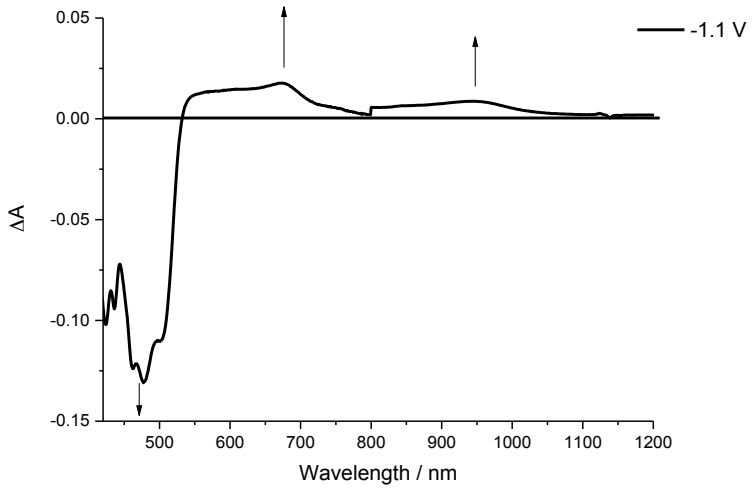

Figure 8.28. Differential absorption spectra obtained upon electrochemical reduction of $C_{38}H_{14}$ in deoxygenated ortho-dichlorobenzene containing $TBAPF_6$ (0.1M) with an applied potential of -1.1 V vs. Ag wire at room temperature.

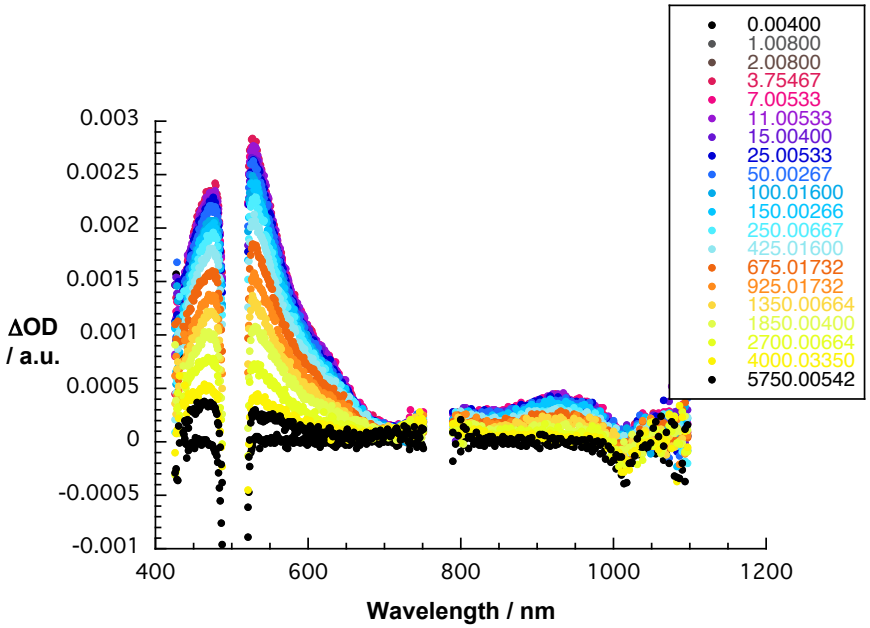

Figure 8.29. Differential absorption spectra obtained upon femtosecond pump probe experiments (480 nm) of truxTTF•$C_{38}H_{14}$ (1:1) in benzonitrile with time delays of 0–5750 ps at room temperature.

When exciting truxTTF•$C_{38}H_{14}$ (1:1) in benzonitrile at 480 nm, $C_{38}H_{14}$ centered transients dominate the spectra (Figure 8.29). Here, no clear assignment to the radical ion species, truxTTF$^{\bullet+}$ and $C_{38}H_{14}^{\bullet-}$, is possible. However, slight changes in the differential absorption in the range between 500 and 700 nm gives rise to the assumption that electronic communication in the excited state is taking place. Furthermore, detailed kinetic analysis corroborates this hypothesis. Multiwavelength analysis yields four major lifetime components. After excitation, a very short lifetime of < 1 ps is followed by a 30-40 ps component. We assign the shorter component to, on one hand, ultrafast charge separation yielding the charge separated state TruxTTF$^{\bullet+}$•$C_{38}H_{14}^{\bullet-}$ and, on the other hand, intrinsic deactivation of non-complexated truxTTF. The longer component is most likely due to intrinsic deactivation of both non-complexated species, i.e. photoexcited truxTTF and $C_{38}H_{14}$. A third component of ~150 ps that is not observed in the single components, reflects the charge recombination to neutral truxTTF•$C_{38}H_{14}$. A fourth component of >5.5 ns can be assigned to the slow deactivation of the $C_{38}H_{14}$ triplet excited state that is

populated by intersystem crossing within non-complexated $C_{38}H_{14}$ and, potentially, charge recombination. In less polar chlorobenzene and toluene no evidence for charge separation was found.

8.2.3. Supramolecular chemistry of trux6CN and hemifullerere $C_{30}H_{12}$

When analyzing the UV/vis titrations of trux6CN, **128**, with the hemifullerene $C_{30}H_{12}$, **105**, in a PhCl we obtained an average value of log K_a = 2.9 ± 0.2.

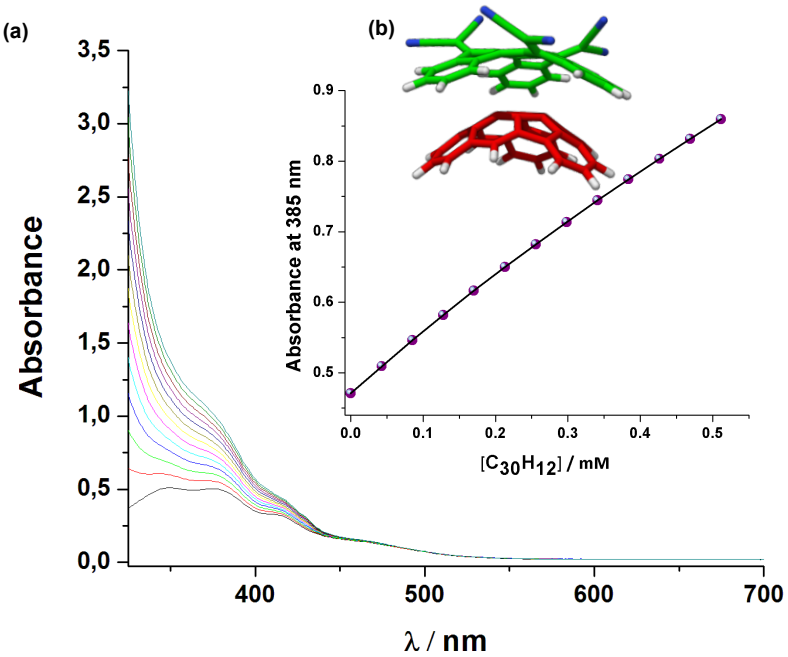

Figure 8.30. (a) Experimental UV/vis spectra as obtained during the titration of trux6CN (2.2 x 10^{-4} M) with $C_{30}H_{12}$ (1.36 x 10^{-3} M) in PhCl at room temperature, inset, experimental (purple dots) and theoretical (black line) binding isotherm at 385 nm. (b) DFT calculated heterodimer for truxTTF•$C_{30}H_{12}$.

The supramolecular aggregate formed by the electron acceptor trux6CN molecule and the hemifullerene $C_{30}H_{12}$ was modeled in four conformations in resemble to the previously studied truxTTF•$C_{30}H_{12}$ complex. Depending on the relative disposition of one moiety with respect to the other, two bowl-in-bowl (**1** and **2**) and two staggered (**3** and **4**) conformations were optimized at the revPBE0-D3/cc-pVTZ level of theory (Figure 8.31).

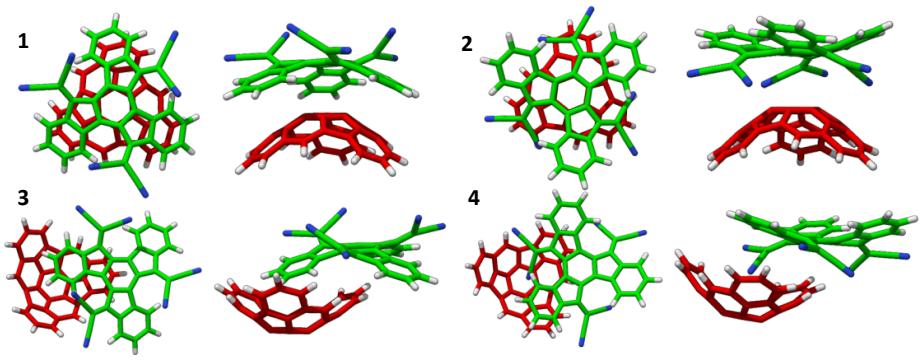

Figure 8.31. Minimum-energy structures (**1**–**4**) computed at the revPBE0-D3/cc-pVTZ level for the most stable conformations of the heterodimer formed by the $C_{30}H_{12}$ fullerene fragment and the electron acceptor trux6CN moiety. Carbon atoms of trux6CN are depicted in green, nitrogen in blue and hydrogen in white. Carbon atoms of $C_{30}H_{12}$ are depicted in red and hydrogen in white.

As shown in Figure 8.32, in structures **1** and **2** the π–π interactions are maximized with short intermolecular contacts in the 3.2-3.6 Å range. On the other hand, staggered arrangements (**3** and **4**) are governed by a mixture of π–π and CH-π interactions, between the electron acceptor trux6CN and the $C_{30}H_{12}$ fullerene fragment with short intermolecular contacts ranging 2.5-3.8 Å (Figure 8.32).

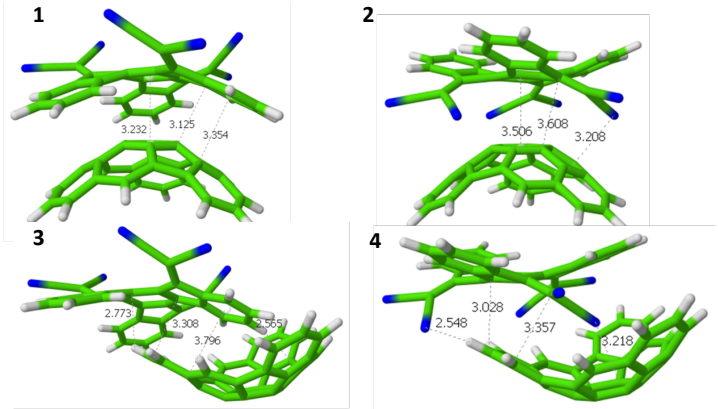

Figure 8.32. Selected intermolecular distances computed for structures **1**–**4** of the trux6CN·$C_{30}H_{12}$ heterodimer at the revPBE0-D3/cc-pVTZ level.

The association energy computed for the different conformers of trux6CN•$C_{30}H_{12}$ are summarized in Table 8.5. As in the case of the

trux6CN•$C_{32}H_{12}$ heterodimer, the arrangements in which the dicyano groups approach to the buckybowl, either in a concave-convex orientation (**2**) or in a staggered disposition (**4**), are computed the less stable with –16.88 and –22.20 kcal/mol, respectively. On the other hand, the arrangements in which the aromatic π-core of the trux6CN gets closer to the hemifullerene fragment, either in a concave-convex (**1**) or in a staggered (**3**) orientation, are computed to be more stable (-23.82 and -24.57 kcal/mol, respectively). This picture contrasts with the relative energies obtained for the truxTTF•buckybowl predicted in the heterodimers of $C_{30}H_{12}$, $C_{32}H_{12}$ and $C_{38}H_{14}$, in which all the staggered conformers exhibit lower energies compared to the concave-convex dispositions. On the other hand, the relative energies computed for the conformers of trux6CN•$C_{30}H_{12}$ compare well with the trends predicted for trux6CN•$C_{32}H_{12}$ (**1-4**) (see Table 8.2), in which the orientations having the aromatic core of the trux6CN close to the fullerene fragment moiety show larger association energies. Moving from the dithiole rings in truxTTF to the dicyano groups in trux6CN, several C-H-π and π-π interactions disappear when forming the supramolecular aggregate with the fullerene fragment. Moreover, the electron lone pairs of the nitrogen atoms (in trux6CN) are substantially worse oriented, especially in conformer **2**, for efficient n-π interactions compared to sulfur atoms in the truxTTF aggregate.

Table 8.5. Association energy (in kcal/mol) for the different conformations of trux6CN•$C_{30}H_{12}$. Association energies for truxTTF•$C_{30}H_{12}$ heterodimer are shown for comparison purposes.

Conformer	truxTTF•$C_{30}H_{12}$	trux6CN•$C_{30}H_{12}$
1	-21.00	-23.82
2	-19.40	-16.88
3	-25.20	-24.57
4	-28.50	-22.20

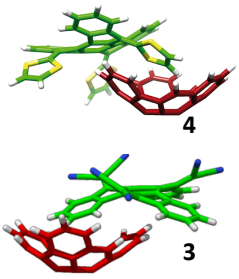

Figure 8.33. Most stable conformer for each heterodimer.

A dramatic change in the electronic properties of the supramolecular associate is predicted when comparing the truxTTF•hemifullerene with the trux6CN•hemifullerene assemblies. The HOMO in truxTTF•$C_{30}H_{12}$ is localized in the donor moiety of truxTTF, whereas the LUMO is completely confined in

the fullerene fragment, which acts as an acceptor (Figure 8.34). Otherwise, the HOMO of trux6CN•$C_{30}H_{12}$ is localized in the hemifullerene fragment which now acts as the electron donor fragment. The LUMO is mainly located in the trux6CN moiety, which is considered as the electron acceptor moiety in the supramolecular associate. This different electron donor/acceptor behavior between the constituting monomers of the supramolecular associates in truxTTF•$C_{30}H_{12}$ and trux6CN•$C_{30}H_{12}$ is also evidenced by computing the accumulated NPA charges borne by the hemifullerene fragment: it has a small but negative charge of -0.010e in truxTTF•$C_{30}H_{12}$ and a positive charge of +0.016e in truxTTF•$C_{30}H_{12}$. These values confirm that the hemifullerene fragment acts as an electron-acceptor (in truxTTF•$C_{30}H_{12}$) or an electron-donor (in trux6CN•$C_{30}H_{12}$) system depending on the nature of the fragment to which is supramolecularly associated.

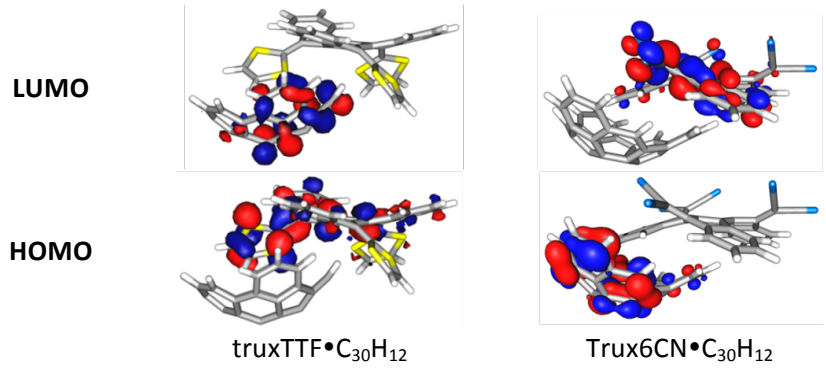

Figure 8.34. Frontier molecular orbitals computed for the most stable conformations of truxTTF•$C_{30}H_{12}$ and trux6CN•$C_{30}H_{12}$.

9.Experimental Section

9. EXPERIMENTAL SECTION

9.1. GENERALITIES

Computational details: Geometry optimization of the supramolecular heterodimers formed by truxTTF or trux6CN and $C_{32}H_{12}$ or $C_{30}H_{12}$ and truxTTF with $C_{38}H_{14}$ was performed within the density functional theory (DFT) framework using the revPBE0 correlation-exchange functional in combination with the Grimme dispersion correction –D3 (revPBE0-D3) in gas phase. The original damping function in the –D3 approach was replaced by the Becke-Johnson damping function to provide a better performance. The correlation-consistent cc-pVTZ basis set was applied throughout. Single-energy calculations at the revPBE0-D3/cc-pVTZ level were performed on the previously optimized structures (heterodimers and isolated moieties) to compute the association binding energies. The three-body contribution to the dispersion energy has been included because it can be significant for medium and large supramolecular systems. The association energy in each heterodimer was computed as the difference between the energy in each heterodimer and the sum of the energies for the two constituting fragments [ΔE_{assoc} = *E*(heterodimer) – *E*(truxTTF or trux6CN) – *E*($C_{30}H_{12}$, $C_{32}H_{12}$ or $C_{38}H_{14}$)]. Geometry optimizations and single-point energy calculations were performed using the ORCA program package (version 3.0.0).

All solvents were dried according to standard procedures.[128] Reagents were used as purchased. All air-sensitive reactions were carried out under argon atmosphere. Flash chromatography was performed using silica gel (Merck, Kieselgel 60, 230-240 mesh, or Scharlau 60, 230-240 mesh). Analytical thin layer chromatography (TLC) was performed using aluminium-coated Merck Kieselgel 60 F_{254} plates. Visualization was made by UV light (λ=254 or 365 nm). NMR spectra were recorded on a Bruker AvanceIII 700 (^{1}H: 700 MHz; ^{13}C 175 MHz) spectrometers at 298 K or on a Varian VNMRS 500 (^{1}H: 500; ^{13}C: 125 MHz), using partially deuterated solvents as internal standards. Coupling constants (J) are denoted in Hz and chemical shifts (d) in ppm. Multiplicities are denoted as follows: s = singlet, d = doublet, t = triplet, m = multiplet, b =

[128] D. D. Perrin, I. F. Amariego, D. R. Perrin, Purification of laboratory Chemicals, Pergamon Press,Oxford, **1980**.

broad. UV/vis spectra were recorded with a Simadzu Spectrophotometer UV-3600 at 298K or with a Varian Cary 50 at 298 K.

9.2. SYNTHESIS OF COMPOUNDS

Truxenequinone trux6CN (128)[127]

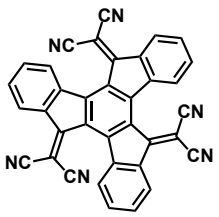

1 Mmol of truxenone (**3**) was dispersed in 65 ml of deoxygenated chlorobenzene. Then, 11.7 mmol of malononitrile were added under Ar followed by the addition of 11.7 mmol of $TiCl_4$ dropwise and 15.6 mmol of dry pyridine. The reaction was stirred at room temperature for 2 h and then it was warmed to 70 °C and stirred overnight. The next day the crude is cooled down to room temperature and 60 ml of water are added to the crude that is extracted with methylene chloride. The organic phases are dried with $MgSO_4$ and filtered. All the solvents were removed under vacuum, leaving a red solid that is purified by column chromatography with methylene chloride as eluent, to yield 192 mg of an orange-red very intense colorful solid (28%).

FT-IR (KBr) 2224 , 1551, 743 cm^{-1}.

^{1}H NMR (700 MHz, $CDCl_3$) δ 8.47 (d, *J* = 7.8 Hz, 1H), 7.78 – 7.72 (m, 2H), 7.68 – 7.63 (m, 1H) ppm.

^{13}C NMR (175 MHz, $CDCl_3$) δ 162.85, 144.60, 138.58, 137.04, 133.48, 133.28, 132.20, 127.50, 125.99, 113.53, 112.63, 79.11 ppm.

MS (MALDI-TOF) m/z calcd ($C_{36}H_{12}N_6$) = 528.52, m/z found = 528.83.

UV/vis (chlorobenzene) λ (nm): 349 (ε= 42826 $M^{-1}cm^{-1}$), 375 (ε= 42174 $M^{-1}cm^{-1}$), 412 (ε= 27000 $M^{-1}cm^{-1}$), 464 (ε= 10870 $M^{-1}cm^{-1}$).

UV/vis (chloroform) λ (nm): 345 (ε= 53521 $M^{-1}cm^{-1}$), 372 (ε= 50696 $M^{-1}cm^{-1}$),

410 (ε= 30739 $M^{-1}cm^{-1}$), 454 (ε= 12434 $M^{-1}cm^{-1}$).

UV/vis (acetone) λ (nm): 341 (52478), 364 (49478), 403 (29435), 454 (12043).

Hemifullerene $C_{30}H_{12}$ (105)[70b,129]

3,3',4,4'-Tetrahydro-[1,2'-binaphthalen]-1'(2'H)-one (122)

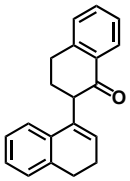

To a stirred solution of α-tetralone (50 g, 0.342 mol) in 500 mL of anhydrous 1,2-dichloroethane at 25°C under N_2, 25 mL of $TiCL_4$ (0.24 mol) were added all at once. The color changes from pale yellow to dark brownish. The reaction mixture is heated under reflux for 4 hours. After that, the reaction mixture is cooled down to room temperature. A mixture of concentrated hydrochloric acid (150 mL) in ice (150 g) was added to quench the reaction. This mixture was stirred until the aqueous layer become fluorescent green. The organic layer was washed with HCl (10 v/v) (2 x 300 mL), and brine (2 x 300 mL), dried with $MgSO_4$ and filtered. All the solvents were removed under vacuum, leaving brownish oil. Recrystallization from hot ethanol yielded 22.6 g (24%) of a pale yellow solid.

^{1}H NMR (500 MHz, $CDCl_3$) δ 8.15 (d, *J* = 7.9 Hz, 1H), 7.52 (td, *J* = 7.5, 1.2 Hz, 1H), 7.37 (t, *J* = 7.6 Hz, 1H), 7.29 (d, *J* = 7.7 Hz, 1H), 7.20 – 7.15 (m, 3H), 7.14 – 7.10 (m, 1H), 5.82 (t, *J* = 4.6 Hz, 1H), 3.87 (dd, *J* = 9.0, 4.6 Hz, 1H), 3.13 – 2.94 (m, 2H), 2.84 – 2.72 (m, 2H), 2.49 – 2.37 (m, 1H), 2.34 – 2.25 (m, 3H) ppm.

1',2',3,3',4,4'-Hexahydro-[1,2':1',2''-ternaphthalen]-1'-ol (124)

[129] S. Hagen, L. T. Scott, *J. Org. Chem.* **1996**, *61*, 7198.

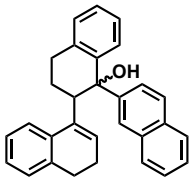

To a stirred solution of 2-bromonaphthalene (9 g, 44 mmol) in 100 mL of anhydrous THF at -78°C under N_2, 4.4 mL of 11M n-buthyllithium in hexanes (44 mmol) were added to form the 2-naphthyl lithium. The solution changes from transparent to yellow. After the solution had been stirred for 2 hours, a solution of ketone **122** (10g, 36 mmol) in 150 mL of anhydrous THF is added dropwise via cannula under N_2. The reaction mixture was stirred for another 45 minutes at -78 °C, and then it was allowed to warm to room temperature and it is stirred overnight, the next day the reaction in quenched with saturated NH_4Cl solution. Diethyl ether was added until all precipitates were dissolved. The organic phase was washed with aqueous NH_4Cl, brine and water, and finally dried over $MgSO_4$ and filtered. After evaporation of the solvents under reduced pressure, the residue was dissolved in hot methanol and allowed to crystallize overnight, yielding 5.4 g (37%) of **124**, white solid.

^{1}H NMR (500 MHz, $CDCl_3$) δ 7.66 – 7.60 (m, 1H), 7.60 – 7.56 (m, 2H), 7.52 (d, *J* = 8.7 Hz, 1H), 7.37 – 7.30 (m, 2H), 7.25 – 7.23 (m, 1H), 7.18 (dd, *J* = 8.6, 1.9 Hz, 1H), 7.12 – 7.09 (m, 2H), 6.83 (d, *J* = 7.3 Hz, 1H), 6.76 – 6.68 (m, 2H), 6.61 (t, *J* = 7.1 Hz, 1H), 6.17 – 6.13 (m, 1H), 3.68 (dd, *J* = 10.5, 2.6 Hz, 1H), 3.15 (s, 1H), 3.13 – 3.04 (m, 2H), 2.64 – 2.58 (m, 2H), 2.35 – 2.25 (m, 2H), 2.19 – 2.09 (m, 1H), 1.98 (m, 1H) ppm.

1,2':1',2''-Ternaphthalene (125)

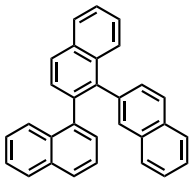

To a stirred solution of alcohol **124** (1.196 g, 2.97 mmol) in 114 mL of benzene, DDQ, 2,3-dichloro-5,6-dicyano-1,4-benzoquinone, (2.6 g, 11.88 mmol) was added and the solution was stirred under reflux for 3 hours. Then 19 mg of *p*-

TsOH (0.11 mmol) were added, and the reaction mixture was stirred for another 2 hours under reflux. After the mixture was cooled to room temperature, the organic phase was extracted with 10% NaOH solution until the aqueous phase remained colorless, then the organic phase was washed with saturated NH_4Cl solution and water. Finally, it was dried over $MgSO_4$, and filtered, followed by evaporation of the solvents. The obtained oily-solid was washed with hot methanol, to yield 718 mg (64%) of a pale yellow solid.

^{1}H NMR (500 MHz, $CDCl_3$) δ 8.00 (dd, *J* = 11.1, 5.9 Hz, 4H), 7.83 (s, 1H), 7.76 (t, *J* = 8.0 Hz, 2H), 7.75 – 7.66 (m, 7H), 7.63 – 7.51 (m, 7H), 7.50 – 7.32 (m, 13H), 7.30 – 7.26 (m, 1H), 7.23 – 7.15 (m, 4H), 7.05 – 7.00 (m, 1H) ppm.

Benzo[c]naphtho [2,1-p]chrysene (126)

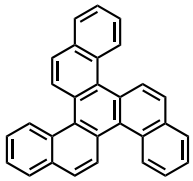

A stirred solution of hydrocarbon **125** (884 mg, 2.3 mmol), iodine (590 mg, 2.33 mmol), in 500 mL of benzene in a quartz flask were purged with N_2 for 15 minutes, then 25 mL of propylene oxide (0.35 mol) are added to the flask and then the solution is irradiated with 450 W medium-pressure mercury UV-lamp for 43 hours. During this time, the lamp has to be refrigerated, and cover with a security shield covered with aluminum foil for protection. After the 43h, the solution is cooled down to room temperature and the solvent is evaporated. The crude of the reaction is recrystallized with ethanol, yielding 492 mg (56%) of a yellow solid.

^{1}H NMR (500 MHz, $CDCl_3$) δ 9.02 – 8.92 (m, 2H), 8.10 – 8.04 (m, 1H), 7.97 (d, *J* = 8.9 Hz, 1H), 7.71 – 7.63 (m, 2H) ppm.

6,12,18-Tribromobenzo[c]naphtho[2,1-*p*]chrysene (127)

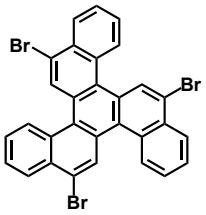

To an oven dry purged with N_2 pressure vessel **126** (364 mg, 0.96 mmol) and 22 mL of chlorobenzene were added. The mixture was heated until the entire solid is dissolved. Then, it was cooled to room temperature and a solution of bromine (0.28 mL, of bromine in 3.6 mL of chlorobenzene) was added dropwise. Then, the reaction mixture was refluxed for 1 hour. After cooling to room temperature the yellow precipitate that appears is collected by vacuum filtration and washed with dichloromethane, yielding 410 mg of a yellow solid (70%), very insoluble in $CDCl_3$.

^{1}H NMR (500 MHz, $CDCl_3$) δ 9.14 (s, 3H), 8.87 – 8.79 (m, 3H), 8.56 – 8.44 (m, 3H), 7.86 – 7.77 (m, 6H) ppm.

Benzo[5,6]-as-indaceno[3,2,1,8,7-mnopqr]indeno[4,3,2,1-cdef]chrysene (105)

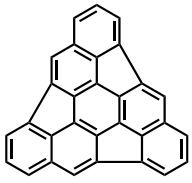

Three separately "Flash Vacuum Pyrolysis" reactions were performed each on 1.0 g of 6,12,18-tribromobenzo[c]naphtho[2,1-p]chrysene (**127**), at 1050°C, with a steady flow of N_2 as a carrier gas, pressure range [0.763-0.758] Torr, capillary length 22.9 cm and 0.25 mm internal diameter. The crude pyrosylate was purified by column chromatography on silica gel with methylene chloride and cyclohexane (1:9) as eluent. The two first fractions in the column yielded 49.9 mg (3%) of a yellow solid.

^{1}H NMR (500 MHz, $CDCl_3$) δ 7.85 (s, 1H), 7.67 (d, *J* = 7.1 Hz, 1H), 7.62 (d, *J* = 8.1

Hz, 1H), 7.38 (t, *J* = 8.1, 7.1 Hz, 1H) ppm.

10. Conclusions

10. CONCLUSIONS

The results obtained in each of the chapters discussed in the present report can be summarized as follows:

Chapter I.

- Molecules **70a** and **81** have been validated as versatile building blocks for the construction of more sophisticated chemical structures of interest.

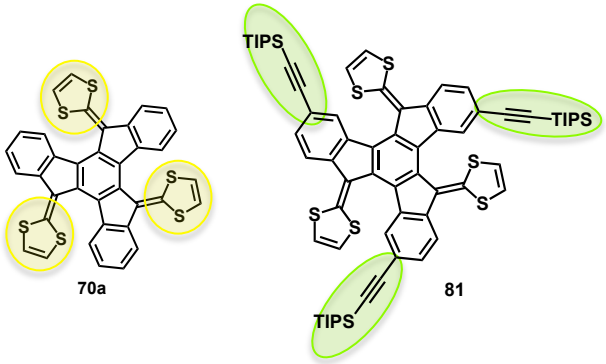

- Three [60]fullerene units were attached to a truxTTF core.

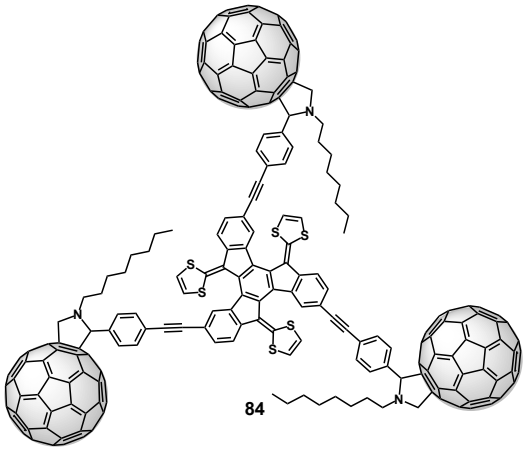

- Five new truxTTF-derivatives featuring multiple anchoring groups have been synthesized. According to their chemical structure, they could have potential applications as sensitizers in Dye Sensitized Solar Cells devices.

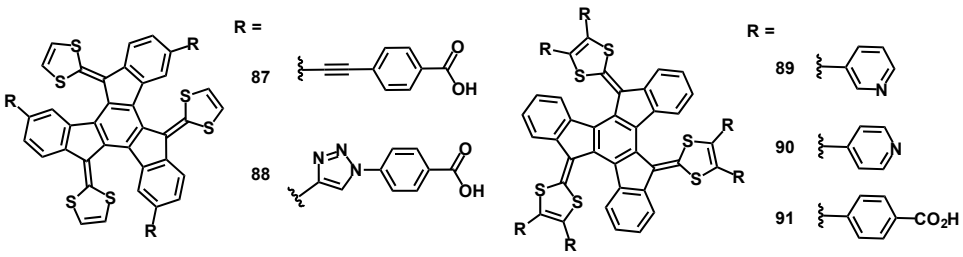

- Molecules **70a** and **73** have been validated as n-type components in BHSCs. A less-explored supramolecular approach has been used for the preparation of efficient small-molecule solar cells. The highest PCE based on a truxTTF was 1.77% while incorporating truxTTF-CO yielded 1.19%. Although, both of them have similar bowl-shape geometries that allow the formation of supramolecular complexes when blended with $PC_{61}BM$ or $PC_{71}BM$, they show different binding constants with fullerenes and also different optical properties. Despite the broader absorption and the deeper HOMO of truxTTF-CO, the stronger non-covalent interactions between the concave shape of the electron donating truxTTF and the surface of the fullerene derivatives lead to higher J_{sc} and FF that could be attributed to a more favorable morphology of the active layer.

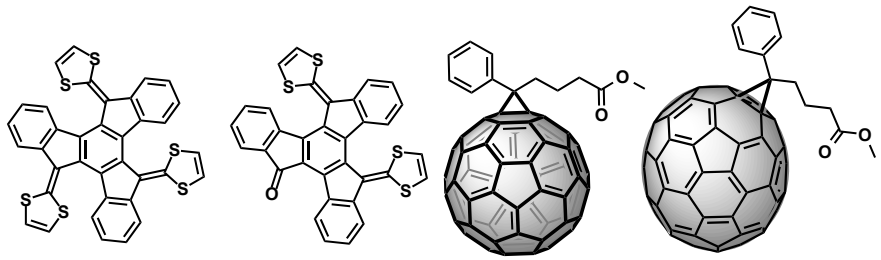

truxTTF (70a) **truxTTF-CO (73)** **$PC_{61}BM$ (94)** **$PC_{71}BM$ (95)**

Chapter II.

- For the very first time, the association of a fullerene fragment, namely hemifullerene $C_{30}H_{12}$, with a bowl-shaped electron-donor, truxTTF has been corroborated.

- The association was investigated experimentally through UV/vis titrations. Quantitatively, we calculated a binding constant of log $K_a = 3.6 \pm 0.3$ in $CHCl_3$ at room temperature, which is comparable to that found for the association

of truxTTF with C_{60}.

- Calculations at the revPBE0-D3/cc-pVTZ level of theory supported the non-covalent interactions between the truxTTF and the $C_{30}H_{12}$; providing insight into the possible structure of the heterodimer and the nature of the changes observed during the UV/vis titration.

- Remarkably, femtosecond pump-probe experiments reveal the formation of a transient species that corresponds to a charge-separated truxTTF$^{\bullet+}$•$C_{30}H_{12}^{\bullet-}$ state. Overall, the latter assignment was backed by both spectroelectrochemical measurements and theoretical calculations. Analysis of the time evolution of these features afforded rate constants of 6.6 x 10^{11} and 1.0 x 10^{10} s^{-1} for the charge separation and charge recombination dynamics respectively.

- This is the first example of a fullerene fragment mimicking the charge transfer behavior of C_{60}.

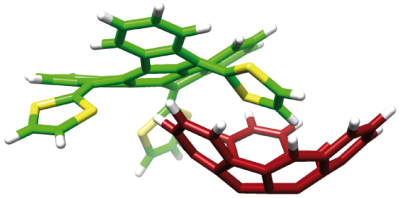

•As done for the truxTTF•$C_{30}H_{12}$ heterodimer, a general systematic study comprising (I) the study of the formation in solution of heterodimers by UV/vis titrations, (II) DTF calculations to support the existence of non-covaent interactions between the components of the heterodimers and (III) photophisical studies to investigate if electron transfer proceses can occur in these new truxene-derivated•buckybowl systems, has been done for truxTTF•$C_{32}H_{12}$, truxTTF•$C_{38}H_{14}$, trux6CN•$C_{30}H_{12}$ and trux6CN•$C_{32}H_{12}$.

11. Summary

11. SUMMARY

11.1. INTRODUCTION

Inspired in the simple benzene molecule, during the past three decades, new carbon nanoforms, namely fullerenes, carbon nanotubes and graphene, have emerged as most appealing carbon materials exhibiting amazing and outstanding properties. Fullerenes were first discovered as 3D carbon spheres forming closed cages. Despite fullerenes are formed by twelve pentagons and a variable number of hexagons ($n \geq 20$) (cyclohexatrienes), they do not follow Hückel's rule and, therefore, they are not aromatic compounds. Fullerenes have been exhaustively studied as electron acceptors in molecular electronics as well as in other different fields, such as hydrogen storage or medicinal chemistry, just to name a few. Carbon nanotubes are 1D carbon-based analogs to fullerenes forming single and multi-wall nanotubes with a variable diameter and constituted exclusively by carbon hexagonal rings. The mechanical and optoelectronic properties of carbon nanotubes have been extensively exploited to construct a wide variety of devices. Finally, 2D graphene is constituted by a single layer of carbon hexagonal rings, thus forming a planar sheet of carbon atoms. Currently, graphene is considered to be the "panacea" of carbon-based technologies. Diverse applications such as transparent electrodes, super-capacitors, extremely sensitive sensors or lightweight high-performance materials have been postulated for it.

Benzene is also the cornerstone of the aromatic systems that will be discussed throughout this memory: classic aromatic systems derived from a curved truxene core and bowl shaped polycyclic aromatic compounds. Both type of systems are at the forefront of aromatic compounds, exhibiting less-known features and a high chemical versatility, which make them aromatic compounds of choice in the search for new applications. A non-comprehensive review on the most significant achievements involving truxenes and bowl shaped polycyclic aromatic compounds will be discussed in their respective chapters.

11.2. CHAPTER I. "Covalent modifications on truxTTF core"

11.2.1. *Background*

The 10,15-dihydro-*5H*-tribenzo[a,f,k]trindene commonly named truxene (**1**), is a planar polycyclic aromatic hydrocarbon (PAH) with C_3-symetry. The high conjugation and the C_3-symetry of the truxene core make it a useful building block for the construction of new materials with diverse and promising applications. By modifying its periphery at will or using structurally analogous systems we can, for example, gain access to: larger polyarenes that might lead to bowl-shaped fullerene fragments or fullerenes, water-soluble anionic fluorophores, candidates for blue light emitting materials, thermally stable cathode buffer materials, effective materials for organic field-effect transistors, (OFETs), liquid crystals and n-type organic semiconductors for thin-film organic solar cells.[7-13]

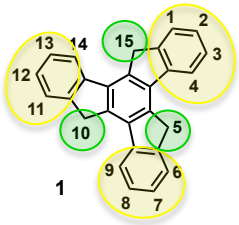

Truxene has fifteen positions that can be functionalized. These positions are grouped in three pentagonal rings and three benzene rings.

Figure 11.1. Truxene core.

Positions C5, C10 and C15 are generally functionalized with saturated alkyl chains to reduce the intermolecular π–π stacking, improving the poor solubility of **1** and therefore facilitating further modifications at other positions.[15] Within the twelve susceptible positions of reaction at the three benzene rings of **1**, C2, C7 and C12 are the most usually functionalized for example by means of electrophilic bromination or Friedel-Crafts reactions.[18-19] Modifying the remaining positions at the aromatic rings requires alternative routes such as previous functionalization at C2, C7 and C12 or by means of condensation of previously modified 1-indanones.[12-19] This latter strategy will give an easy acces to truxenes modified even at the most hindered positions C4, C9 and C13. The truxene core can also contain heteroatoms in its structure.[21]

The truxene core has also been exploited for the construction of receptors for fullerenes using truxenone as the starting material.[38,40] Truxenone is a feasible scaffold to build receptor for fullerenes because it has an extended π-delocalized core, which provides a large aromatic surface suitable for establishing non-covalent interactions towards fullerenes. Furthermore, the planar geometry of the original core is bended by performing a three-fold Wittig-Horner olefination reaction on truxenone **3** (Scheme 11.1).

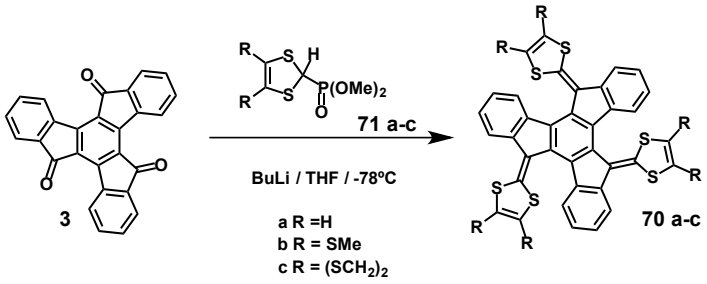

Scheme 11.1. Synthesis of the truxene-TTF derivatives **70 a-c**.

In order to accommodate the three dithiole rings, the planar geometry of the original truxenone adopts an all-*cis* sphere-like geometry.

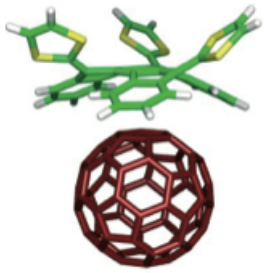

Figure 11.2. truxTTF•C_{60}

This bowl shape adopted by the truxene core is complementary in shape and size with the fullerenes, which should maximize the van der Waals and π–π interactions between the receptor and C_{60}.[38, 40]

One of the potential applications for truxene-based materials is their application in solar cells devices. There are some examples in the literature in which a truxene core has been used as π-bridge in the design of dyes for DSSCs[31-32] and some electron-deficient truxene derivatives have been used as non-fullerene type of acceptors or n-type semiconductors for BHSCs.[17,34]

The working mode of a DSSCs follows three main steps:[28] (1) the anchored sensitizer molecules absorb incidental light, (2) then charge separation occurs at the interface dye-TiO_2 through photoinduced electron injection from the excited dye to the conduction band of the TiO_2, creating holes in the ground

state of the dye, (3) the electrons reach the TCO electrode and the hole-transporter material regenerates the ground state of the dye (Figure 11.3).

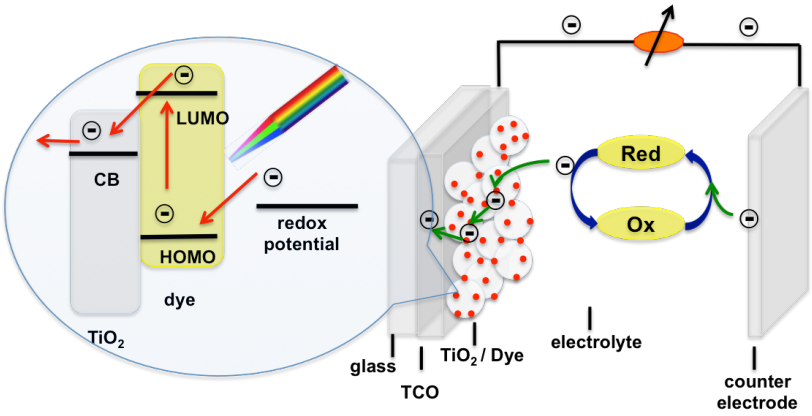

Figure 11.3. Schematic DSSC device.

Regarding the dye, many types of compounds have been synthesized like metal-organic complexes, metal-free organic compounds, Zn-porphyrins and Zn-phthalocyanines. Metal-free organic dyes are rare metal free, tunable at will, low cost and also present high molecular extinction coefficients, for all this, they are good candidates for DSSCs devices. The schematic structure of a dye for DSSCs is depicted in Figure 11.4. A donor group, a π–bridge and an acceptor group, which usually acts as the anchoring group towards the TiO_2, are the usual components of a dye.[28]

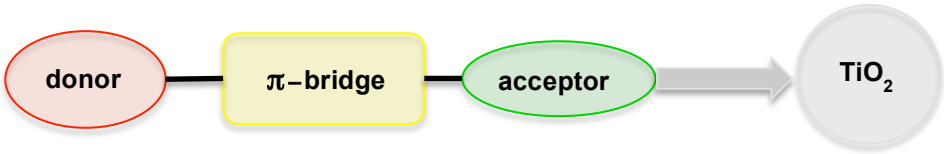

Figure 11.4. Schematic design for a metal-free organic dye.

The elements that usually form a BHJ solar cell are a mixed film of a conjugated polymer or a small molecule as donor and an acceptor material, usually a fullerene derivative. This film is sandwiched in between an ITO (indium tin oxide) anode and a low work function metal cathode. When the donor component is photoexcited, an exciton is created. The exciton created in the donor material has to diffuse to the donor-acceptor interface. When an exciton reaches the D-A interface it is broken up into free electron-hole pairs. This charge separation requires an optimal energy offset between the LUMO

of the donor and the LUMO of the acceptor materials (approximately a 0.3-0.4 eV gap between them). Finally, the last step is the free charge carrier transport and collection at the electrodes. The whole photoinduced process needs high charge-carrier mobility.[33]

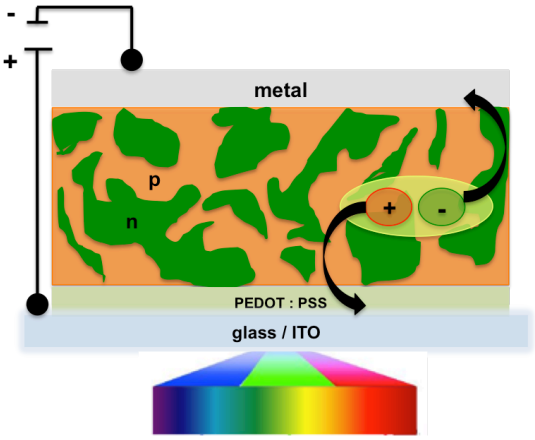

Figure 11.5. Schematic BHJ OSC device and representation of the fundamental photoinduced process.

A key factor affecting the efficiency of such devices is their morphology at the D-A interface. In our research group with the aim of constructing nanostructured optoelectronic devices, we look for suitable electron-donor partners for fullerenes in order to form supramolecular donor-acceptor pairs. A suitable electron donor partner for fullerenes must show three main features, (i) to have a good electron-donor character, (ii) to present efficient light absorption, preferably in the visible region and, (iii) to have the ability to self-assemble with these fullerenes. In this regard, the molecular and supramolecular properties of truxene-TTF derivatives make them a valuable option to test as complementary partners for the fullerenes derivatives in organic photovoltaic devices.

11.2.2. *Objectives*

Our aim in this study is to exploit the potential applicability of the truxene-TTF derivatives already reported in our group, as well as constructing new truxene-TTF based molecules that could have potential applications in organic electronics. To do so, we will divide the *Results and Discusion* section of this Chapter I according to the following objectives:

• Synthesis of building blocks

We will present the synthesis of two suitable functionalized building blocks that will give access to more sophisticated chemical structures of interest for further objectives.

• Covalent linkage of three fullerenes to a truxTTF core

The aim is to cover the synthesis and characterization of unprecedented truxTTF-fullerene molecular tetrads, where the central truxene core is connected to three C_{60} units forming DA_3 photo and electroactive systems.

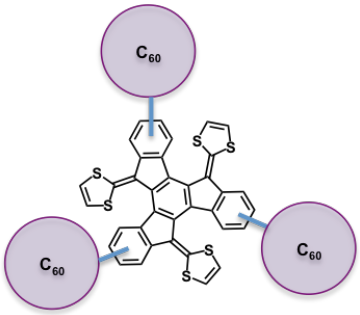

Figure 11.6. tetrad truxTTF-C_{60}

• TruxTTF derivatives for DSSCs

We will report on the synthesis of five truxTTF-based dyes that, according to their chemical structure, could have potential applications as sensitizers in Dye Sensitized Solar Cells devices.

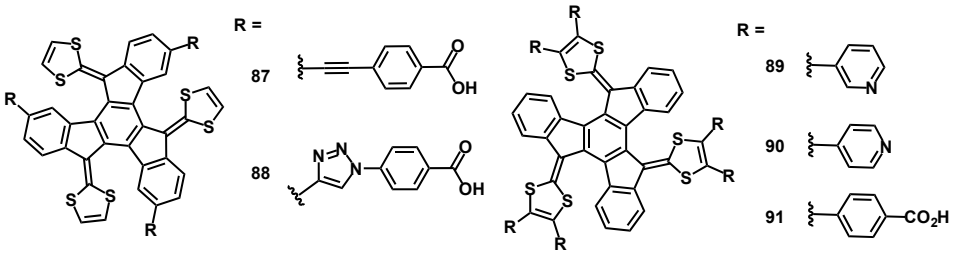

Figure 11.7. truxTTF-based dyes

• TruxTTF derivatives for BHSCs

The aforementioned interest of the truxene core for DSSCs can be extended to the use of suitably functionalized truxene derivatives, namely truxTTF (**70a**) and truxTTF-CO (**73**) molecules in Bulk Heterojunction Solar Cells devices. Remarkably, to the best of our knowledge, the use of curved molecules for photovoltaic (PV) applications has not been properly addressed in the

literature. Therefore, this study could give a valuable hint on the interest of these molecules for PV purposes.

11.2.3. *Results and discussion*

• Synthesis of building Blocks

The truxTTF molecule, offers the possibility of modifying its structure in a covalent manner, either at its 1,3-dithiole rings (highlighted in yellow in Figure 11.8) or at its aromatic core (highlighted in green in Figure 11.8).

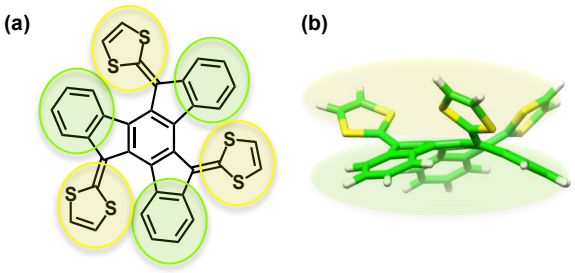

Figure 11.8. (a) Chemical structure of truxTTF (**70a**). Susceptible regions for being covalently modified highlited in yellow and green. (b) View of the biconcave disposition adopted by the truxene core and the 1,3-dithiole rings in **70a**.

70a is synthesized by attaching three 1,3-dithiole rings by a three-fold Horner-Wadsworth-Emmons olefination reaction on truxenone (**3**) (Scheme 11.2). It is also possible to perform a two-fold Horner-Wadsworth-Emmons olefination reaction on truxenone (**3**), to get a truxTTF derivative, the truxTTF-CO (**73**). This compound **73**, as well as truxTTF, will be tested for BHSC.

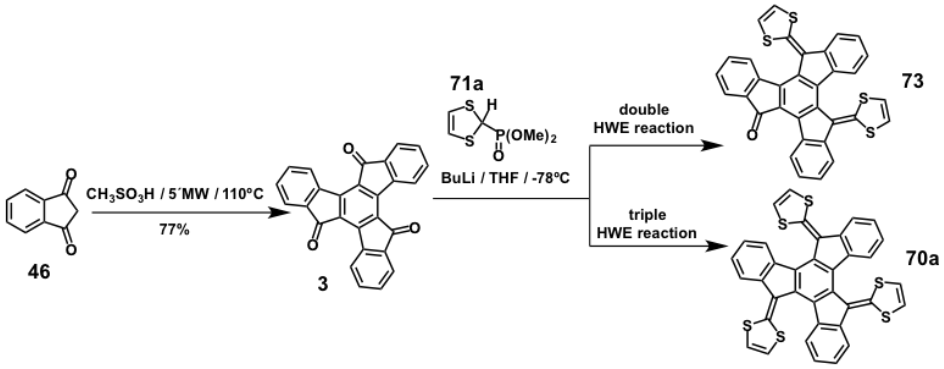

Scheme 11.2. Synthesis of **73** and truxTTF (**70a**).[38,40]

In order to design a useful and versatile building block that will conduce to

truxTTF derivatives decorated on its aromatic periphery; we have to resort to the synthesis of a suitably functionalized truxenone. Tribromotruxenone **75** provides a suitable truxene core functionalized with three carbonyl groups and three bromine atoms at its periphery.

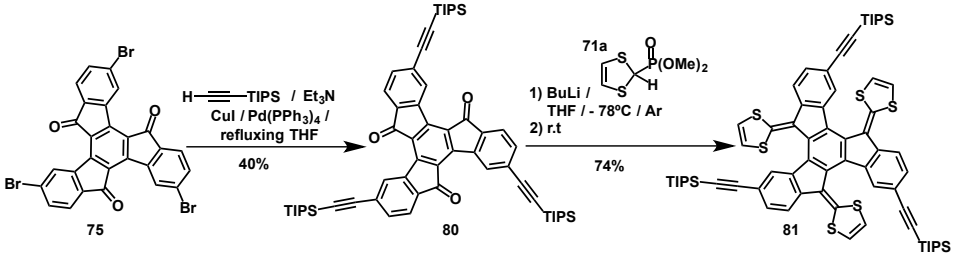

Scheme 11.3. Synthesis of building block **81**.

The carbonyl groups allow their substitution with 1,3-dithiole rings, and the bromine atoms provide an easy way to functionalize the molecule at its aromatic periphery by cross-coupling reactions.

As expected, **81** shows the biconcave morphology with triple helical quirality observed for truxTTF. As for truxTTF, we just found the enantiomeric pair *P*, *P*, *P* / *M*, *M*, *M*. As well as **70a**, compound **81** is able to bind [60]fullerene.

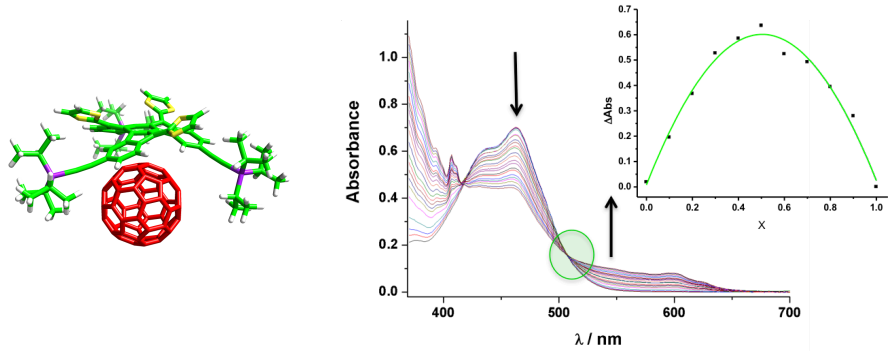

Figure 11.9. Left, amber simulated complex **81**•C_{60}. Right, changes in the UV/vis absorption spectra of **81**, upon addition of C_{60} showing log K_a= 4.5 ± 0.5, (PhCl, r.t). Inset Job plot confirming a 1:1 stoichiometry for the complex **81**•C_{60}.

Building **70a** and **81** will give access to more sophisticated truxene-TTF derivatives.

- **Covalent linkage of three fullerenes to a truxTTF core**

Although several donor-fullerene molecular dyads based on exTTF have previously been reported in our group as well as the supramolecular behavior between the C_{60} and the truxTTF (**70a**), the covalent linkage of truxTTF to fullerenes has not been addressed in our group so far.

Our building block of choice is molecule **81**, a truxTTF derivative with alkyne chains at its aromatic periphery that will allow the further covalent linkage of three C_{60} units to the truxene core of the truxTTF. The successful synthetic strategy followed for the preparation of the truxTTF-$(C_{60})_3$ derivative, implies (I) deprotection of **81**, which is accomplished with tetra-n-butylammonium fluoride (TBAF) in THF at room temperature affording **83**, (II) triple Sonogashira coupling in refluxing THF of **83** with 4-iodobenzaldehyde that gives **85** and (III) a three-fold 1,3-dipolar cycloaddition reaction on trialdehyde **85** with n-octyl glycine, and C_{60} in refluxing toluene we obtained the desired compound **84**. (Scheme 11.4)

84 resulted a good receptor for fullerenes. It exploits fullerene-fullerene and truxene-fullerene interactions to bind [70]fullerene giving a log K_a = 6.8 ± 0.5 (*o*-DCB, r.t). Unfortunately upon femtosecond flash photolysis experiments, the sample decomposed. It was impossible to determine whether there were or not intermolecular o intramolecular charge transfer processes.

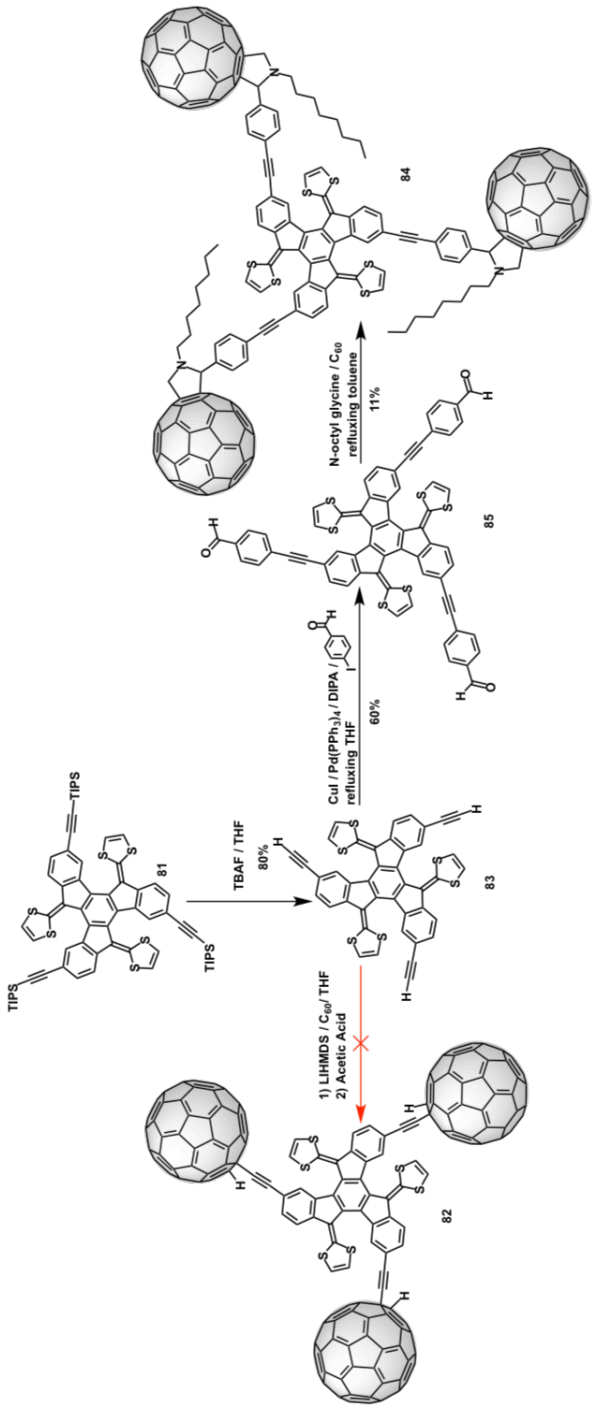

Scheme 11.4. Synthetic strategy towards a truxTTF core linked to three C_{60} units.

- **TruxTTF derivatives for DSSCs**

The truxTTF molecule provides a truxene aromatic core, this is, a π-conjugated bridge (Figure 11.10, highlighted in green) and three 1,3-dithiole units, that behaves as three donor units (Figure 11.10, highlighted in yellow). The presence of appropriate anchoring groups would allow synthesizing a suitable functionalized sensitizer.

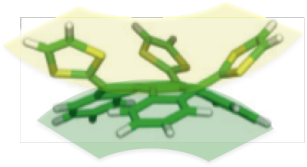

Figure 11.10. truxTTF molecule **70a**.

The biconcave disposition of the truxTTF molecule offers not only a hindrance to prevent the aggregation of the dye but also the possibility of organizing donor groups, π-bridge and anchoring groups.

There are several studies on systems with multiple anchoring groups.[47] This "multi-anchoring" exhibits some advantages, namely: dye-bonding enhancement on the surface of the photo-electrode, superior electron injection efficiency and reduced recombination rate. Most of the donor-acceptor π-conjugated (D-π-A) organic dyes have carboxyl groups in order to link the dye to the TiO_2 surface. The carboxyl group forms strong ester linkage with Brönsted acid sites of the TiO_2 surface, enabling good electron communication between the dye and the TiO_2. Just a few years ago, the use of a pyridine ring as electron-withdrawing and anchoring group in dyes was reported.[48] The pyridine ring forms a strong coordinated bond between the lone pair of electrons of the nitrogen atom and the Lewis acid sites of the TiO_2. This new type of D-π-A dye gave electron injection efficiencies comparable to, or even higher, than the equivalent dye featuring carboxyphenyl group as anchoring group.

The three dithiole-rings of the truxTTF can be easily modified by direct C-H arylation with palladium catalysis in one-pot reaction (Scheme 11.5).

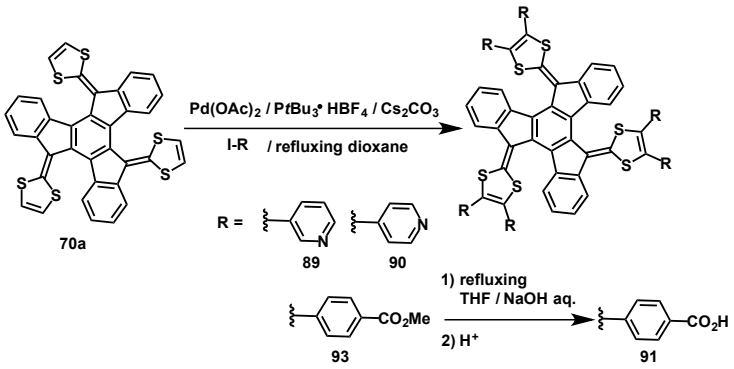

Scheme 11.5. Synthesis of truxTTF derivatives with six anchoring groups.

Building block **81** provides three alkyne groups that can be modified. To do so we followed two strategies (Scheme 11.6): (1) modification via three-fold Sonogashira coupling reaction and (2) modification via "click chemistry". Both strategies start with the cleavage of the protecting groups TIPS with tetra-n-butylammonium fluoride (TBAF) in THF at room temperature to afford molecule **83**.

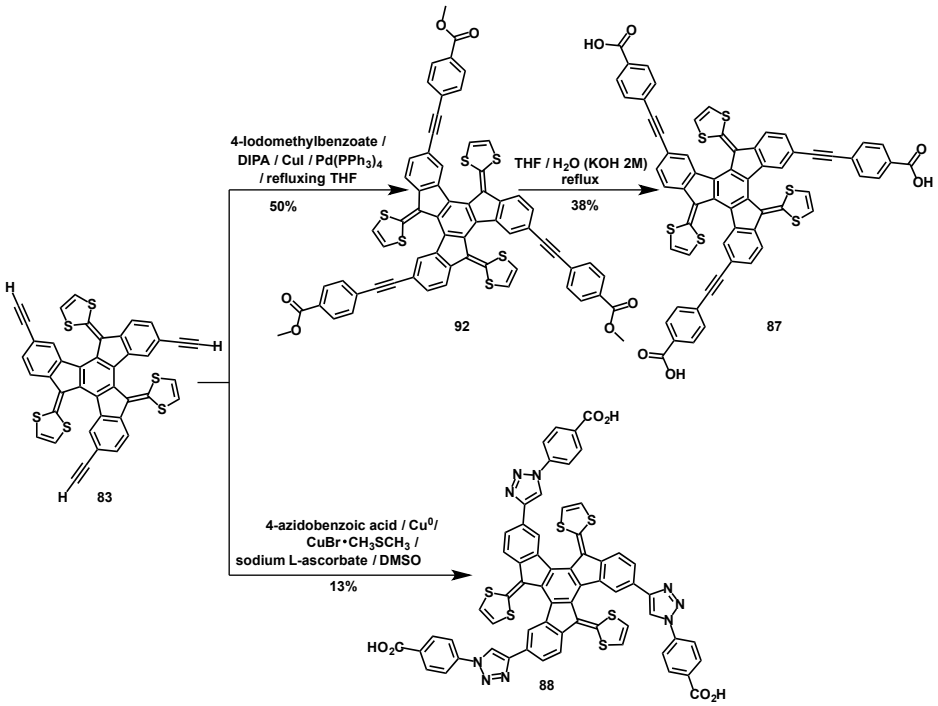

Scheme 11.6. Synthesis of truxTTF-derivatives with three anchoring groups.

- **TruxTTF derivatives for BHSCs**

The following results have been extracted from the article " Organic solar cells based on bowl-shape small molecules".

Agustín Molina-Ontoria, María Gallego, Luis Echegoyen, Emilio M. Pérez and Nazario Martín. *RSC* Adv., **2015**, *5*, 31541.

A less-explored supramolecular approach has been used for the preparation of efficient small-molecule solar cells. The highest PCE based on a truxTTF was 1.77% while incorporating truxTTF-CO yielded 1.19%. Although, both of them posess similar bowl-shape geometries that allow the formation of supramolecular complexes when blended with $PC_{61}BM$ or $PC_{71}BM$, they show different binding constants with fullerenes and also different optical properties. Despite the broader absorption and the deeper HOMO of truxTTF-CO, the stronger non-covalent interactions between the concave shape of the electron donating truxTTF and the surface of the fullerene derivatives lead to higher J_{sc} and FF, attributed to a more favorable morphology of the active layer.

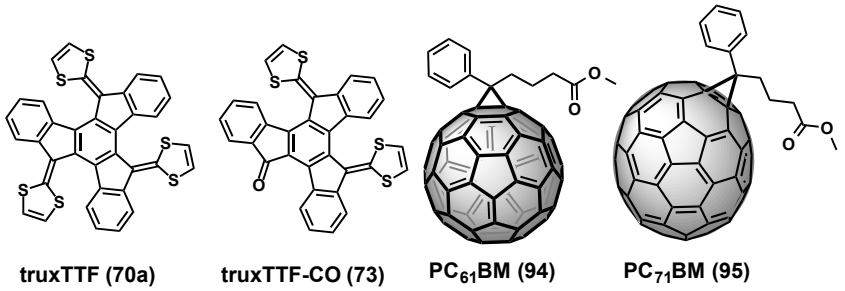

Figure 11.11. Chemical structures of bowl-shape electron-donors truxTTF and truxTTF-CO and electron acceptors phenyl-C_{60}-butyric acid methyl ester ($PC_{61}BM$) and phenyl-C_{70}-butyric acid methyl ester ($PC_{71}BM$).

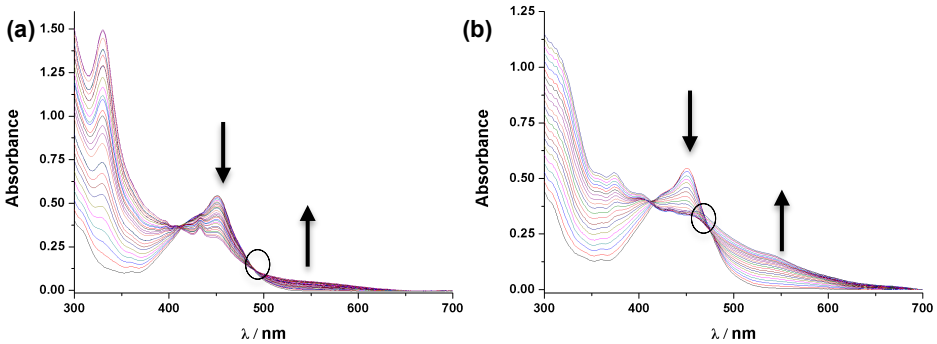

Figure 11.12. UV/vis spectra as obtained during the titration of truxTTF with (a) $PC_{61}BM$ and (b) $PC_{71}BM$. The corresponding binding values are log K_a= 3.44±0.03 (PhCl, r.t) for truxTTF•$PC_{61}BM$ and log K_a= 4.1±0.8 (PhCl, r.t) for truxTTF•$PC_{71}BM$.

11.3. CHAPTER II: *"Supramolecular complexation of truxene derivatives with bowl-shaped PAHs"*

11.3.1. *Background*

The synthesis of curve PAHs (open geodesic cages) is currently a mayor topic in chemistry. The curvature of curve PAHs is given by the five-membered rings inserted in their benzoid structure, which force them to adopt non-planar equilibrium geometries. The reason why these open geodesic cages are so appealing to scientists owes to the unique electronic properties that the curvature surface gives to these curved PAHs, as it gives to fullerenes.

Different preparation procedures[70] as well as covalent chemical modifications have been reported during the last recent years.[71] Furthermore, several authors noticing the shape complementarity among the π-faces of the C_{60} and corannulene, the smallest elemental bowl-shape subunit of C_{60}, designed several corannulene-based receptors for fullerenes,[89-93] featuring one or more corannulene units. The choice of corannulene as the recognition motif for fullerenes follows one of the many strategies to find adequate receptors to associate fullerenes, which is to exploit the complementarity host-guest shape that will maximize π–π interactions; this is, to design concave receptors that will match the convex surface of fullerenes. However, to the best of our knowledge the supramolecular chemistry of these curve PAHs with

complementary concave-convex partners has not been properly addressed so far.

11.3.2. *Objectives*

In this chapter we will present our studies directed to the supramolecular understanding between curved PAHs and electron-donor (truxTTF, **70a**) and electron acceptor (trux6CN, **128**) as efficient recognition partners of choice in order to determine the main supramolecular interactions governing the complexation process. Thus the following topics are discussed in this Chapter II:

• Supramolecular chemistry of truxTTF and $C_{30}H_{12}$. A singular case of study

We will study the association of a fullerene fragment, the hemifullerene $C_{30}H_{12}$ (**105**), with an electron-donating bowl-shaped tetrathiafulvalene derivative (truxTTF, **70a**).

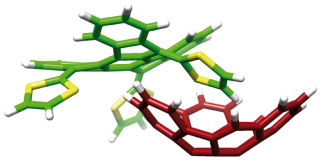

Figure 11.13. truxTTF•$C_{30}H_{12}$ complex.

• Extension to other curved PAHs systems. A comparative study

Encouraged by the good results obtained for the previous study, we decided to widen the scope and explore the complexation processes between bowl-shaped PAHs **112** ($C_{32}H_{12}$) and **113** ($C_{38}H_{14}$) molecules with truxTTF, as well as to explore if the n/p electronic behavior of the buckybowls **105** ($C_{30}H_{12}$) and **112** ($C_{32}H_{12}$) could be tuned depending on the counterpart in the formed complexes, to do so we resort to an electron acceptor truxene derivative, the trux6CN (**128**).

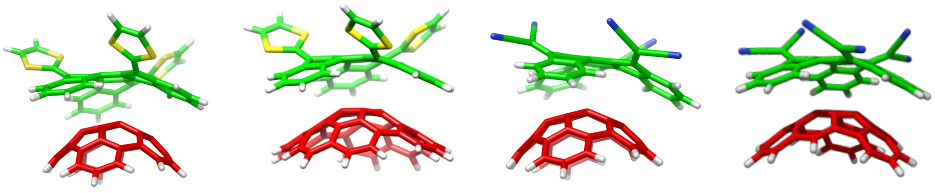

truxTTF•$C_{32}H_{12}$ truxTTF•$C_{38}H_{14}$ Trux6CN•$C_{32}H_{12}$ Trux6CN•$C_{30}H_{12}$

11.3.3. *Results and discussion*

• Supramolecular chemistry of truxTTF and $C_{32}H_{12}$, a singular case of study

The following results have been extracted from the published article "Electron Transfer in a Supramolecular Associate of a Fullerene Fragment".

María Gallego, Joaquín Calbo, Juan Aragó, Rafael M. Krick Calderón, Fernando H. Líquido, Takahiro Iwamoto, Allison K. Greene, Edward. A. Jackson, Emilio M. Pérez, Enrique Ortí, Dirk M. Guldi, Lawrence T. Scott, Nazario Martín, *Angew. Int. Ed.* **2014**, *53*, 2170.

Herein, we investigate the association of a fullerene fragment, hemifullerene $C_{30}H_{12}$, with an electron-donating bowl-shaped tetrathiafulvalene derivative (truxTTF). UV/vis titrations and DFT calculations support the formation of the complex, for which an association constant of log K_a = 3.6 ± 0.3 in $CHCl_3$ at room temperature was determined. Remarkably, electron transfer from truxTTF to $C_{30}H_{12}$ to form the fully charge-separated species takes place upon irradiation of the associate with light, constituting the first example in which a fullerene fragment mimics the electron accepting behavior of fullerenes within a supramolecular complex.

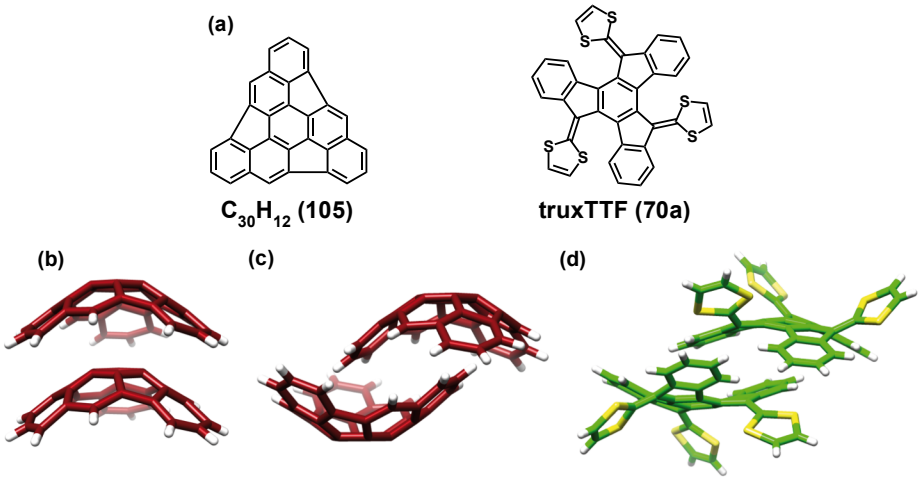

Figure 11.14. (a) Chemical structures of hemifullerene $C_{30}H_{12}$ and truxTTF. (b), (c) Structures of the dimers formed by $C_{30}H_{12}$ in its trigonal and orthorhombic crystal polymorphs, respectively. (d) Structure of the dimers formed by truxTTF in its crystal packing.

Several syntheses[70] and two crystal structures[80] of hemifullerene $C_{30}H_{12}$ were reported a few years ago. In the solid state, two polymorphs were found, each of which showed a different packing motif, originating from the interaction between the $C_{30}H_{12}$ molecules. In the trigonal polymorph, bowl-in-bowl columnar stacks were found, an arrangement in which π–π interactions are maximized (Figure 11.14(b)). In the orthorhombic polymorph, each hemifullerene inserts one of its six-membered rings into the cavity of a neighboring molecule, forming dimers in which both CH–π and π–π interactions play a primary role (Figure 11.14(c)). On the other hand, in truxTTF, a bowl-in-bowl arrangement is prevented by the protruding dithiole rings and, consequently, only the dimeric form in which one of the aromatic rings of each monomer is placed inside the cavity of the other is found (Figure 11.14(d)). Because of their concave shape both $C_{30}H_{12}$ and truxTTF are inherently chiral,[109] consequently, each is obtained as a racemic mixture of two enantiomers.

Considering the ability of truxTTF to associate fullerenes,[38,40] and its electron-donating character, we reasoned that it should also be able to bind $C_{30}H_{12}$, forming hetero-molecular bowl-bowl complexes. To explore this possibility, we first carried out density functional theory (DFT) calculations on four different supramolecular truxTTF•$C_{30}H_{12}$ models, which were rationally constructed from the crystallographic information on both $C_{30}H_{12}$ and truxTTF. All of the models proposed were fully optimized using the revPBE0-D3 functional, which is capable of capturing the dispersion effects and is one of the best density functional to accurately describe supramolecular complexes governed by π–π interactions.[111]

Figure 11.15 displays the minimum-energy structures (**1**-**4**) computed for the truxTTF•$C_{30}H_{12}$ heterodimer at the revPBE0-D3/cc-pVTZ level.

In structures **1** and **2** the convex surface of the $C_{30}H_{12}$ bowl perfectly matches the two concave cavities of the truxTTF host; that is, either through the cavity formed by the carbon backbone (structure **1**) or through the cavity formed by the central benzene ring and the three dithiole rings (structure **2**). Both structures can be thus seen as bowl-in-bowl arrangements where π–π interactions are maximized. The concave cavities of truxTTF and $C_{30}H_{12}$ can also interact, giving rise to heterodimers in which either a benzene ring or a dithiole ring of the truxTTF molecule is placed inside the concave cavity of the

hemifullerene bowl (structures **3** and **4,** respectively). The optimized heterodimeric structures **1**-**4** all show close intermolecular contacts in the 2.5-3.7 Å range, which is indicative of the positive non-covalent interactions between both molecular bowls.

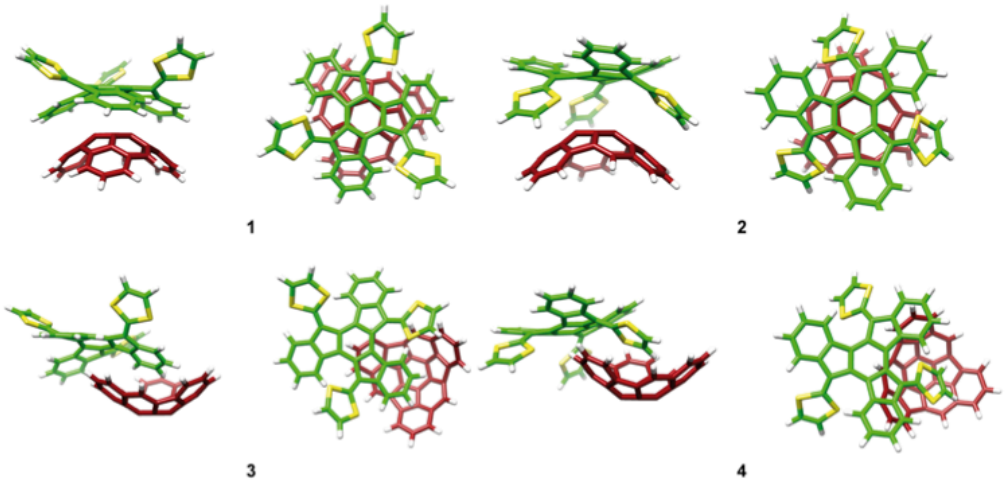

Figure 11.15. Minimum-energy structures (**1**-**4**) computed for the truxTTF•$C_{30}H_{12}$ heterodimer at the revPBE0-D3/cc-pVTZ level.

The association of the hemifullerene $C_{30}H_{12}$, with the truxTTF was corroborated experimentally through UV/vis titrations to do so, truxTTF (1.7 x 10^{-4} M) was titrated with $C_{30}H_{12}$ (0.8 x 10^{-3} M) in $CHCl_3$ at room temperature. The electronic absorption spectra resulting from this titration experiment are depicted in Figure 11.16(a). A decrease in the intensity of the truxTTF absorption at λ = 450 nm was observed, accompanied by the increase of a broad band and a charge-transfer band in the 500-600 nm region. These features are clearly indicative for the truxTTF•$C_{30}H_{12}$ heterodimer in solution. These spectral changes are analogous to those found in the titration of truxTTF vs. C_{60}, albeit with a significantly less intense charge-transfer feature. The results of three separate titration experiments were analyzed with Reactlab Equilibria software, affording a binding constant of log K_a = 3.6 ± 0.3, which is comparable to that found for the association of truxTTF with C_{60}. Calculations at the revPBE0-D3/cc-pVTZ level of theory supported the non-covalent interactions between the truxTTF and the $C_{30}H_{12}$; providing insight

into the possible structure of the heterodimer and the nature of the changes observed during the UV/vis titration.

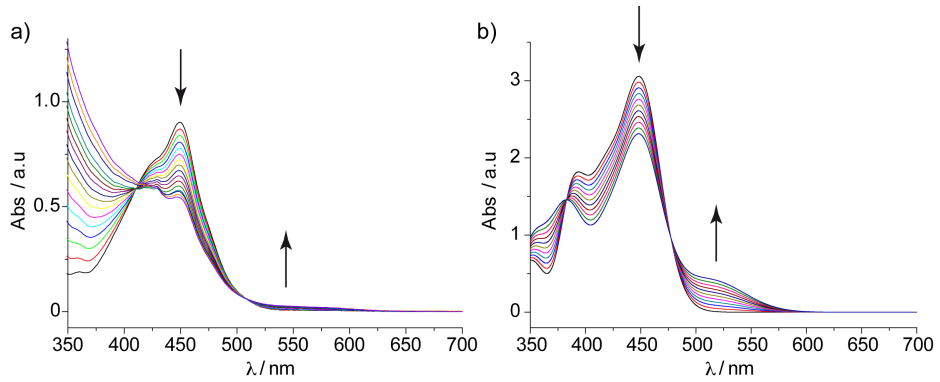

Figure 11.16. (a) Experimental UV/vis spectra as obtained during the titration of truxTTF (1.7×10^{-4} M) with $C_{30}H_{12}$ (0.8×10^{-3} M) in $CHCl_3$ at room temperature. Each addition corresponds to 0.2 eq. (b) TDDFT simulation of the absorption spectra of truxTTF as the ratio of truxTTF•$C_{30}H_{12}$ increases from 0 to 100% (B3LYP/cc-pVDZ calculations including $CHCl_3$ as solvent).

Remarkably, femtosecond pump-probe experiments revealed the formation of a transient species that corresponds to a charge-separated truxTTF$^{\bullet+}$•$C_{30}H_{12}^{\bullet-}$ state. Overall, the latter assignment was backed by both spectroelectrochemical measurements and theoretical calculations. Analysis of the time evolution of these features afforded rate constants of 6.6 x 10^{11} and 1.0 x 10^{10} s^{-1} for the charge separation and charge recombination dynamics respectively. This is the first example of a fullerene fragment mimicking the charge transfer behavior of C_{60}, which paves the way to the study of other related known fullerene fragments, thus opening a new avenue for these electronically less-known carbon-based materials.

• Extension to other PAHs curved systems, a comparative study

Encouraged by the aforementioned results we decided to extend these systematic studies to two more buckybowls **112** and **113**, provided by Prof. Yao-Ting Wu from the National Cheng Kung University (Taiwan). To do so, we studied the supramolecular complexation among truxTTF molecule and these two new buckybowls. Notice that if **105** could be seen as the hemifullerene of C_{60}, **113** could be seen as the analogous hemifullerene of C_{70}.

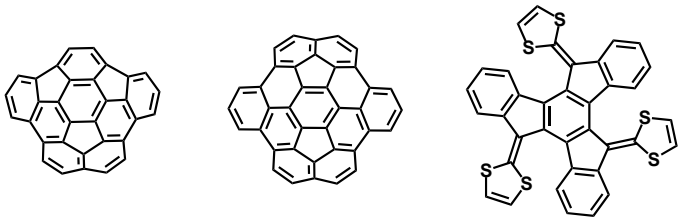

$C_{32}H_{12}$ (**112**) $C_{38}H_{14}$ (**113**) truxTTF (**70a**)

Figure 11.17. Chemical structures of buckybowls **112**, **113**, and truxTTF **70a**.

We also wanted to explore if the n/p electronic behavior of the buckybowls can be tuned depending on the counterpart in the formed complexes. For this purpose, we have firstly investigated the association behavior in solution of buckybowls $C_{32}H_{12}$ **112** and $C_{30}H_{12}$ **105** towards truxene derivative molecule **128** the trux6CN. Please note that **128** is the analogous acceptor system to truxTTF in which the three 1,3-dithiole rings are replaced by three cyanovinylene units.

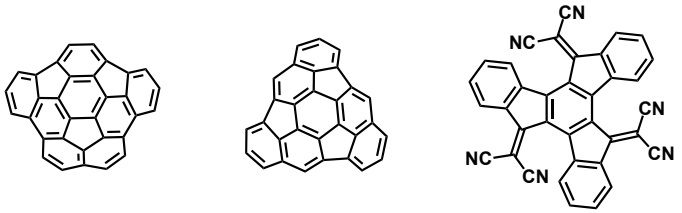

$C_{32}H_{12}$ (**112**) $C_{30}H_{12}$ (**105**) Trux6CN (**128**)

Figure 11.18. Chemical structures of buckybowls **112** and **105**, and truxene acceptor derivative **128**.

Electron acceptor trux6CN (**128**) was synthesized following the method described by V. Khodorkovsky and co-workers,[127] buckybowl **112** was provided by Y. T. Wu, and $C_{30}H_{12}$ (**105**) was synthesized at the laboratory of L. T. Scott.

Again the formation of supramolecular heterodimers of truxene-derivatives and buckybowls was studied in solution. Once that we have experimentally proven the formation of these heterodimers we turn to density functional theory (DFT) calculations to further explore these complexes (done by the group of Prof. E. Ortí). The supramolecular aggregate formed by the electron donor truxTTF molecule and the $C_{32}H_{12}$ or the $C_{38}H_{14}$ buckybowl was modeled in several conformations in resemble to the previously studied truxTTF•$C_{30}H_{12}$.

The same kind of study was carried out for the supramolecular aggregate formed by the electron acceptor trux6CN molecule and the $C_{30}H_{12}$ or the $C_{32}H_{12}$ fullerene fragment.

As schematized in Figure 11.19, π–π interactions are maximized in bowl-in-bowl arrangements (**1** and **2**). The concave cavities of truxTTF and $C_{30}H_{12}$ can also interact, giving rise to heterodimers in which either a benzene ring or a dithiole ring of the truxTTF molecule is placed inside the concave cavity of the hemifullerene bowl structures **3** and **4**, in these staggered arrangements a mixture of π–π and CH–π interactions govern the arrangement between the bowls. For both truxTTF•$C_{32}H_{12}$ and truxTTF•$C_{38}H_{14}$, the staggered arrangement in which a dithiole ring interacts with the cavity of the buckybowls was computed to be the most stable, as it was already reported for the truxTTF•$C_{30}H_{12}$ hetherodimer.

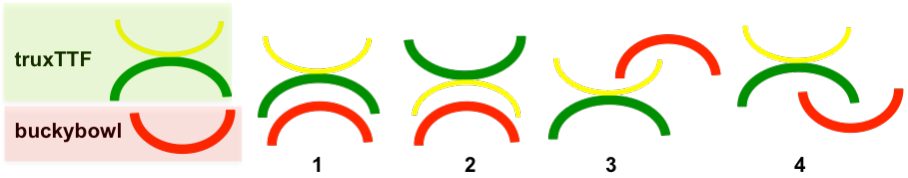

Figure 11.19. Possible ways of arrangement among truxTTF and a buckybowl.

In table 11.1 the most stable conformers calculated for each truxene-derivative•buckybowl heterodimer are shown, as well as the binding constant obtained for each system in PhCl at room temperature.

Table 11.1. Most stable conformers calculated for each truxene-derivative•buckybowl heterodimer.

truxTTF•$C_{32}H_{12}$	truxTTF•$C_{38}H_{14}$	trux6CN• $C_{30}H_{12}$	trux6CN• $C_{32}H_{12}$
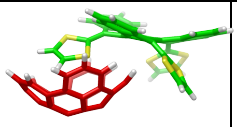	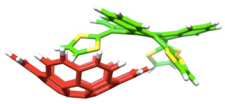	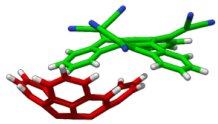	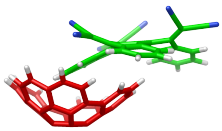
log K_a = 3.19±0.02	log K_a = 3.4±0.1	log K_a = 2.9±0.2	log K_a = 3.2±0.2

As schematized below (Figure 11.20), again π–π interactions are maximized in bowl-in-bowl arrangements (**1** and **2**). The concave cavities of trux6CN and a buckybowl can also interact, in a staggered way, giving rise to heterodimers in which either a benzene ring or a cyanovinylene unit of the trux6CN molecule,

is placed inside the concave cavity of the hemifullerene bowl structures **3** and **4**. In these staggered arrangements a mixture of π–π and CH–π interactions govern the arrangement between the bowls, but some of these interactions are weaker in comparison with arrangements involving the truxTTF. Furthermore, electron lone pairs of nitrogen atoms are worse oriented for efficient n-π interactions compared to sulfur atoms in truxTTF. For both trux6CN•$C_{32}H_{12}$ and trux6CN•$C_{32}H_{12}$, the staggered arrangement in which the aromatic truxene core interacts with the cavity of the buckybowls (**4**) was computed to be the most stable.

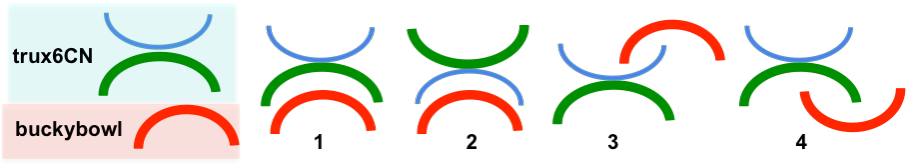

Figure 11.20. Possible ways of arrangement among trux6CN and a buckybowl.

As for the others truxTTF•fullerene heterodimers, the truxTTF behaves as an electron-donor system through its dithiole rings (HOMO localized in the truxTTF moiety and LUMO in $C_{30}H_{12}$, Figure 11.21). A dramatic change in the electronic properties of the supramolecular associate is predicted when comparing the truxTTF•buckybowl with the trux6CN•buckybowl assemblies. The HOMO in truxTTF•$C_{30}H_{12}$ is localized in the donor moiety of truxTTF, whereas the LUMO is completely confined in the fullerene fragment, which acts as an acceptor (Figure 11.21). Otherwise, the HOMO of trux6CN•$C_{30}H_{12}$ is localized in the hemifullerene fragment, which now acts as the electron donor fragment. The LUMO is mainly located in the trux6CN moiety, which is considered as the electron acceptor moiety in the supramolecular associate. This different electron donor/acceptor behavior between the constituting monomers of the supramolecular associates in truxTTF•$C_{30}H_{12}$ and trux6CN•$C_{30}H_{12}$ is also evidenced by computing the accumulated NPA charges borne by the hemifullerene fragment: it has a small but negative charge of -0.010e in truxTTF•$C_{30}H_{12}$ and a positive charge of +0.016e in truxTTF•$C_{30}H_{12}$. These values confirm that the hemifullerene fragment acts as an electron-acceptor (in truxTTF•$C_{30}H_{12}$) or an electron-donor (trux6CN•$C_{30}H_{12}$) system depending on the nature of the fragment to which is supramolecularly associated. The same behavior was found for the truxTTF•$C_{32}H_{12}$ and

trux6CN•$C_{32}H_{12}$ heterodimers.

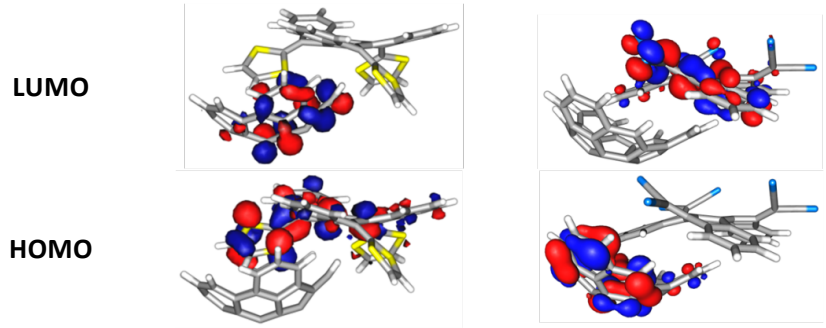

Figure 11.21. Frontier molecular orbitals computed for the most stable conformations of truxTTF•$C_{30}H_{12}$ and trux6CN•$C_{30}H_{12}$.

As for the others truxTTF•buckybowl heterodimers, the truxTTF behaves as an electron-donor system through its dithiole rings in the truxTTF•$C_{38}H_{14}$ heterodimer (HOMO localized in the truxTTF moiety and LUMO in $C_{38}H_{14}$, Figure 11.22).

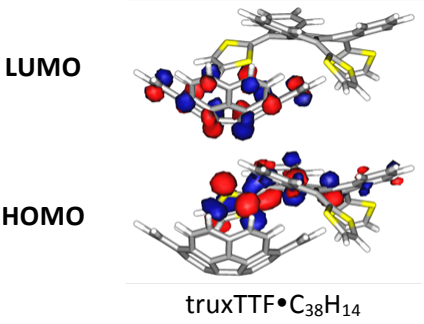

Figure 11.22. Frontier molecular orbitals computed for the most stable conformation of truxTTF•$C_{38}H_{14}$.

Preliminary photophysical studies, done by the group of Prof. D. M. Guldi, reveal a possible electron transfer process in the truxTTF•$C_{38}H_{14}$ heterodimer. When exciting truxTTF•$C_{38}H_{14}$ (1:1) in benzonitrile at 480 nm, $C_{38}H_{14}$ centered transients dominate the spectra (Figure 11.23). Here, no clear assignment to the radical ion species, truxTTF$^{\bullet+}$ and $C_{38}H_{14}^{\bullet-}$, is possible. However, slight changes in the differential absorption in the range between 500 and 700 nm gives rise to the assumption that electronic communication in the excited state is taking place. Furthermore, detailed kinetic analysis corroborates this hypothesis. Multiwavelength analysis yields four major lifetime components. After excitation, a very short lifetime of < 1 ps is followed by a 30-40 ps

component. We assign the shorter component to, on one hand, ultrafast charge separation yielding the charge separated state truxTTF$^{\bullet+}$•$C_{38}H_{14}^{\bullet-}$ and, on the other hand, intrinsic deactivation of non-complexated truxTTF. The longer component is most likely due to intrinsic deactivation of both non-complexated species, i.e. photoexcited truxTTF and $C_{38}H_{14}$. A third component of ~150 ps that is not observed in the single components, reflects the charge recombination to neutral truxTTF•$C_{38}H_{14}$. A fourth component of >5.5 ns can be assigned to the slow deactivation of the $C_{38}H_{14}$ triplet excited state that is populated by intersystem crossing within non-complexated $C_{38}H_{14}$ and, potentially, charge recombination. In less polar chlorobenzene and toluene no evidence for charge separation was found.

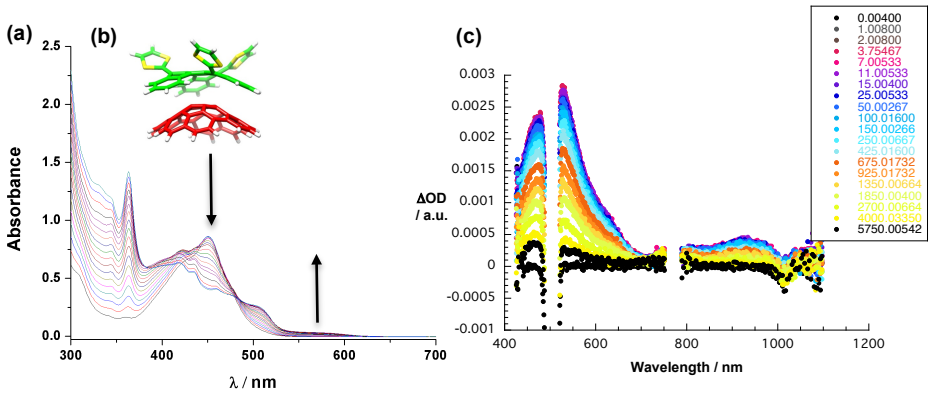

Figure 11.23. (a) Experimental UV/vis spectra as obtained during the titration of truxTTF (1.5 x 10^{-4} M) with $C_{38}H_{14}$ (7.7 x 10^{-4} M) in PhCl at room temperature. (b) DFT calculated heterodimer for truxTTF•$C_{38}H_{14}$. (c) Differential absorption spectra obtained upon femtosecond pump probe experiments (480 nm) of truxTTF•$C_{38}H_{14}$ (1:1) in benzonitrile with time delays of 0–5750 ps at room temperature.

11.4. CONCLUSIONS

The results obtained in each of the chapters discussed in the present report can be summarized as follows:

Chapter I.

•Molecules **70a** and **81** have been validated as versatile building blocks for the construction of more sophisticated chemical structures of interest.

•Three [60]fullerene units were attached to a truxTTF core in molecule **84**.

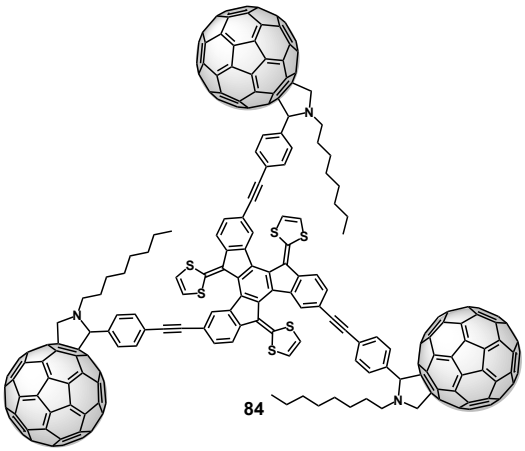

•Five new truxTTF-derivatives featuring multiple anchoring groups have been synthesized. According to their chemical structure, they could have potential applications as sensitizers in Dye Sensitized Solar Cells devices.

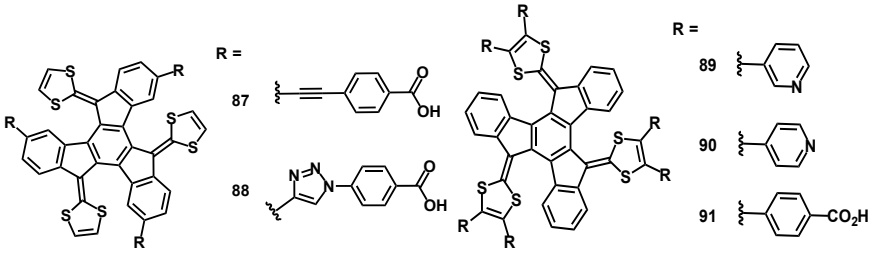

•Molecules **70a** and **73** have been validated as n-type components in BHSCs. A less-explored supramolecular approach has been used for the preparation of efficient small-molecule solar cells. The highest PCE based on a truxTTF was 1.77% while incorporating truxTTF-CO yielded 1.19%. Although, both of them have similar bowl-shape geometries that allow the formation of supramolecular complexes when blended with $PC_{61}BM$ or $PC_{71}BM$, they show different binding constants with fullerenes and also different optical properties. Despite the broader absorption and the deeper HOMO of truxTTF-CO, the stronger non-covalent interactions between the concave shape of the electron donating truxTTF and the surface of the fullerene derivatives lead to higher J_{sc} and FF that could be attributed to a more favorable morphology of the active layer.

Chapter II.

•For the very first time, the association of a fullerene fragment, namely hemifullerene $C_{30}H_{12}$, with a bowl-shaped electron-donor, truxTTF has been corroborated. The association was investigated experimentally through UV/vis titrations. Quantitatively, we calculated a binding constant of log K_a = 3.6 ± 0.3 in $CHCl_3$ at room temperature, which is comparable to that found for the association of truxTTF with C_{60}. Calculations at the revPBE0-D3/cc-pVTZ level of theory supported the non-covalent interactions between the truxTTF and the $C_{30}H_{12}$; providing insight into the possible structure of the heterodimer and the nature of the changes observed during the UV/vis titration.

•Remarkably, femtosecond pump-probe experiments reveal the formation of a transient species that corresponds to a charge-separated truxTTF$^{\bullet+}$•$C_{30}H_{12}^{\bullet-}$ state. Overall, the latter assignment was backed by both spectroelectrochemical measurements and theoretical calculations. Analysis of the time evolution of these features afforded rate constants of 6.6 x 10^{11} and 1.0 x 10^{10} s^{-1} for the charge separation and charge recombination dynamics respectively. This is the first example of a fullerene fragment mimicking the charge transfer behavior of C_{60}.

•As done for the truxTTF•$C_{30}H_{12}$ heterodimer, a general systematic study comprising (I) the study of the formation in solution of heterodimers by UV/vis titrations, (II) DTF calculations to support the existence of non-covalent interactions between the components of the heterodimers and (III) photophisical studies to investigate if electron transfer proceses can occur in these new truxene-derivated•buckybowl systems, has been done for truxTTF•$C_{32}H_{12}$, truxTTF•$C_{38}H_{14}$, trux6CN•$C_{30}H_{12}$.

12. Resumen

12. RESUMEN

12.1. INTRODUCCIÓN

Hasta hace 30 años tan solo se conocían dos alótropos del carbono, el diamante y el grafito. Sin embargo, en las últimas tres décadas hemos asistido al descubrimiento de otras formas alotrópicas de este elemento, siendo las más representativas los fullerenos, nanotubos de carbono y grafeno. El interés despertado en la comunidad científica por los materiales basados en estas nuevas nanoformas de carbono, que evocan la estructura simple del anillo de benceno, radica en sus exóticas y fascinantes propiedades. Los fullerenos son estructuras tridimensionales de carbono de geometría geodésica, jaulas de carbono de alta simetría formadas por 12 pentágonos y un número variable de hexágonos (ciclohexatrienos) igual o mayor a 20. Estas moléculas no siguen la regla de Hückel y, por lo tanto, son compuestos no aromáticos. Los fullerenos han sido exhaustivamente estudiados como materiales electroaceptores en electrónica molecular y su potencial aplicabilidad se está estudiando también en campos tan dispares como el almacenamiento de hidrógeno o la química médica. Los nanotubos de carbono son los análogos monodimensionales de los fullerenos, estos cilindros de carbono pueden ser de pared simple o múltiple, de diámetro variable y, en ausencia de defectos estructurales, están constituidos exclusivamente por anillos hexagonales de carbono. Se ha construido una amplia variedad de dispositivos explotando las propiedades mecánicas y optoelectrónicas de estos materiales. Finalmente, el grafeno está constituido por una lámina bidimensional de anillos hexagonales de carbono de espesor monoatómico, para el que se han postulado múltiples aplicaciones y, actualmente, se le considera la panacea de los materiales para las tecnologías basadas en carbono.

El benceno es también la piedra angular de los sistemas aromáticos que se discuten en la presente memoria: sistemas aromáticos clásicos derivados de estructuras curvadas de truxeno y compuestos aromáticos policíclicos con forma de cuenco. Estos dos tipos de sistemas están en la vanguardia de los compuestos aromáticos, ya que presentan características menos conocidas que los sistemas aromáticos clásicos y una alta versatilidad química, lo que les

convierte en sistemas aromáticos de elección en la búsqueda de nuevas aplicaciones. En la presente memoria se realizará un repaso de los avances más representativos en estos dos tipos de sistemas, en sus correspondientes capítulos.

12.2. CAPÍTULO I. "Modificaciones covalentes en el esqueleto de truxTTF"

12.2.1. ANTECEDENTES

El truxeno (**1**) es un hidrocarburo aromático plano con simetría C3. Su alta conjugación y su simetría, lo convierten en un bloque de construcción molecular muy útil para la síntesis de nuevos materiales orgánicos con aplicaciones diversas. Modificando la periferia de **1** o utilizando análogos estructurales, se puede, por ejemplo, tener acceso a fragmentos de fullereno, fullerenos, fluoróforos solubles en agua, materiales emisores de luz azul, materiales para OFETs, cristales líquidos o semiconductores orgánicos de tipo n para células solares orgánicas.[7-13]

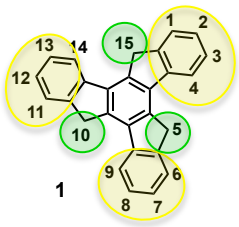

Figura 12.1. Estructura química del truxeno.

El truxeno tiene 15 posiciones susceptibles de ser modificadas covalentemente. Estas 15 posiciones se agrupan en 3 anillos pentagonales y 3 anillos de benceno (Figura 12.1).

Las posiciones C5, C10 y C15 de **1** se funcionalizan habitualmente con cadenas alquílicas saturadas para impedir el empaquetamiento π–π intermolecular. De esta forma, se mejora la solubilidad del truxeno, lo que facilita la posterior modificación de su esqueleto en otras posiciones.[15] De las doce posiciones aromáticas de **1** susceptibles de ser funcionalizadas, C2, C7 y C12 son las que generalmente se modifican, por ejemplo, por reacciones de Friedel-Crafts o por bromaciones electrofílicas.[18-19] La modificación de las restantes posiciones del esqueleto de truxeno requiere rutas alternativas, como la modificación previa de las posiciones C2, C7 y C12 o la síntesis de truxenos con 1-indanonas

previamente funcionalizadas, siendo esta última estrategia muy útil también para la obtención de truxenos modificados en las posiciones más impedidas, C4, C9 y C13.[19] Los esqueletos de truxeno pueden, además, contener heteroátomos en su estructura.[21]

El esqueleto de truxeno se validó como unidad de reconocimiento molecular en receptores de fullerenos, de tipo truxeno-tetratiafulvaleno, preparados a partir de truxenonas modificadas por reacciones de olefinación de tipo Wittig-Horner (Esquema 12.1).[38,40]

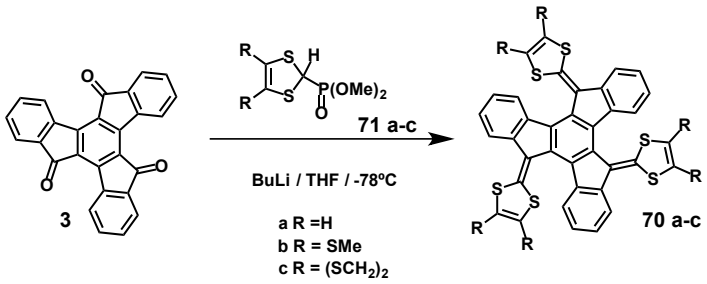

Esquema 12.1. Síntesis de derivados de truxeno-TTF.

En estos derivados, el esqueleto aromático original de la truxenona y los anillos de ditiol quedan dispuestos de manera ecuatorial.

La geometría cóncava resultante del esqueleto de truxeno es complementaria en forma y tamaño a la superficie de los fullerenos (Figura 12.2), lo que permite maximizar las interacciones de van der Waals y las de tipo π–π entre el receptor y los fullerenos.[38,40]

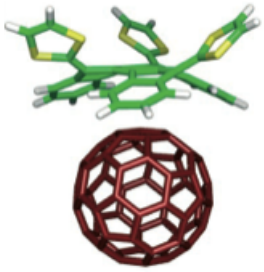

Figura 12.2. Heterodímero truxTTF•C_{60}.

Una de las potenciales aplicaciones de los materiales basados en truxeno sería su implementación en dispositivos fotovoltaicos. En la bibliografía existen ejemplos en los que el esqueleto de truxeno se ha utilizado como puente tipo π en el diseño de colorantes para células solares orgánicas sensibilizadas por colorantes (DSSCs),[31-32] también llamadas dispositivos de tipo Graetzel. En la bibliografía queda, además, recogida la síntesis de algunos derivados electrodeficientes de truxeno como semiconductores tipo n-, que se utilizaron

como alternativa a los derivados fullerénicos en células solares de heterounión masiva (BHSCs).[17,34]

12.2.2. OBJETIVOS

- **Síntesis de bloques de construcción molecular**

Se pretende llevar a cabo la síntesis de los bloques de construcción molecular **70ª** y **81** que son moléculas adecuadas para la síntesis de estructuras de interés derivadas de truxTTF.

- **Unión covalente de tres fullerenos al esqueleto de truxTTF**

Nos proponemos el diseño, síntesis y caracterización de una tétrada molecular de tipo DA_3 compuesta por un esqueleto de truxTTF al que se le unirán por la periferia aromática tres unidades de [60]fullereno.

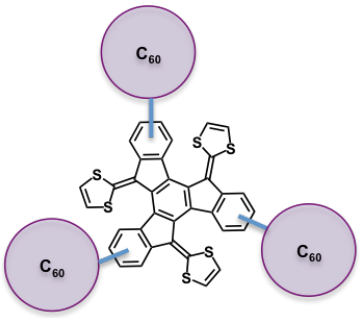

Figura 12.3. Tétrada truxTTF-3C_{60}

- **Derivados de truxTTF para DSSCs**

Presentaremos la síntesis de cinco derivados de truxTTF que, atendiendo a su estructura química, podrían ser colorantes de interés para dispositivos de DSSCs.

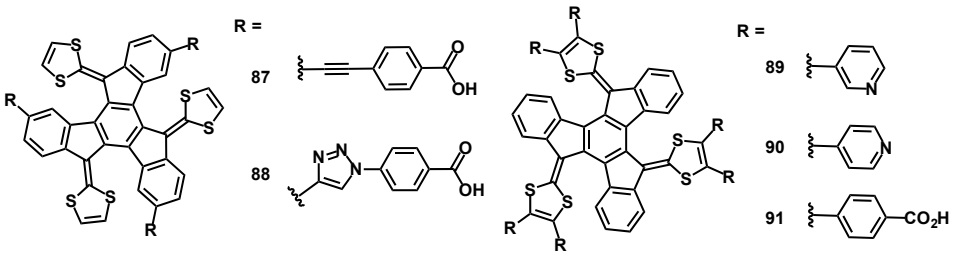

Figure 12.4. Derivados de truxTTF para DSSCs.

- **Derivados de truxTTF para BHSCs**

Nos proponemos estudiar la aplicabilidad de derivados de truxTTF en dispositivos de tipo BHSCs como semiconductores tipo p- junto con los derivados de fullereno [71]PCBM y [61]PCBM.

12.2.3. EXPOSICIÓN Y DISCUSIÓN DE RESULTADOS

- **Síntesis de bloques de construcción molecular**

La molécula de truxTTF (**70ª**) ofrece la posibilidad de modificar su estructura de manera covalente en los anillos de 1,3-ditiol (resaltados en amarillo en la Figura 12.5) o en su esqueleto aromático (resaltado en verde en la Figura 12.5).

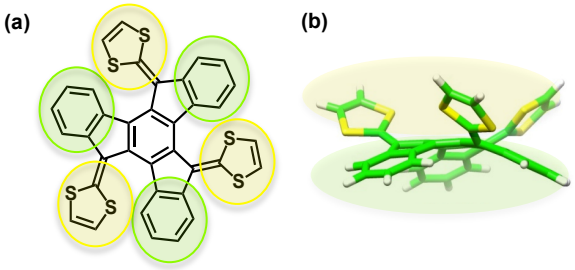

Figura 12.5. (a) Estructura química del truxTTF (**70a**). Resaltadas en verde y 237emperat las 237empera susceptibles de ser covalentemente modificadas. (b) Vista de la disposición 237emperatu adoptada por los anillos de 1,3-ditiol y el esqueleto de truxeno en la molécula **70a**.

El compuesto **70ª** es, en sí mismo, un bloque de construcción molecular adecuado para la modificación covalente en los anillos de 1,3-ditiol. Esta molécula se sintetiza a partir de la truxenona (**3**) mediante una triple reacción de olefinación de tipo Wittig-Horner con el fosfonato **71ª**. De la misma manera, mediante una doble reacción de olefinación de tipo Wittig-Horner con el fosfonato **71ª** sobre la truxenona se obtiene el derivado truxTTF-CO (**73**) (Esquema 12.2).[38,40]

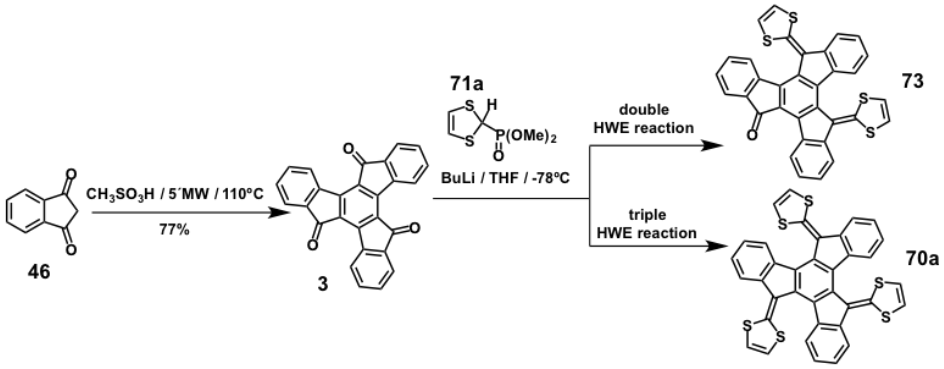

Esquema 12.2. Síntesis de **73** y de truxTTF (**70a**).

Recurrimos a la síntesis de una truxenona previamente funcionalizada, concretamente a la tribromotruxenona **75** para la síntesis de un bloque de construcción molecular que permita posteriormente modificaciones periféricas del esqueleto de truxeno. Esta truxenona proporciona un *core* de truxeno funcionalizado con tres carbonilos y tres átomos de bromo en su periferia. Los carbonilos permitirán la sustitución por grupos de 1,3-ditiol y los bromos proporcionan una forma sencilla de funcionalización mediante reacciones de acoplamiento cruzado de tipo C-C.

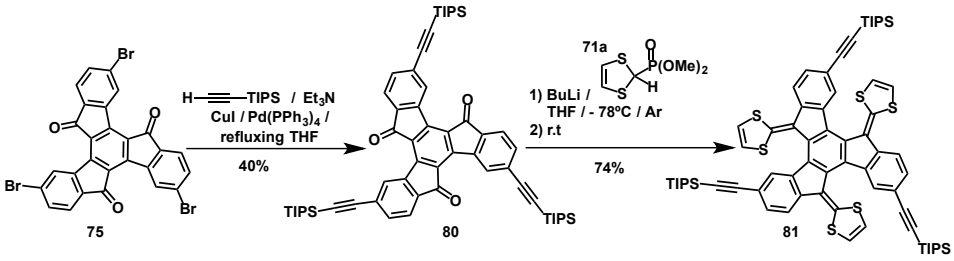

Esquema 12.3. Síntesis del bloque de construcción molecular **81**.

Como era de esperar, el bloque de construcción molecular **81** presenta la misma quiralidad helicoidal que el truxTTF, encontrando para esta estructura sólo el par enantiomérico *P,P,P / M,M,M*. Se comprueba además que, aunque se haya modificado el esqueleto aromático de truxeno, **81** mejora la capacidad de asociar fullerenos (Figura 12.6).

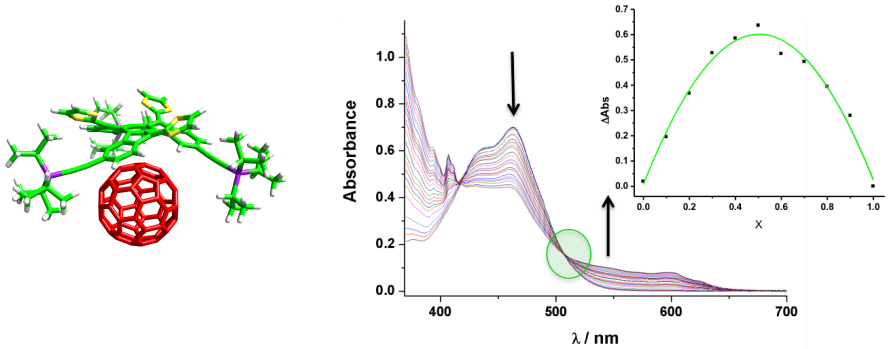

Figura 12.6. Izquierda, simulación del complejo **81**•C_{60}. Derecha, cambios en el espectro de absorción UV/vis de la molécula **81**, al añadir alícuotas de C_{60} (log K_a= 4.5 ± 0.5, PhCl, r.t). La gráfica de Job insertada confirma la estequiometría 1:1 para el complejo **81**•C_{60}.

- **Unión covalente de tres fullerenos al esqueleto de truxTTF**

En nuestro grupo de investigación se han descrito díadas moleculares basadas en exTTF, como unidades dadoras, y fullerenos como unidades aceptoras. Sin embargo, hasta ahora no se había descrito la síntesis de una molécula que incluyera en su estructura la unión covalente de un truxTTF y fullerenos.

Para afrontar la síntesis de esta molécula recurrimos al bloque de construcción molecular **81**, un derivado de truxeno que presenta tres alquinos en su periferia. La ruta sintética que condujo a la unión del esqueleto de truxTTF a las tres unidades de [60]fullereno tiene tres etapas: (i) desprotección de los grupos triisopropilsililacetileno con TBAF en THF, para obtener el alquino **83**, (ii) triple reacción de acoplamiento C-C de tipo Sonogashira entre el alquino **83** y el 4-iodobenzaldehído catalizada por paladio que conduce al derivado de truxTTF **85** y, finalmente, (iii) una triple reacción de cicloadición 1,3-dipolar sobre el aldehído **85** con octilglicina y C_{60} en tolueno a reflujo, para obtener la molécula objetivo **84**.

84 resultó ser un buen receptor de C_{70} que explota las interacciones fullereno-fullereno y truxeno-fullereno. Se obtuvo una constante de log K_a = 6.8 ± 0.5 (*o*-DCB, r.t). Desafortunadamente fue imposible determinar la existencia o no de procesos de transferencia de carga inter o intramolecular para este

sistema ya que cuando se somete esta molécula a experimentos fotofísicos de tipo fotólisis ultrarrápida de femtosegundo la muestra descompone.

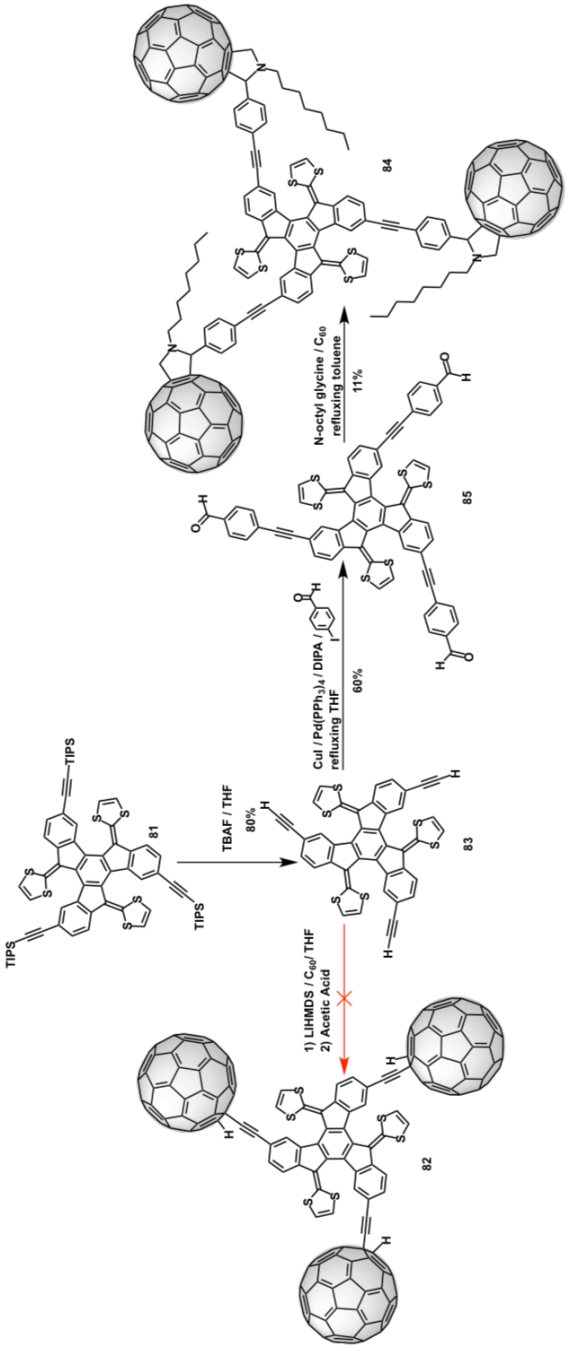

Esquema 12.4. Estrategias sintéticas seguidas para la obtención de un esqueleto de truxTTF unido covalentemente a tres unidades de C_{60}.

- **Derivados de truxTTF para dispositivos fotovoltaicos DSSCs**

Como se ha comentado anteriormente, el truxTTF proporciona un esqueleto aromático que podría actuar de puente tipo π en el diseño de colorantes para células de tipo de Graetzel. Un colorante adecuado para este tipo de sistemas consta fundamentalmente de unidades dadoras de electrones, un puente tipo π que conduce los electrones cedidos a un grupo aceptor de electrones que, generalmente, actúa además como grupo de anclaje que inyectará al óxido de titanio los electrones. La geometría bicóncava del truxTTF impide la autoagregación molecular y su estructura permite la incorporación de múltiples puntos de anclaje. La multivalencia de puntos de anclaje se ha descrito ya para varios colorantes y se cree que puede tener ventajas como serían una mayor eficiencia en la inyección electrónica desde el colorante al óxido de titanio.[47]

La mayoría de los colorantes conjugados de tipo D-π-A diseñados para DSSCs tienen ácidos carboxílicos como grupos de anclaje, que permiten una buena comunicación electrónica entre el colorante y el TiO_2. Igualmente, se han descrito colorantes con anillos de piridina que actúan tanto de grupo electroaceptor como de grupo de anclaje al óxido de titanio mediante enlace coordinado, dando rendimientos de inyección electrónica comparables a los que se obtiene con ácidos carboxílicos.[48]

La incorporación de grupos de anclaje al truxTTF (**70ª**) se realiza de una manera sencilla en un solo paso. Mediante una séxtuple reacción de arilación de C-H catalizada por paladio se han obtenido las moléculas **89** y **90** mediante la reacción del truxTTF con la correspondiente yodopiridina y **91** mediante reacción del truxTTF con 4-yodobenzoato de metilo para obtener **93**. La posterior hidrólisis en medio básico proporciona el derivado de truxTTF decorado con seis grupos carboxilo. (Esquema 12.5).

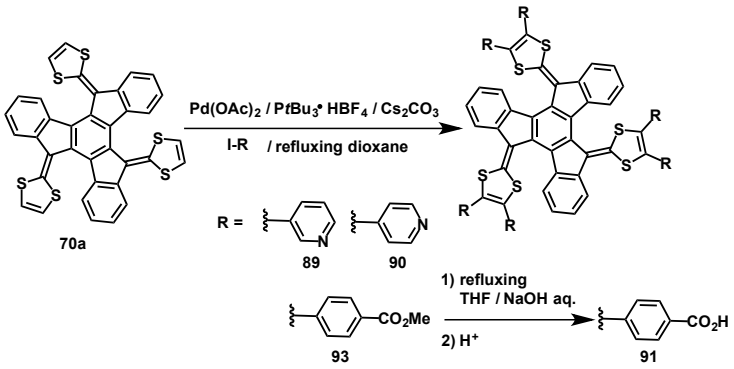

Esquema 12.5. Síntesis de derivados de truxTTF con seis grupos de anclaje.

El bloque de construcción molecular **81** permite el diseño de colorantes con tres grupos de anclaje siguiendo dos estrategias: (i) modificación vía triple acoplamiento C-C de tipo Sonogashira y (ii) modificación mediante una triple reacción de cicloadición 1,3-dipolar catalizada por Cu(I) entre los alquinos del derivado de truxTTF **81** y el ácido 4-azidobenzoico. Estas dos estrategias comienzan con la desprotección de los alquinos de **81** en THF a temperatura ambiente con TBAF para obtener el derivado **83** (Esquema 12.6).

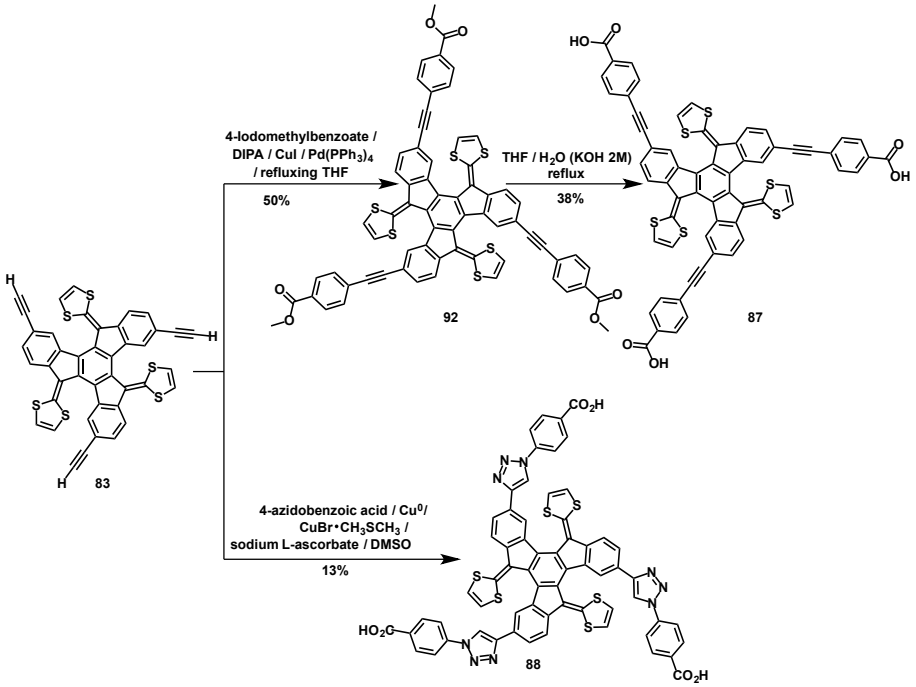

Esquema 12.6. Síntesis de derivados de truxTTF con tres grupos de anclaje.

- **Derivados de truxTTF para células de heterounión masiva (BHSCs)**

Los elementos que componen una célula solar orgánica de tipo BHSC son una película de un polímero conjugado o molécula pequeña como material dador de electrones y, habitualmente, un derivado fullerénico como material aceptor electrónico. Esta película se dispone entre los electrodos. Cuando el componente dador o aceptor se fotoexcita se crea un excitón que difunde hasta la interfase dador-aceptor, donde se escinde en un par de cargas libres. El electrón es entonces conducido por el material electroaceptor hacia el ánodo, y el hueco generado hacia el cátodo metálico (Figura 12.7). El proceso global requiere una alta movilidad de carga.[33]

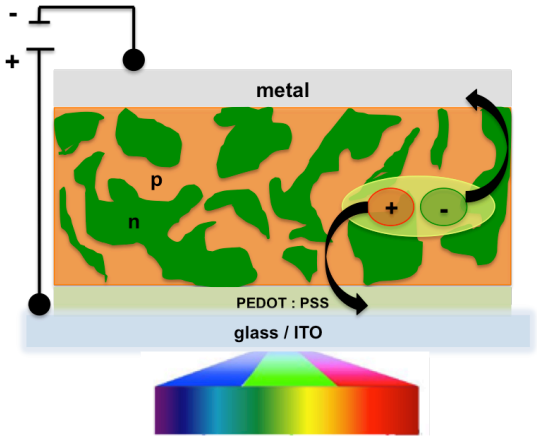

Figura 12.7. Representación esquemática del funcionamiento de un dispositivo BHJ.

Un factor clave que afecta a la eficiencia de este tipo de dispositivos es la morfología de la interfase, esto es, el ordenamiento de los componentes dador-aceptor a escala nanométrica. En nuestro grupo de investigación, con el objetivo de lograr la nanoestructuración de los componentes dadores y aceptores en los dispositivos fotovoltaicos, diseñamos receptores de fullerenos para su aplicación en fotovoltaica orgánica. Un buen receptor de fullerenos debe reunir tres características principales: (i) ser un buen material electro-dador, (ii) ser eficientre frente a la absorción de luz y (iii) tener la capacidad de autoensamblarse con estos fullerenos. En este sentido, hace ya algunos años, validamos truxTTF (**70ª**) y al truxTTF-CO (**73**) como buenos receptores para el C_{60} y C_{70} mediante estudios de complejación en disolución.[38,40] Además, los estudios fotofísicos realizados en estas moléculas

los confirman como buenos sistemas dadores de electrones. Por lo tanto, en principio, estos sistemas serían candidatos adecuados para su estudio como semiconductores tipo p- junto con el [71]PCBM y el [61]PCBM como semiconductores tipo n- en dispositipos de tipo BHSCs.

Los resultados que se exponen a continuación se han extraído del artículo publicado " Organic Solar Cells Based on Bowl-Shape Small Molecules". Los resultados descritos en la publicación original han sido complementados con la síntesis y caracterización de otro derivado del truxTTF, el 3F-truxTTF.

Agustín Molina-Ontoria, María Gallego, Luis Echegoyen, Emilio M. Pérez and Nazario Martín. *RSC* Adv., **2015**, *5*, 31541.

Se recurre a una aproximación supramolecular para la construcción de dispositivos de tipo BHSCs de molécula pequeña, buscando una complementariedad geométrica y electrónica entre los semiconductores tipo n- y tipo p- , con el objetivo de maximizar las interacciones intermoleculares en la interfase D-A de la célula solar que, en principio, debería conducir a una mejor morfología y a una mejora en la eficiencia de los dispositivos.

Atendiendo a esta aproximación molecular, se empleará como semiconductores tipo p- el truxTTF (**71a**) y el truxTTF-CO (**73**) y [71]PCBM y [61]PCBM como semiconductores tipo n- (Figura 12.8).

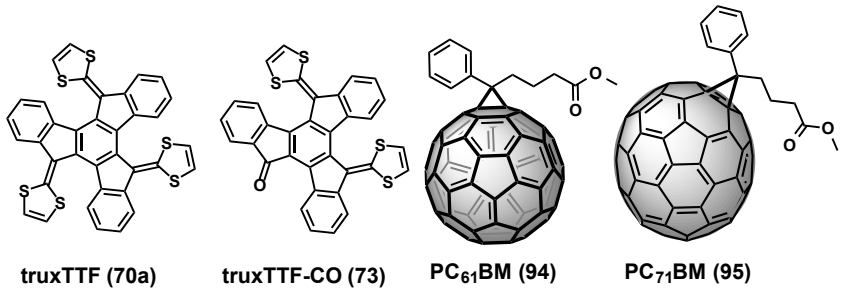

Figura 12.8. Estructura química de los 245 emperatur electro-dadores truxTTF y truxTTF-CO, y electro-aceptores $PC_{61}BM$ y $PC_{71}BM$.

Se ha estudiado la asociación supramolecular en disolución del [61] y [71]PCBM con **70ª** y **73**, obteniéndose constantes de asociación de magnitud análoga a las obtenidas para estos receptores con el C_{60} y C_{70}.[38,40] (Figura 12.9). Cuando se prepararon los dispositivos fotovoltaicos con estos componentes

se alcanzó una eficiencia de 1.77% para el dispositivo que incorporaba truxTTF como material dador de electrones y [71]PCBM como material aceptor de electrones. Sin embargo, cuando en lugar de truxTTF se utilizó truxTTF-CO se alcanzó una eficiencia de 1.19%, a pesar de la mayor capacidad de absorción de luz del truxTTF-CO. El hecho de que el truxTTF reconozca en disolución al C_{70} y al [71]PCBM mejor que el truxTTF-CO, podría tener como consecuencia una morfología más favorable, dando lugar a una mejor eficiencia en el dispositivo.

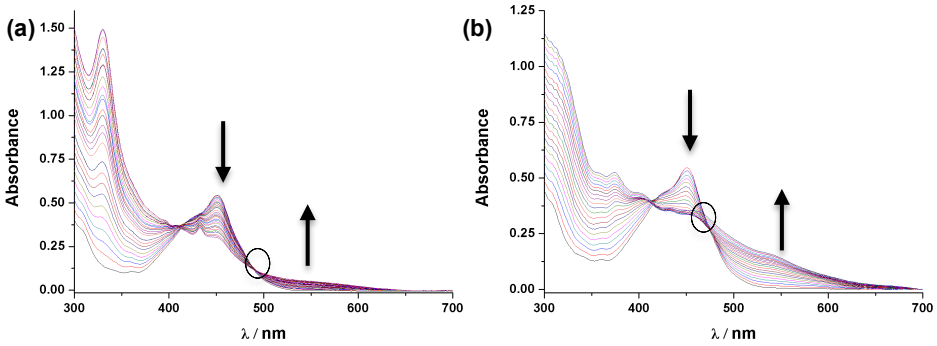

Figura 12.9. Espectros UV/vis obtenidos en la valoración del truxTTF con (a) $PC_{61}BM$ y (b) $PC_{71}BM$. Los correspondientes valores de asociación obtenidos fueron log K_a= 3.44 ± 0.03 (PhCl, r.t) para el complejo truxTTF•$PC_{61}BM$ y log K_a= 4.1 ± 0.8 (PhCl, r.t) para el complejo truxTTF•$PC_{71}BM$.

12.3. CAPÍTULO II: "Complejación supramolecular de compuestos aromáticos policíclicos curvados con derivados curvados de truxeno"

12.3.1. ANTECEDENTES

La síntesis de hidrocarburos aromáticos policíclicos curvados es un tema de gran actualidad en química. El interés suscitado por estos compuestos radica en su inherente curvatura, que les confiere propiedades electrónicas que no manifiestan sus análogos planos y que recuerdan, en cierto modo, a las de los fullerenos. En la bibliografía encontramos una amplia variedad de estos hidrocarburos aromáticos policíclicos curvados,[71] preparados de diversas maneras y sobre los que se han llevado a cabo múltiples modificaciones químicas, algunas análogas a las que se pueden realizar sobre los fullerenos.[64]

Además, algunos autores, basándose en la complementariedad geométrica entre las superficie π-convexa del [60]fullereno y la superficie π-cóncava de estos hidrocarburos, diseñaron una serie de receptores para fullerenos que explotaban como unidad de reconocimiento molecular una o varias unidades de coranuleno.[87-89] Sin embargo, el reconocimiento supramolecular de estos hidrocarburos aromáticos policíclicos curvados, así como síntesis de receptores adecuados para los mismos, son aspectos comparativamente muy poco explotados.

12.3.2. OBJETIVOS

Nos proponemos, por tanto, estudiar el reconocimiento molecular de algunos hidrocarburos aromáticos policíclicos mediante derivados curvados de truxeno. Este segundo capítulo se ha subdividido en las siguientes secciones:

- **Química supramolecular del truxTTF y el hemifullereno $C_{30}H_{12}$, un caso singular de estudio**

Estudiaremos la asociación entre el hemifullereno $C_{30}H_{12}$ (**105**) y un derivado curvado electrodador de truxeno: el truxTTF.

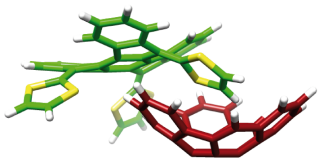

Figura 12.10. Complejo truxTTF•$C_{30}H_{12}$.

- **Química supramolecular de otros hidrocarburos aromáticos policíclicos curvados con derivados curvados de truxeno, un estudio sistematico**

Alentados por los buenos resultados obtenidos en el estudio previo, se ha llevado a cabo un estudio sistemático sobre otros hidrocarburos aromáticos policíclicos curvados, más específicamente los compuestos **112** ($C_{32}H_{12}$) y **113** ($C_{38}H_{14}$). En este apartado utilizaremos como unidades de reconocimiento molecular para estos sistemas de nuevo el truxTTF y el trux6CN. Este último es un derivado curvado de truxeno pero de marcado carácter electroaceptor. (Figura 12.11)

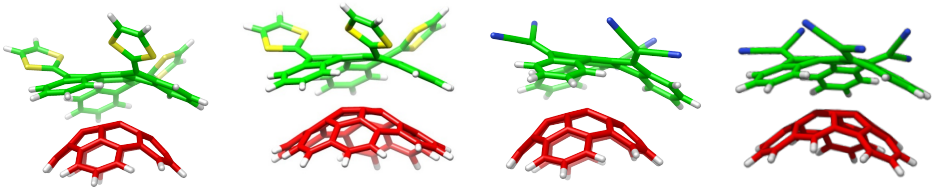

truxTTF•$C_{32}H_{12}$ truxTTF•$C_{38}H_{14}$ Trux6CN•$C_{32}H_{12}$ Trux6CN•$C_{30}H_{12}$

Figura 12.11. complejos heteromoleculares (derivado de truxeno)•(sistema aromático policíclico curvado) objeto de estudio.

12.3.2. EXPOSICIÓN Y DISCUSIÓN DE LOS RESULTADOS

- **Química supramolecular del truxTTF y el hemifullereno $C_{30}H_{12}$, un caso singular de estudio**

Los resultados expuestos a continuación se han extraído del artículo publicado bajo el título "Electron Transfer in a Supramolecular Associate of a Fullerene Fragment". Los resultados descritos en la publicación original se han complementado con la síntesis y la caracterización del hemifullereno $C_{30}H_{12}$, que se llevaron a cabo durante mi estancia pre-doctoral en el Boston College bajo la supervisión del Prof. L. T. Scott.

María Gallego, Joaquín Calbo, Juan Aragó, Rafael M. Krick Calderón, Fernando H. Líquido, Takahiro Iwamoto, Allison K. Greene, Edward A. Jackson, Emilio M. Pérez, Enrique Ortí, Dirk M. Guldi, Lawrence T. Scott, Nazario Martín, *Angew. Chem. Int. Ed.* **2014**, 2170.

En este trabajo investigamos la asociación de un fragmento de fullereno, el hemifullereno $C_{30}H_{12}$, con un derivado electro-dador de truxeno tetratíafulvaleno de geometría bicóncava, el truxTTF. La formación del complejo truxTTF•$C_{30}H_{12}$ está basada en estudios computacionales DFT y en los estudios de complejación en disolución monitorizados por espectroscopia ultravioleta-visible, los cuales han permitido obtener un valor medio de asociación de log K_a = 3.6 ± 0.3 en cloroformo a temperatura ambiente. Además, los estudios fotofísicos en disolución confirman que bajo irradiación del complejo truxTTF•$C_{30}H_{12}$, se produce un proceso de transferencia electrónica fotoinducida, desde el truxTTF al hemifullereno $C_{30}H_{12}$ lo que origina un estado de separación de cargas. Este descubrimiento constituye el

primer ejemplo descrito en la literatura en el cual un fragmento de fullereno mimetiza el comportamiento eletro-aceptor del propio [60]fullereno en un complejo supramolecular.

El hemifullereno $C_{30}H_{12}$ es un hidrocarburo aromático policíclico curvado sobre el que se encuentra mucha información en la bibliografía, datos cristalográficos,[80] diversos métodos de síntesis,[70] etc. El interés suscitado por esta molécula nace del descubrimiento de los fullerenos. Durante mucho tiempo se pensó que la unión de dos unidades de este fragmento de fullereno conduciría, idealmente, a la molécula del [60]fullereno.[70] El truxTTF es un derivado del truxeno con capacidad dadora de electrones, que tiene tres anillos de 1,3-ditiol en su estructura que fuerzan al esqueleto de truxeno a abandonar su geometría plana y adoptar una geometría cóncava que es complementaria en forma y tamaño con el [60]fullereno y [70]fullereno. Los buenos resultados obtenidos en los estudios de complejación supramolecular con fullereno lo ratifican como un buen sistema de reconocimiento para diferentes unidades electroaceptoras.

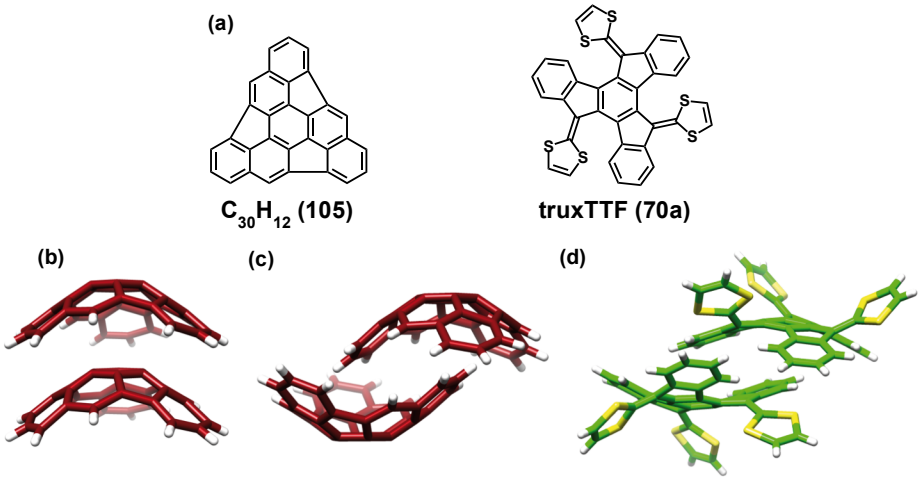

Figura 12.13. (a) Estructuras químicas del hemifullereno $C_{30}H_{12}$ y del truxTTF. (b), (c) Estructuras diméricas formadas por el $C_{30}H_{12}$ en su empaquetamiento polimorfo ortorrómbico. (d) Estructura adoptada por los dímeros de truxTTF en su empaquetamiento cristalino.

Considerando la habilidad del truxTTF para asociar fullerenos en disolución y su carácter electro-dador,[38,40] razonamos que podría ser capaz también de

reconocer al hemifullereno $C_{30}H_{12}$ y formar el complejo heteromolecular truxTTF•$C_{30}H_{12}$. Mientras que para el truxTTF•C_{60} tan sólo había una disposición espacial posible para las dos subunidades del complejo, aquella en la que el esqueleto cóncavo aromático del truxTTF interacciona con la superficie convexa del C_{60}, para el truxTTF•$C_{30}H_{12}$ se razonaron cuatro posibles disposiciones. Estas disposiciones se estudiaron mediante cálculos computacionales DFT (Figura 12.14). Todos los modelos propuestos se optimizaron con el funcional revPBE0-D3.

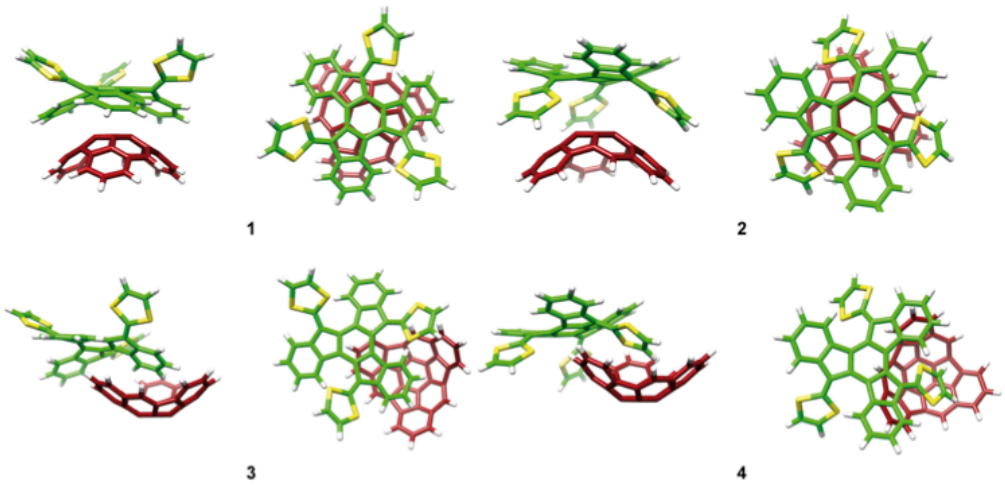

Figura 12.14. Estructuras de 250 emper energía (**1**-**4**) computadas para el heterodímero truxTTF•$C_{30}H_{12}$ (revPBE0-D3/cc-pVTZ).

Como puede apreciarse en la Figura 12.14, en las estructuras **1** y **2** se maximiza la complementariedad geométrica cóncavo-convexo, esto es, bien entre el esqueleto cóncavo de truxeno del truxTTF y la superficie convexa del hemifullereno (estructura **1**) o bien, a través de la cavidad cóncava que crean los anillos de ditiol del truxTTF con la superficie convexa del $C_{30}H_{12}$. Tanto en **1** como en **2** se han maximizado las interacciones π–π. Alternativamente, estas moléculas pueden interaccionar de manera que se dispongan "cóncavo-cóncavo" como se observa para las estructuras **3** y **4**. Es decir, un anillo de benceno del truxTTF, en **3**, o un anillo de ditiol, en **4**, queda insertado en la cavidad cóncava del hemifullereno, maximizando las interacciones de tipo CH-π. La optimización de todas las posibles disposiciones espaciales pone de manifiesto distancias de contacto intermoleculares en el rango de valores de

2.5-3.7 Å. Estas distancias justifican la existencia de interacciones no covalentes que propiciarían la formación del complejo supramolecular truxTTF•$C_{30}H_{12}$.

La formación del complejo truxTTF•$C_{30}H_{12}$ se llevó a cabo experimentalmente mediante valoraciones ultravioleta-visible (Figura 12.15 (a)). Para ello, a una disolución de truxTTF (1.7 x 10^{-4} M, $CHCl_3$) se le fueron añadiendo alícuotas de una disolución de $C_{30}H_{12}$ (0.8 x 10^{-3} M, $CHCl_3$) a temperatura ambiente. Los espectros de absorción obtenidos se muestran en la figura 12.15. Es notable la disminución de la intensidad de la banda centrada en $\lambda = 450$ nm. Esta disminución de intensidad viene acompañada de la aparición de una nueva banda de transferencia de carga que se extiende en el rango de los 500-600 nm. Las características encontradas en estos estudios de complejación son análogas a las observadas en los realizados para la complejación del [60]fullereno con el truxTTF, si bien, con una notable menor intensidad en la banda de transferencia de carga. Los resultados obtenidos para tres experimentos de complejación independientes se analizaron con el software ReactLab Equilibria^{TM}. El análisis proporcionó una constante de asociación de log K_a = 3.6 ± 0.3. El valor de esta constante de asociación es comparable al obtenido en el estudio de complejación del C_{60} con truxTTF.

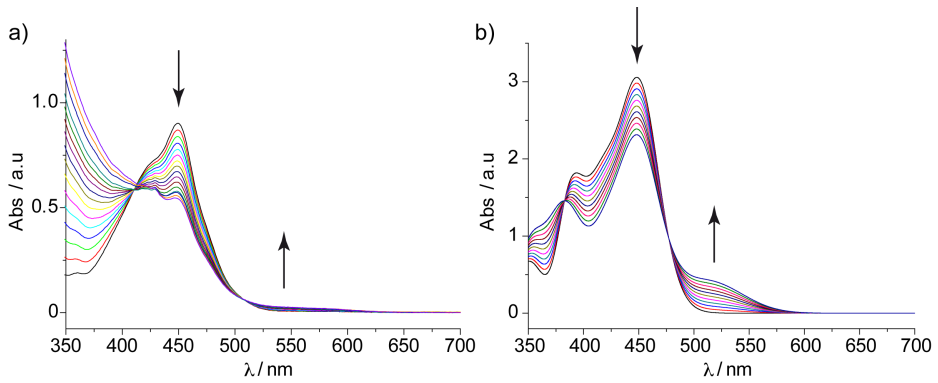

Figura 12.15. (a) Espectros UV/vis obtenidos durante la valoración del truxTTF (1.7 × 10^{-4} M) con $C_{30}H_{12}$ (0.8 × 10^{-3} M) en $CHCl_3$ a temperature ambiente. Cada adición corresponde a 0.2 eq. (b) Simulación TDDFT de los espectros de absorción del truxTTF según aumenta el ratio de truxTTF•$C_{30}H_{12}$ de 0 a 100% (Cálculos B3LYP/cc-pVDZ que incluyean al $CHCl_3$ como disolvente).

Los estudios de espectroscopía de absorción a tiempo resuelto demostraron

la formación de especies transitorias que corresponden al estado de separación de cargas del complejo heteromolecular, esto es, al truxTTF$^{\bullet+}$•$C_{30}H_{12}^{\bullet-}$. El análisis de los datos obtenidos por estos estudios permitieron obtener valores de 6.6 x 10^{11} s^{-1} y 1.0 x 10^{10} s^{-1} para los procesos de separación y recombinación de cargas, respectivamente. Este comportamiento fue, además, apoyado por medidas espectroelectroquímicas y por cálculos teóricos. La importancia de los datos obtenidos radica en que nos encontramos ante el primer ejemplo en el que se demuestra que un fragmento de fullereno es capaz de mimetizar el comportamiento de transferencia de carga que se encuentra para los fullerenos. Se abre así la puerta a futuros estudios con otras estructuras relacionadas y, por lo tanto, a un nuevo campo de investigación para estos materiales de carbono cuyo comportamiento electrónico es poco conocido.

- **Química supramolecular de otros hidrocarburos aromáticos policíclicos curvados con derivados curvados de truxeno: un estudio sistematico**

Alentados por los resultados obtenidos descritos en el apartado anterior, nos propusimos extender el estudio realizado a otros sistemas aromáticos policíclicos curvados. En esta sección se estudiarán los sistemas truxTTF•$C_{32}H_{12}$, trux6CN•$C_{32}H_{12}$, truxTTF•$C_{38}H_{14}$ y trux6CN•$C_{30}H_{12}$. Los fragmentos de fullereno **112** y **113**, fueron proporcionados por el Prof. Yao-Ting Wu de la National Cheng Kung University (Taiwan). El trux6CN (**128**), análogo electro-aceptor del truxTTF se preparó siguiendo la metodología descrita por Khodorkovsky y colaboradores.[127] (Figura 12.16)

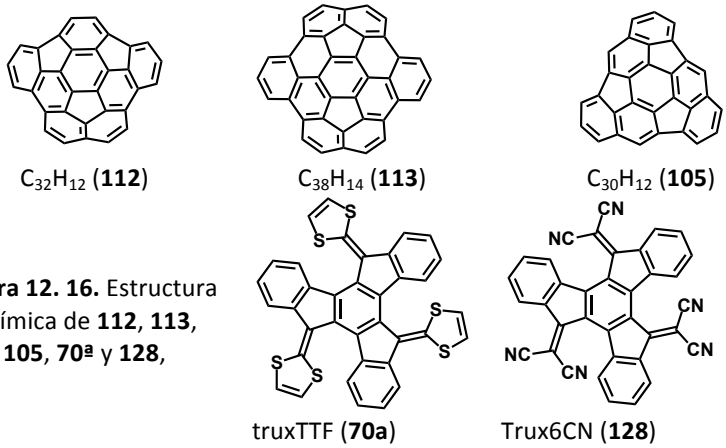

$C_{32}H_{12}$ (**112**) $C_{38}H_{14}$ (**113**) $C_{30}H_{12}$ (**105**)

truxTTF (**70a**) Trux6CN (**128**)

Figura 12. 16. Estructura química de **112**, **113**, **105**, **70ª** y **128**,

La formación de todos los complejos heteromoleculares (derivado de truxeno)•(sistema aromático policíclico curvado) fue estudidada en disolución mediante valoraciones ultravioleta-visible. Los datos obtenidos de estas valoraciones fueron tratados nuevamente con el software ReactLab Equilibria^{TM}, que nos proporciona las constantes de asociación que se muestran en la tabla 12.1. Para estos nuevos heterodímeros, el grupo del Prof. Enrique Ortí realizó los estudios computacionales pertinentes análogos a los realizados para el estudio del dímero truxTTF•$C_{30}H_{12}$. De manera esquemática en las Figuras 12.17 y 12.18 se muestran las posibles disposiciones espaciales relativas que pueden adoptar los derivados de truxeno y fragmentos de fullereno en los nuevos complejos heteromoleculares, y en la tabla 12.1, se muestra la configuración que resulta más estable para cada caso particular.

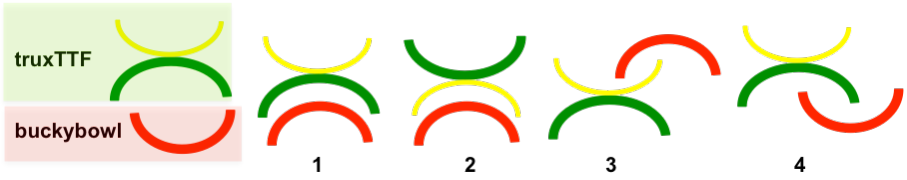

Figura 12.17. Posibles disposiciones espaciales relativas adoptadas por los 253emperatur de los heterodímeros de tipo truxTTF•(sistema aromático policíclico curvado).

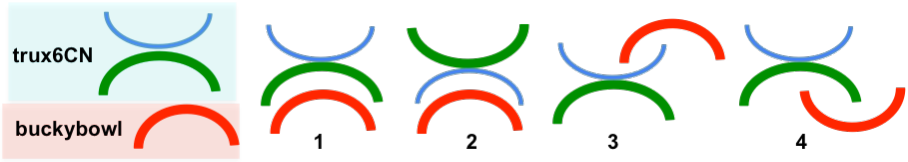

Figure 12.18. Posibles disposiciones espaciales relativas adoptadas por los 253emperatur de los heterodímeros de tipo trux6CN•(sistema aromático policíclico curvado).

Tabla 12.1. Confórmeros más estables calculados para :			
truxTTF•$C_{32}H_{12}$	truxTTF•$C_{38}H_{14}$	trux6CN• $C_{30}H_{12}$	trux6CN• $C_{32}H_{12}$
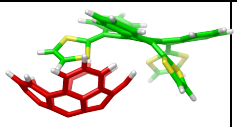	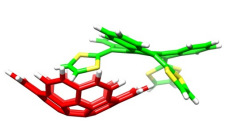	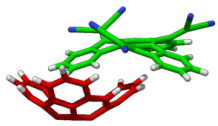	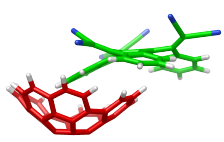
log K_a = 3.19±0.02	log K_a = 3.4±0.1	log K_a = 2.9±0.2	log K_a = 3.2±0.2

Como se esquematiza en la Figura 12.17, las interacciones de tipo π–π quedan maximizadas en las disposiciones **1** y **2**. En las disposiciones "cóncavo-cóncavo"

3 y **4**, encontramos mezclas de interacciones π–π ,CH-π y S-π o π–π y CH-π respectivamente. Estas posibles disposiciones para truxTTF•$C_{32}H_{12}$ y truxTTF•$C_{38}H_{14}$ son análogas a que se propusieron en su momento para el truxTTF•$C_{30}H_{12}$. En la Figura 12.18 se muestran las posibles disposiciones para los heterodímeros trux6CN•$C_{32}H_{12}$ y trux6CN•$C_{30}H_{12}$. En este caso cabe destacar que las disposición **3** no está muy favorecida ya que los pares de electrones solitarios del nitrógeno no se encuentran orientados de una manera adecuada para la interacción con el esqueleto aromático del fragmento de fullereno. La interacción N-π es en este caso, menos eficiente en comparación con la S-π existente en los dímeros que contienen truxTTF. En otras palabras, los grupos dicianometilenos proporcionan menos estabilización covalente que los anillos de ditiol. La conformación **4** es aparentemente la más favorable para los dímeros trux6CN•$C_{32}H_{12}$ y trux6CN•$C_{30}H_{12}$.

Como ocurría en los dímeros truxTTF•C_{60} y truxTTF•$C_{30}H_{12}$, el truxTTF se comporta como sistema electro-dador a través de sus anillos de ditiol. El HOMO queda localizado en el truxTTF y el LUMO en el $C_{32}H_{12}$ o $C_{38}H_{14}$ para los dímeros truxTTF•$C_{32}H_{12}$ y truxTTF•$C_{38}H_{14}$ respectivamente. Sin embargo, para los complejos trux6CN•$C_{30}H_{12}$ y trux6CN•$C_{32}H_{12}$ el HOMO se localiza en el fragmento de fullereno y el LUMO está localizado en el derivado de truxeno electro-aceptor (Figura 12.19).

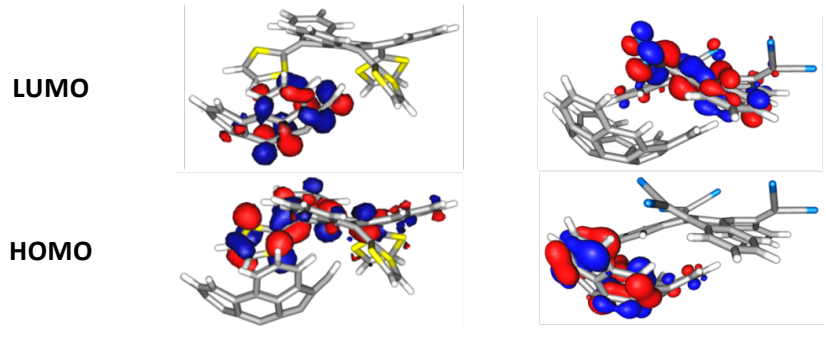

Figura 12.19. Orbitales frontera calculados 254emperat conformaciones más estables de truxTTF•$C_{30}H_{12}$ y trux6CN•$C_{30}H_{12}$.

El grupo del Prof. Dirk M. Guldi está realizando los estudios fotofísicos de estos nuevos sistemas. Como datos preliminares, podemos citar la posible

existencia de procesos de transferencia electrónica para el heterodímero truxTTF•$C_{38}H_{14}$ (Figura 12.20 (b)).

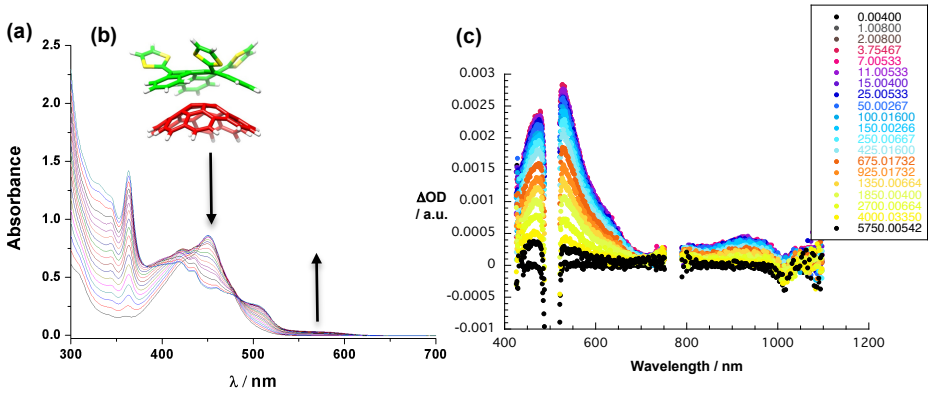

Figura 12.20. (a) Espectros de absorción obtenidos durante la valoración UV/vis del truxTTF (1.5 x 10^{-4} M) con $C_{38}H_{14}$ (7.7 x 10^{-4} M) en PhCl a 255emperature ambiente. (b) heterodímero de truxTTF•$C_{38}H_{14}$. (c) Espectros de absorción diferencial obtenidos al irradiar con laser pulsado de femtosegundo (480 nm) una muestra de truxTTF•$C_{38}H_{14}$ (1:1) en benzonitrilo a temperature ambiente.

12.4. CONCLUSIONES

Los resultados obtenidos en cada uno de los capítulos expuestos anteriormente pueden resumirse de la siguiente manera:

Capítulo I.

Las moléculas **70ª** y **81** han sido validadas como bloques de construcción molecular adecuados para la síntesis de estructuras derivadas de truxTTF de interés.

Se logró la unión covalente de tres unidades de [60]fullereno al truxTTF para formar la tétrada DA_3 (**84**).

Se han sintetizado cinco colorantes basados en la estructura de truxTTF con múltiples puntos de anclaje de tipo ácido carboxílico o piridina que podrían actuar como sensibilizadores en dispositivos fotovoltaicos de tipo Graetzel.

Las moléculas **70ª** y **73** se validaron como semiconductores tipo n- en dispositivos fotovoltaicos de tipo BHSCs.

Capítulo II.

La formación del complejo heteromolecular truxTTF•$C_{30}H_{12}$ fue confirmada tanto experimentalmente como mediante cálculos teóricos.

La fotoexcitación del complejo truxTTF•$C_{30}H_{12}$ conduce a un estado con separación de cargas, constituyendo el primer caso en el que un fragmento de fullereno imita el comportamiento aceptor de la molécula de C_{60} en un complejo supramolecular.

El estudio de cuatro nuevos heterodímeros supramoleculares derivados de truxeno (truxTTF•$C_{32}H_{12}$, truxTTF•$C_{38}H_{14}$, trux6CN•$C_{30}H_{12}$, trux6CN•$C_{32}H_{12}$), tanto a nivel teórico como experimental indica la formación de los complejos deseados, con constantes de asociación en el rango de log K_a = 2.9 – 3.4.

Los estudios fotofísicos preliminares indican que la transferencia electrónica fotoinducida también tiene lugar en el nuevo heterodímero truxTTF•$C_{38}H_{14}$.

13. Bibliography

[1] (a) W. H. Brock, "The Norton History of Chemistry", p. 257 "The Triumph of Structural Theory", **1992**; (b) K. Hafner, "August Kekulé—The Architect of Chemistry Commemorating the 150th Anniversary of His Birth", *Angew. Chem. Int. Ed. Engl.* **1979**, *18,* 641; (c) D. H. Wilcox Jr, F. R. Greenbaum, "Kekule's benzene ring theory: A subject for lighthearted banter", *J. Chem. Ed.,* **1965**, *42*, 266; (d) A. Kekulé, "Sur la constitution des substances aromatiques", *Bull. Soc. Chim. Paris,* **1865**, 98.

[2] A. T. Balaban, P.v. R. Schleyer, H. S. Rzepa, "Crocker, Not Armit and Robinson, Begat the Six Aromatic Electrons", *Chem. Rev*. **2005**, *105*, 3436.

[3] A. J. Rocke, "It Began with a Daydream: The 150th Anniversary of the Kekulé Benzene Structure", *Angew. Chem. Int. Ed*. **2015**, *54*, 1.

[4] (a) J. Hausmann, "Einwirkung von *o*-Cyanbenzylchlorid auf Natriummalonester. Untersuchung des α-Hydrindons", *Ber. Dtsch. Chem. Ges*. **1889**, *22*, 2019; (b) F. S. Kipping, "The formation of the hydrocarbon "truxene" from phenylpropionic acid, and from hydrindone", *J. Chem. Soc*. **1894**, 269.

[5] (a) E. Dietzel, U.S. Patent 2,216,001, 1940; Chem. Abstr. 1941, 35, 4584; (b) K. F. Lang, M. Zander, E. A. Teiling, "Isotruxen", *Chem. Ber*. **1960**, *93*, 321; (c) G. Merz, *Synthesis* **1972**, 614.

[6] Y. N. Oded, I. Agranat, "A simple synthesis of truxene, a building block for optoelectronics and fullerene fragments", *Tetrahedron Lett.* **2014**, *55*, 636.

[7] (a) B. Gómez-Lor, O. de Frutos, A. M. Echavarren, "Synthesis of 'crushed fullerene' $C_{60}H_{30}$", *Chem. Commun*. **1999**, 2431; (b) L. T. Scott, M. M. Boorum, B. J. McMahon, S. Hagen, J. Mack, J. Blank, H. Wegner, A. de Meijere, "A rational chemical synthesis of C_{60}", *Science* **2002**, *295*, 1500; (c) K. Y. Amsharov, M. Jansen, "A C_{78} Fullerene Precursor: Toward the Direct Synthesis of Higher Fullerenes", *J. Org. Chem*. **2008**, *73*, 2931; (d) K. Amsharov, M. Jansen, "Synthesis of a higher fullerene precursor-an "unrolled" C_{84}fullerene", *Chem. Commun.* **2009**, 2691; (e) G. Otero, G. Biddau, C. Sánchez-Sánchez, R, Caillard, M. F. López, C. Rogero, F. J. Palomares, N. Cabello, M. A. Basanta, J. Ortega, J. Méndez, A. M. Echavarren, R. Pérez, B. Gómez-Lor, J. A, Martín-Gago, "Fullerenes from aromatic precursors by surface-catalysed cyclodehydrogenation"*Nature* **2008**, *445*, 865; (f) K. Amsharov, N. Abdurakhmanova, S. Stepanow, S. Rauschenbach, M. Jansen, K. Kern, "Towards the Isomer-Specific Synthesis of Higher Fullerenes and Buckybowls by the Surface-Catalyzed Cyclodehydrogenation of Aromatic Precursors", *Angew. Chem. Int. Ed*. **2010**, *49*, 9392.

[8] N. Earmrattana, M. Sukwattanasinitt, P. Rashatasakhon, "Water-soluble anionic fluorophores from truxene", *Dyes and Pigments* **2012**, *93*, 1428.

[9] J. Luo, Y. Zhou, Z.Q. Niu, Q.F. Zhou, Y. Ma, J. Pei, "Three-Dimensional Architectures for Highly Stable Pure Blue Emission", *J. Am. Chem. Soc*. **2007**, *129*, 11314.
[10] H. Tsuji,Y. Ota, S. Furukawa, C. Mitsui, Y. Sato, E. Nakamura, "Tripyridyltruxenes: Thermally Stable Cathode Buffer Materials for Organic Thin-Film Solar Cells", *Asian J. Org. Chem*. **2012**, *1*, 34.
[11] Y. Sun, K. Xiao, Y. Liu, J. Wang, J. Pei, G. Yu, D. Zhu, "Oligothiophene-Functionalized Truxene: Star-Shaped Compounds for Organic Field-Effect Transistors", *Adv. Funct. Mater*. **2005**, *15*, 818.
[12] (a) K.Q. Zhao, C. Chen, H. Monobe, P. Hu, B.Q. Wang, Y. Shimizu, *"*Three-chain truxene discotic liquid crystal showing high charged carrier mobility*", Chem. Commun.* **2011**, *47*, 6290; (b) K. Isoda, T. Yasuda, T. Kato, "Truxene-Based Columnar Liquid Crystals: Self-Assembled Structures and Electro-Active Properties", *Chem. Asian J*. **2009**, *4*, 1619.
[13] C.B. Nielsen, E. Voroshazi, S. Holliday, K. Cnops, B. P. Rand, I. McCulloch, "Efficient truxenone-based acceptors for organic photovoltaics", *J. Mater. Chem*. A, **2013**, *1*, 73.
[14] E. V. Dehmlow, T. Kelle, "Synthesis of New Truxene Derivatives: Possible Precursors of Fullerene Partial Structures?", *Synth. Commun.* **1997**, *27*, 2021.
[15] S. Diring, R. Ziessel, "Facile pathways to multichromophoric arrays based on a truxene platform", *Tetrahedron lett.* **2009**, *50*, 1203.
[16] L. Sánchez, N. Martín, E. González-Cantalapiedra, A. M. Echavarren, G. M. A. Rahman, D. M. Guldi, "Molecular Panels for Energy Transduction in C_{60}-Based Conjugates", *Org. Let.* **2006**, *8*, 2451.
[17] E. González-Cantalapiedra, M. Ruiz. B. Gómez-Lor, B. Alonso, D. García-Cuadrado, D. J. Cárdenas, A. M. Echavarren, "New Building Blocks Based on Truxene Cores: Synthesis of Functionalized *syn*-Tri- and -Hexasubstituted Derivatives", *Eur. J. Org. Chem*. **2005**, 4127.
[18] X. Y. Cao, W. B. Zhang, J. L. Wang, X. H. Zhou, H. Lu, J. Pei, "Extended π-Conjugated Dendrimers Based on Truxene", *J. Am. Chem. Soc*. **2003**, *125*, 12430.
[19] B. Gómez-Lor, O. de Frutos, P. A. Ceballos, T. Granier, A. M. Echavarren, "Synthesis of New C_{3h} and C_{3v} Truxene Derivatives", *Eur. J. Org. Chem.* **2001**, 2107.
[20] Y. Xie, X. Zhang, Y. Xiao, Y. Zhang, F. Zhou, J. Qi, J. Qu, "Fusing three perylenebisimide branches and a truxene core into a star-shaped chromophore with strong two-photon excited fluorescence and high photostability", *Chem. Commun*. **2012**, *48*, 4338.
[21] (a) J. Bergman, B. Egestad, "Cyclocondensation of 3(2*H*)-benzofuranone", *Tetrahedron lett.* **1978**, 3143; (b) J. Bergman, B. Egestad, *Tetrahedron* **1986**,

42, 763; (c) M. Franceschin, L. Ginnari-satriani, A. Alvino, G. Ortaggi, A. Bianco, "Study of a Convenient Method for the Preparation of Hydrosoluble Fluorescent Triazatruxene Derivatives", *Eur. J. Org. Chem*. **2010**, 134.
[22] H. K. Bisoyi, S. Kumar, "Discotic nematic liquid crystals: science and technology", *Chem. Soc. Rev.* **2010**, *39*, 264.
[23] B. Gómez-Lor, A. Echavarren, "Synthesis of a Triaza Analogue of Crushed-Fullerene by Intramolecular Palladium-Catalyzed Arylation", *Org. Lett.* **2004**, *6*, 2993.
[24] W. Y Lai, Q. Y He, R. Zhu, Q. Q Chen, W. Huang, "Kinked Star-Shaped Fluorene/ Triazatruxene Co-oligomer Hybrids with Enhanced Functional Properties for High-Performance, Solution-Processed, Blue Organic Light-Emitting Diodes", *Adv. Funct. Mater.* **2008**, *18*, 265.
[25] X. Quian, Y. Z. Zhu, J. Song, X. P. Gao, J. Y. Zheng, "New Donor-π-Acceptor Type Triazatruxene Derivatives for Highly Efficient Dye-Sensitized Solar Cells", *Org. Lett*. **2013**, *15*, 6034.
[26] L. Sanguinet, J. C. Williams, Z. Yang, R. J. Twieg, G. Mao, K. D. Singer, G. Wiggers, R. G. Petscheck, "Synthesis and Characterization of New Truxenones for Nonlinear Optical Applications", *Chem. Mater.* **2006**, *18*, 4259.
[27] J. Y. Wang, J. Yan, l. Ding, Y. Ma, J. Pei, "One-Dimensional Microwires Formed by the Co-Assembly of Complementary Aromatic Donors and Acceptors", *Adv. Funct. Mater.* **2009**, *19*, 1746.
[28] (a) A. Mishra, M. K. R. Fischer, P. Bäulerle, "Metal-free Organic Dyes for Dye-Sensitized Solar Cells: From Structure Property Relationships to Design Rules", *Angew. Chem. Int. Ed.* **2009**, *48*, 2472; (b) S. Zhang, X. Yang, Y. Numata, L. Han, "Highly efficient dye-sensitized solar cells: progress and future challenges", *Energy Environ. Sci.* **2013**, *6*, 1443.
[29] http://www.nrel.gov
[30] M. K. Nazeeruddin, P. Péchy, T. Renouard, S. M. Zakeeruddin, R. Humphry-Baker, P. Compte, P. Liska, L. Cevey, E. Costa, V. Shklover, L. Spiccia, G. B. Deacon, C. A, Bignozzi, M. Grätzel, "Engineering of Efficient Panchromatic Sensitizers for Nanocrystalline TiO_2-Based Solar Cells", *J. Am. Chem. Soc.* **2011**, *123*, 1613. (b) S. Mathew, A. Yella, R. Humphry-Baker, B. Curchod, N. Ashari-Astani, I. Tavernelli, U. Rothlisberger, M. K. Nazeeruddin, M. Grätzel, *Nature Chem.* **2014**, *6*, 262.
[31] L. Yu, J. Xi, H. T. Chan, T. Su, L. J. Antrobus, B. Tong, Y. Dong, W. K. Chan, D. L. Philips, "Novel Organic D-π-2A Sensitizer for Dye Sensitized Solar Cells and Its Electron Transfer Kinetics on TiO_2 Surface", *J. Phys. Chem. C,* **2013**, *117*, 2041.

[32] Z. Wang. M. Liang, H. Wang, P. Wang, F. Cheng, Z. Sun, X. Song, "Joint Electrical, Photophysical, and Photovoltaic Studies on Truxene Dye-Sensitized Solar Cells: Impact of Arylamine Electron Donors", *ChemSusChem* **2014**, *7*, 795.
[33] (a) A. Mishra, P. Bäuerle, *Angew. "*Small Molecule Organic Semiconductors on the Move: Promises for Future Solar Energy Technology*", Chem. Int. Ed.* **2012**, *51*, 2020; (b) J. L. Delgado, P.A. Bouit, S. Filippone, M. A. Herranz, N. Martín, "Organic photovoltaics: a che3mical approach", *Chem. Commun.* **2010**, *46*, 4853.
[34] C. B. Nielsen, E. Voroshazi, S. Holliday, K. Cnops, D. Chenys, I. McCulloch, "Electron-deficient truxenone derivatives and their use in organic photovoltaics", *J. Mater. Chem. A* **2014**, *2*, 12348.
[35] T. Bura, N. Leclerc, R. Bechara, P. Lévêque, T. Heiser and R. Ziessel, "Triazatruxene-Diketopyrrolopyrrole Dumbbell-Shaped Molecules as Photoactive Electron Donor for High-Efficiency Solution Processed Organic Solar Cells", *Adv. Energy Mater.* **2013**, *3*, 1118.
[36] http://www.orgworld.de/
[37] (a) F. G. Brunetti, J. L. López, C. Atienza, N. Martín, "π-Extended TTF: a versatile molecule for organic electronics", *J. Mater. Chem.* **2012**, *22*, 4188. (b) N. Martín, L. Sánchez, M. A. Herranz, B. Illescas, D. M. Guldi, "Electronic Communication in Tetrathiafulvalene (TTF)/C_{60} Systems: Toward Molecular Solar Energy Conversion Materials?", *Acc. Chem. Res.* **2007**, *40*(*10)*, 1015; (c) Y. Yamashita, Y. Kobayashi, T. Miyasi, "*p*-Quinodimethane Analogues of Tetrathiafulvalene", *Angew. Chem. Int. Ed.* **1989**, *28*, 1052.
[38] E.M. Pérez, M. Sierra, L. Sánchez, M. R. Torres, R. Viruela, P. M. Viruela, E. Ortí, N. Martín, "Concave Tetrathiafulvalene-Type Donors as Supramolecular Partners for Fullerenes", *Angew. Chem. Int. Ed.* **2007**, *46*, 1847.
[39] K. Isoda, T. Yasuda, T. Kato, "Truxene-Based Columnar Liquid Crystals: Self-Assembled Structures and Electro-Active Properties", *Chem*. *Asian*. *J.* **2009**, *4*, 1619.
[40] H. Isla, B. Grimm, E. M. Pérez, M. R. Torres, M. A. Herranz, R. Viruela, J. Aragó, E. Ortí, D. M. Guldi, N. Martín, "Bowl-shape electron donors with absorptions in the visible range of the solar spectrum and their supramolecular assemblies with C_{60}", *Chem. Sci.* **2012**, *3*, 498.
[41] (a) N. Martín, L. Sánchez, M. A. Herranz and D. M. Guldi, "Evidence for Two Separate One-Electron Transfer Events in Excited Fulleropyrrolidine Dyads Containing Tetrathiafulvalene (TTF)", *J. Phys. Chem. A* **2000,** *104*, 4648.;(b) Y. Takano, M. A. Herranz, N. Martín, S. Gayathri-Radhakrishnan, D. M. Guldi, T. Tsuchiya, S. Nagase, T. Akasaka, "A Molecular Ce2@ IhC80 Switch-Unprecedented Oxidative Pathway in Photoinduced Charge Transfer Reactivity", *J. Am. Chem. Soc.* **2010**, *132,* 8048; (c) F. Giacalone, J. L. Segura, N.

Martín, J. Ramey, D. M. Guldi,"Probing Molecular Wires: Synthesis, Structural, and Electronic Study of Donor–Acceptor Assemblies Exhibiting Long-Range Electron Transfer", *Chem. Eur. J.* **2005**, *11*, 4819; (d) D. M. Guldi, F. Giacalone, G. de la Torre, J. L. Segura, N. Martín, "Topological Effects of a Rigid Chiral Spacer on the Electronic Interactions in Donor–Acceptor Ensembles", *Chem. Eur. J.* **2005**, *11*, 7199; (e) S. Handa, F. Giacalone, S. A. Haque, E. Palomares, N. Martín. J. R. Durran, "Solid Film versus Solution-Phase Charge-Recombination Dynamics of exTTF–Bridge–C_{60} Dyads", *Chem. Eur. J.* **2005**, *11*, 7440; (f) L. Sánchez, M. Sierra, N. Martín, D. M. Guldi, M. W. Wienk, R. J. A. Janssen, "C_{60}–exTTF–C_{60} Dumbbells: Cooperative Effects Stemming from Two C_{60}s on the Radical Ion Pair Stabilization", *Org. Lett.* **2005**, *7*, 1691; (g) C. Atienza, N. Martín, D. M. Guldi, "Tuning electron transfer through *p*-phenyleneethynylene molecular wires", *Chem. Commun.* **2006**, 3202; (h) B. M. Illestcas, J. Santos, M. Wielopolski, C. M. Atienza, N. Martín, D. M. Guldi, "Electron transfer through exTTF bridges in electron donor–acceptor conjugates", *Chem. Commun.* **2009**, *74*, 5374; (i) D. M. Guldi, B. M. Illescas, C. M. Atienza, M. Wielopolski, N. Martín, "Fullerene for organic electronics", *Chem . Soc. Rev.* **2009**, *38*, 1587.

[42] (a) H. L. Anderson, R. Faust, Y. Rubin, F. Diederich, "Fullerene–Acetylene Hybrids: On the Way to Synthetic Molecular Carbon Allotropes", *Angew. Chem. Int. Engl.* **1994**, *33*, 1366; (b) K. Komatsu, Y. Murata, N. Takimoto, S. Mori, N. Sugita, T. S. Wan, "Synthesis and Properties of the First Acetylene Derivatives of C_{60}", *J. Org. Chem.* **1994**, *59*, 6101; (c) G. V. Vives, J. M. Tour, "Synthesis of Single-Molecule Nanocars", *Acc. Chem. Res.* **2009**, *42*, 473.

[43] J.-L. Wang, X.-F. Duan, B. Jiang, L.-B. Gan, J. Pei, "Nanosized Rigid π-Conjugated Molecular Heterojunctions with Multi[60]fullerenes: Facile Synthesis and Photophysical Properties", *J. Org. Chem.* **2006**, *71*, 4400.

[44] Z. Ning, Y. Fu, H. Tian, "Improvement of dye-sensitized solar cells: what we know and what we need to know", *Energy Environ. Sci.* **2010**, *3*, 1170.

[45] A. Amacher, C. Yi, J. Yang, M. P. Bircher, Y. Fu, M. Cascella, M. Grätzel, S. Decurtis, S.-X. Liu, "A quinoxaline-fused tetrathiafulvalene-based sensitizer for efficient dye-sensitized solar cells", *Chem. Commun.* **2014**, *50*, 6540.

[46] (a) S. Wenger, P.-A. Bouit, Q. Chen, J. Teuscher, D. Di Censo, R. Humphry-Baker, J.-E Moser, J. L. Delgado, N. Martín, S. M. Zakeeruddin, M. Gräetzel, "Efficient Electron Transfer and Sensitizer Regeneration in Stable π-Extended Tetrathiafulvalene-Sensitized Solar Cells", *J. Am. Chem. Soc.* **2010**, *132*, 5164; (b) C. A. Echeverry, M. A. Herranz, A. Ortiz, B. Insuasty, N. Martín, "Rhodanine-3-acetic acid and π-extended tetrathiafulvalene (exTTF) based systems for dye-sensitized solar cells", *New J. Chem.* **2014**, *38*, 5801.

[47] (a) S. P. Singh, M. S. Roy, K. R. J. Thomas, S. Balaiah, K. Bhanuprakash, G. D. Sharma, "New Triphenylamine-Based Organic Dyes with Different Numbers

of Anchoring Groups for Dye-Sensitized Solar Cells", *J. Phys. Chem. C* **2012**, *116*, 5941; (b) D. Cao, J. *Peng*, Y. Hong, X. Fang, L. Wang, H. Meier, "Enhanced Performance of the Dye-Sensitized Solar Cells with Phenothiazine-Based Dyes Containing Double D−A Branches", *Org. Lett.* **2011**, *13*, 1610; (c) Y.-S. Yen, W.-T Chen, C.-Y. Hsu, H.-H Chou, J. T. Lin, M.-C. P. Yeh, "Arylamine-Based Dyes for p-Type Dye-Sensitized Solar Cells", *Org. Lett.* **2011**, *13*, 4930.

[48] (a) Y. Ooyama, S. Inove, T. Nagano, K. Kushimoto, J. Ohshita, I. Imae, K. Komaguchi, Y. Harima, "Dye-Sensitized Solar Cells Based On Donor–Acceptor π-Conjugated Fluorescent Dyes with a Pyridine Ring as an Electron-Withdrawing Anchoring Group", *Angew*. *Chem*. **2011**, *123*, 7567. (b) Y. Ooyama, T. Nagano, S. Inoue, I. Imae, K. Komaguchi, J. Ohshita, Y. Harima, "Dye-Sensitized Solar Cells Based on Donor-π-Acceptor Fluorescent Dyes with a Pyridine Ring as an Electron-Withdrawing-Injecting Anchoring Group", *Chem. Eur. J*. **2011**, *17*, 14837.

[49] H. C. Kolb, M. G. Finn, K. B. Sharpless, "Click Chemistry: Diverse Chemical Function from a Few Good Reactions", *Angew. Chem. Int. Ed.* **2001**, *40*, 2004.

[50] (a) Y. Mitamura, H. Shima, A. Osuka, "Straightforward access to aryl-substituted tetrathiafulvalenes bypalladium-catalysed direct C–H arylation and their photophysical and electrochemical properties", *Chem. Sci*. **2011**, *2*, 2017; (b) S. Bivaud, S. Goeb, V. Croeué, P. I. Dron. M. Allain, M. Sallé, "Self-Assembled Containers Based on Extended Tetrathiafulvalene", *J. Am. Chem. Soc.* **2013**, *135*, 10018.

[51] (a) B. C. Thompson, J. M. Frechet, "Polymer–Fullerene Composite Solar Cells", *Angew. Chem. Int. Ed.* **2008**, *47*, 58; (b) A. J. Moulé, K. Meerholz, "Morphology Control in Solution-Processed Bulk-Heterojunction Solar Cell Mixtures", *Adv. Funct. Mater.* **2009**, *19*, 3028; (c) G. Dennler, M. C. Scharber, C. J. Brabec. "Polymer-Fullerene Bulk-Heterojunction Solar Cells", *Adv. Mater.* **2009**, *21*, 1323; (d) F. Yang, M. Shttein, S. R. Forrest, "Controlled growth of a molecular bulk heterojunction photovoltaic cell", *Nat*. *Mater.* **2004**, *4*, 37; (e) J. Peet, M. L. Senatore, A. J. Heeger, G. C. Bazan, "The Role of Processing in the Fabrication and Optimization of Plastic Solar Cells", *Adv. Mater.* **2009**, *21*, 1521; (f) X. Yang, J. Loos, "Toward High-Performance Polymer Solar Cells: The Importance of Morphology Control", *Macromolecules*, **2007**, *40*, 1353; (g) Y. Huang, E. J. Kramer, A. J. Heeger, G. C. Bazan, "Bulk Heterojunction Solar Cells: Morphology and Performance Relationships", *Chem. Rev.* **2014**, *114*, 7006.

[52] (a) J. Peet, J. Y. Kim, N. E. Coates, W. L. Ma, D. Moses, A. J. Heeger, G. C. Bazan, "Efficiency enhancement in low-bandgap polymer solar cells by processing with alkane dithiols", *Nat. Mater.* **2007**, *6*, 497; (b) S. J. Lou, J. M. Szarko, T. Xu, T. J. Marks, L. X. Chen, "Effects of Additives on the Morphology of Solution Phase Aggregates Formed by Active Layer Components of High-

Efficiency Organic Solar Cells", *J. Am. Soc.* **2011**, *133*, 20661; (c) J. K. Lee, W. L. Ma, C. J. Brabec, J. Yuen, J. S. Moon, J. Y. Kim, K. Kee, G. C. Bazan, A. J. Heeger, "Processing Additives for Improved Efficiency from Bulk Heterojunction Solar Cells", *J. Am. Chem. Soc*. **2008**, *130*, 3619.

[53] (a) G. Li, V. Shrotriya, J. Huang, Y. Yao, T. Moriarty, K. Emery, Y. Yang, "High-efficiency solution processable polymer photovoltaic cells by self-organization of polymer blends", *Nat. Mater.* **2005**, *4*, 864; (b) G. Li, Y. Yao, H. Yang, V. Shrotriya, G. Yang, Y. Yang, ""Solvent Annealing" Effect in Polymer Solar Cells Based on Poly(3-hexylthiophene) and Methanofullerenes", *Adv. Funct. Mater.* **2007**, *17*, 1636; (c) W. Ma, C. Yang, X. Gong, K. Lee, A. J. Heeger, "Thermally Stable, Efficient Polymer Solar Cells with Nanoscale Control of the Interpenetrating Network Morphology", *Adv. Funct. Mater.* **2005**, *15*, 1617; (d) M. Campoy-Quiles, T. Ferenczi, T. Agostinelli, P. G. Etchegoin, Y. Kim, T. D. Anthopoulos, P. N. Stavrinou, D. D. C. Bradley, J. Nelson, "Morphology evolution via self-organization and lateral and vertical diffusion in polymer: fullerene solar cell blends", *Nat. Mater.* **2008**, *7*, 158; (e) S. Miller, G. Franchini, Y. Y. Lin, C. Li, C. W. Chen, W. F. Su, M. Chowalla, "Investigation of nanoscale morphological changes in organic photovoltaics during solvent vapor annealing", J. Mater. Chem. **2008**, *18*, 306; (f) G. Wei, S. Wang, K. Sun, M. E. Thompson, S. R. Forrest, "Solvent-Annealed Crystalline Squaraine: $PC_{71}BM$ (1:6) Solar Cells", *Adv. Energy Mater.* **2011**, *1*, 184; (g) G. Wei, R. R. Lunt, K. Sun, S. Wang, M. E. Thompson, S. R. Forrest, "Efficient, Ordered Bulk Heterojunction Nanocrystalline Solar Cells by Annealing of Ultrathin Squaraine Thin Films", *Nano Lett.* **2010**, *10*, 3555; (h) T. A. Bull, L. S. C. Pingree, S. A. Jenekhe, D. S. Ginger, C. K. Luscombe, "The Role of Mesoscopic PCBM Crystallites in Solvent Vapor Annealed Copolymer Solar Cells", *ACS Nano*, **2009**, *3*, 627.

[54] (a) R. D. Kennedy, A. L. Ayzner, D. D. Wanger, C. T. Day, M. Halim, S. I. Khan, S. H. Tolbert, B. J. Schwartz, Y. Rubin, "Self-assembling fullerenes for improved bulk-heterojunction photovoltaic devices", *J. Am. Chem. Soc.* **2008**, *130*, 17290; (b) C. J. Tassone, A. L. Ayzner, R. D. Kennedy, M. Halim, M. So, Y. Rubin, S. H. Tolbert, B. J. Schwartz, "Using Pentaarylfullerenes to Understand Network Formation in Conjugated Polymer-Based Bulk-Heterojunction Solar Cells", *J. Phys. Chem. C.* **2011**, *115*, 22563.

[55] (a) N. C. Cates, R. Gysel, Z. Beiley, C. E. Miller, M. F. Tonet, M. Heeney, I. McCulloch, M. D. McGehee, "Tuning the Properties of Polymer Bulk Heterojunction Solar Cells by Adjusting Fullerene Size to Control Intercalation", *Nano Lett.* **2009**, *9*, 4153; (b) C. Bruner, N. C. Miller, M. D. McGehee, R. H. Dauskardt, "Molecular Intercalation and Cohesion of Organic Bulk Heterojunction Photovoltaic Devices", *Adv. Funct. Mater.* **2013**, *23*, 2863; (c) N.

C. Miller, S. Sweetnam, E. T. Hoke, R. Gysel, C. E. Miller, J. A. Barlet, X. Xie, M. F. Toney, M. D. McGehee, "Molecular Packing and Solar Cell Performance in Blends of Polymers with a Bisadduct Fullerene", *Nano Lett.* **2012**, *12*, 1566.
[56] (a) K. H. Lam, T. R. B. Foong, Z. E. Ooi, J. Zhang, A. C. Grimsdale, Y. M. Lam, "Enhancing the performance of solution-processed bulk-heterojunction solar cells using hydrogen-bonding-induced self-organization of small molecules", *ACS Appl. Mater. Interfaces,* **2013**, *5*, 13265; (b) B. M. Schulze, N. T. Shewmon, J. Zhang, D. L. Watkins, J. P. Mudrick, W. Cao, R. B. Zerdan, A. J. Quartararo, I. Ghiviringa, J. Xue, R. K. Castellano, "Consequences of hydrogen bonding on molecular organization and charge transport in molecular organic photovoltaic materials", *J. Mater. Chem. A*. **2014**, *2*, 1541; (c) A. Ruiz-Carretero, T. Aytun, C. J. Bruns, C. J. Newcomb, W. W. Tsai, S. I. Stupp, "Stepwise self-assembly to improve solar cell morphology", *J. Mater. Chem. A.* **2013**, *1*, 11674; (d) C. H. Huang, N. D. McClenaghan, A. Kuhn, J. W. Hofstraat, D. M. Bassani, "Enhanced Photovoltaic Response in Hydrogen-Bonded All-Organic Devices", *Org. Lett*. **2005**, *7*, 3409.
[57] (a) S. J Kang, J. B. Kim, C. Y. Chiu, S. Ahn, T. Schiros, S. S. Lee, K. G. Yager, M. F. Toney, Y. L. Loo, C. Nuckolls, "A supramolecular complex in small-molecule solar cells based on contorted aromatic molecules", *Angew. Chem. Int. Ed.* **2012**, *51*, 8594; (b) S. J. Kang, S. Ahn, J. B. Kim, C. Schenck, A. M. Hiszpanski, S. Oh, T. Schiros, Y. L. Loo, C. Nuckolls, "Using Self-Organization To Control Morphology in Molecular Photovoltaics", *J. Am. Chem. Soc.* **2013**, *135*, 2207.
[58] (a) E. M. Pérez, N. Martín, "Curves ahead: molecular receptors for fullerenes based on concave–convex complementarity", *Chem. Soc. Rev.* **2008**, *37*, 1512; (b) M. Gallego, J. Calbo, J. Aragó, R. M. K. Calderón, F. H. Líquido, A. Iwamoto, A. K. Greene, E. A. Jackson, E. M. Pérez, E. Ortí, D. M. Guldi, L. T. Scott, N. Martín, "Electron Transfer in a Supramolecular Associate of a Fullerene Fragment", *Angew. Chem. Int. Ed.* **2014**, *53*, 2170.
[59] (a) V. D. Mihailetchi, H. X. Xie, B. de Boer, L. J. A. Koster, P. W. M. Blom, "Charge Transport and Photocurrent Generation in Poly(3-hexylthiophene): Methanofullerene Bulk-Heterojunction Solar Cells", *Adv. Funct. Mater.* **2006**, *16*, 699; (b) B. Qui, J. Wang, "Fill factor in organic solar cells", *Phys. Chem. Chem. Phys.* **2013**, *15*, 8972; (c) D. Gupta, S. Mukhopadhyay, K. S. Narayan, "Fill factor in organic solar cells", *Sol. Energy. Mater. Sol. Cells,* **2010**, *94*, 1309; (d) G. Li, R. Zhu, Y. Yang, "Polymer solar cells", *Nature Photonics*, **2012**, *6*, 153.
[60] (a) C. R. McNeill, S. Westenhoff, C. Groves, R. h. Friend, N. C. Greenham, "Influence of Nanoscale Phase Separation on the Charge Generation Dynamics and Photovoltaic Performance of Conjugated Polymer Blends: Balancing

Charge Generation and Separation", *J. Phys. Chem. C.* **2007**, *111*, 19153; (b) Y. Yao, J. Hou, Z. Xu, G. Li, Y. Yang, "Effects of Solvent Mixtures on the Nanoscale Phase Separation in Polymer Solar Cells", *Adv. Funct. Mater.* **2008**, *18*, 1783.
[61] D. D. Perrin, I. F. Amariego, D. R. Perrin, Purification of laboratory Chemicals, Pergamon Press,Oxford, **1980**.
[62] J. C. Hummelen, B. W. Knight, F. LePeq, F. Wudl, "Preparation and Characterization of Fulleroid and Methanofullerene Derivatives", *J. Org. Chem.* **1995**, *60*, 532.
[63] (a) M. Gingras, "One hundred years of helicene chemistry. Part 1: non-stereoselective syntheses of carbohelicenes", *Chem. Soc. Rev.* **2013**, *42*, 968; (b) M. Gingras, G. Félix, R. Peresutti, "One hundred years of helicene chemistry. Part 2: stereoselective syntheses and chiral separations of carbohelicenes", *Chem. Soc. Rev.* **2013**, *42*, 1007; (c) M. Gingras, "One hundred years of helicene chemistry. Part 3: applications and properties of carbohelicenes", *Chem. Soc. Rev.* **2013**, *42*, 1051.
[64] L. T. Scott, H. E. Bronstein, D. V. Preda, R. B. M. Ansems, M. S. Bratcher, S. Hagen, "Geodesic polyarenes with exposed concaves surfaces", *Pure & Appl. Chem*. **1999**, *71*, 209.
[65] (a) W. E. Barth, R. G. Lawton, "Dibenzo[*ghi,mno*]fluoranthene", *J. Am. Chem. Soc.* **1966**, *88*, 380; (b) R. G. Lawton, W. E. Barth, "The Synthesis of Corannulene", *J. Am. Chem. Soc.* **1971**, *93*, 1730.
[66] H. W.Kroto, J. R. Heath, S. C. O´Brien, R. F. Curl, R. E. Smalley, "C_{60}: Buckminsterfullerene", *Nature,* **1985**, *318*, 162.
[67] W. Krätschmer, L. D. Lamb, K. Fostiropoulos, D. R. Huffman, "Solid C_{60}: a new form of carbon", *Nature*, **1990**, *347*, 354.
[68] (a) D. M. Guldi, N. Martín, "Fullerenes: From synthesis to Optoelectronic Properties", Kluwer Academic Publishers, **2002**; (b) A. Hirsh, M. Brettreich, "Fullerenes", Wiley-VCH: New York, NY, **2005***;* (c) F. Langa, J. F. Nierengarten, "Fullerenes: Principles and Applications", RSC Nanoscience and Nanotechnology, **2007**; (d) N. Martin, J. F. Nierengarten, "Supramolecular Chemistry of Fullerenes and Carbon Nanotubes", Wiley-VCH Verlag GmbH and Co. KGaA, **2010**; For references on the aromaticity in fullerenes see (e) A. Hirsch, Z. Chen, H. Jiao, " Spherical Aromaticity in I_h symmetrical fullerenes: The $2(N+1)^2$ Rule", *Angew. Chem. Int. Ed.* **2000**, *39*, 3915; (f) A. rodriguez-Fortea, N. Alegret, A. L. Balch, J. M. Poblet, "The maximum pentagon separation rule provides a guideline for the structures of endohedral metallofullerenes", *Nature Chem*. **2010**, *2*, 955; (g) M. García-Borrás, S. Osuna, M. Swart, J. M. Luis, M. Solá, "Maximum Aromaticity as a Guiding Principle for the Most Suitable Hosting Cages in Endohedral Metallofullerenes", *Angew. Chem. Int. Ed.* **2013**, *52*, 9275.

[69] Z. Yoshuda, E. Osawa, *Aromaticity*. Chemical Monograph Series 22. Kyoto: Kagaku-dojin, **1971**, p. 174.
[70] (a) A. H. Abdouzarak, Z. Marcinow, A. Sygula, R. Sygula, P. W. Rabideau, "Buckybowls 2. Toward the Total Synthesis of Buckminsterfullerene (C_{60}): Benz[5,6]-*as*-indaceno[3,2,1,8,7-*mnopqr*]indeno[4,3,2,1-*cdef*]chrysene", *J. Am. Chem. Soc.* 1995, *117*, 6410; (b) S. Hagen, M. S. Bratcher, M. S. Erickson, G. Zimmermann, L. T. Scott, "Novel Syntheses of Three $C_{30}H_{12}$ Bowl-Shaped Polycyclic Aromatic Hydrocarbons", *Angew. Chem. Int. Ed.* **1997**, *36*, 406.
[71] M. A. Petrukhina, L. T. Scott, *Fragments of Fullerenes and Carbon Nanotubes: Designed Synthesis, Unusual Reactions, and Coordination Chemistry,* Wiley, Hoboken **2012**.
[72] (a) L. T. Scott, "Methods for the Chemical Synthesis of Fullerenes ", *Angew. Chem. Int. Ed.* **2004**, *43*, 4994; (b) V. M. Tsefrikas, L. T. Scott, "Geodesic Polyarenes by Flash Vacuum Pyrolysis", *Chem. Rev.* **2006**, *106*, 4868.
[73] E. Maroto, A. de Cózar, S. Filippone, A. Martín-Domenech, M. Suarez, F. P. Cossío, N. Martín, "Hierarchical Selectivity in Fullerenes: Site-, Regio-, Diastereo-, and Enantiocontrol of the 1,3-Dipolar Cycloaddition to C_{70}", *Angew. Chem. Int. Ed.* **2011**, *50,* 6060.
[74] L. T. Scott, M. M. Hashemi, M. S. Bratcher, "Corannulene bowl-to-bowl inversion is rapid at room temperature", *J. Am. Soc.* **1992**, *114*, 1920.
[75] M. A. Petrukhina, K. W. Andrenini, J. Mack, L. T. Scott, "X-ray Quality Geometries of Geodesic Polyarenes from Theoretical Calculations: What Levels of theory are Reliable", *J. Org. Chem.* **2005**, *70*, 5713.
[76] A. Sygula, H. E. Folsom, R. Sygula, A. H. Abdourazak, Z. Marcinow, R. Fronczek, P. W. Rabideau, "Bowl stacking in curved polynuclear aromatic hydrocarbons: crystal and molecular structure of cyclopentacorannulene", *Chem. Soc., Chem. Commun.* **1994**, 2571.
[77] Y. T. Wu, J. S. Siegel, "Aromatic Molecular-Bowl Hydrocarbons: Synthetic Derivatives, Their Structures, and Physical Properties", *Chem. Rev.***2006**, *106*, 4843.
[78] (a) T. C. Wu, M. K. Chen, Y. W. Lee, M. Y. Kuo, Y. T. Wu, "Bowl-Shaped Fragments of C_{70} or Higher Fullerenes: Synthesis, Structural Analysis, and Inversion Dynamics", *Angew. Chem. Int. Ed.* **2013**, *52*, 1289; (b) Y. T. Wu, T. C. Wu, M. K. Chen, H. J. Hsin, "Synthetic and structural considerations on highly curved bowl-shaped fragments of fullerenes", *Pure Appl. Chem.* **2014**, *86*, 539.
[79] (a) L. T. Scott, M. S. Bratcher, S. Hagen, *J. Am. Chem. Soc.* **1996**, *118*, 8743; (b) R. B. M. Ansems, L. T. Scott, "Circumtrindene: A Geodesic Dome of Molecular Dimensions. Rational Synthesis of 60% of C_{60}", *J. Am. Chem*. *Soc.* **2000**, *122*, 2719.

[80] M. A. Petrukhina, K. W. Andrenini, L. Peng, L. T. Scott, "Hemibuckminsterfullerene $C_{30}H_{12}$: X-ray Crystal Structures of the Parent Hydrocarbon and of the Two-Dimensional Organometallic Network $\{[Rh_2(O_2CCF_3)_4]_3 \cdot (C_{30}H_{12})\}$", *Angew. Chem. Int. Ed.* **2004**, *43*, 5477.
[81] M. A. Petrukhina, L. T. Scott, *Fragments of Fullerenes and Carbon Nanotubes: Designed Synthesis, Unusual Reactions, and Coordination Chemistry,* Wiley, Hoboken **2012**, p. 413.
[82] A. A. Popov, S. Yang, L. Dunsch, "Endohedral Fullerenes", *Chem. Rev.* **2013**, *113*, 5989.
[83] P. A. Vecci, C. M. Alvarez, A. Ellern, J. Angelici, A. Sygula, P. W. Rabideau, "Synthesis and Structure of a Dimetallated Buckybowl: Coordination of One $\{Cp^*Ru\}^+$ Unit toEach side of Corannulene", *Angew. Int. Ed.* **2004**, *43*, 4497.
[84] T. Amaya, H. Sakane, T. Hirao, "A Concave-Bound CpFe Complex of Sumanene as a Metal in a π Bowl", *Angew. Chem. Int. Ed.* **2007**, *46*, 8376.
[85] M. A. Petrukhina, L. T. Scott, "Coordination chemistry of buckybowls: from corannulene to a hemifullerene", *Dalton Trans.* **2005**, 2969.
[86] (a) E. M. Pérez, N. Martín, *Chem. Soc. Rev.* **2008**, *37*, 1512; (b) D. Canevet, E. M. Pérez, N. Martín, "Wraparound Host for Fullerenes: Tailored Macrocycles and Cages", *Angew. Int. Ed.* **2011**, *50*, 9248.
[87] S. Mizyed, P. E. Georghiou, M. Bancu, B. Cuadra, A. K. Rai, P. Cheng, L. T. Scott, "Embracing C_{60} with Multiarmed Geodesic Partners", *J. Am. Chem. Soc.* **2001**, *123*, 12770.
[88] L. N. Dawe, T. A. AlHujran, H. A. Tran, J. I. Mercer, E. A. Jackson, L. T. Scott, P. E. Georghiou, "Corannulene and its penta-*tert*-butyl derivative co-crystallize 1:1 with pristine C_{60}-fullerene", *Chem. Commun.* **2012**, *48*, 5563.
[89] P. E. Georghiou, A. H. Tran, S. Mizyed, M. Bancu, L. T. Scott, "Concave Polyarenes with Sulfide-Linked Flaps and Tentacles: New Electron-Rich Host for Fullerenes", *J. Org. Chem.* **2005**, *70*, 6158.
[90] A. Sygula, F. R. Fronczek, R. Sygula, P. W. Rabideau, M. M Olmstead, " A Double Concave Hydrogen Buckycatcher", *J. Am. Chem. Soc.* **2007**, *129*, 3842.
[91] M. Yanney, A. Sygula, "Tridental molecular clip with corannulene pincers: is three better than two?", *Tetrahedron Lett.* **2013**, *54*, 2604.
[92] M. C. Stuparu, "Rationally Designed Polymer Host for Fullerene", *Angew. Chem. Int. Ed.* **2013**, *52*, 7786.
[93] M. Yamada, K. Ohkubo, M. Shionoya, S. Fukuzumi, "Photoinduced Electron Transfer in a Charge-Tranfer Complex Formed between Coranulenne anf $Li^+@C_{60}$ by Concave-Convex π–π interactions", *J. Am. Chem. Soc*. **2014**, *136*, 13240.

[94] D. Miyajima, K. Tashiro, F. Araoka, H. Takezoe, J. Kim, K. Kato, M. Takata, T. Aida, "Liquid Crystalline Corannulene Responsive to Electric Field", *J. Am. Chem. Soc.* **2009**, *131*, 44.
[95] T. Amaya, S. Seki, T. Moriuchi, K. Nakamoto, T. Nakata, H. Sakane, A. Saeki, S. Tagawa, T. Hirao, "Anisotropic Electron Transport Properties in Sumanene Crystal", *J. Am. Chem. Soc.* **2009**, *131*, 408.
[96] L. T. Scott, E. A. Jackson, Q. Zhang, B. D. Steinberg, M. Bancu, B. Li, "A Short, Rigid, Structurally Pure Carbon Nanotube by Stepwise Chemical Synthesis", *J. Am. Chem. Soc*. **2012**, 134, 107.
[97] J. L. Delgado, M. A. Herranz, N. Martín, "The nano-forms of carbon", *J. Mater. Chem.* **2008**, *18*, 1417.
[98] (a) N. Martín, "New challenges in fullerene chemistry", *Chem. Commun.* **2006**, 2093; (b) J. Delgado, S. Filippone, F. Giacalone, M. Herranz, B. Illescas, E. Pérez, N. Martín, "Buckyballs", *Top. Curr. Chem.* **2014**, *350*, 1.
[99] *Carbon Nanotubes And Related Structures: Synthesis, Characterization, Functionalization, and Aplications* (Eds. D. M. Guldi, N. Martín), Wiley-VCH, Weinheim, **2010**.
[100] (a) M. J. Allen, V. C. Tung, R. B. Kaner, "Honeycomb Carbon: A Review of Graphene", *Chem. Rev.* **2010**, *110*, 132; (b) C. N. R. Rao, A. K. Sood, K. S. Subrahmanyam, A. Govindaraj, "Graphene: The New Two-Dimensional Nanomaterial", *Angew. Chem., Int. Ed.* **2009**, *48*, 7752; (c) A. K. Geim, "Graphene: Status and Prospects", *Science* **2009**, *324*, 1530; (d) A. K. Geim, K. S. Novoselov, "Progress Article abstract", *Nat. Mater.* **2007**, *6*, 183; (e) L. Rodríguez-Pérez, M. A. Herranz, N. Martín, "The chemistry of pristine graphene", *Chem. Commun.* **2013**, *49,* 3721; (f) K. Dirian, M. A. Herranz, G. Katsukis, J. Malig, L. Rodríguez-Pérez, C. Romero-Nieto, V. Strauss, N. Martín, D. M. Guldi, "Low dimensional nanocarbons – chemistry and energy/electron transfer reactions", *Chem. Sci.,* **2013**, *4,* 4335.
[101] (a) D. Wróbel, A. Graja, "Photoinduced electron transfer processes in fullerene-organic cromophore systems", *Coord. Chem. Rev.* **2011**, *255*, 2555; (b) S. Fukuzumi, T. Kojima, "Photofunctional nanomaterials composed of multiporphyrins and carbon-based π-electron acceptors", *J. Mater. Chem.* **2008**, *18*, 1427; (c) H. Imahori, "Porphyrin–fullerene linked systems as artificial photosynthetic mimics", *Org. Biomol. Chem.* **2004**, *2*, 1425.
[102] (a) G. Dennler, M. C. Scharber, C. J. Brabec, "Polymer-Fullerene Bulk-Heterojunction Solar Cells", *Adv. Mater.* **2009**, *21*, 1323; (b) M. Helgesen, R. Søndergaard, F. C. Krebs, "Advanced materials and processes for polymer solar cell devices", *J. Mater. Chem.* **2010**, *20*, 36; (c) C. J. Brabec, S. Gowrisanker, J. J. M. Halls, D. Laird, S. Jia, S. P. Williams, "Polymer–Fullerene Bulk-Heterojunction Solar Cells", *Adv. Mater.* **2010**, *22*, 3839; (d) H. Hoppe, N.

S. Sariciftci, "Morphology of polymer/fullerene bulk heterojunction solar cells", *J. Mater. Chem.* **2006**, *16*, 45.
[103] (a) J. M. Schnorr, T. M. Swager, "Emerging Applications of Carbon Nanotubes", *Chem. Mater.* **2011**, *23*, 646; (b) C. Wang, K. Takei, T. Takahashi, A. Javey, "Carbon nanotube electronics moving forward", *Chem. Soc. Rev.* **2013**, *42*, 2592; (c) S. Park, M. Vosguerichian, Z. Bao, "A review of fabrication and applications of carbon nanotube film-based flexible electronics", *Nanoscale* **2013**, *5*, 1727. (d) S. N. Kim, J. F. Rusling, F. Papadimitrakopoulos, "Carbon Nanotubes for Electronic and Electrochemical Detection of Biomolecules", *Adv. Mater.* **2007**, *19*, 3214.
[104] (a) S. Bae, H. Kim, Y. Lee, X. Xu, J.-S. Park, Y. Zheng, J. Balakrishnan, T. Lei, H. R. Kim, Y. I. Song, Y.-J. Kim, K. S. Kim, B. Oezyilmaz, J.-H. Ahn, B. H. Hong, S. Iijima, "Roll-to-roll production of 30-inch graphene films for transparent electrodes", *Nat. Nanotechnol.* **2010**, *5*, 574; (b) X. Li, Y. Zhu, W. Cai, M. Borysiak, B. Han, D. Chen, R. D. Piner, L. Colombo, R. S. Ruoff, "Transfer of Large-Area Graphene Films for High-Performance Transparent Conductive Electrodes", *Nano Lett.* **2009**, *9*, 4359; (c) K. S. Kim, Y. Zhao, H. Jang, S. Y. Lee, J. M. Kim, K. S. Kim, J.-H. Ahn, P. Kim, J.-Y. Choi, B. H. Hong, "Large-scale pattern growth of graphene films for stretchable transparent electrodes", *Nature* **2009**, *457*, 706; d) X. Wang, L. Zhi, K. Müllen, "Transparent, Conductive Graphene Electrodes for Dye-Sensitized Solar Cells", *Nano Lett.* **2008**, *8*, 323.
[105] (a) C.-H. Lu, H.-H. Yang, C.-L. Zhu, X. Chen, G.-N. Chen, "A graphene platform for sensing biomolecules", *Angew. Chem. Int. Ed.* **2009**, *48*, 4785; (b) J. T. Robinson, F. K. Perkins, E. S. Snow, Z. Wei, P. E. Sheehan, "Reduced Graphene Oxide Molecular Sensors", *Nano Lett.* **2008**, *8*, 3137; (c) F. Schedin, A. K. Geim, S. V. Morozov, E. W. Hill, P. Blake, M. I. Katsnelson, K. S. Novoselov, "Detection of individual gas molecules adsorbed on graphene", *Nat. Mater.* **2007**, *6*, 652.
[106] (a)Y. Zhu, S. Murali, M. D. Stoller, K. J. Ganesh, W. Cai, P. J. Ferreira, A. Pirkle, R. M. Wallace, K. A. Cychosz, M. Thommes, D. Su, E. A. Stach, R. S. Ruoff, "Carbon-Based Supercapacitors Produced by Activation of Graphene", *Science* **2011**, *332*, 1537; (b) K. Zhang, L. L. Zhang, X. S. Zhao, J. Wu, *Chem. Mater.* **2010**, *22*, 1392; (c) Y. Wang, Z. Shi, Y. Huang, Y. Ma, C. Wang, M. Chen, Y. Chen, "Supercapacitor Devices Based on Graphene Materials", *J. Phys. Chem. C* **2009**, *113*, 13103.
[107] H. Hu, Z. Zhao, W. Wan, Y. Gogotsi, J. Qiu, "Ultralight and Compressible Graphene Aerogels", *Adv. Mater.* **2013**, *25*, 2219.
[108] X. Huang, Z. Yin, S. Wu, X. Qi, Q. He, Q. Zhang, Q. Yan, F. Boey, H. Zhang, "Graphene-Based Materials: Synthesis, Characterization, Properties, and Applications", *Small* **2011**, *7*, 1876.

[109] A. Dalla Cort, L. Mandolini, C. Pasquini, L. Schiaffino, ""Inherent chirality" and curvature", *New J. Chem.* **2004**, *28*, 1198.
[110] (a) Y. Zhang, W. Yang, "Generalized Gradient Approximation Made Simple", *Phys. Rev. Lett.* **1998**, *80*, 890; (b) S. Grimme, J. Antony, S. Ehrlich, H. Krieg, "A consistent and accurate *ab initio* parametrization of density functional dispersion correction (DFT-D) for the 94 elements H-Pu", *J. Chem. Phys.* **2010**, *132*, 154104.
[111] W. Hujo, S. Grimme, "Performance of the van der Waals Density Functional VV10 and (hybrid)GGA Variants for Thermochemistry and Noncovalent Interactions", *J. Chem. Theory Comput.* **2011**, *7*, 3866.
[112] F. G. Brunetti, H. Isla, J. Aragó, E. Ortí, E. M. Pérez, N. Martín, "Exploiting multivalent nanoparticles for the supramolecular functionalization of graphene with a nonplanar recognition motif", *Chem. Eur. J.* **2013**, *19*, 9843.
[113] S. Grimme, S. Ehrlich, L. Goerigk, "Effect of the damping function in dispersion corrected density functional theory", *J. Comput. Chem.* **2011**, *32*, 1456.
[114] P. Jurecka, J. Sponer, J. Cerny, P. Hobza, "Benchmark database of accurate (MP2 and CCSD(T) complete basis set limit) interaction energies of small model complexes, DNA base pairs, and amino acid pairs", *PCCP* **2006**, *8*, 1985.
[115] J. Řezáč, K. E. Riley, P. Hobza, "S66: A Well-balanced Database of Benchmark Interaction Energies Relevant to Biomolecular Structures", *J. Chem. Theory Comput.* **2011**, *7*, 2427.
[116] W. Hujo, S. Grimme, "Performance of the van der Waals Density Functional VV10 and (hybrid)GGA Variants for Thermochemistry and Noncovalent Interactions", *J. Chem. Theory Comput.* **2011**, *7*, 3866.
[117] (a) S. Grimme, W. Hujo, B. Kirchner, "", *Phys. Chem. Chem. Phys.* 2012, 14, 4875; (b) M. K. Rana, H. S. Koh, J. Hwang, D. J. Siegel, "Comparing van der Waals Density Functionals for CO_2 Adsorption in Metal Organic Frameworks", *J.* Phys*. Chem. C.* **2012**, *116*, 16957; (c) A. Tkatchenko, O. A von Lilienfeld, *Phys. Rev*. *B* **2008**, *78*, 045116; (d) F. Goltl, J. Hafner, "Alkane adsorption in Na-exchanged chabazite: the influence of dispersion forces", *J. Chem. Phys.* **2011**, *134*, 064102.
[118] J. T. H. Dunning, "Gaussian Basis Sets for Use in Correlated Molecular Calculations. I. The Atoms Boron Through Neon and Hydrogen", *J. Chem. Phys.* **1989**, *90*, 1007.
[119] K. Eichkorn, O. Treutler, H. Öhm, M. Häser, R. Ahlrichs, "Auxiliary basis sets to approximate Coulomb potentials", *Chem. Phys. Lett.* **1995**, *240*, 283.
[121] S. Grimme, "Supramolecular Binding Thermodynamics by Dispersion-Corrected Density Functional Theory", *Chem. Eur. J.* **2012**, *2*, 9955.

[122] F. Neese. *WIREs Comput. Mol. Sci.* **2012**, *2*, 73.
[123] http://www.chemcraftprog.com
[124] E. M. Casida, C. Jamorski, K. C. Casida, D. R. Salahub, "Molecular excitation energies to high-lying bound states from time-dependent density-functional response theory: Characterization and correction of the time-dependent local density approximation ionization threshold", *J. Chem. Phys.* **1998**, *108*, 4439.
[125] Gaussian 09, revisión D.01, M. J. Frisch, G. W Trucks, H. B. Schlegel, G. E. Scuseria, M. A. Robb, J. R. Cheeseman, G. Scalmani, V. Barone, B. Mennucci, G. A. Petersson, H. Nakatsuji, M. Caricato, X. Li, H. P. Hratchian, A. F. Izmaylov, J. Bloino, G. Zheng, J. L. Sonnenberg, M. Hada, M. Ehara, K. Toyota, R. Fukuda, J. Hasegawa, M. Ishida, T. Nakajima, Y. Honda, O. Kitao, H. Nakai, T. Vreven, J. A. Montgomery, J. E. Peralta, F. Ogliaro, M. Bearpark, J. J. Heyd, E. Brothers, K. N. Kudin, V. N. Staroverov, R. Kobayashi, J. Normand, K. Raghavachari, A. Rendell, J. C. Burant, S. S. Iyengar, J. Tomasi, M. Cossi, N. Rega, J. M. Millam, M. Klene, J. E. Knox, J. B. Cross, V. Bakken, C. Adamo, J. Jaramillo, R. Gomperts, R. E Stratmann, O. Yazyev, A. J. Austin, R. Cammi, C. Pomelli, J. W. Ochterski, R. L. Martin, K. Morokuma, V. G. Zakrzewski, G. A. Voth, P. Salvador, J. J. Dannenberg, S. Dapprich, A. D. Daniels, Farkas, J. B. Foresman, J. V. Ortiz, J. Cioslowski, D. J. Fox, Gaussian, Inc., Wallingford CT, **2009**.
[126] (a) J. Tomasi, M. Perisco, "Molecular Interactions in Solution: An Overview of methods Based on Continuous Distributions of the Solvent", *Chem. Rev.* **1994**, 2027; (b) C. S. Cramer, D. G. *Solvent Effects and Chemical reactivity;* Kluwer: Dordrecht, 1996.
[127] K. Jacob, J. Y. Becker, A. Ellern, V. Khodorkovsky*, "*Synthesis of Novel Truxenequinone Based Electron Acceptors", *Tetrahedron Lett.* **1999**, *40*, 8625.
[128] D. D. Perrin, I. F. Amariego, D. R. Perrin, Purification of laboratory Chemicals, Pergamon Press Oxford, **1980**.
[129] S**.** Hagen, L. T. Scott, "A Convenient Synthesis of Benzo[*c*]naphtho[2,1-*p*]chrysene" *J. Org. Chem.* **1996**, *61*, 7198**.**